FLUID-STRUCTURE INTERACTION SIMULATION OF BILEAFLET AND MONOLEAFLET MECHANICAL HEART VALVE FLOW DYNAMICS

By

MORTEZA KIMIAGHALAM

Bachelor of Science in Mechanical Engineering

Ferdowsi University of Mashhad

Mashhad, Iran

2010

Submitted to the Faculty of the
Graduate College of the
Oklahoma State University
in partial fulfillment of
the requirements for
the Degree of
MASTER OF SCIENCE IN MECHANICAL ENGINEERING
May, 2013

FLUID-STRUCTURE INTERACTION SIMULATION OF BILEAFLET AND MONOLEAFLET MECHANICAL HEART VALVE FLOW DYNAMICS

Thesis Approved:

Dr. Wei Yin

Thesis Adviser

Dr. David Rubenstein

Dr. David Lilley

Dr. Sheryl A. Tucker

Dean of the Graduate College

.

ACKNOWLEDGEMENT

Foremost, I would like to acknowledge my supervisor Dr. Wei Yin for her incredible support and patience to walk me through this thesis.

I would like to acknowledge Dr. Rubenstein and Dr. Lilley for serving on my thesis committee.

Thank you to all my friends and colleagues who have given me support, especially Saravan, Mazdak and Nasim.

My final thanks are reserved for my parents, who believed in me and my ability and encouraged me to be the best that I could be.

TABLE OF CONTENTS

LIST OF TABLES

Table Page

LIST OF FIGURES

Figure Page

CHAPTER I

INTRODUCTION

Heart valve diseases affect more than 5 million Americans each year[1]. Heart valve disease is the situation in which the valve does not function properly; it can develop before birth or during life as a result of a variety of diseases[2]. One of the treatments for heart valve diseases is to replace the afflicted valve with a prosthetic heart valve (PHV). Almost 60,000 patients in the United States undergo heart valve replacement surgery each year[3].

The most commonly used PHVs are mechanical heart valves (MHVs) and bioprosthetic heart valves (BHVs). MHVs in general have long term mechanical durability[4]. The major limitations of MHVs include its high chance of thrombosis and the requirement of life long anticoagulation treatment[4]. On the other hand, bioprosthetic heart valves are made of chemically treated animal tissue and have lower likelihood of eliciting a thrombogenic response[4]. However, they have a shorter life time due to structural changes such as leaflet wear and calcification (deposition of calcium on the heat valve tissue)[4].

St. Jude Medical bileaflet heart valves are the most commonly used mechanical heart valves in the US market, with more than 1.3 million valves implanted in patients. The bileaflet

heart valves are composed of three parts: two leaflets attached to a valve ring by small hinges. These leaflets can open almost parallel to the mainstream flow, hence presenting a minimum obstruction of flow. Monoleaflet heart valves are not as popular, due to an increased potential in flow obstruction and higher pressure drop[5;6]. However, it has been demonstrated that monoleaflet heart valves can actually have better hemodynamic performance compared to bileaflet heart valves by employing an optimum valve orientation and opening angle for the leaflet[7-12]. Bjork Shiley monoleaflet heart valves, composed of a leaflet secured to the valve ring through a strut, are one of the most successful monoleaflet valves with the lowest occurrence of complications[13]. The opening angle for bileaflet valves usually ranges from 75^{o} to 90^{o}; and that for monoleaflet valves is from 60^{o} to 80^{o}[14].

To design a mechanical heart valve, several aspects should be considered, including the tendency to cause hemolysis (destruction of red blood cells) and thrombosis, durability, and other biochemical responses. Hemodynamic performance of a valve reveals its potential to cause hemolysis and platelet activation in short and long terms. Hemodynamic performance can be evaluated by the obstruction of forward flow, flow separation, regions of high velocity flow (squeeze flow), high shear stress regions, cavitation (formation of low pressure bubbles), and turbulence.

Under physiological conditions, the opening of a heart valve is very fast (in order of 25 to 35 msec) and the valve reaches its fully opened position when the peak flow through the valve reaches less than 75% of its maximum[15]. This will result in the minimum obstruction of the forward flow and less energy loss. Nerem et al.[16] reported that under normal conditions, the fluid flow in the valve region remains laminar most of the time, but the Reynolds number might reach up to 4500 at peak flow. The physiological range of shear stress on heart valve tissues is 0.3 - 8 Pa, with the maximum shear stress occurring at peak systole[17].

The hemodynamic performance of an artificial heart valve can be tested using different methods. *In vivo* studies can provide the most physiologically relevant data on the performance of PHVs. But these experiments are very complicated since they require the implantation of heart valves into living animals. *In vitro* experiments are relatively easier and they usually require an experimental set up which can mimic the flow environment of the heart. Left ventricular assist device (LVAD) is well suited for this purpose; however, it is very expensive to be widely used in basic science research[40]. In order to reduce the costs of *in vitro* experiments with PHVs, a flow chamber with similar properties of a LVAD was developed by Ngwe[18]. Besides *in vitro* experiments, computational fluid dynamics (CFD) methods have been used by Ngwe to evaluate flow conditions in the flow chamber with the presence of PHVs. However, like most of the CFD models, his model did not simulate the valve motion and did not have sufficient temporal resolution[19]. A Fluid Structure Interaction (FSI) approach will be used in this study to simulate flow through monoleaflet and bileaflet MHVs in the flow chamber.

The major goal of this thesis was to develop a high resolution numerical model to simulate the diaphragm motion of the flow chamber and corresponding valve leaflet motions, to provide a more accurate estimation of the flow conditions in the Ngwe's flow chamber design[18], using the FSI modeling approach.

The specific aims of this study were as the following:

Specific Aim 1: to develop two dimensional and three dimensional numerical models to simulate the diaphragm motion and corresponding bileaflet valve motions using a FSI modeling approach, and evaluate flow dynamics around the valve area during systole and diastole.

Specific Aim 2: to develop two dimensional and three dimensional numerical models to simulate the diaphragm motion and corresponding monoleaflet valve motions using a FSI

modeling approach, and evaluate flow dynamics around the valve area during systole and diastole.

Specific Aim 3: to investigate the optimum opening angle for the monoleaflet mechanical heart valve and compare its hemodynamic performance to that of bileaflet heart valves.

In this study complete 2D and 3D FSI models were developed to simulate the opening and closing behavior of monoleaflet and bileaflet mechanical valves, as well as associated dynamic flow conditions. The FSI model used the arbitrary Lagrangian-Eulerian (ALE) method for moving boundaries, and coupled with dynamic equations for leaflets and diaphragm motion. Valve motion was determined by fluid dynamics inside the flow chamber; and the diaphragm motion was controlled by a pulsatile pump, simulating the setup in Ngwe's *in vitro* experiments. This model was developed based on the flow chamber's geometrical parameters and proper boundary conditions. Therefore, it can be used as a numerical tool to assist *in vitro* studies to analyze hemodynamic performance of various heart valve designs.

CHAPTER II

BACKGROUND

2.1 ANATOMY OF THE HEART

The major function of the heart is to circulate blood throughout the body. Blood circulation is responsible for the transferring of the nutrients and oxygen to organs and tissues and simultaneously removing waste materials and carbon dioxide generated by cells. The proper operation of the heart is vital for the healthy performance of all body tissues[20].

The human heart has four chambers: the right atrium, the left atrium, the right ventricle and the left ventricle. The right and left atrium are separated from the right and left ventricle by coronary sulcus. Posterior interventricular sulcus separates the right side of the heart from the left side[21]. The right atrium receives deoxygenated blood through superior and inferior vena cava. The right ventricle pushes deoxygenated blood through the pulmonary arteries into the lungs where it becomes oxygenated. The oxygen rich blood goes to the left side of the heart, and it is then pumped by the left ventricle through the aorta to the rest of the body[22].

The heart has four valves: tricuspid A-V valve, pulmonary valve, mitral valve and the aortic valve. Each heart valve acts as a one way valve, and it directs the blood flow in the right direction. Each valve has two or three cusps of tissue which are called leaflets. The blood pressure changes within each chamber controls the opening and closing behavior of each valve.

The tricuspid AV valve is located between the right atrium and the right ventricle. The pulmonary valve is located between the right ventricle and the pulmonary artery. The mitral valve separates the left atrium from the left ventricle. The aortic valve separates the left ventricle from the aorta[22]. Figure 2.1 illustrates the location of individual heart valves as well as different chambers.

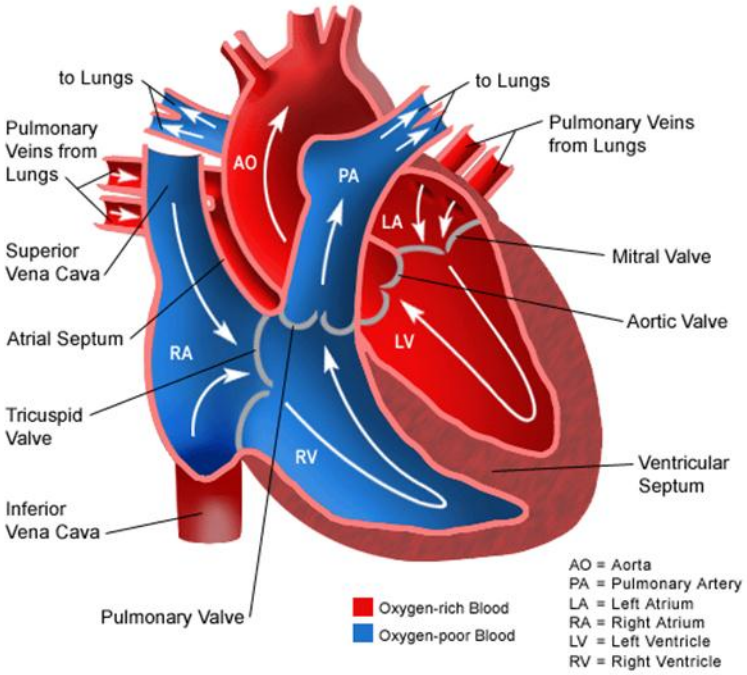

Figure 2.1 Location of different valves and heart chambers[23].

A cardiac cycle is the interval between two subsequent heartbeats. The cardiac cycle has two different periods: systole and diastole. Systole is the phase in which the ventricles contract and push blood out of the heart. During diastole, the heart is relaxed, and the ventricles are filled

with blood[22]. Blood pressure reaches its highest and lowest during systole and diastole respectively. The cardiac output can be defined as the volume of blood which is pushed out of the heart per minute. Cardiac output is dependent on stroke volume (SV) and heart rate (HR). Stroke volume is the volume of blood which is pushed out of the heart at each heartbeat, which is about 70 to 80 mL. Stroke volume is dependent on the end diastolic volume and end systolic volume. End diastolic volume (EDV) is the volume of blood in the ventricle before the ventricular contraction (at the end of ventricular diastole). The end systolic volume (ESV) is the amount of blood in the ventricle right after the ventricular contraction (at the end of ventricular systole). Stroke volume can be calculated as the difference between EDV and ESV. The product of stroke volume and the heart rate gives the cardiac output which is about between 5 and 6 L/min for an average adult.

2.2 HEART VALVE DISEASE

Heart valve disease affects more than 5 million Americans each year and can be defined as the situation in which heart valves do not work properly[24]. Heart valve diseases can be divided in two main classes: stenosis (narrowing) and incompetence (regurgitation). The stenotic heart valve occurs when the valve tissue is stiffened and prevents the valve to open fully. Incompetence occurs when a valve does not close properly and blood can flow backwards across the valve[25].

Heart valve disease can develop before birth (congenital valve disease) or can be developed sometime during the lifetime (acquired valve disease). Congenital valve disease mostly affects the aortic or pulmonic valve. In case of acquired valve disease, a variety of diseases or infections such as rheumatic fever and endocarditis may change the structure of the valve[25].

Finally, other heart diseases such as heart attack, coronary artery disease, heart muscle disease, connective tissue disease, and high blood pressure may also result in a heart valve disease[24]. In any of these conditions, the pupillary muscles which support the heart valves can be injured, so that the valve does not close tightly. Some heart valve diseases are caused by tumors, radiation, and some types of drugs[24].

2.3 PROSTHETIC HEART VALVES

Nowadays prosthetic heart valves (PHVs) are commonly used for the replacement of the diseased heart valves. Almost 60,000 patients in the United States are undergoing heart valve replacement surgery each year[3]. PHVs are made of synthetic materials (mechanical or polymeric heart valves) or biological tissue (bio prosthetic heart valves). Mechanical heart valves (MHVs) are commonly used in the heart valve replacement surgeries (nearly half of the replacement valves[26]). Dr. Charles Hufnagel implanted the first MHV in 1952[27]. Figure 2.2 shows the evaluation of mechanical heart valve since 1952.

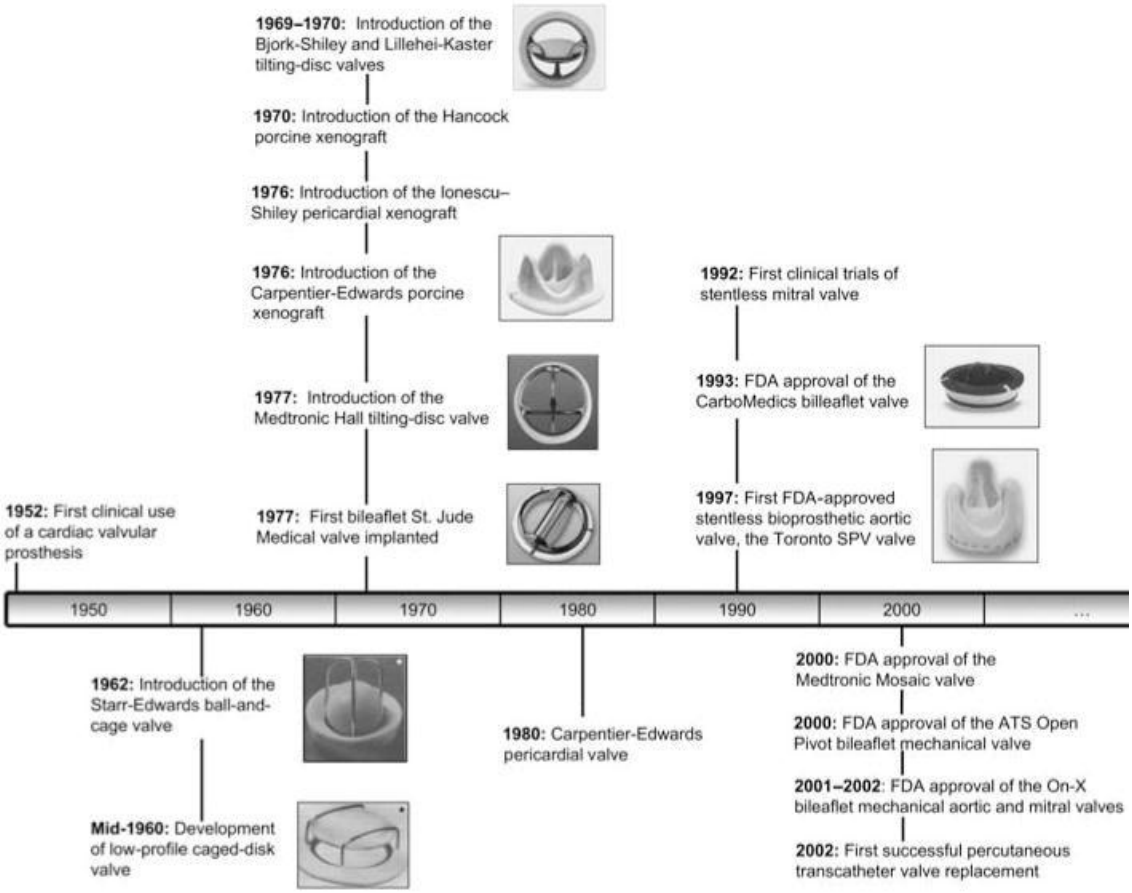

Figure 2.2 Prosthetic heart valve evaluations since 1952[20].

Three main designs of MHVs include ball and cage valve, tilting disc valve, and the bileaflet valve (Figure 2.3). All these MHV designs are made of three main components including occluder, housing, and sewing ring. The occluder is usually a rigid body such as a ball (as in the caged ball valves), a disc (as in the Bjork-Shiley monoleaflet valves) or a hinged leaflet (as in the St. Jude bileaflet valves). The housing may include a cage-like structure and a ring structure. The function of the housing is to guide and restrict the occludar's movement (cage-like structure) and to provide a seat for the occludar (ring structure). The sewing ring is for the implantation of the valve[28].

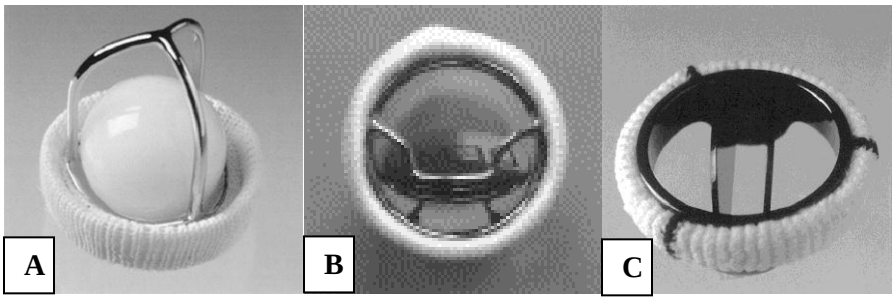

Figure 2.3 Three main designs of MHVs include the caged ball valve (A), the tilting disc valve (B), and the bileaflet valve (C)[28].

The first commercially available MHV was the Starr-Edwards ball in cage valve, which was presented in 1960[28]. So far about 200,000 of these valves have been implanted, and they have the longest clinical usage history compared to other MHV designs[28]. The original Starr-Edwards MHV was made of a ball, a sewing ring, and a cage-like structure. The valve is closed when the ball is seating in the sewing ring, and it opens when the ball moves forward into the cage (Figure 2.3A)[29]. Some of the complications of the Starr-Edwards MHVs were reported as ball damage (cracks) and thrombus formation due to the central flow obstruction by the ball[25].

In late 1969 the Bjork Shiley monostrut valve was introduced which was the first successful tilting disk valve. Tilting disc valve models include the Medtronic Hall valve, the

Omnicarbon valve, the Sorin Allcarbon tilting disc valve, and the Bjork-Shiley monostrut valve. Monoleaflet valves are composed of a single disk and a strut (Figure 2.3B). The function of the strut is to guide and restrict the occludar movement and to prevent its loss into the bloodstream[25]. Monoleaflet valves provide better hemodynamic performance due to a better central flow[26]. Some of the complications of the monoleaflet valves are strut fracture and thrombus formation[26].

Nowadays the majority (about 80%) of the implanted MHVs are bileaflet mechanical heart valves. Bileaflet valves include the ATS valve, ST. Jude valve, and Sorin Bicarbon valve. The St. Jude Medical (SJM) bileaflet valve has acceptable hemodynamic performance and is usually considered as the "golden standard", among all mechanical heart valves[30]. It is composed of two leaflets which are held by butterfly hinges (Figure 2.3C). Bileaflet valves provide a symmetric flow through the valve (if aligned properly) which reduces the possibility of flow separation. Due to the results of a study by Butany et al.[26], bileaflet valves provide more central flow compared to the monoleaflet valves. However, further progress should be made with bileaflet mechanical heart valves in terms of durability and thrombogenicity.

To overcome the disadvantages of MHVs, Bioprosthetic heart valves (BHV) were presented. BHVs are made from porcine valves or bovine pericardium. Porcine valves are most commonly used, and they usually fall into two categories: Hancock valves (Figure 2.4A) and Carpentier-Edwards valves (Figure 2.4B). Since BHVs are natural valves they provide a better hemodynamic performance and less thrombogenicity[31]. However, they come with the risk of calcification and possible immune responses. Calcification could result in stiffened leaflet cusps and stenotic heart valve[31]. In late 1976 Carpentier-Edwards valve was introduced to improve the BHV design. However, the Carpentier-Edwards valve is only a reliable choice as a tissue valve in the mitral position and for patients more than 60 years old[31]. More recently (1992), stentless porcine valves were introduced (Figure 2.4C). Stentless valves do not have any frame in their structure. Removing the stent from the valve reduces the resistance against the flow and lowers

the transvalvular pressure gradient. Therefore, stentless valves have better hemodynamic performance compared to previous stented designs[32].

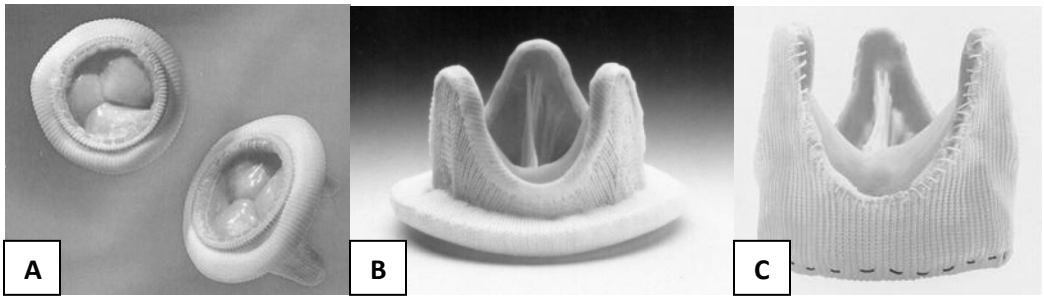

Figure 2.4 Different designs of BHVs including: the Hancock valve (A), the Carpentier-Edwards valve (B), and the Toronto SPV valve (C)[32;33].

There is an ongoing need to improve the currently available PHV designs due to some major limitations. Mechanical heart valves are vulnerable to thrombosis and thromboembolism and require long-term anticoagulation treatment[30]. On the other hand, bioprosthetic valves have a limited life time due to structural changes such as leaflet wear and calcification[30].

Some of the main design factors to be considered in the future heart valve designs include short and long term hemodynamic performance, durability, and biological response to the implant. Hemodynamic performance of the valve can be improved by valve designs which provide higher orifice area. A large orifice area will decrease the pressure gradients across the valve which leads to less energy loss[25]. It can also lower chances of flow transitioning into the turbulent region and reduce the blood cell damage in the valve area. High durability can be achieved by use of materials which are resistant to mechanical and structural wear and are non-degradable in the physiological environment. The new design needs to also minimize trauma to

the endothelial tissue of the cardiovascular structure and risks of platelet and thrombus deposition[34].

2.4 VENTRICULAR ASSIST DEVICE

The testing of prosthetic heart valves and analysis of flow characteristics in a physiologically relevant replication of the human heart is necessary.

Different experimental set ups have been introduced to test the hemodynamic performance of prosthetic heart valves. Dual chamber pulse duplicators, ventricular assist devices (VADs), and different mock loop systems are employed in different experimental studies. Dual chamber pulse duplicators can replicate ventricular and atrial muscle contraction and relaxation with independent hydraulic systems. These test devices can be used to investigate flow parameters such as pressure gradient, orifice area, leakage level, and velocity profiles in the valve area[35]. Mock loop systems are simplified hydraulic simulators of the cardiovascular system that have been employed to test heart valves. In vitro mock loops can provide reliable and quantitative data about the performance of heart valve implants[36-38]. Ventricular assist device (VAD) can also be used along with laser doppler velocimetry (LDV) and digital particle image velocimetry (DPIV) to reveal flow patterns downstream of the valves[39].

The first VADs were developed for short-term use until a donor heart could be found. VADs are particularly well suited to assess the hemodynamic performance of aortic and mitral prosthetic heart valves since they can provide a similar flow environment as a normal heart[40]. However, the high cost for the VAD prevents it from being widely used for research purposes[40]. In this context, a flow chamber with similar properties of a VAD and lower cost was developed by Ngwe et al.[18]. This system was composed of two compartments. The top compartment was designed for heart valve testing and the bottom compartment was a water chamber, which could be connected to a reciprocating pump. In the present study, flow conditions in the top flow chamber were investigated, where the heart valves were placed.

2.5 COMPUTATIONAL FLUID DYNAMICS

Besides in vitro, ex vivo and in vivo studies, computational fluid dynamics (CFD) is an effective alternative to study the hemodynamic performance of heart valves. The advantages of using CFD to study the performance of artificial heart valves include: relatively low cost, high speed, and ability to simulate real conditions. CFD simulations can be performed in a short period of time and provide engineering data early in the design process. Some of the flow processes in a MHV cannot be easily measured by experiments (e.g. high speed jet flow during the valve closure); however, CFD is capable of theoretically simulating any physical condition.

In the early 1970s (almost a decade after the introduction of the first mechanical heart valve) the first CFD model was developed to study the flow dynamics of MHVs. The primary CFD models of prosthetic heart valves were two dimensional models, focusing mainly on simulating the large scale flow parameters in mechanical heart valves[41-45]. They were also used to assess the efficiency of diverse numerical methods and to compare the results with experimental fluid mechanics outcomes[42;45]. More CFD models were developed in the early 1990s with the invention of more powerful computer units. It was in this period that Gill-Jeong and Chandran[42] studied the transient closing behavior of Bjork-Shiley monoleaflet MHV. They employed the governing equations of motion with fluid pressure and gravitational force to calculate the position of the leaflet at each time step. They reported a closing time of 10-15 msec and a maximum backflow velocity of about 1.5-2.5 m/sec. Their results were in agreement with an experimental study conducted by Chandran et al.[46] They assumed that the flow was laminar and one-dimensional in the axial direction.

Krafczyk et al.[45] simulated 3D transient physiological flow in bileaflet MHVs with different opening angles. They used a Lattice–Boltzmann scheme with nearly 6 million nodes to predict the flow pattern. They studied three dimensional flow parameters when the valve was kept

stationary at each specific opening angle. They estimated a maximum forward velocity of 0.3 m/s at the center of the tube and a peak shear stress magnitude of 10 N/m^2 in the gap between the leaflets. The shear stress values estimated in this study were in agreement with the experimental results reported by Lee and Chandran[47]. The limitation of this study was that it neglected the effects of leaflet fluid interaction and the elasticity of the artery.

King et al.[43] used CFD to study the effect of opening angle on the flow dynamics through a carbomedics bileaflet MHV. In their study, they employed a commercial package called FIDAP (Fluid Dynamics International Applications Package) which was based on the Galerkin form of weighted residuals method. This study demonstrated that variation in the opening angle significantly affected the downstream flow and that opening angles greater than 80^o were preferable for the bileaflet valves. The weakness of this study was the use of steady laminar simulation without considering the leaflet motion. Later in 1997, King et al.[25] studied the same problem of the optimal opening angle for a bileaflet MHV by employing a three dimensional transient CFD model. This time their results demonstrated that the maximum shear rate and the maximum velocity increased with an increase in the opening angle from 78^o to 80^o. The maximum shear rate was 42000 Sec^{-1} and 38000 Sec^{-1} for the 85 and 78 degrees of opening angle respectively and occurred on the edge of the leaflet adjacent to the valve ring. The maximum velocity was 1.6 m/s and 1.5 m/s for the 85 and 78 degrees of opening angle respectively. In the valve with 85 degrees of opening angle the gap between the leaflets was smaller in they fully opened position and as a result the maximum velocity was increased. They concluded that the geometry of the central flow also needs to be taken into the consideration.

Aluri and Chandran[41] studied cavitation possibility during the closure of a typical bileaflet MHV in the mitral position. They used grids with 2048 and 56,192 nodes in 2D and 3D models respectively. Their model solved conservation of mass and Navier–Stokes equations to capture the pressure and flow patterns during the valve closure. They reported a maximum

velocity of 13 m/s and 4.73 m/s and a maximum shear stress of 4000 Pa and 725 Pa in the gap between the leaflet and the wall at the instant of valve closure in the 3D and 2D models respectively. They also reported a maximum pressure difference of 130,389 Pa and 13,332 Pa across the valve in the 3D and 2D models respectively. The shear stress values reported in this study were above the physiological range (0.3 – 8 Pa) for heart valve tissue[58]. The major weakness of this study was avoiding the leaflet fluid interaction during the valve closure.

Lai et al.[48] presented a computational model to study a typical bileaflet MHV closure process. They used a grid of 9830 nodes with an arbitrary Lagrange-Euler solver to study the effect of leaflet geometry on the pressure in the valve region during closure. This study has established that the arbitrary Lagrange-Euler solver modeling can serve in CFD modeling of valve designs. They reported that, for a valve closure time of 33.156 msec, the maximal velocity in the gap between the leaflet and the wall at the instant of valve closure was 13 m/s. Limitation of this study was the use of a simplified 2D geometry for the leaflets and avoiding the leaflet fluid interaction during the valve closure.

Rosenfeld et al.[49] numerically studied the flow across a tilting disk MHV. They used a 2D grid with 20,000 nodes to investigate the flow parameters near the leaflet. They utilized both moving and fixed mesh grids for the valve. In the moving mesh case, the maximum pressure drop at the valve fully open position was 2130 Pa, while the mean was 400 Pa. They pointed out that leaflet motion had a significant effect on flow characteristics when the valve was fully open. The major limitation of this study was that only simplified 2D geometry was used.

Krishnan et al[50] numerically studied the relationship between shear stress and platelet activation in a Medtronic bileaflet mechanical valve during the valve closure phase. They employed 2D Navier–Stokes Equations in the non-dimensional form. Due to the results of this study, the maximum velocity and shear stress were 20 m/s and 11000 Pa in the gap between the

leaflet and the wall at the instant of valve closure. Results from this study showed that the jet flow through the gap between the leaflet and the wall was the main cause of platelet activation in this region. Estimated shear stress values in this study were also higher than physiological range of shear stress in case of heart valve tissues (0.3 – 8 Pa)[58]. The weakness of this study was the use of fixed grid Cartesian mesh and the 2D geometry for the leaflets.

Yin et al.[51] compared the relationship between shear stress and the platelet activation in bileaflet and monoleaflet MHVs. They used Wilcox $k-\omega$ turbulence method and a platelet activation model to study the effect of shear stress on platelet activation in these two different valve designs. The 2D grid consisted of 89,000 nodes and 23,000 elements. This study indicated that the bileaflet mechanical valves induced higher shear stress compared to the monoleaflet valves, which resulted in higher tendency for platelet activation. The limitation of the computational model was neglecting the effect of leaflet motion and the flow dynamics in the valve hinge regions.

Simon et al[52] studied the 3D flow parameters in the valve hinge regions of a bileaflet MHV in the aortic position. They employed Cartesian sharp interference immersed boundary approach combined with a second-order accurate fraction step method. Their results demonstrated that the flow fields in the valve hinge area were highly prone to platelet aggregation and thrombosis. This model was not able to simulate the flow dynamics at the instant of valve closure, and blood was also modeled as an incompressible Newtonian fluid.

Most recent models tried to numerically couple the motion of heart valve leaflets with the fluid flow to improve model accuracy. In addition, these studies used more realistic three dimensional valve leaflet geometries and improved the assumption criteria by including important local flow properties such as turbulence and cavitation. de Hart[53] studied the effect of fluid structure interaction (FSI) for the aortic valve opening and closing phases. He used a Lagrange

multiplier based fictitious domain method coupled with a finite element method for the fluid. Results from this study showed that the combined fictitious domain and arbitrary Lagrange-Euler method is a useful numerical tool for FSI analyses of the aortic valve.

Govindarajan et al.[54] conducted a 2D FSI simulation of the closing behavior of a Bjork-Shiley monostrut MHV in the mitral position. The leaflet motion was calculated based on the external forces and momentum applied on the leaflet surfaces from the surrounding fluid. They estimated that it took the leaflet 35 s to reach the closed position (a 70^{o} movement). The maximum shear stress and fluid velocity in the gap between the leaflet and the wall at the fully closed position was 7536 Pa and 41.8 m/s. The major limitation of this study was that they initialized the simulation with fluid being stationary and the valve being at the fully open position. The opening motion of the mitral valve during diastole and the corresponding flow conditions could have affected the closing characteristics of the valve. Cheng et al.[55] studied the three dimensional unsteady flow in a typical bileaflet MHV in the mitral position during the valve closure phase by employing the FSI method. Arbitrary Lagrangian–Eulerian method was used in the FSI model. The forces exerted by the fluid on the leaflets were computed and applied to the leaflet equation of motion to predict the leaflet position. The 3D geometry was consisted of a total number of 226090 nodes with 210000 elements. In this model, the pressure was assumed to be constant at zero in the arterial side of the valve while the ventricular pressure was increasing at a rate of 266644 Pa/s. Such initial conditions for the pressure resulted in development of significant local positive and negative pressures around the leaflet surface. At the instant of valve closure, the maximum negative pressure in the valve region was −79593 Pa with the corresponding maximum positive pressure of 81592 Pa. The maximum velocity and shear stress were 28 m/s and 18 kPa respectively in the gap between the leaflet and the wall. The weakness of this study was the use of an unrealistic and simplified geometry for leaflets.

Nobili et al.[56] numerically studied the flow dynamics in a St. Jude bileaflet MHV using the FSI method. They used Arbitrary Lagrangian-Eulerian method in their model. They reported that it took 0.04 seconds for the valve leaflets to reach their fully opened position (85^{o}). The maximum transvalvular pressure measured during systole was 2933 Pa and the maximum velocity was 1.4 m/s at the peak systole. They conducted validation experiments using a mock loop. Since their model was not able to model the contact between the leaflet and the wall, they had to model the leaflets smaller than their actual size. This resulted in a smaller moment of inertia for the leaflets and consequently higher opening velocities in the numerical simulation compared to the experimental results. Also, compliance of the aortic root and the friction forces due to the presence of the hinge mechanism were neglected in their numerical simulation.

According to Sotiropoulos[57], recent development of FSI capabilities gives us the ability to simulate the monoleaflet and bileaflet MHV flows under physiologic conditions and with high resolutions.

The present project followed Ngwe's[18] study to evaluate three dimensional flow patterns induced by different MHVs in a flow chamber. In his study, numerical simulation was conducted under steady conditions without considering the movement of valve leaflets. He demonstrated that flow was prominently laminar in the flow chamber during one cardiac cycle. The transvalvular pressure across the outlet valve during systole was 57.2 Pa, that across the inlet valve during diastole was 37.8 Pa. The maximum velocity was reported as 0.35 m/s in both valves. The major goal of the present study was to develop a high resolution numerical model to simulate the diaphragm motion and corresponding valve leaflet motions, to provide a more accurate estimation of the flow conditions in the flow chamber, using the FSI modeling approach.

CHAPTER III

MODELING PROCEDURE

3.1 GEOMETRY

3.1.1 FLOW CHAMBER GEOMETRY

The flow chamber was designed to provide a physiologically relevant mechanical environment to evaluate the performance of artificial heart valves. It followed the original design of a left ventricular assist device (LVAD)[59]. The whole system was composed of two compartments, separated by a diaphragm (Figure 3.1). The top compartment was designed for heart valve testing and the bottom compartment was a water chamber, which could be connected to a reciprocating pump. Two artificial heart valves can be placed on each side of the top flow chamber to control the direction of flow, driven by a reciprocating pump through the diaphragm at the bottom of the chamber (Figure 3.1)[60]. To generate the physiological flow conditions of a normal heart, the stroke volume was set at 80 mL, stroke rate at 72 min^{-1}, and systole/diastole ratio at 3/8. Since the bottom flow chamber was not in direct contact with the heart valves, flow condition in this chamber was not simulated. The focus of the present study is the flow conditions in the top flow chamber, where the heart valves were placed. The geometry of the flow chamber was constructed in ANSYS ICEM CFD 13.0, in both 2D and 3D.

For the 2D model, the cross section of the flow chamber was constructed as a segment (of a circle) with a base of 0.093 m and a height of 0.031 m. The centers of the inlet and outlet channels (0.0254 m in diameter, where the valves were placed) were 0.05 m apart, on each side of the chamber[60]. The height of the inlet and outlet channels was 0.072 m. The details of the 2D geometry are shown in Figure 3.2.

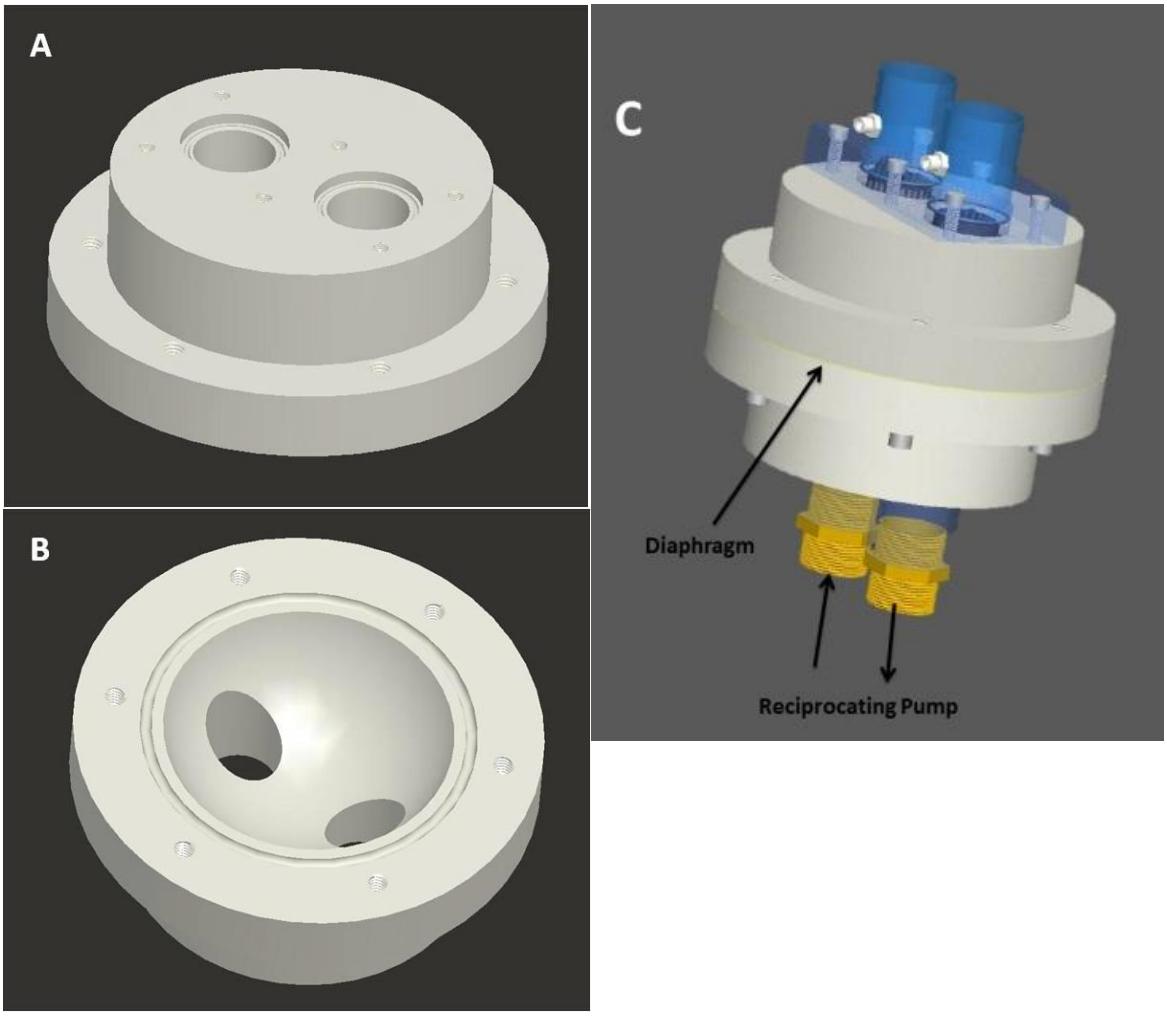

Figure 3.1 3D CAD model of the flow chamber. (A) The top surface of the fluid chamber, where the heart valves would be placed. (B) The bottom surface of the fluid chamber. It served as a water chamber to drive the movement of the diaphragm. (C) Assembled flow chamber. Picture from reference 18 with modification.

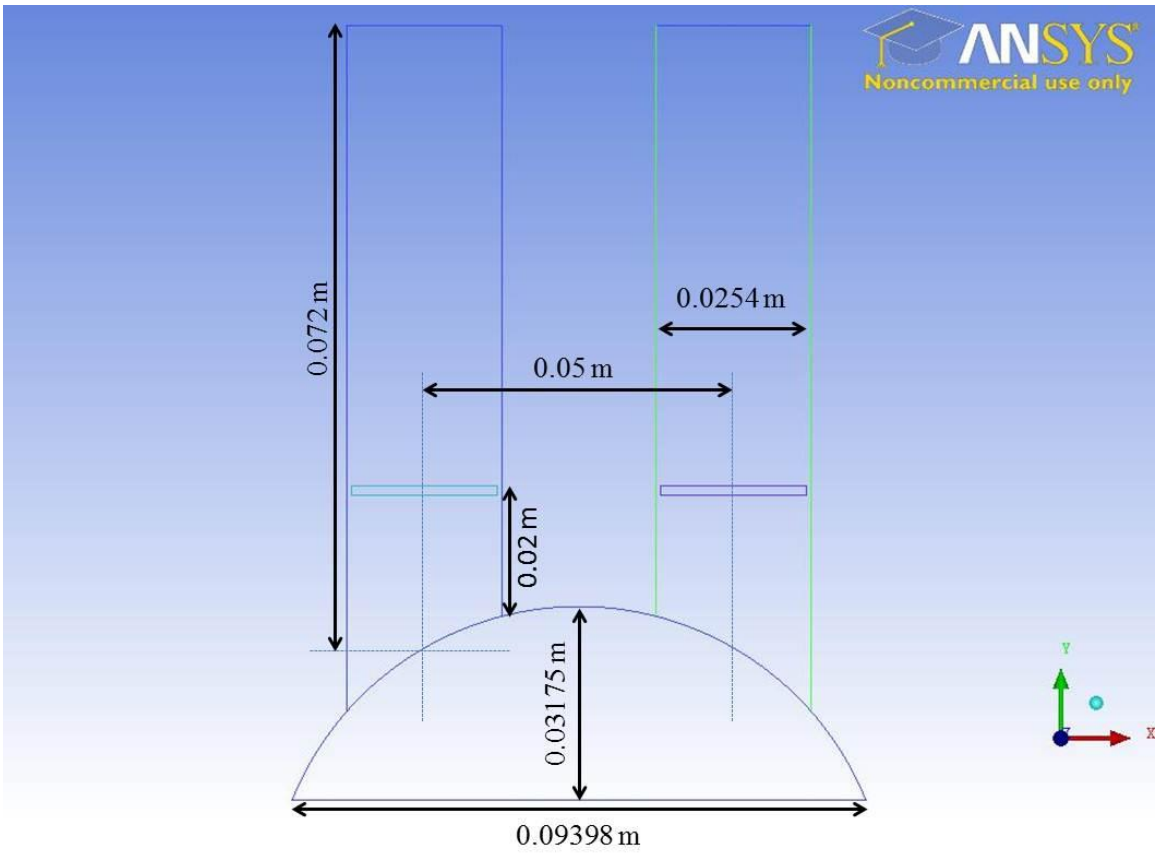

Figure 3.2 2D geometry of flow chamber constructed using ICEM CFD.

For the 3D model (Figure 3.3), the geometry was considered as a dome. The diameter of the base was 0.09398 m and the height was 0.03175 m. Similar to the 2D model, the inlet and outlet channels were placed on each side of the chamber, and the centers of the two channels were 0.05 m apart. The height of the channels was 0.072 m. The total volume of the flow chamber was 127 mL.

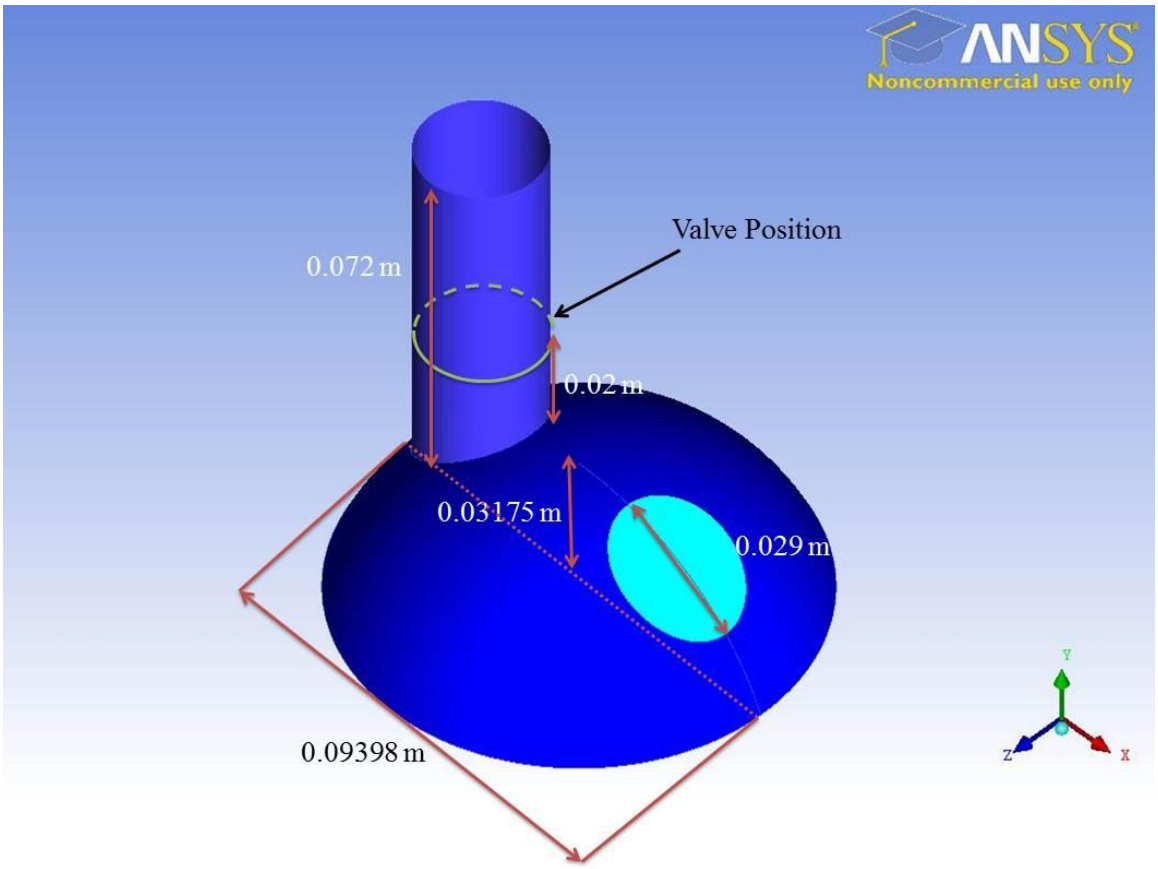

Figure 3.3 3D geometry of flow chamber constructed using ICEM CFD

3.1.2 THE BILEAFLET HEART VALVE GEOMETRY

Two St. Jude bileaflet mechanical heart valves were used in the numerical model as the control valves. The external diameter of the St. Jude bileaflet heart valve used in this study was 25 mm (without the suture ring) and its geometry is shown in Figure 3.4. When fully open, the valve leaflet was set at 5^{o} with respect to the y axis; and when fully closed, the valve leaflet was set at a 25^{o} angle, reference to the x axis. Therefore, the leaflet moved 60° from the fully closed position to the fully open position. In Figure 3.4, the direction of flow during diastole is shown by the thin blue arrow and that during systole by the thick red arrow. In the 2D simulation, the cross-section of the leaflet was close to a rectangle (shown in Figure 3.4) with a width of 0.000899 m and a length of 0.0139 m. The leaflet rotated around rotation center O, which was located on the rectangle centerline and 0.0014 m away from the leaflet inner edge. For the 3D model, the leaflet was defined as half of a disk, with a diameter of 0.0139 m and a thickness of 0.000899 m. The axis of rotation was defined as a line passing through the leaflet, 0.0014 m away from the leaflet inner edge[61]. Figure 3.5 shows the constructed 2D and 3D geometries of the valve leaflets at the fully closed position in ICEM CFD.

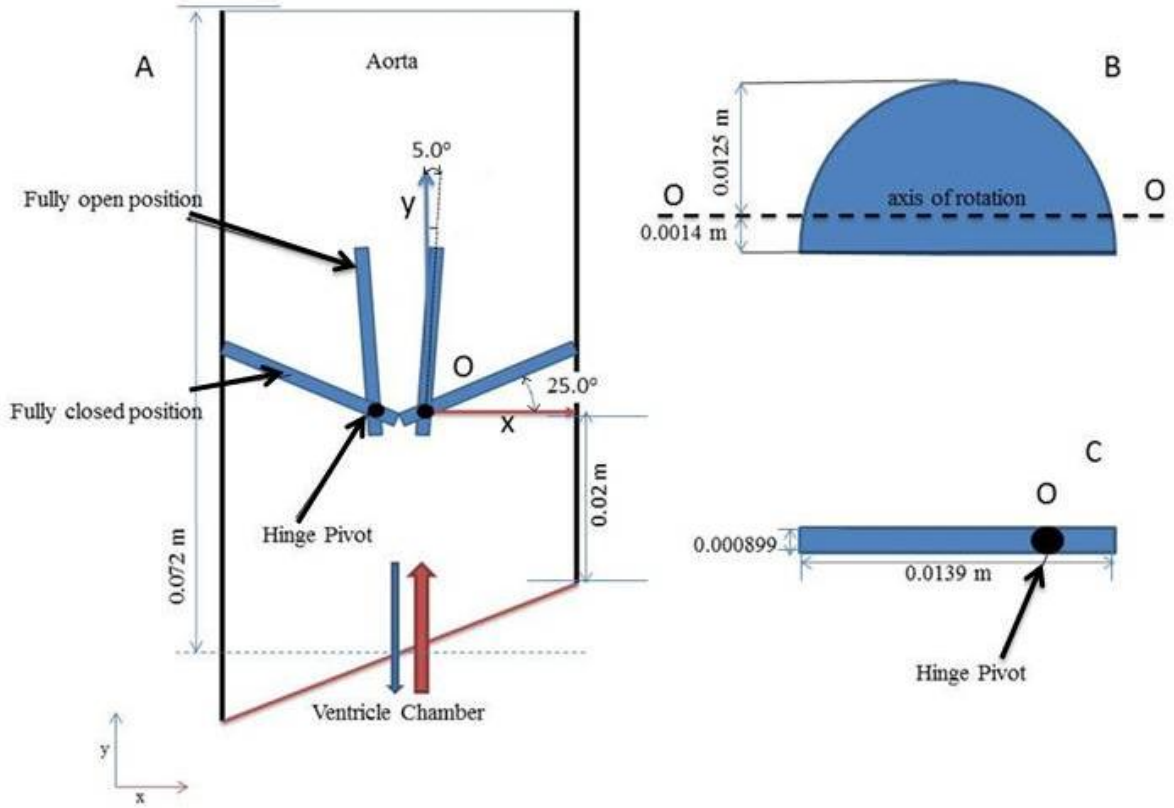

Figure 3.4: The side view of the outlet tube showing the fully open and closed positions of the valve (A), The top view of the St. Jude medical heart valve leaflet (B), Side view of the St. Jude medical leaflet (C). Picture was redrawn based on reference [61].

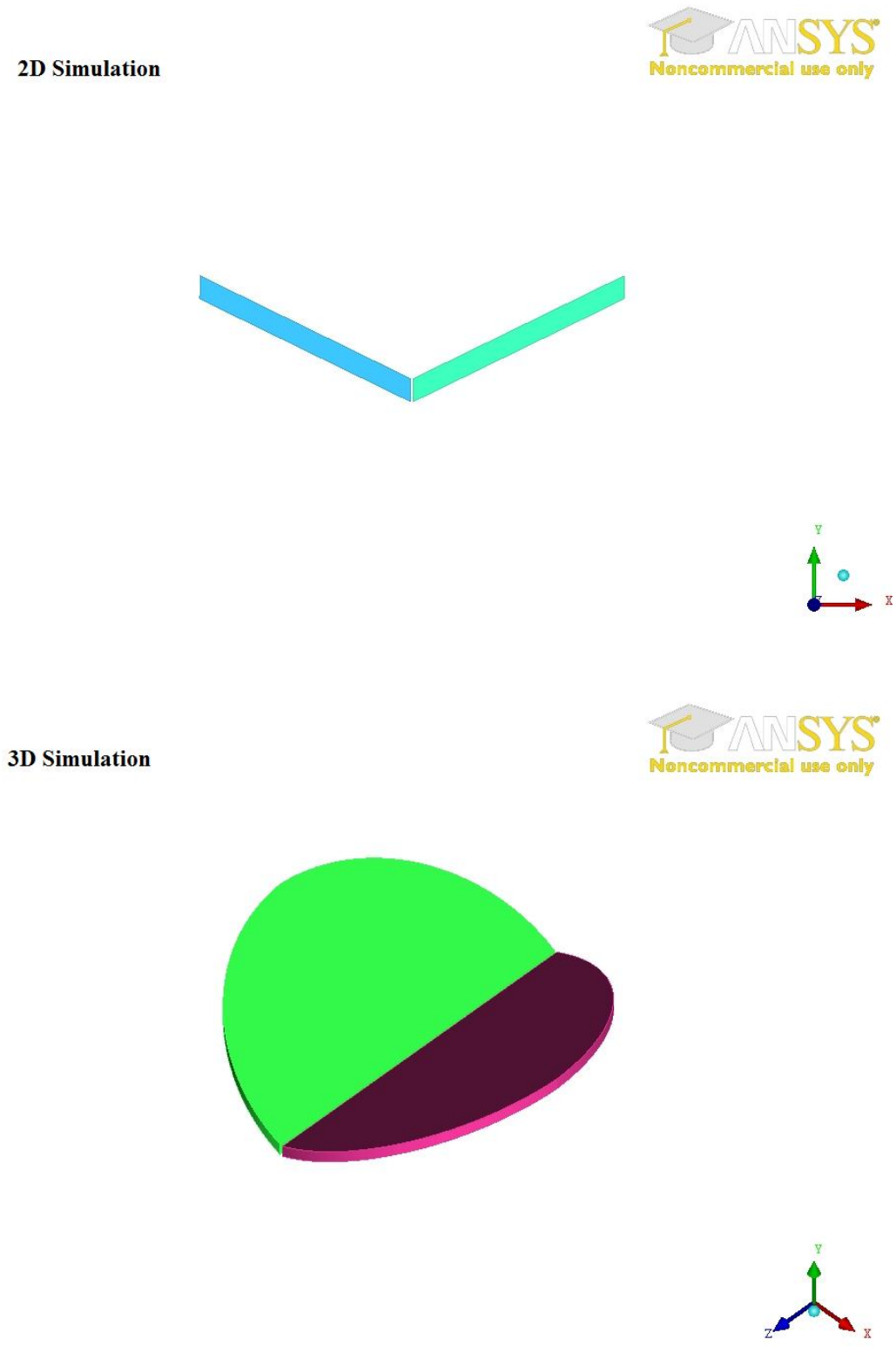

Figure 3.5 St. Jude Medical bileaflet heart valve geometry in 2D and 3D, constructed in ICEM CFD

3.1.3 THE MONOLEAFLET HEART VALVE GEOMETRY

A monoleaflet heart valve was designed based on the geometry of a 25 mm Bjork Shiley tilting disc valve, and its hemodynamic performance was evaluated in the present study. For the 2D model, the leaflet geometry was defined as a rectangle with a width of 0.0015 m and a length of 0.024 m. The leaflet rotated around the rotation center O, which was located 0.006 m off the center on one side of the leaflet[62]. For the 3D model, the leaflet was defined as a disk with a diameter of 0.024 m and a thickness of 0.0015 m. The axis of rotation was defined as a line passing through the leaflet, 0.006 m away from the leaflet edge. There was a 0.00005m- gap between the leaflet and the wall when the valve was fully closed[62]. The geometry specifications of the monoleaflet valve are shown in Figure 3.6. In the present study, we wanted to investigate the effect of monoleaflet heart valve opening angle on flow conditions, therefore, in our CFD simulations, the valve opening angle, Θ (valve inclination angle with respect to x axis), was defined to range from 45^{o} to 85^{o}. The fully closed position for the valve was set to be 0° (to x axis). In Figure 3.6, the direction of flow during diastole is shown by the thin blue arrow and that during systole by the thick red arrow. Figure 3.7 shows the constructed 2D and 3D geometries of the valve leaflet at the fully closed position in ICEM CFD.

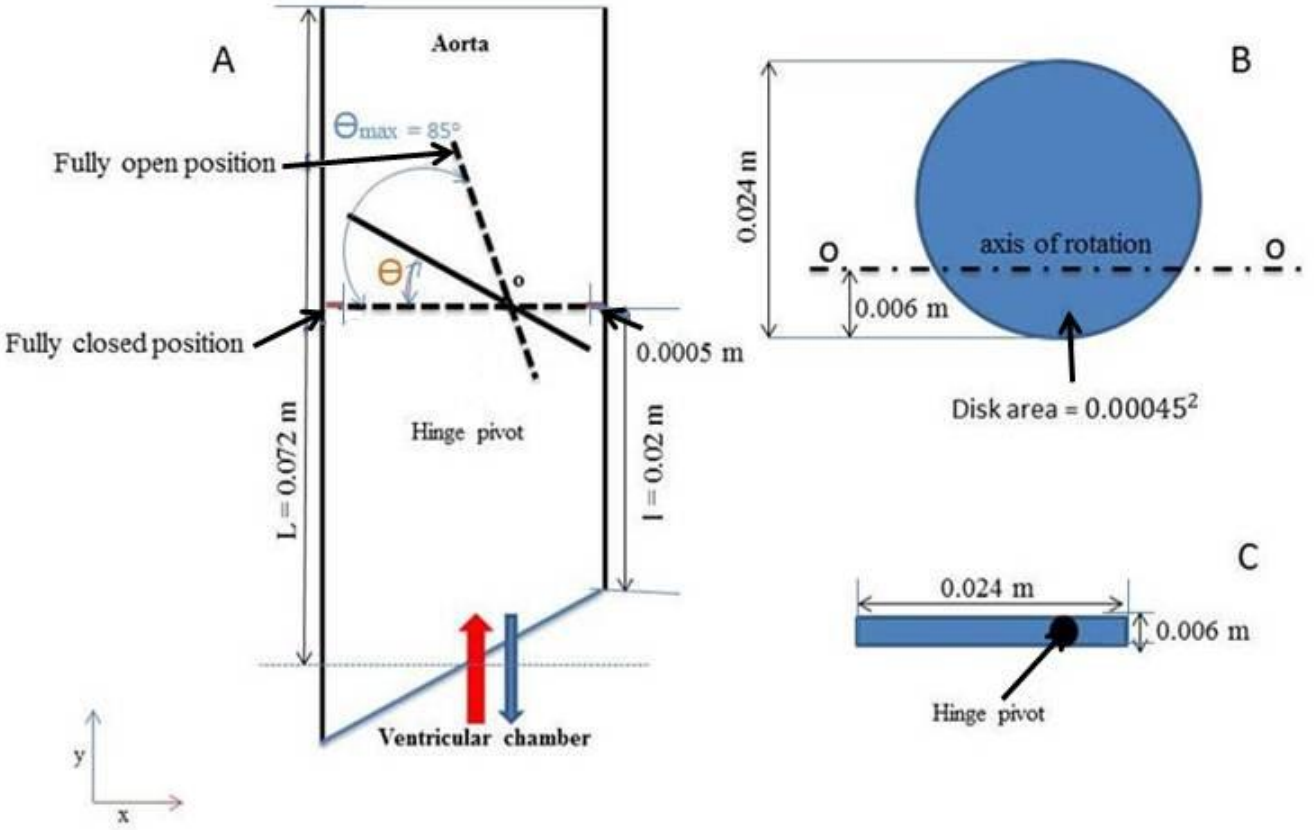

Figure 3.6: Side view of the outlet tube showing the fully open and closed valve positions (A). Top view of the Bjork-Shiley monoleaflet valve (B). The side view of the Bjork-Shiley monoleaflet valve (C). Picture was redrawn based on reference [62].

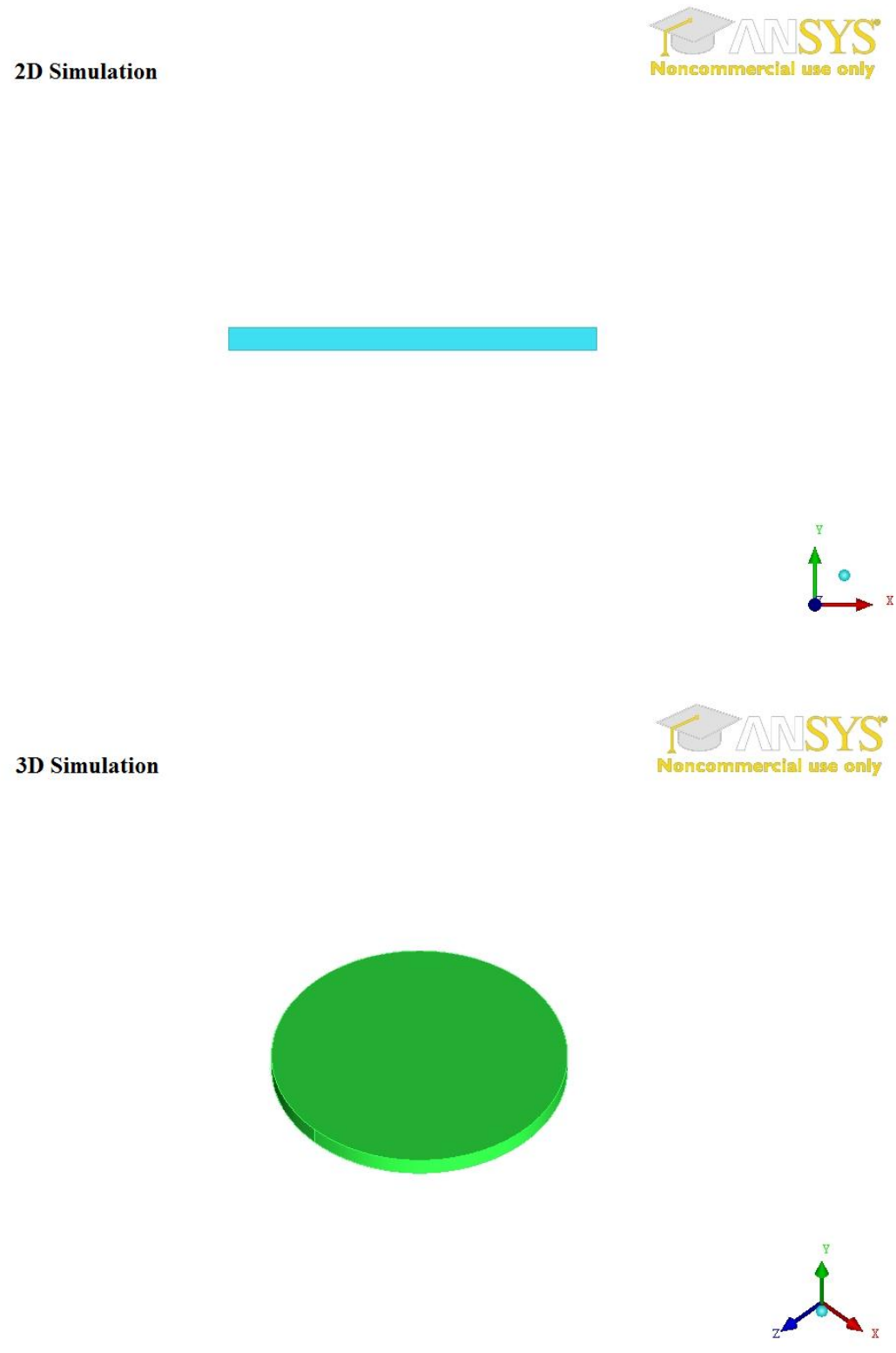

Figure 3.7 The monoleaflet valve geometry in 2D and 3D, constructed in ICEM CFD

3.2 NUMERICAL MODEL

3.2.1 MESHING

3.2.1.1 TWO-DIMENSIONAL MODEL

The 2D monoleaflet and bileaflet heart valve models were meshed with robust mesh method using tetrahedral/mixed mesh elements in ANSYS ICEM CFD 13.0.1. Robust tetra/mixed mesh method generated tetra volume mesh with prism layers. The meshing parameters were defined by surface meshing. The maximum surface mesh size differed from one surface to another depending on the complication of the fluid flow in that region and the possibility of mesh motion.

3.2.1.1.1 THE BILEAFLET HEART VALVE

Due to the simplicity of the 2D model, both valves had a uniform fine mesh throughout the whole geometry. All results from the simulation were tested for mesh independency. Figure 3.8 shows the meshing of the bileaflet heart valve and the fluid chamber. Table 3.1 summarizes the maximum mesh size, and number of nodes and elements in the model for each surface.

Table 3.1 Mesh information of each individual surface for SJM heart valve

Part Name	Mesh Motion	Maximum Mesh Size	Number of Elements	Number of Nodes
Diaphragm	Yes	0.1	115	78
Housing	No	0.1	72	54
Inlet	No	0.1	152	102
Outlet	No	0.1	48	34
Inlet Interface	No	0.1	39	26
Outlet Interface	No	0.1	38	26
Inlet Right Leaflet	Yes	0.01	352	174
Inlet Left Leaflet	Yes	0.01	352	174
Outlet Right Leaflet	Yes	0.01	352	174
Outlet Left Leaflet	Yes	0.01	352	174
Inlet Symmetry	No	0.02	32685	174
Outlet Symmetry	No	0.02	32685	21204
Housing Symmetry	No	0.02	10332	21204
Inlet Wall	No	0.05	1279	828
Outlet Wall	No	0.05	1279	298

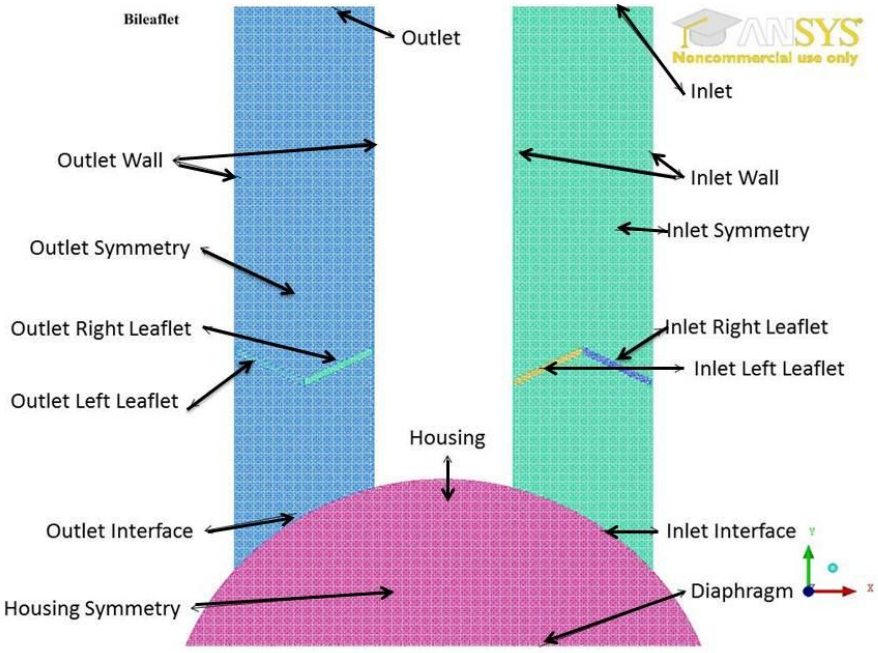

Figure 3.8 Two dimensional surface meshing of bileaflet heart valve along with the fluid chamber

3.2.1.1.2 The MONOLEAFLET HEART VALVE

Table 3.2 summarizes the maximum mesh size, and number of nodes and elements in the monoleaflet heart valve model for each surface. Figure 3.9 shows the meshing of monoleaflet heart valve and the fluid chamber.

Table 3.2 Mesh information of each individual surface for the monoleaflet heart valve

Part Name	Mesh Motion	Maximum Mesh Size	Number of Elements	Number of Nodes
Diaphragm	Yes	0.1	142	78
Housing	No	0.1	82	54
Inlet	No	0.1	156	102
Outlet	No	0.1	48	34
Inlet Interface	No	0.1	41	26
Outlet Interface	No	0.1	38	26
Inlet Valve	Yes	0.01	2304	1330
Outlet Valve	Yes	0.01	2304	1330
Inlet Symmetry	No	0.02	23877	12232
Outlet Symmetry	No	0.02	23867	12225
Housing Symmetry	No	0.02	18744	9636
Inlet Wall	No	0.05	452	828
Outlet Wall	No	0.05	448	268

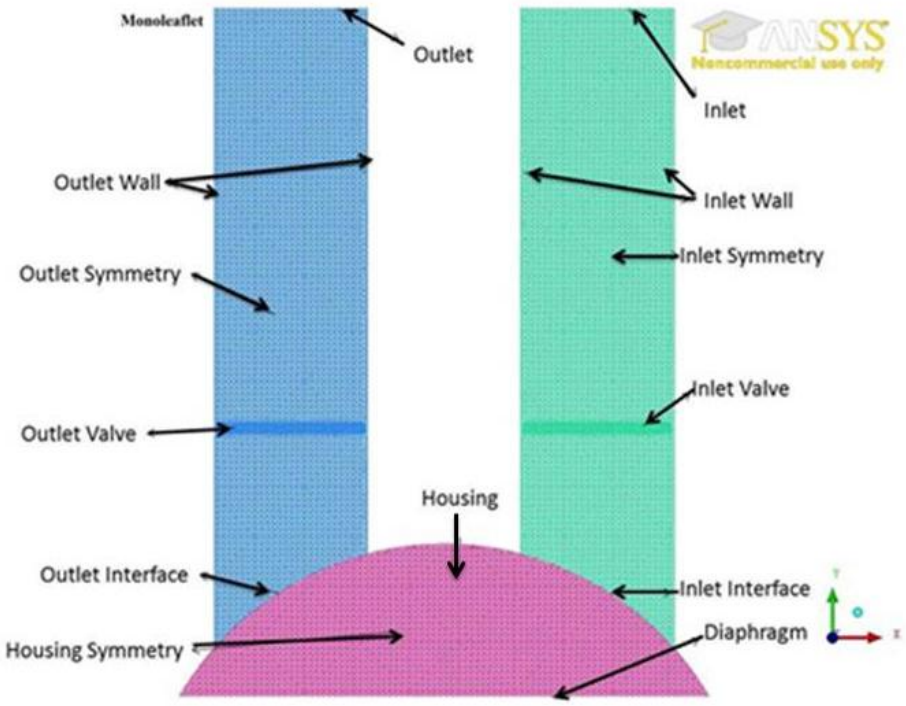

Figure 3.9 Two dimensional surface meshing of monoleaflet heart valve along with the fluid chamber.

3.2.1.2 THREE-DIMENSIONAL MODEL

The 3D models of the monoleaflet and bileaflet valves were meshed with a similar robust mesh method, using tetrahedral/mixed mesh element type in ANSYS ICEM CFD 13.0.1. Due to the computational memory limitation (Intel 3.2 GHz dual processor, 12 Gb RAM), the 3D model geometry was simplified. During systole, since the inlet valve remained closed, the model contained only the flow chamber and the outlet channel with the valve; while during diastole, since the outlet valve remained closed, the model contained only the flow chamber and the inlet channel with the valve. The 3D models were meshed with different mesh density for different volumes, based on the required resolution and region of interest. The areas around the valves and the diaphragm were finely meshed because of their motion. Meshing for the 3D simulation was checked for mesh independency. Tables 3.3 to 3.6 demonstrate the maximum mesh size and number of nodes and elements in each model for each volume. Figures 3.10 and 3.11 show the 3D meshing for the bileaflet and monoleaflet heart valves and the fluid chamber.

Table 3.3 Mesh information of each individual volume for the bileaflet heart valve during systole

Part Name	Mesh Motion	Maximum Mesh Size	Number of Elements	Number of Nodes
Diaphragm	Yes	0.1	3574	1878
Housing	No	0.1	8876	4751
Outlet	No	0.05	4362	2182
Inlet Interface	No	0.02	6925	3570
Outlet Interface	No	0.02	6919	3578
Outlet Right Leaflet	Yes	0.01	27813	13615
Outlet Left Leaflet	Yes	0.01	27813	13593
Outlet Tube	No	0.05	131450	26825

Table 3.4 Mesh information of each individual surface for the bileaflet heart valve during diastole

Part Name	Mesh Motion	Maximum Mesh Size	Number of Elements	Number of Nodes
Diaphragm	Yes	0.1	3574	1878
Housing	No	0.1	8876	4751
Inlet	No	0.05	4362	2182
Inlet Interface	No	0.02	6925	3570
Outlet Interface	No	0.02	6919	3578
Inlet Right Leaflet	Yes	0.01	27813	13615
Inlet Left Leaflet	Yes	0.01	27813	13593
Inlet Tube	No	0.05	131450	26825

Table 3.5 Mesh information of each individual surface for the monoleaflet heart valve during systole

Part Name	Mesh Motion	Maximum Mesh Size	Number of Elements	Number of Nodes
Diaphragm	Yes	0.1	3574	1873
Housing	No	0.1	8876	4738
Outlet	No	0.05	4331	2152
Inlet Interface	No	0.02	6918	3564
Outlet Interface	No	0.02	6899	3562
Outlet Valve	Yes	0.01	455	204
Outlet Tube	No	0.05	222368	45088

Table 3.6 Mesh information of each individual surface for the monoleaflet heart valve during diastole

Part Name	Mesh Motion	Maximum Mesh Size	Number of Elements	Number of Nodes
Diaphragm	Yes	0.1	3574	1873
Housing	No	0.1	8876	4738
Inlet	No	0.05	4331	2152
Inlet Interface	No	0.02	6918	3564
Outlet Interface	No	0.02	6899	3562
Inlet Valve	Yes	0.01	455	204
Inlet Tube	No	0.05	222368	45088

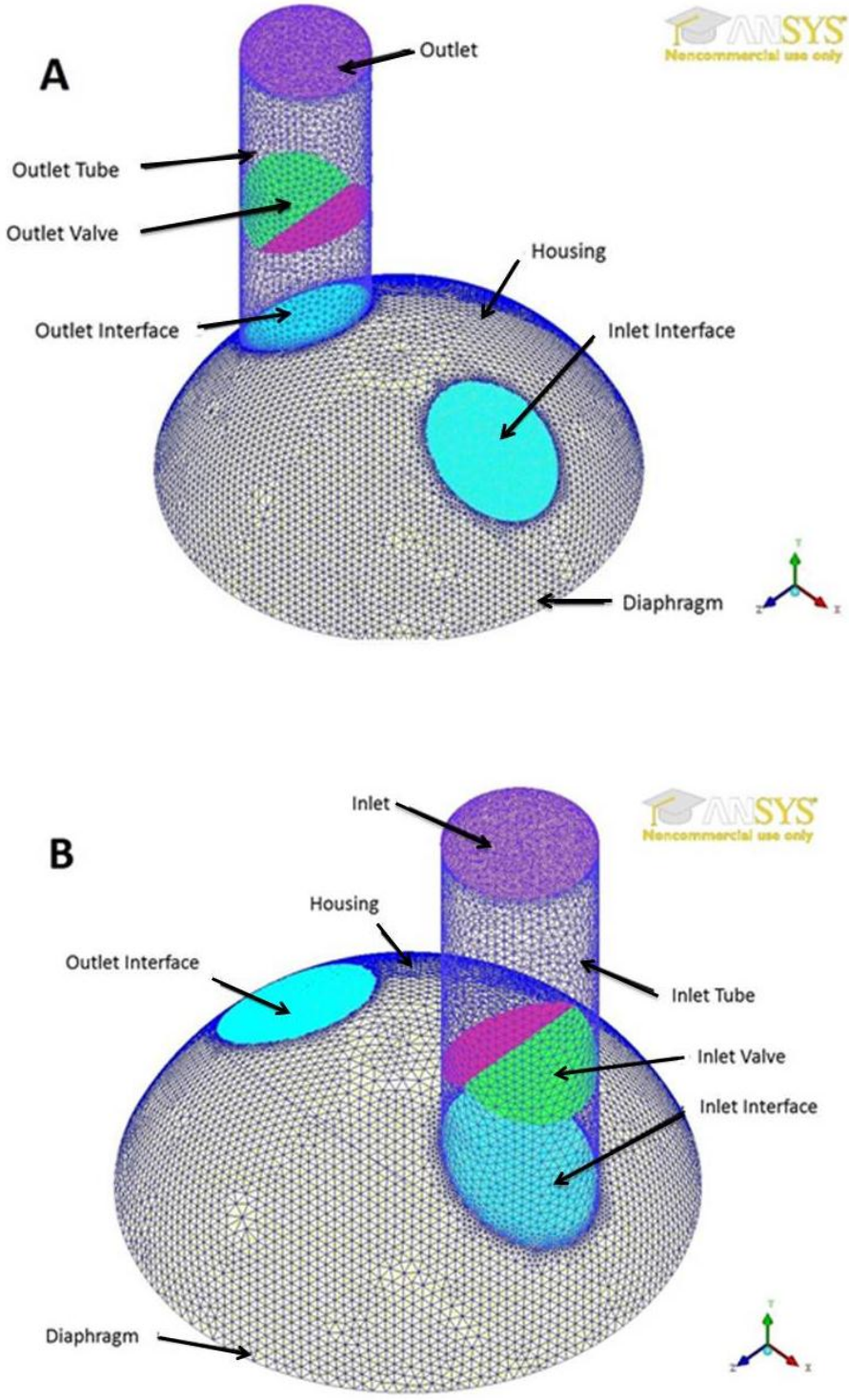

Figure 3.10 Three dimensional volume meshing of bileaflet heart valve along with the fluid chamber at the beginning of systole (A) and diastole (B).

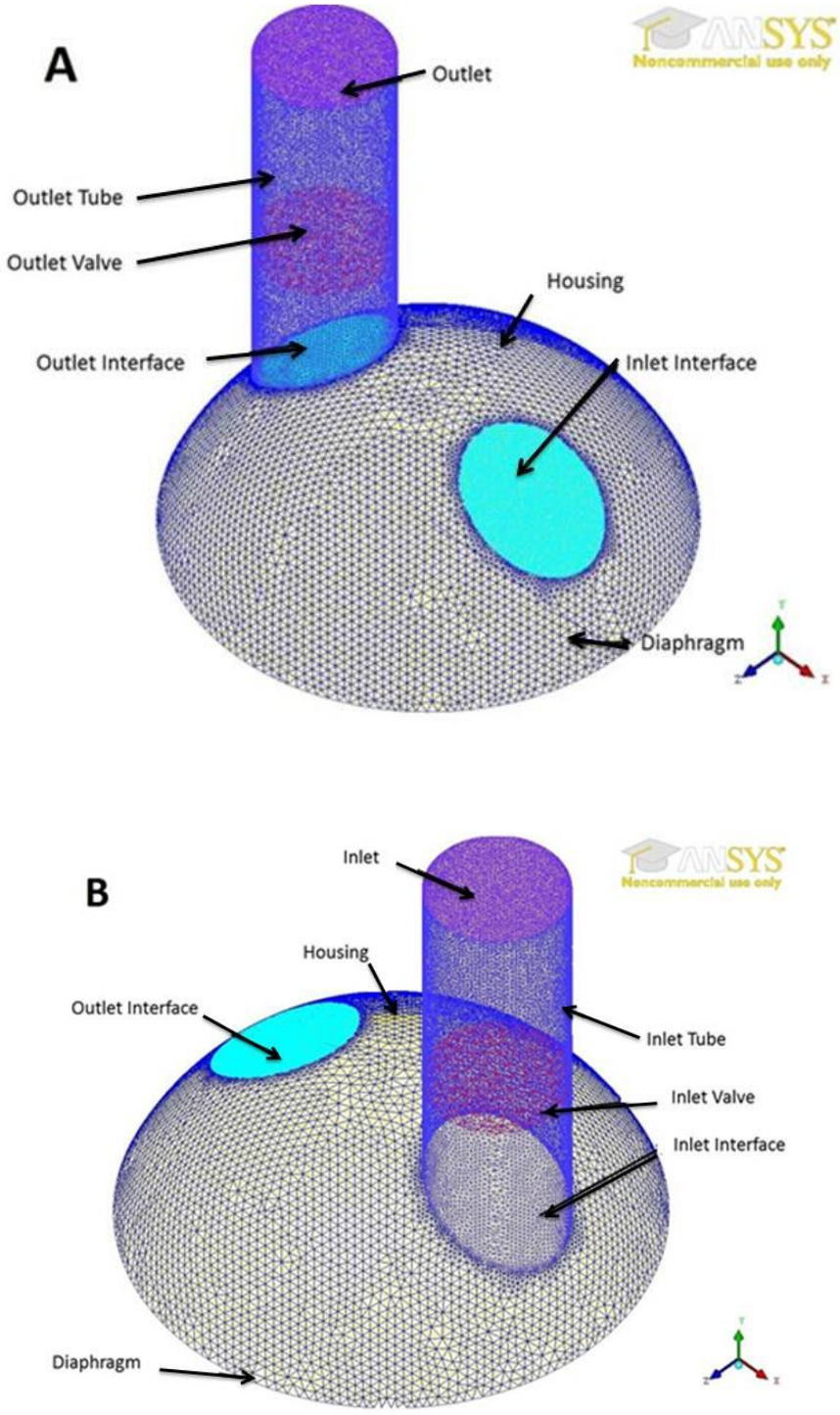

Figure 3.11 Three dimensional volume meshing of the monoleaflet heart valve along with the fluid chamber. Systolic model (A), diastolic model (B).

3.2.2 DIAPHRAGM AND VALVE LEAFLET MOTION

3.2.2.1 DIAPHRAGM MOTION

In the current model the movement of the diaphragm caused the two valves to open and close. The volume change induced by the diaphragm in one cardiac cycle was 80 mL, matching the stroke volume. The equation for the diaphragm motion was developed in 2D and 3D forms using MATLAB R2011a.

Here, we assumed that the diaphragm was in the shape of a spherical cap at each time step during systole and diastole (Figure 3.12). Volume covered by this spherical cap was equal to the amount of water pushed in by the pump, and the amount of blood pushed out of the chamber by the diaphragm.

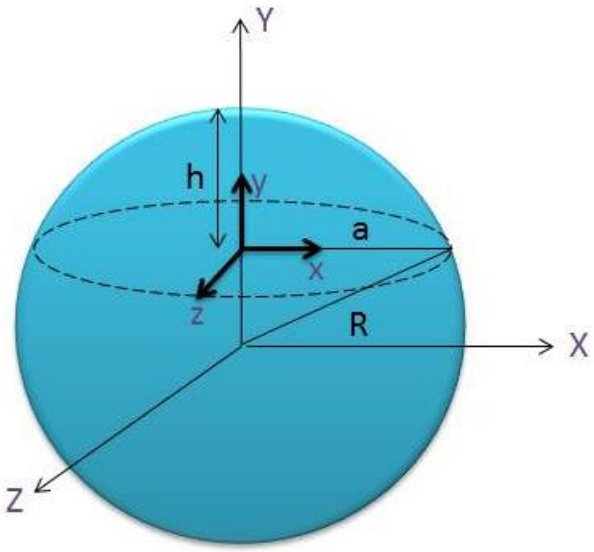

Figure 3.12 The volume occupied by the diaphragm at each time step is considered as the volume of a spherical cap. a is the initial radius of the diaphragm at t=0, h is the height, and R is the radius of the base sphere.

Knowing the stroke volume (SV = 80 mL) and the durations of systole and diastole (0.2454 s for systole and 0.6546 s for diastole), two different scalar coefficients were derived to describe the relationship between the accumulated simulation time and the spherical cap volume. These coefficients could be determined by the average flow rate moving out or into the flow chamber, which were derived by dividing the maximum volume (80 mL) by the duration of systole (0.2454 sec) and diastole (0.6546 sec) respectively. At each time step, the spherical cap volume was calculated by Equations 3.1 and 3.2 during systole and diastole respectively:

$$V = 3.26E\text{-}4 * t \qquad \text{(Equation 3.1)}$$

$$V = 1.22E\text{-}4 * t \qquad \text{(Equation 3.2)}$$

where V was the volume under the spherical cap in m^3 and t was accumulated time in seconds. The volume of a spherical cap can be approximated using Equation 3.3.

$$V_{cap} = \frac{1}{6}\,\pi\, h\,(3a^2 + h^2) \qquad \text{(Equation 3.3)}$$

where a is the initial radius of the diaphragm (at equilibrium), and h is the height of the spherical cap at each time step (Figure 3.12), and h can be solved as:

$$h = \left[\left(\frac{9V^2}{\pi^2} + a^6\right)^{\frac{1}{2}} + \frac{3V}{\pi}\right]^{\frac{1}{3}} - \frac{a^2}{\left[\left(\frac{9V^2}{\pi^2} + a^6\right)^{\frac{1}{2}} + \frac{3V}{\pi}\right]^{\frac{1}{3}}} \qquad \text{(Equation 3.4)}$$

For the base sphere (Figure 3.12),

$$X^2 + Y^2 + Z^2 = R^2 \qquad \text{(Equation 3.5)}$$

where X, Y, and Z are the coordinates of any node located on the surface of the sphere and R is the base sphere radius. A secondary coordinate system (x, y, and z) was created at the center of the diaphragm (Figure 3.12). For nodes on the sphere surface X and Z coordinates were the same

as x and z, but for Y and y coordinates, they follow the relationship descripted in Equation 3.6, as:

$$Y = y + R - h \qquad \text{(Equation 3.6)}$$

Substituting Y in Equation 3.5, we could determine the coordinates of each mesh node on the diaphragm in the (x, y, z) coordinate system:

$$x^2 + (y + R - h)^2 + z^2 = R^2 \qquad \text{(Equation 3.7)}$$

Since $R^2 = a^2 + (R - h)^2$ (from the Pythagorean Theorem), R in the above equation can be replaced by $R = (a^2 + h^2)/2h$; and y was solved as:

$$y = \frac{(a^4 + 2a^2h^2 + h^4 - 4h^2x^2 - 4h^2z^2)^{\frac{1}{2}} - a^2 + h^2}{2h} \qquad \text{(Equation 3.8)}$$

where h was defined by Equation 3.4. By inputting a (initial radius of the diaphragm), h (height of the spherical cap), and x and y coordinates of each node in the above equation, the displacement (y) was calculated in MATLAB for all time steps. The displacement of the diaphragm during systole (0-0.2454s) is shown in Figure 3.13 (plotted in Matlab). During diastole, the diaphragm moved from the location with the maximum displacement to the initial equilibrium position (Figure 3.14, which is opposite from Figure 3.13).

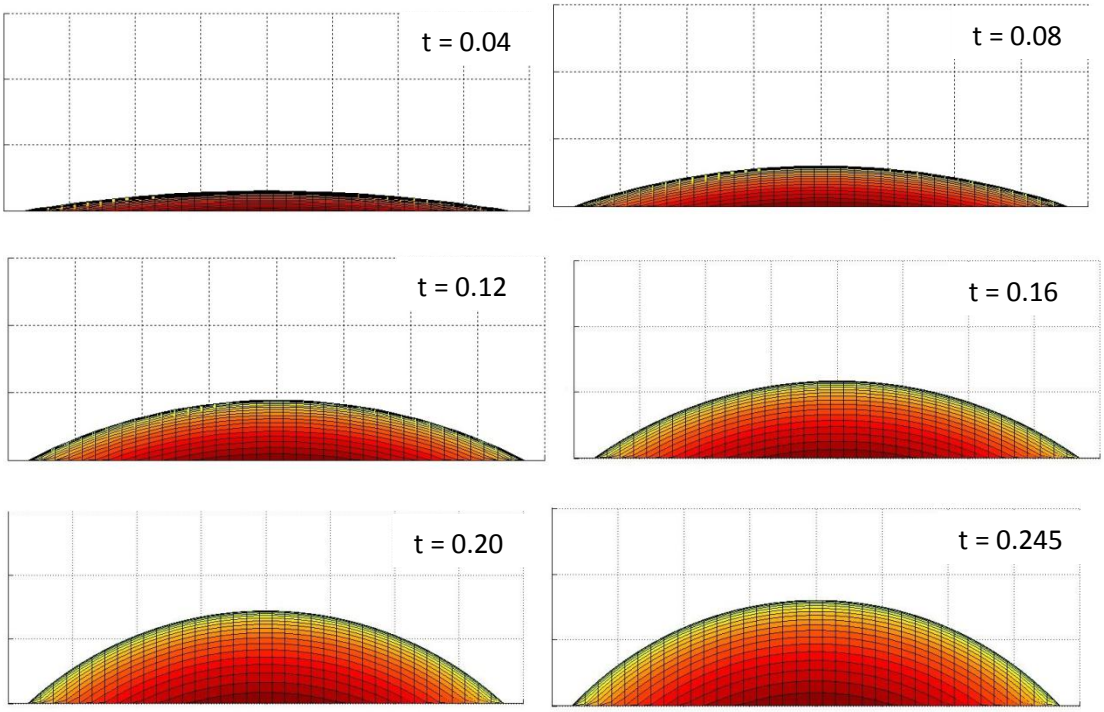

Figure 3.13 Diaphragm displacement calculation during systole using MATLAB software

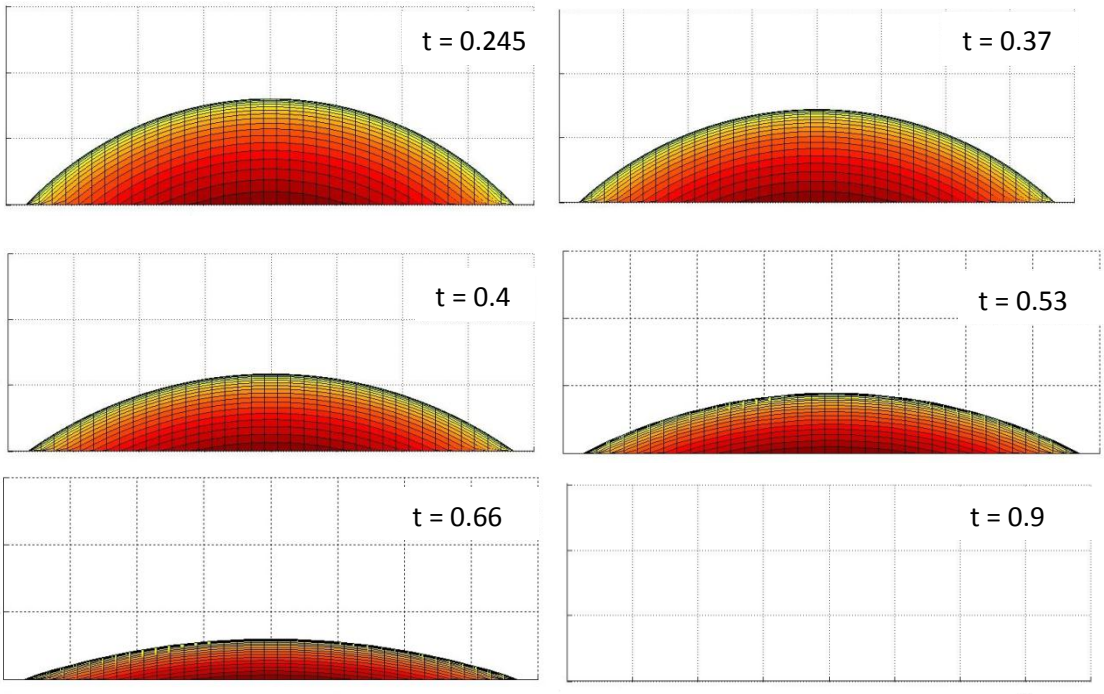

Figure 3.14 Diaphragm displacement calculation during diastole using MATLAB software

3.2.2.1.1 2D DIAPHRAGM MOTION

To simulate the diaphragm motion in the 2D model, z value was set at 0. Therefore, by solving Equation 3.8 when z = 0, the diaphragm motion for the 2D models can be described using Equation 3.9:

$$y = \frac{(a^4 + 2a^2h^2 + h^4 - 4h^2x^2)^{\frac{1}{2}} - a^2 + h^2}{2h} \qquad \text{(Equation 3.9)}$$

The diaphragm motion during systole and diastole in 2D models are shown in Figure 3.15 and Figure 3.16 (taken from ANSYS).

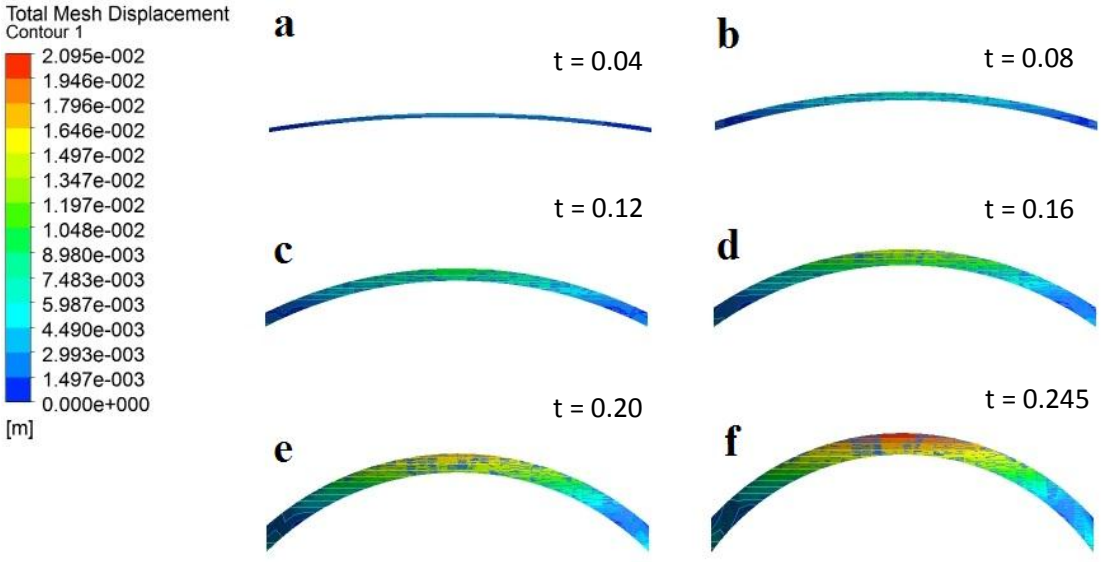

Figure 3.15 (a-f) contours of total mesh displacement during the systole for 2D models

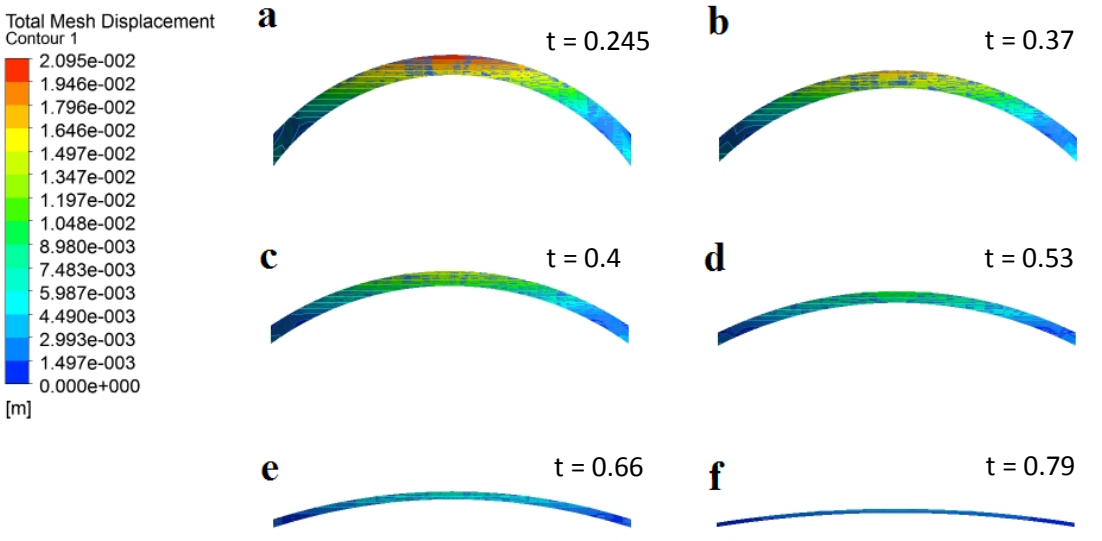

Figure 3.16 (a-f) contours of total mesh displacement during the diastole for 2D models

3.2.2.1.2 3D DIAPHRAGM MOTION

For 3D simulations, the displacement equation (3.8) was directly imported to ANSYS CFX to calculate diaphragm motion. At each time step this equation was solved to calculate the value of diaphragm displacement in y direction. Figures 3.17 and 3.18 show the contours of diaphragm displacement during systole and diastole respectively (taken from ANSYS).

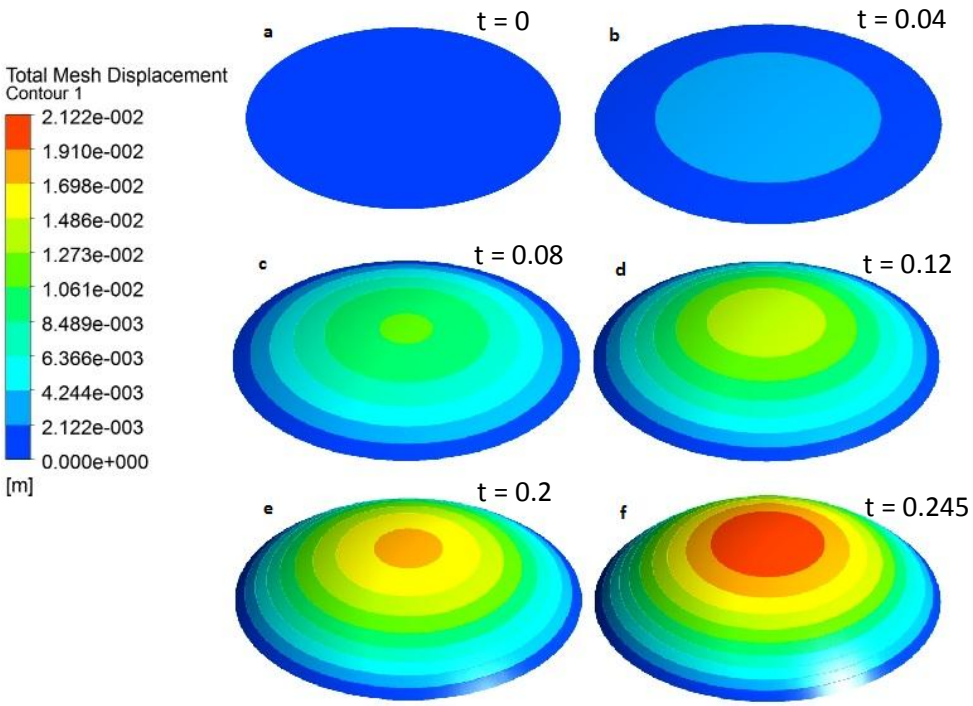

Figure 3.17 (a-f) contours of total mesh displacement during the systole for 3D models

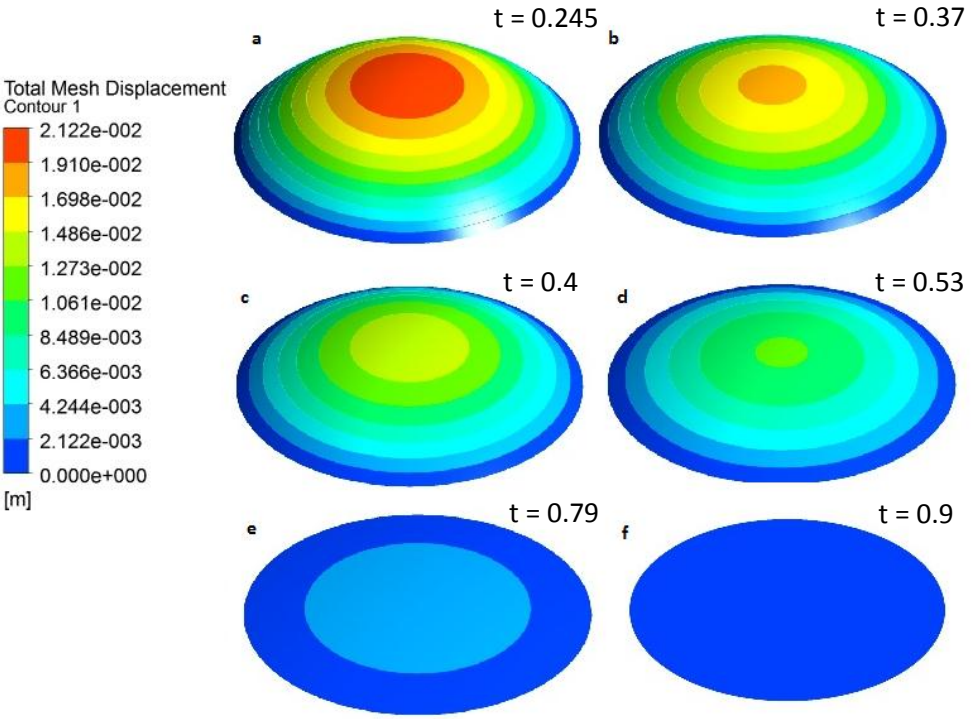

Figure 3.18 (a-f) contours of total mesh displacement during the diastole for 3D models

3.2.2.1.3 DIAPHRAGM MESH DIFFUSION

The motion of all the other nodes in the flow chamber was determined by the displacement diffusion method. Using this method, the displacement of the mesh nodes on the diaphragm was diffused to the mesh nodes of the flow chamber (Figure 3.19 and 3.20). The equation used for this purpose is as the following:

$$\nabla \cdot \left(\Upsilon_{\text{disp}} \nabla \delta \right) = 0 \qquad \text{(Equation 3.10)}$$

where $\boldsymbol{\delta}$ is the relative displacement of the flow chamber mesh and Υ_{disp} is the mesh stiffness. Mesh stiffness was defined as the ability of the mesh nodes to move together without being skewed[63]. To prevent negative mesh volume during the mesh movement, we used the mesh displacement diffusion option with a mesh stiffness value of 1.0 (m^5 s^-1)/volcvol. The variable volcvol (volume of finite volumes) is a predefined variable related to the local mesh element volume. The mesh stiffness was defined as inversely proportional to the mesh element size[63]. Therefore, the regions of smaller elements (regions which were prone to experience mesh folding) had higher stiffness.

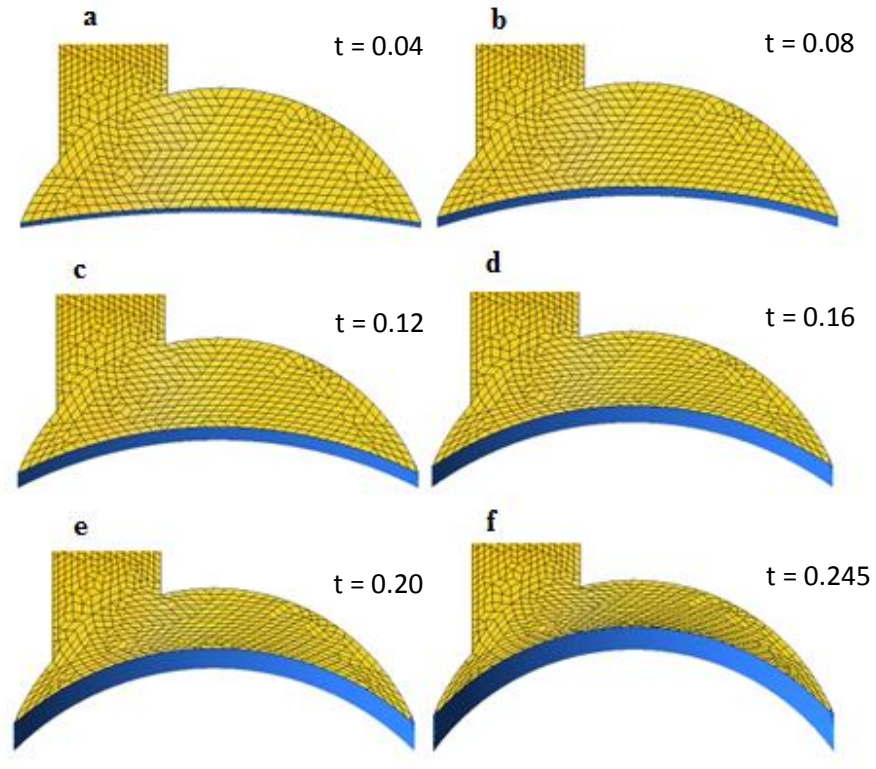

Figure 3.19 (a-f) diffusion of diaphragm mesh displacement to the flow chamber mesh nodes in the 2D model.

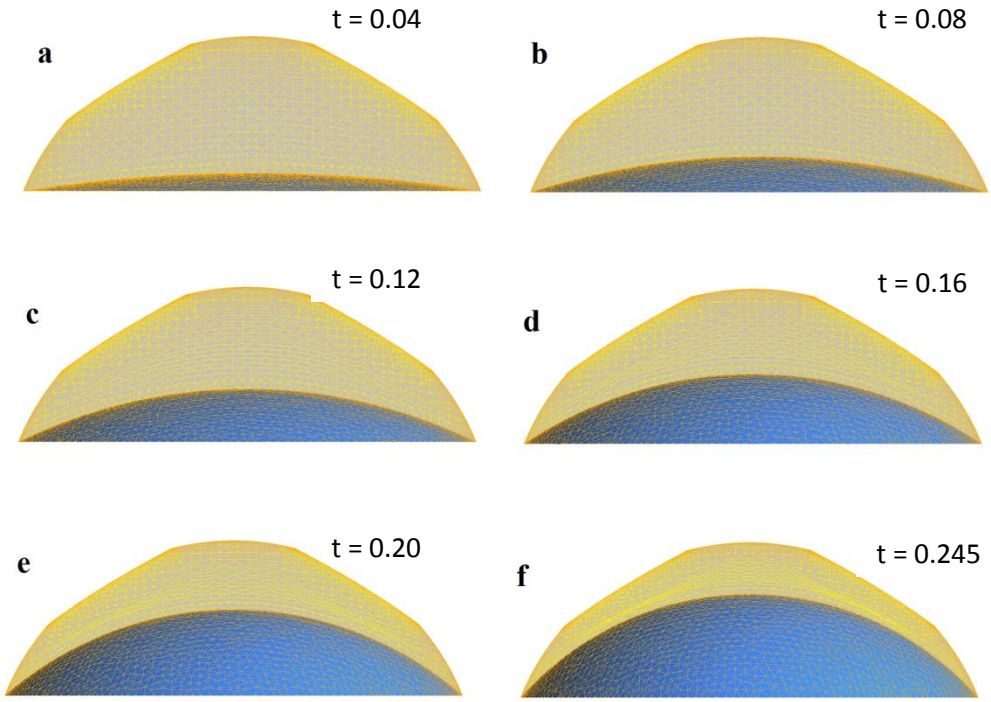

Figure 3.20 (a-f) diffusion of diaphragm mesh displacement to the flow chamber mesh nodes in the 3D model.

3.2.2.2 VALVE LEAFLET MOTION

For valve motion, since the movement of the valve leaflet was very fast (0.016-0.022 sec), we were not able to model it with the mesh displacement method employed to describe the diaphragm motion. In here, a fluid structure interaction method was employed using an ANSYS CFX feature called "six degrees-of-freedom Rigid Body Solver". A rigid body was defined as a solid domain which can move through a fluid domain without any deformation. A rigid body could be modeled in two different ways. The first method was to define the 2D regions of the rigid body as different faces and apply mesh motion criteria to each face. Alternatively, the whole rigid body could be modeled as an immersed solid. Using this method, the motion of the immersed solid was calculated by solving the rigid body motion equations. These motion equations are known as Euler's laws which include the following two laws:

$$\sum \mathrm{F} = \frac{\mathrm{d}}{\mathrm{dt}} (\mathrm{G}) \qquad \text{(Equation 3.11)}$$

$$\sum \mathrm{M_o} = \frac{\mathrm{d}}{\mathrm{dt}} (\mathrm{H_o}) \qquad \text{(Equation 3.12)}$$

where F is the force exerted on the rigid body, G is the translational motion of the rigid body, M_o is the moment force applied on the body around the rigid body center of rotation (O), and H_o is the angular momentum of the rigid body around its center of rotation. The first law describes how the sum of forces applied on the rigid body affects the rigid body translational motion and the second law defines how the rigid body angular momentum is affected by the exerted moment forces and couples.

In this study, the leaflet was defined as an immersed solid. The leaflet motion was determined by solving the interaction force between fluid and the leaflet. The leaflet had one degree of freedom, rotating around the Z-axis in the local coordinate frame (Figure 3.21).

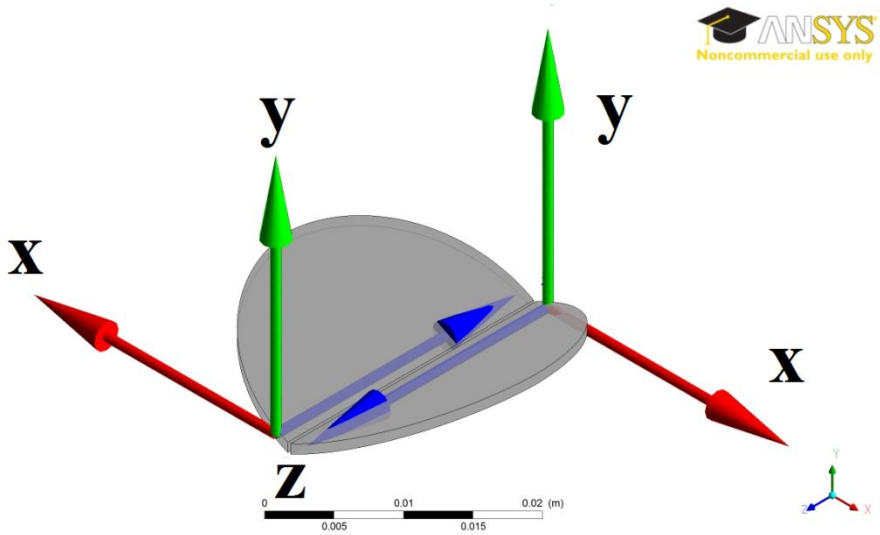

Figure 3.21 The Z-axis of the local coordinate frame was passing throw the rotation axis of each leaflet.

The other parameters that were defined include: leaflet mass, center of gravity, gravity magnitude, moment of inertia, initial velocities and accelerations, and orientation. The center of gravity was calculated by ANSYS CFX-Solver automatically; the initial velocities and accelerations were all set to zero. Other parameters were calculated using the geometrical measurements presented in the geometry section (refer to Table 3.1 through 3.6) and they are listed in Table 3.7 and Table 3.8 for the bileaflet and monoleaflet valves respectively. The same parameters were used in 2D and 3D models. The ANSYS rigid body solver calculated the moments acting on the leaflet, which were induced by the fluid pressure (M_p), frictional shear stress (M_f), and gravitational force (M_g) over the leaflet surface ($M = M_p + M_f + M_g$). The rigid body solver was able to calculate these forces and moments to determine the leaflet angle, velocity, and position.

Starting with the initial local coordinates (XYZ) defined for each leaflet (Figure 3.21), a composition of three intrinsic rotations can be used to reach and determine the new orientation of the valve leaflet frame during the rigid body rotation. The values for these rotations are known as Euler Angles and they are shown by α, β, and γ[63]. The position of the leaflet was determined using these angles as follows: First, Euler angle α rotates the XYZ-system about the Z-axis and

modifies the initial orientation; Euler angle β then further modifies the orientation by a rotation about the (modified) Y-axis; finally, Euler Angle γ further modifies the orientation by a rotation about the (twice modified) X-axis (Figure 3.22).

Table 3.7 Physical properties of the bileaflet valve leaflet (one leaflet)

Parameter	Value
Moment of Inertia (I)	8.1 E-9 kg m^2
Mass	4.38786E-4 Kg
Volume (V)	2.19393E-7 m^3
Density (ρ)	2000 kg/m^3

Table 3.8 Physical properties of monoleaflet valve leaflet

Parameter	Value
Moment of Inertia (I)	1.21E-7 kg m^2
Mass	1.682E-3 kg
Volume (V)	6.7824E-7 m^3
Density (ρ)	2000 kg/m^3

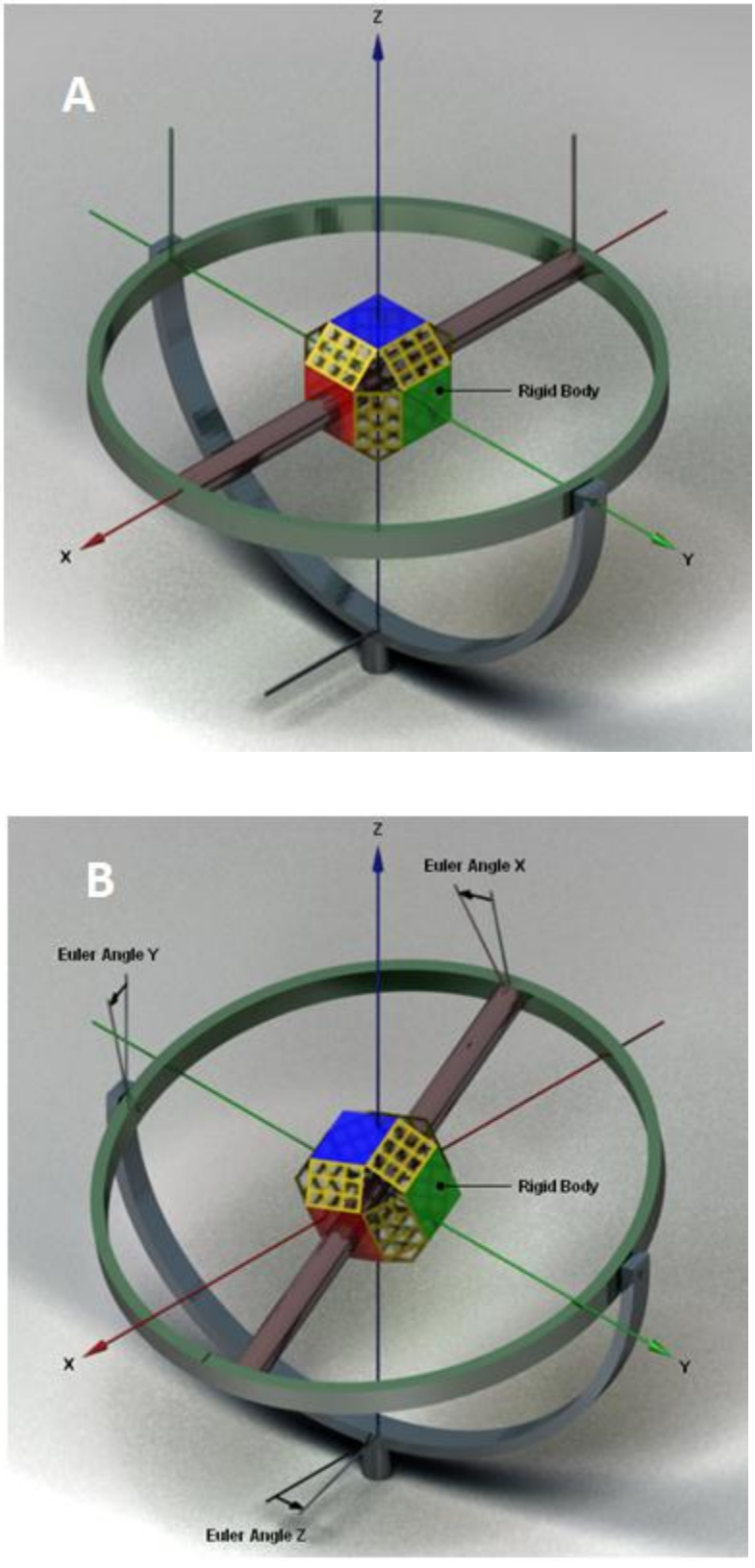

Figure 3.22 Rectangular coordinate (xyz) (A) and Euler angles (X,Y and Z) after reorientation (B)[63].

One major limitation of the rigid body solver is that it cannot model a collision. Therefore, the rotating motion of the valve leaflet would not stop even when the leaflet touched the vessel wall (i.e., at its fully open position). To solve this problem, we defined an expression in ANSYS CFX PRE to monitor the leaflet angle; when the leaflet reached a specified angle (e.g., 85^{o} for the bileaflet valve) the motion would be stopped. This expression was defined by the following CFX command: "rbstate(Euler Angle X)@RigidBody". As soon as the value returned by this expression exceeded a specified value, (e.g., 85^{o} for the maximum valve opening for the bileaflet valve) the rigid body solver was turned off and the leaflet was kept stationary.

Another problem associated with defining valves as immersed solids was that, due to the low momentum of the leaflet, the leaflet could be mildly permeable to the flow. This generally means that the motion of the fluid nodes which lie inside the immersed solid might not match the immersed solid mesh motion. ANSYS CFX treats an immersed solid as a general momentum source. A momentum source was defined as a momentum value per unit volume in a specific direction. In order to make the fluid (within the immersed solid) velocity match the immersed solid velocity, the solver applied the same momentum source to the fluid nodes that lie inside the immersed solid, by defining a momentum source scalar coefficient (this coefficient can control how close the immersed solid velocity matches the fluid velocity). By applying a scaling factor to the momentum sources scalar coefficient, we were able to accurately match the velocity of the fluid within the immersed solid to that of the immersed solid. In the 3D model, the momentum source coefficient was increased by 30% without causing any problem. However, for the 2D model, any slight increase in the momentum source caused serious robustness problems that resulted in diverging solutions. Therefore, no scaling factor was defined in the 2D model, which may have slightly reduced the accuracy of the leaflet motion calculation in 2D simulations compared to the 3D models.

3.2.3 COMPUTATIONAL FLUID DYNAMICS

3.2.3.1 BASIC THEORY

ANSYS CFX was used to solve the unsteady Navier-Stokes equations in their conservation form (i.e. conservation of mass, conservation of momentum, and conservation of energy). The instantaneous mass, momentum, energy conservation equations are listed below[63].

The continuity equation:

$$\frac{\partial \rho}{\partial t} + \nabla \cdot (\rho U) = 0 \qquad \text{(Equation 3.13)}$$

Conservation of momentum equation:

$$\frac{\partial (\rho U)}{\partial t} + \nabla \cdot (\rho U \otimes U) = -\nabla p + \nabla \cdot \tau + S_M \qquad \text{(Equation 3.14)}$$

where τ is defined by the following equation:

$$\tau = \mu \left(\nabla U + (\nabla U)^T - \frac{2}{3} \delta \nabla \cdot U \right) \qquad \text{(Equation 3.15)}$$

The total energy equation:

$$\frac{\partial (\rho h_{tot})}{\partial t} - \frac{\partial p}{\partial t} + \nabla \cdot (\rho U h_{tot}) = \nabla \cdot (\lambda \nabla T) + \nabla \cdot (U \cdot \tau) + U \cdot S_M + S_E \qquad \text{(Equation 3.16)}$$

where $h_{tot} = h + \frac{1}{2}U^2$, $\nabla \cdot (U \cdot \tau)$ represents viscous stress work, and $U \cdot S_M$ represents the work due to external momentum source. In these equations ρ is fluid density (density of water in this case which is 997 kg/m^3), μ is fluid viscosity (1 cP in this case), p is pressure, T is the temperature, $\lambda = -\frac{2}{3}\mu$, S_E is the external source of energy, and U is the velocity.

The continuity and momentum equations were used in the numerical model for the calculation of the fluid motion. For the interaction between the fluid domain and the solid domain, ANSYS used the Euler method for the fluid domain and the Lagrange method for the structural domain, and the Euler-Lagrange method for fluid-structure interaction (FSI) for the interaction between the two. The Lagrange method used a flexible mesh which could deform due to the forces applied to it from the neighboring elements. This enabled the solver to model the motion of the structure using a neighboring fluid element. On the other hand, the Euler method used a fixed mesh and it was suitable for the fluids due to their relatively large movement. The Euler-Lagrange method could be used to simulate a variety of fluid dynamics problems. It used both flexible mesh vertices as in the Lagrange method and fixed mesh vertices as in the Euler method. This method also employed mesh vertices that would move in any prescribed manner[64].

3.2.3.2 BOUNDARY CONDITIONS

The boundary conditions were defined as the following:

- Opening: The flow inlet and outlet surfaces were defined as opening boundaries. The opening boundary condition was defined using the mass and momentum option. The relative pressure was set at 12665.8 Pa and 10665.8 Pa for the outlet and inlet respectively (Fig 3.23).
- Wall: The diaphragm, boundary of the flow chamber, valve leaflet and the outlet/inlet tubes were defined as wall.
- Immersed Solid: The two valves were defined as immersed solid domains and their motion was defined using the rigid body solver.
- Symmetry: In order to import a 2D mesh in ANSYS CFX PRE, the mesh needs to have a thickness. This left the 2D model with two separate surfaces on the front and back sides

of the model. These faces were then defined as symmetry boundaries in order for the ANSYS CFX SOLVER to solve the 2D models properly.

Boundary conditions were defined the same for the bileaflet valve models and the monoleaflet valve models.

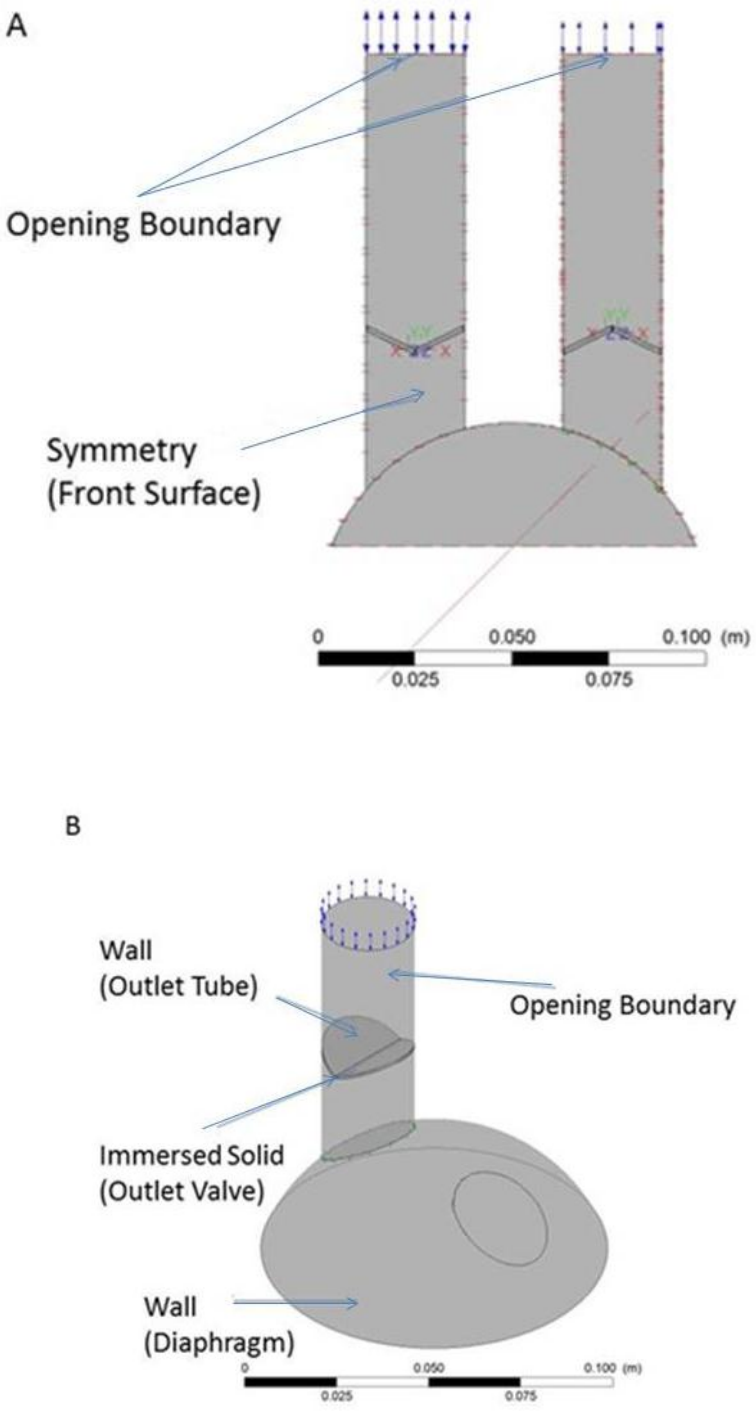

Figure 3.23 Boundary conditions for the 2D (a) and 3D (b) models

3.2.4 FLOW ANALYSIS

The geometry of the flow chamber with valves was first constructed and then meshed using ANSYS ICEM CFD 13.0. The meshed geometries were then imported to ANSYS CFX-Pre 13.0 for boundary setup and surface definition. The models were solved using ANSYS CFX-Solver 13.0 and the results were exported to ANSYS CFD-Post 13.0 for post processing.

3.2.4.1 ASSUMPTIONS

- Fluid Medium: water was used from the ANSYS CFX material database as our fluid medium.
- Flow Chamber Initial Relative Pressure: The initial relative pressure inside the flow chamber was set at 5 Pa, to prevent overflow complications in the model.
- Leaflet Initial Velocity and Acceleration: the leaflet initial velocity and acceleration were set at zero.
- Leaflet Degrees of Freedom: it was assumed that each leaflet had only one degree of freedom – rotating around the rotational axis (Z-axis) and all other degrees were fixed by the hinges.
- No Slip Boundary Condition: for all the wall boundaries in this simulation, the no-slip boundary condition was applied.
- The flow was assumed to be laminar at the beginning of each simulation. If during the simulation CFX SOLVER found any signs of turbulent flow, the simulation would restart using the shear stress transport method. This method can reduce the over flow possibility during the simulation. For all the 2D models the turbulent method (shear stress transport method) was activated. Results from the

2D models revealed that there was no significant increase in turbulent kinetic energy which revealed that the flow was prominently laminar. The preliminary 3D analysis also revealed that the flow was laminar. Therefore, 3D models were simulated utilizing the laminar method.

3.2.4.2 ANALYSIS TYPE

The analysis was run as a transient model with a total time of 0.2454s for systole and 0.6546s for diastole. For the 2D mode, the time step was 0.002 sec, and that for the 3D mode was 0.0005 sec to aid the convergence of the simulation.

3.2.4.3 SOLVER CONTROL

The maximum number of iterations per time step was set to 10 and the minimum number of iterations to 2. Thus, the solver would at least complete 2 but no more than 10 iterations during each time step. The CFX solver was set to update the rigid body solver every iteration. In order to aid the convergence of our models, the solver at each time step was initialized using the values from the previous time step. RMS (root mean square) residual type and a residual target of 1E-4 were used for the governing equation residuals (i.e., momentum, continuity, energy, and turbulent).

3.3 DATA ANALYSIS

Results from this study included the velocity profile, pressure distribution, turbulence kinetic energy (TKE) distribution, valve effective orifice area, and the valve opening and closing time in systole and diastole for bileaflet and monoleaflet valves.

The intensity of turbulent flow was measured by assessing the TKE values throughout the fluid domain, which demonstrated the degree of turbulence. The TKE per unit mass equation is given in Equation 3.17.

$$\mathrm{TKE} = \mathrm{e} = \frac{1}{2}\left(\mathrm{u}'^2 + \mathrm{v}'^2 + \mathrm{w}'^2\right) \qquad \text{(Equation 3.17)}$$

TKE is directly related to the velocity fluctuations and can be used as a turbulent flow indicator (i.e. TKE increases when the boundary layer becomes more turbulent; and it decreases as the boundary layer becomes less turbulent).

For the 3D simulation, values for effective orifice area (EOA) were calculated. EOA was a measure of how efficient a valve used its internal orifice area. The higher the EOA the more efficient the valve would be, and it would be less likely for the valve leaflet to obstruct blood flow through the valve. EOA was calculated using the following equation[65]:

$$\mathrm{EOA} = \frac{\mathrm{Q_{rms}}}{51.6\sqrt{\Delta \mathrm{P}}} \qquad \text{(Equation 3.18)}$$

where Q_{rms} is the root-mean-square forward flow rate in cm^3/s and ΔP is the forward flow pressure drop in mm Hg. In order to calculate ΔP, two planes in a distance of 0.02 m were placed before and after the valve. ΔP was then defined as the difference between the average pressures on these planes.

CHAPTER IV

RESULTS

4.1 2D MODEL

4.1.1 THE BILEAFLET VALVE

4.1.1.1 THE BILEAFLET OUTLET VALVE OPENING

Flow conditions in the flow chamber with the bileaflet heart valve during systole were calculated with the valve opening and closing angles being at 85^{o} and 25^{o} respectively. Table 4.1 contains the maximum axial velocity, as well as mean and maximum transvalvular pressure across the outlet valve during systole. Transvalvular pressure was defined as the difference between the average pressure on two planes 0.02 m apart, before and after the valve. Figure 4.1 shows the velocity stream line during systole. Figure 4.2 shows velocity vectors in the vicinity of the valve. Figure 4.3 depicts pressure distribution through systole. It took 0.16 sec for the valve to reach its fully opened position. When the valve was open, flow separated around the valve leaflet, rushing into three orifices. A recirculation zone developed approximately 10 mm in the outlet channel before the valve (t=0.16 sec), due to the velocity gradient. Most of the flow passed through the left lateral orifice with a skewed flow profile (Figure 4.1). The maximum velocity

was 0.3099 m/sec, occurring at the end of systole (t = 0.2454 s, Figure 4.4). The mean transvalvular pressure was 91.60 Pa (Figure 4.5), which is less than the *in vivo* mean pressure gradient across St. Jude Medical bileaflet valves in the aortic position (Δp mean = 586.61 Pa) reported by Laske et al.[66]. The maximum transvalvular pressure was 3500 Pa (Figure 4.5), which occurred right before valve opening (t = 0.001 s). Laske et al[66]. reported that the maximal pressure gradient at the moment of valve opening was 2199.81 Pa. No significant increase in turbulent kinetic energy (TKE) was observed (the average TKE = 8.12e-6 s^{-1}, maximum TKE = 4.53e-3 s^{-1} and minimum TKE = 3.066e-9 s^{-1}), indicating that the flow was prominently laminar.

Table 4.1 The bileaflet outlet valve opening behavior.

Parameter	Value
Maximum Axial Velocity	0.3099 m/s
Maximum Pressure Drop Across the Valve	3500 Pa
Average Pressure Drop Across the Valve	91.60 Pa
Valve Opening Time	0.16 s

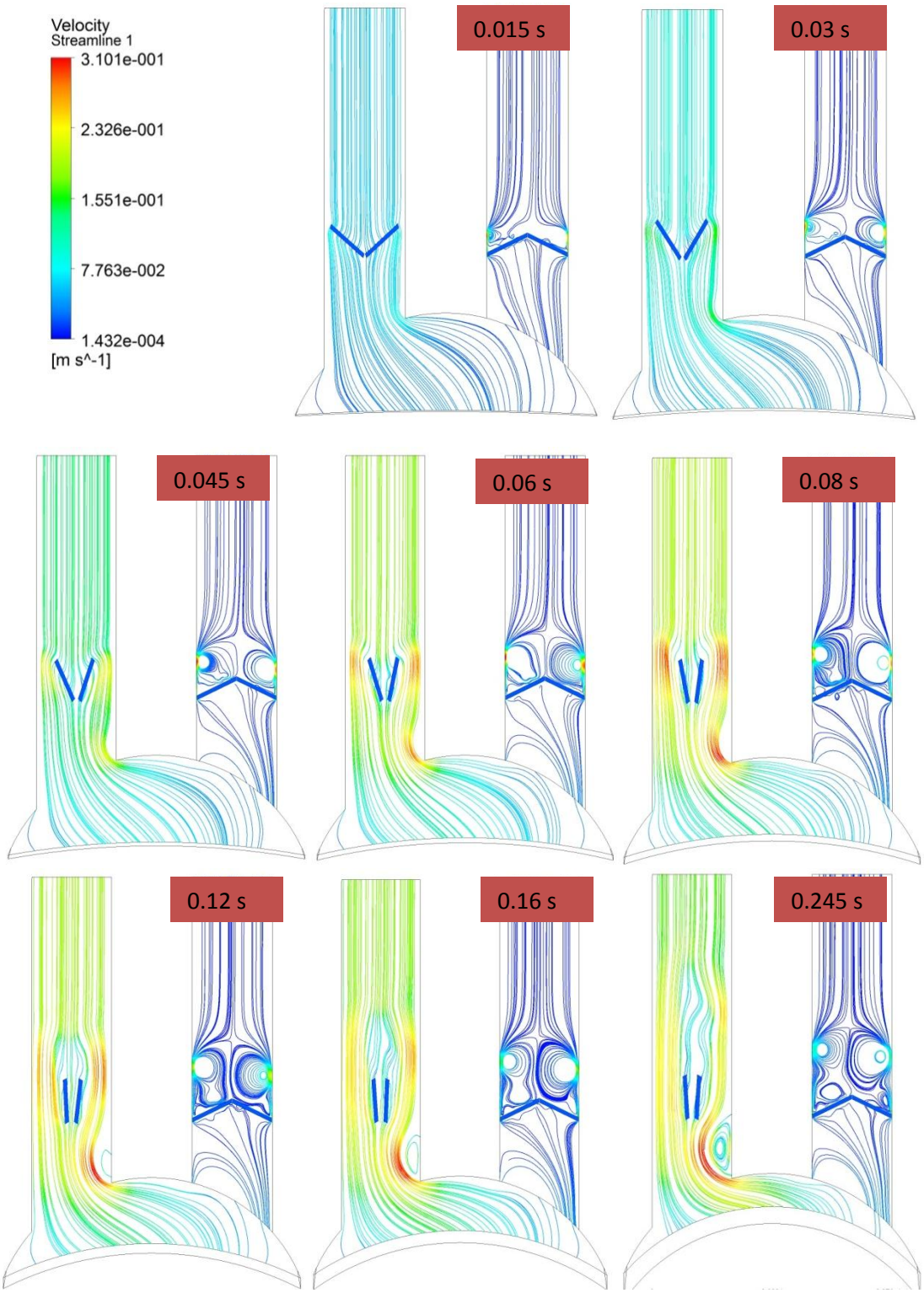

Figure 4.1 Velocity streamline during systole when the bileaflet valve opens.

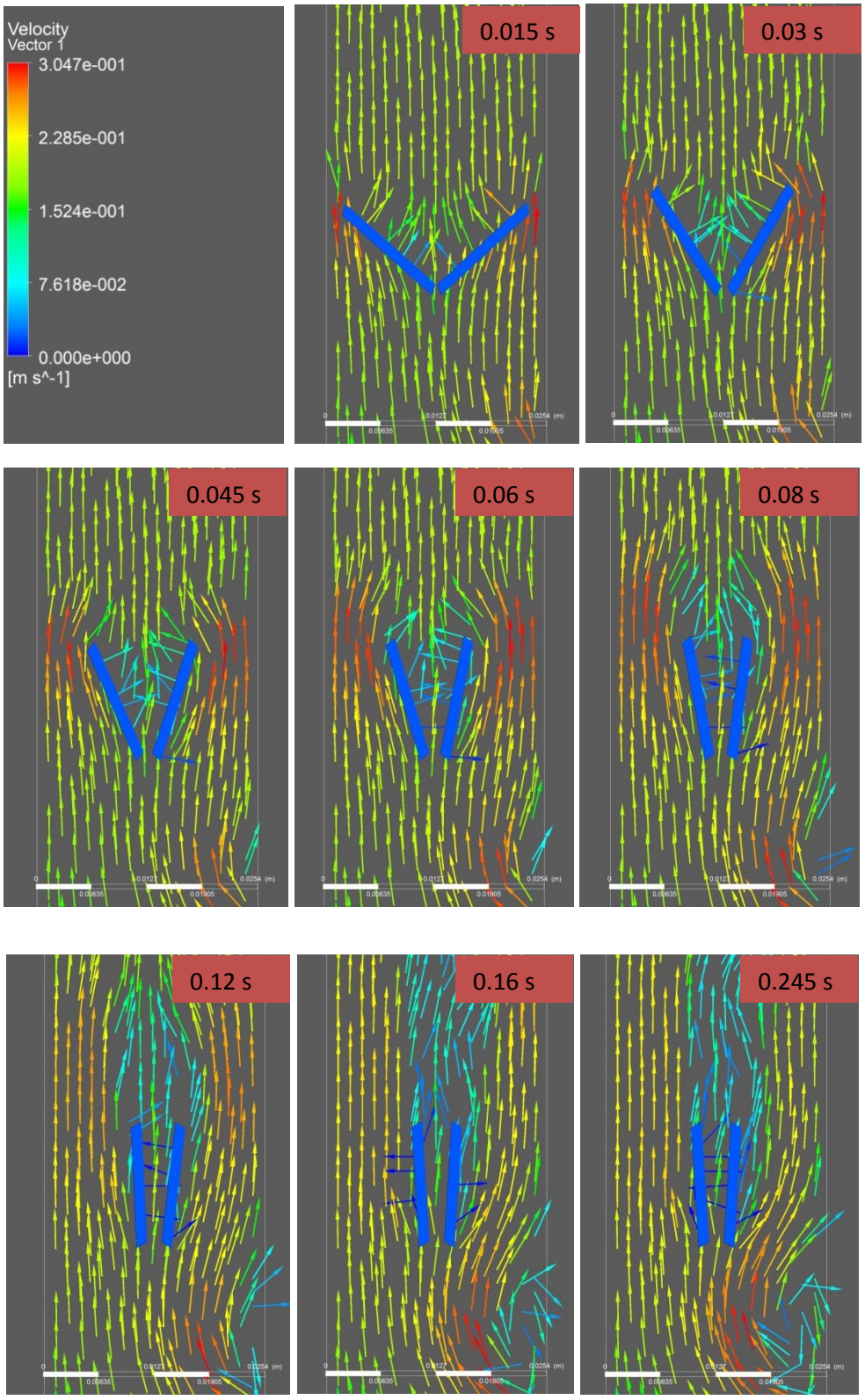

Figure 4.2 Velocity vectors in the bileaflet valve region during systole.

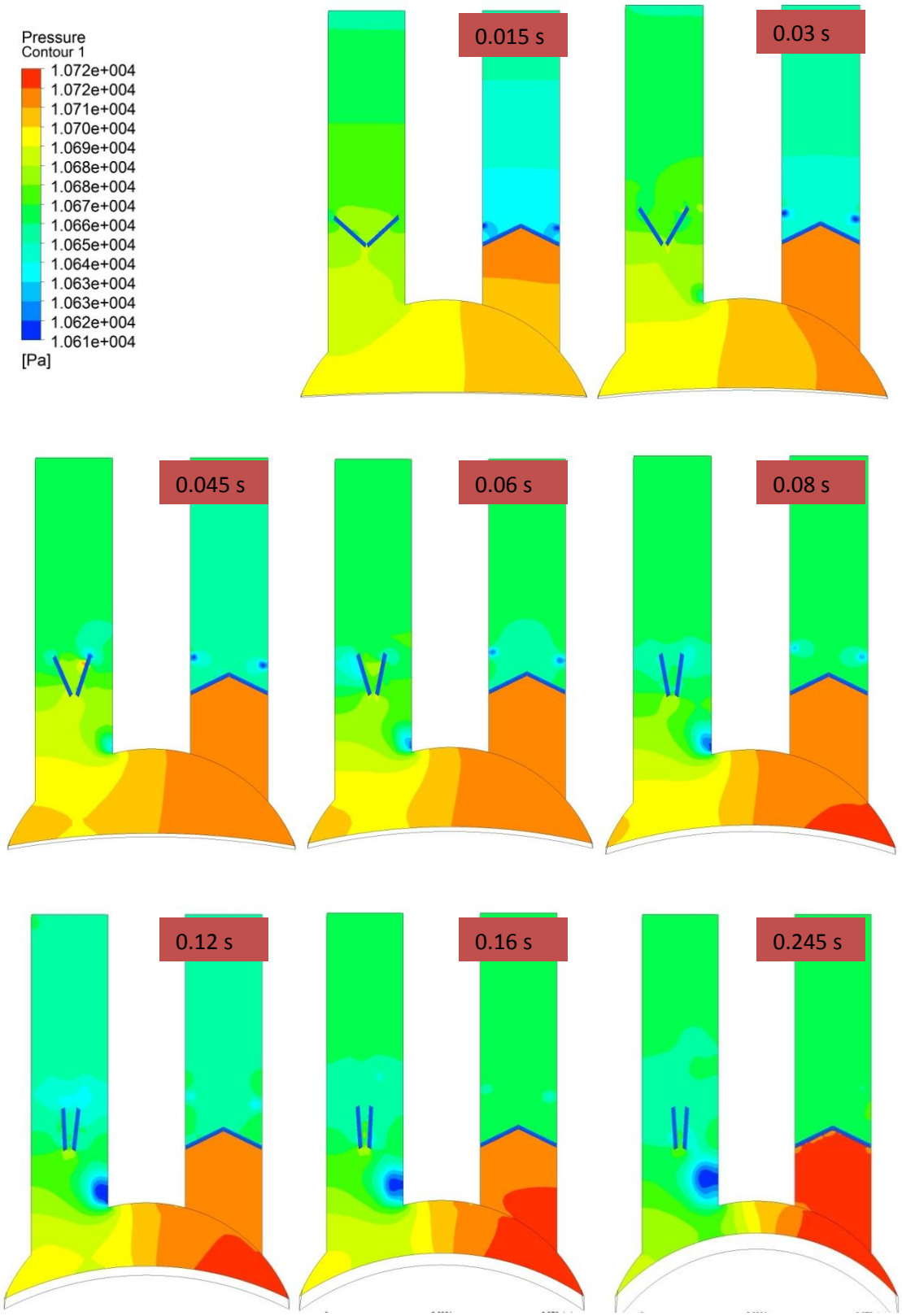

Figure 4.3 Pressure distribution during systole when the bileaflet outlet valve opens.

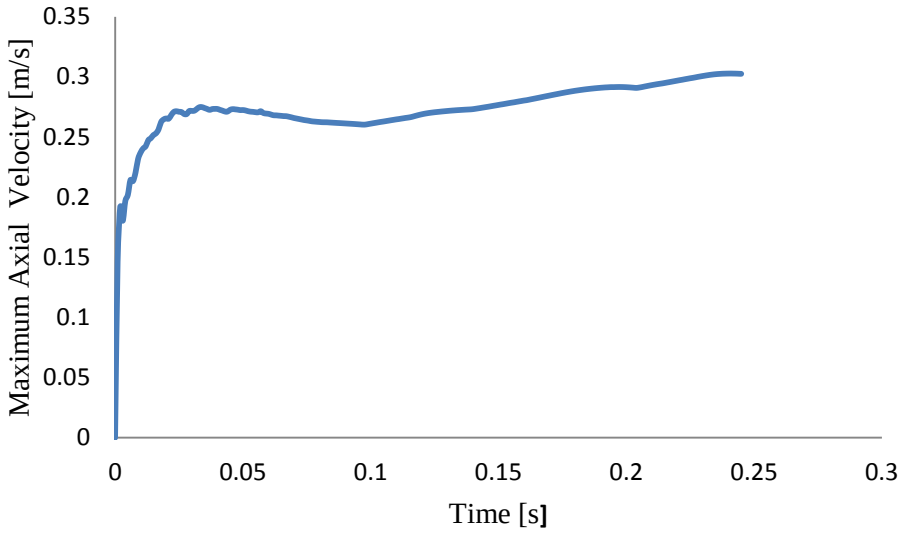

Figure 4.4 Maximum axial velocity versus time for the bileaflet outlet valve opening measured on XY plane in the outlet tube.

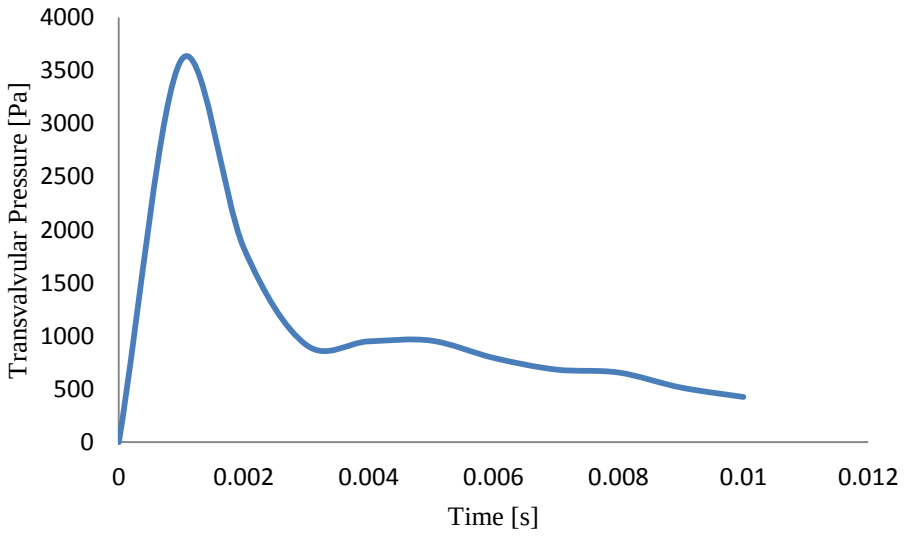

Figure 4.5 Transvalvular pressure versus time for the bileaflet outlet valve opening measured as the difference between average pressures on two planes 0.02 m apart before and after the valve.

4.1.1.2 THE BILEAFLET OUTLET VALVE CLOSING

Table 4.2 lists the maximum backflow velocity and pressure conditions during the outlet valve closing (from the 85^{o} opened position to the 25^{o} closed position). In this table, transvalvular pressure was defined as the difference between average pressure on two planes 0.02 m apart before and after the valve. Figure 4.6 depicts velocity distribution through the valve closing phase. Figure 4.7 shows velocity vectors in the vicinity of the valve and Figure 4.8 demonstrates pressure distribution. It took 0.042 sec for the valve to reach the fully closed position (25°). The maximum backflow velocity was 0.745 m/sec before the valve closure (t = 0.2834 s, Figure 4.9). Two recirculation zones developed at the tip of each leaflet as they were moving towards the outlet wall. Low pressure regions developed around these recirculation zones as the valve closed. The mean transvalvular pressure was 3034.97 Pa. The maximum transvalvular pressure was 15500 Pa and it occurred at t = 0.25 s (Figure 4.10). No big change in the turbulent kinetic energy was observed (the average TKE = 1.152e-11 s^{-1}, maximum TKE = 9.289e-1 s^{-1} and minimum TKE = 3.093e-13 s^{-1}), indicating that the flow was prominently laminar.

Table 4.2 Flow parameters related to the bileaflet outlet valve closing, when the opening and closing angles were 85^{o} and 25^{o} respectively.

Parameter	Value
Maximum Backflow Velocity	-0.745 m/s
Maximum Pressure Drop Across the Valve	15500 Pa
Average Pressure Drop Across the Valve	3034.97 Pa
Valve Closing Time	0.042 s

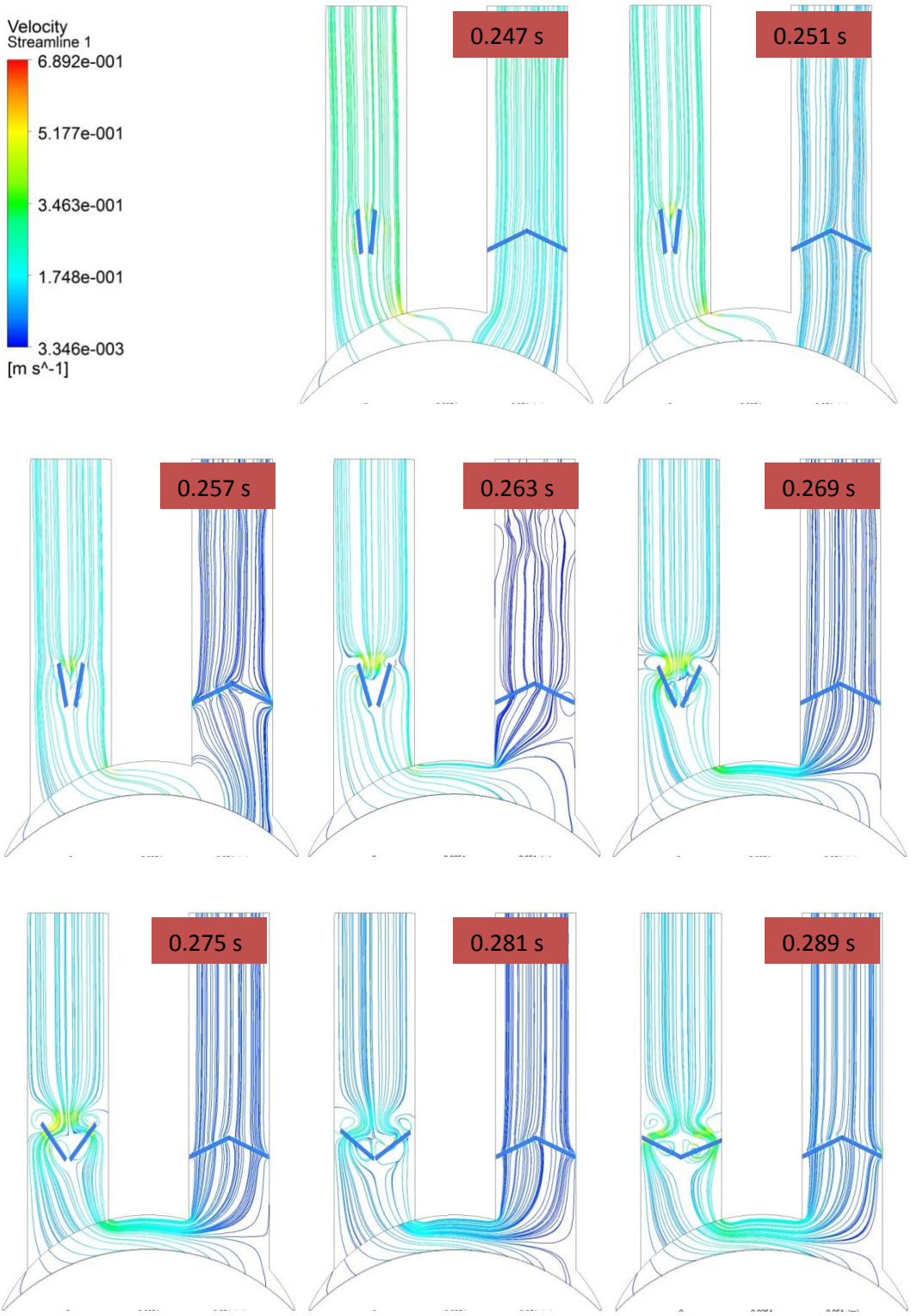

Figure 4.6 Velocity streamline during diastole when the bileaflet outlet valve closes.

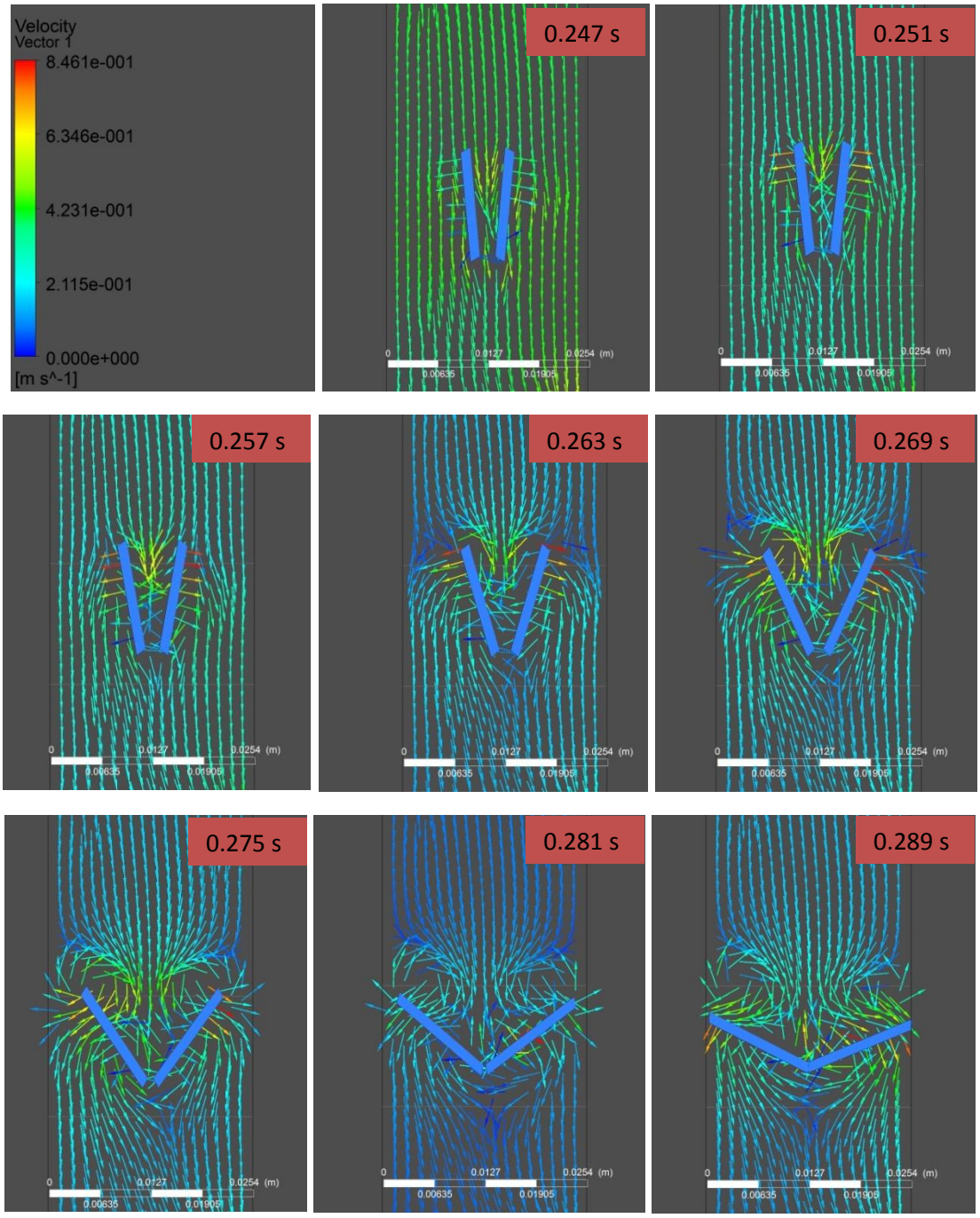

Figure 4.7 Velocity vectors around the bileaflet outlet valve region at the end of systole.

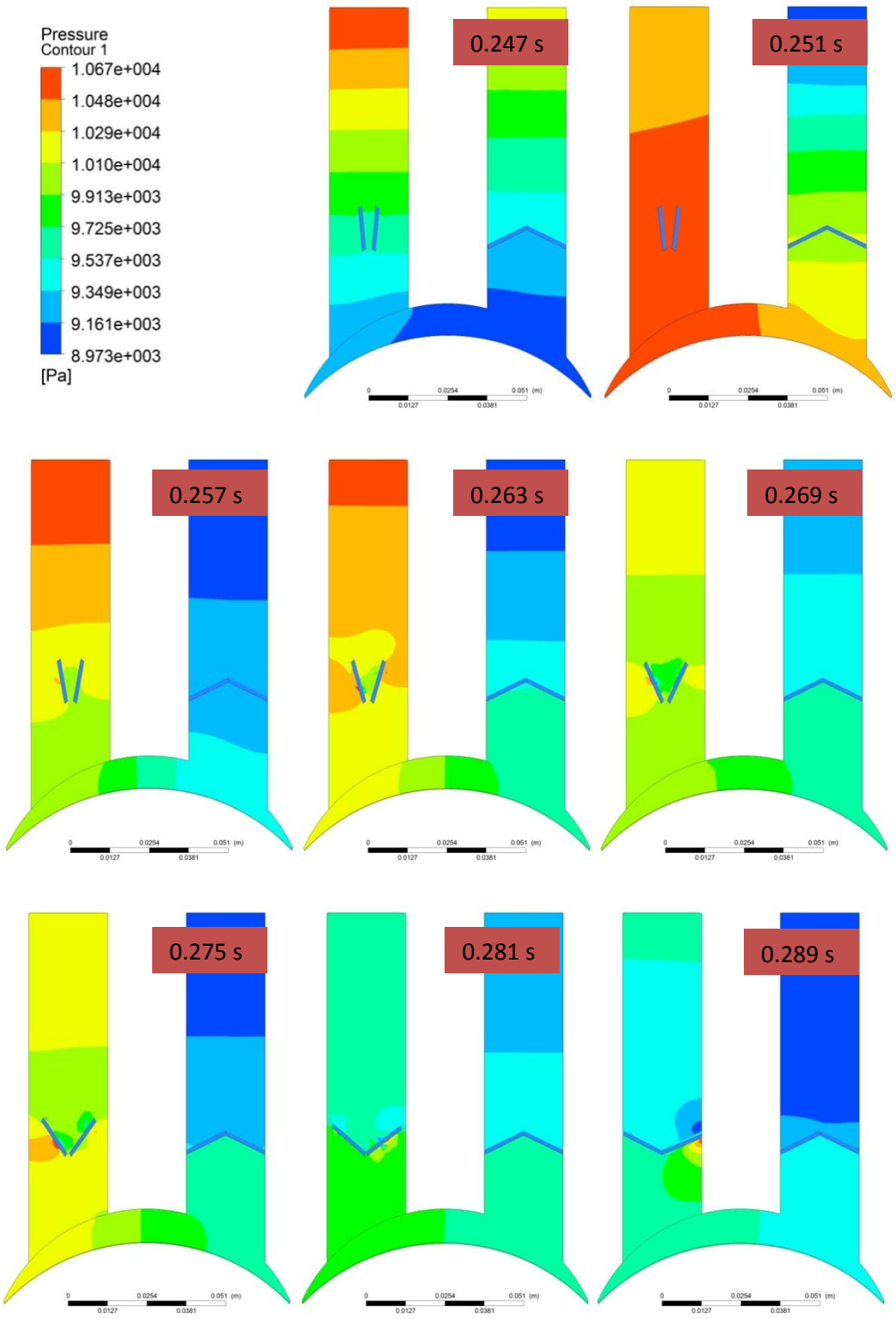

Figure 4.8 Pressure distribution during diastole when the bileaflet outlet valve closes

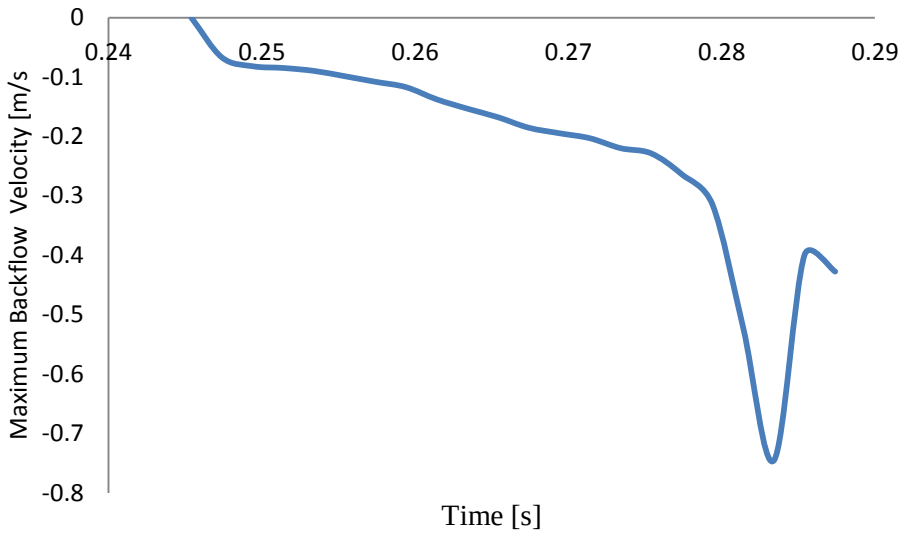

Figure 4.9 Maximum backflow velocity versus time for the bileaflet outlet valve closing measured on XY plane in the outlet tube.

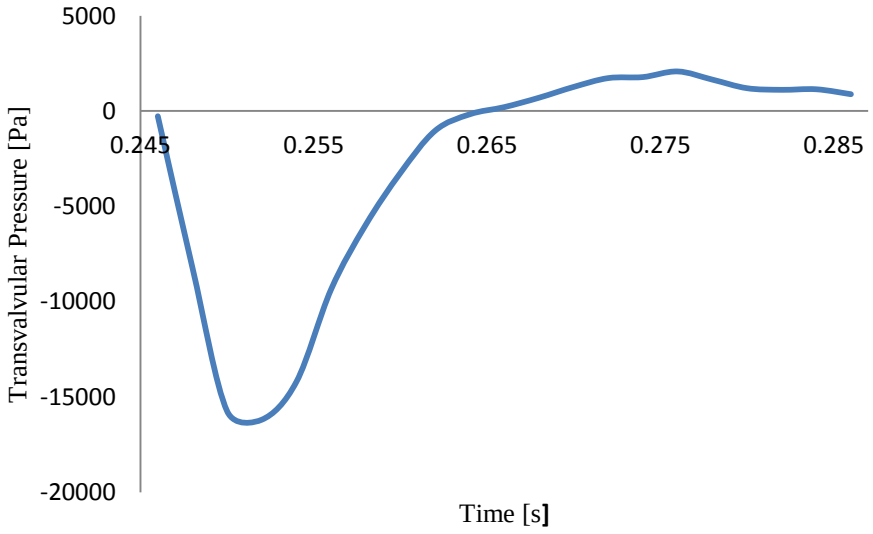

Figure 4.10 Transvalvular pressure versus time for the bileaflet outlet valve closing measured as the difference between average pressures on two planes 0.02 m apart before and after the valve.

4.1.1.3 THE BILEAFLET INLET VALVE OPENING

During diastole, the outlet valve remained closed and the inlet valve opened. The opening angle of the inlet valve was 85° (closed angle was 25°). Table 4.3 lists the maximum axial velocity and pressure conditions during the inlet valve opening. Again, transvalvular pressure was defined as the difference between the average pressure on two planes 0.02 m apart before and after the valve. Figure 4.11 depicts velocity distribution through diastole. Figure 4.12 shows velocity vectors in the vicinity of the valve; and Figure 4.13 depicts pressure distribution through diastole. It took 0.106 sec for the valve to reach the fully opened position (from 25° to 85°). The maximum velocity was 2.5 m/sec, occurring at the beginning of the inlet valve opening in the gap between the right leaflet and the wall (t = 0.293 s, Figures 4.12 and 4.14). A region of high velocity jet flow developed in the gap between the two leaflets when the valve reached its fully opened position. Figure 4.15 shows the pressure gradient across the valve as a function of time during inlet valve opening. The mean transvalvular pressure was 227.436 Pa. The maximum negative transvalvular pressure of 3071 Pa (average pressure on the lower plane minus average pressure on the upper plane) occurred at t = 0.393 s and initiated the valve opening process. The value for mean transvalvular pressure agrees with the data reported by Zoghbe et al.[67], that the mean pressure gradient across the mitral valve during diastole was less than 666.6 Pa. No big difference in the turbulent kinetic energy was observed (the average TKE = 6.06e-10 s^{-1}, maximum TKE = 5.02e-5 s^{-1} and minimum TKE = 7.12e-12 s^{-1}), indicating that the flow was prominently laminar.

Table 4.3 The bileaflet inlet valve opening behavior.

Parameter	Value
Maximum Axial Velocity	-2.5 m/s
Maximum Pressure Drop Across the Valve	3071 Pa
Average Pressure Drop Across the Valve	227.436 Pa
Valve Opening Time	0.106 s

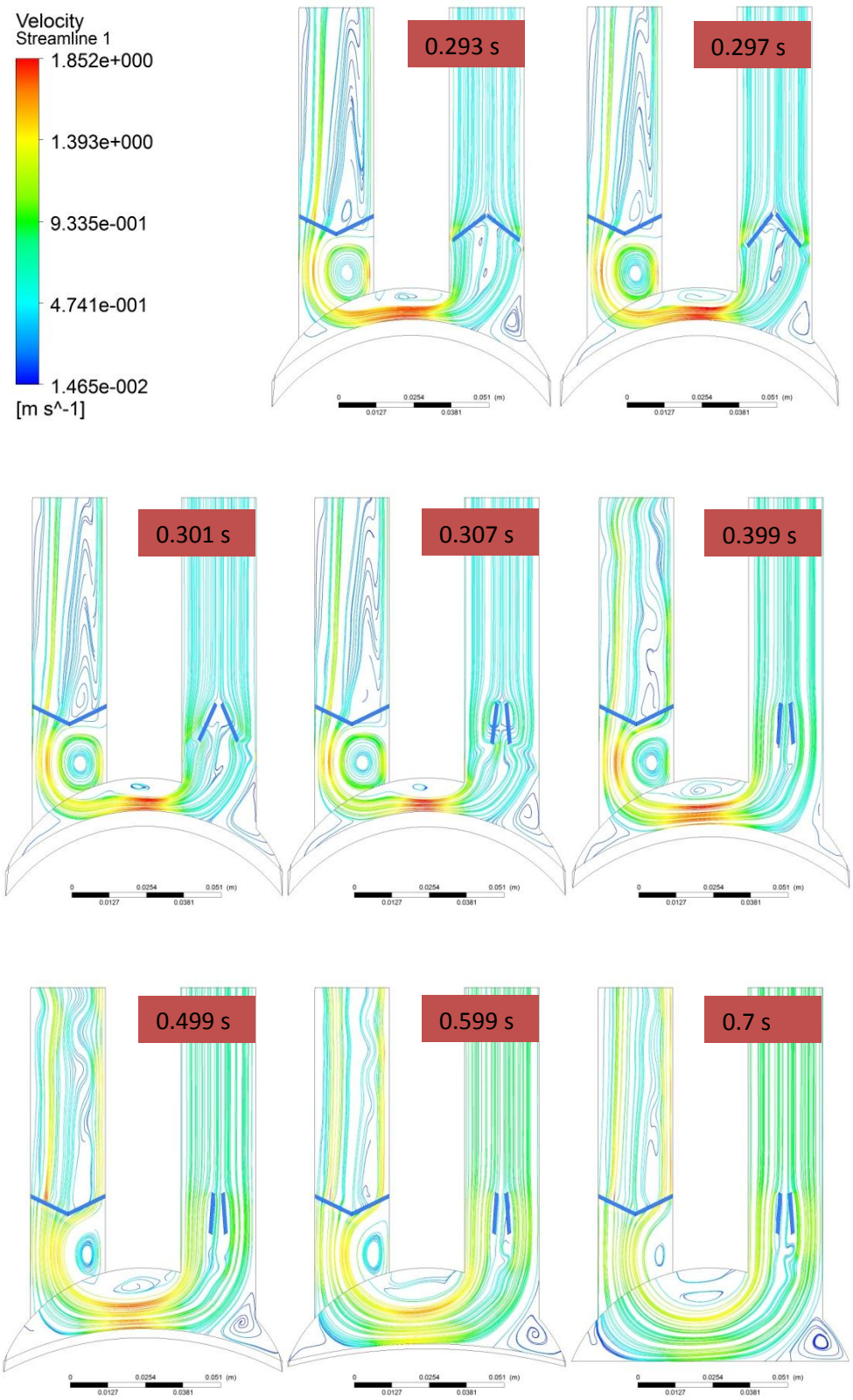

Figure 4.11 Velocity streamline for the bileaflet inlet valve opening.

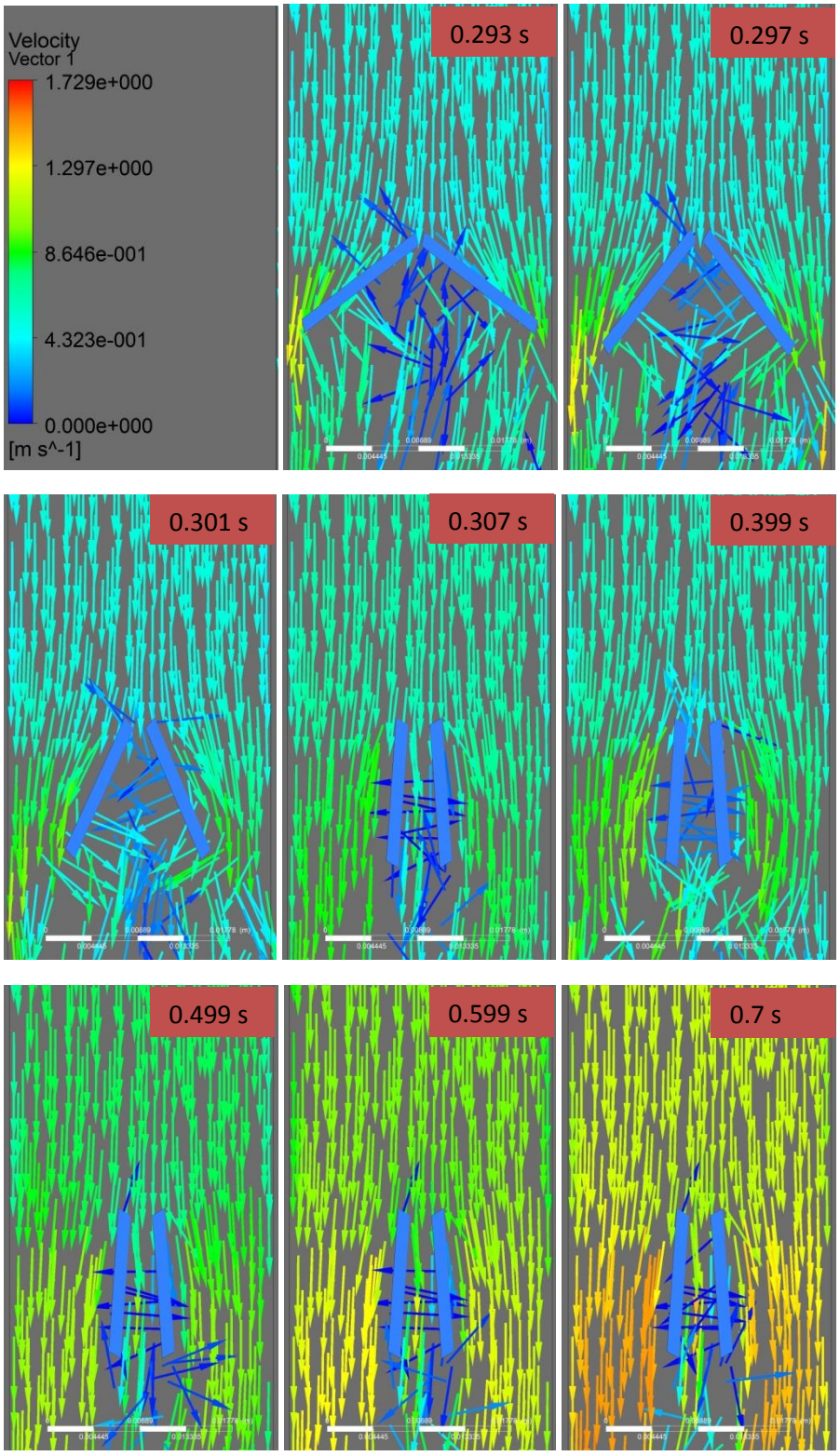

Figure 4.12 Velocity vectors for the bileaflet inlet valve opening.

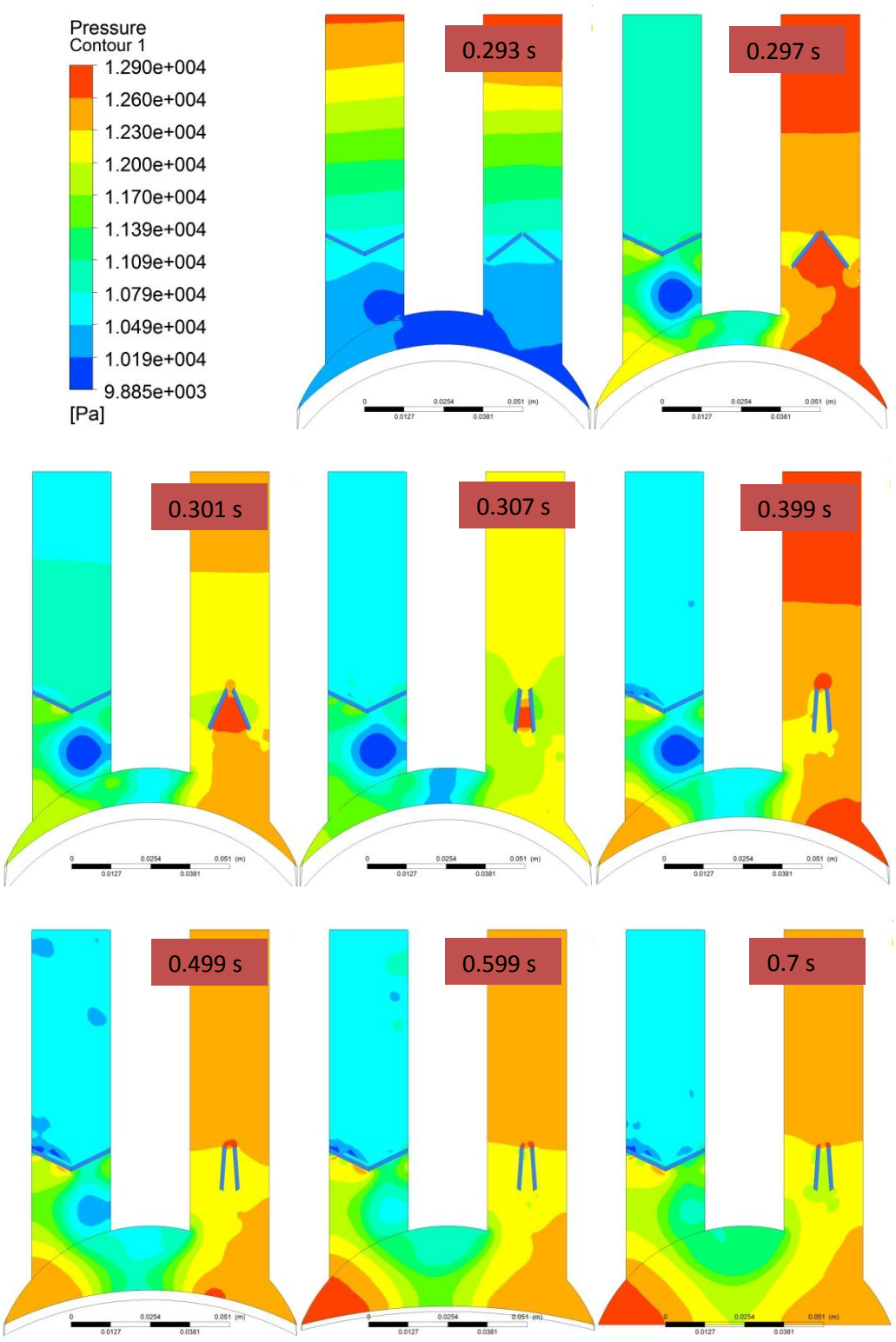

Figure 4.13 Pressure distribution during the opening of the bileaflet inlet valve.

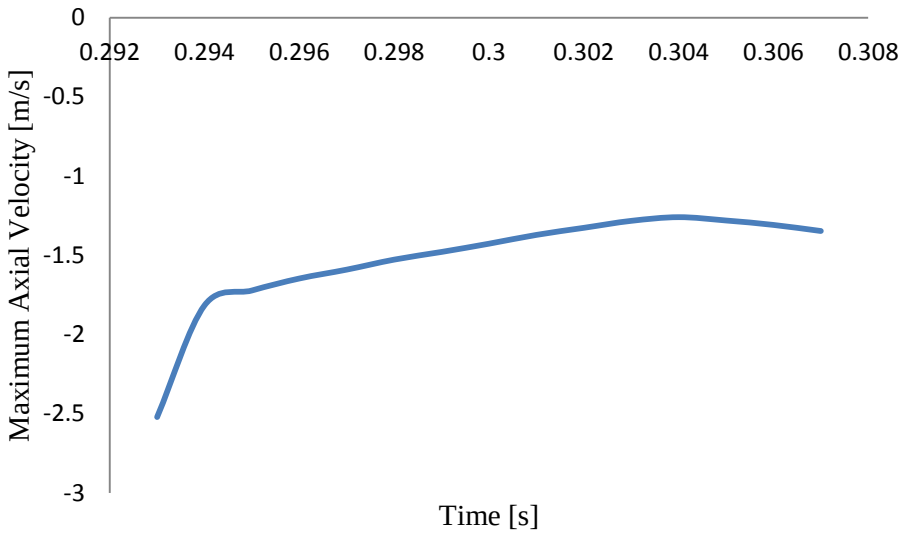

Figure 4.14 Maximum backflow velocity versus time for the bileaflet inlet valve opening measured on XY plane in the inlet tube.

.

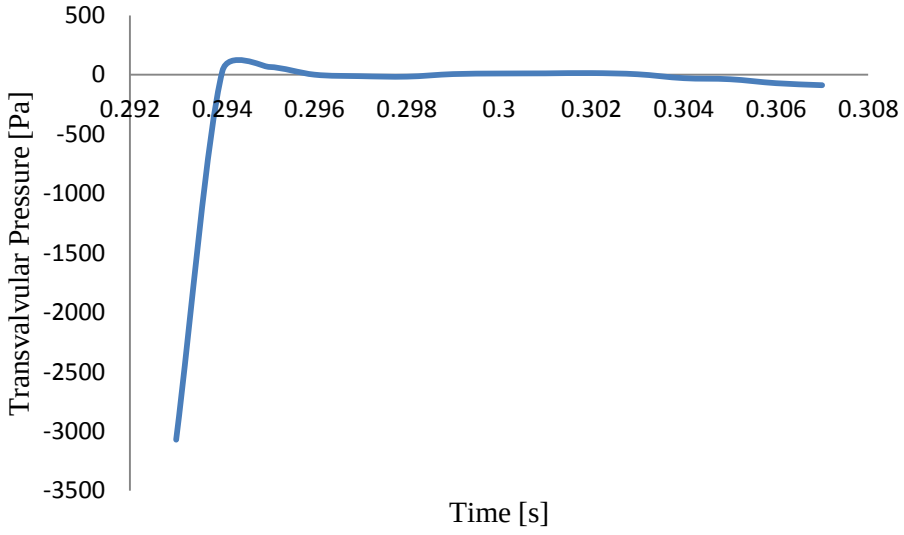

Figure 4.15 Transvalvular pressure versus time for the bileaflet inlet valve opening measured as the difference between average pressures on two planes 0.02 m apart before and after the valve.

4.1.1.4 THE BILEAFLET INLET VALVE CLOSING

Table 4.4 lists the maximum axial velocity and pressure conditions during the inlet valve closing, from the 85° opened position to the 25° closed position. Figure 4.16 depicts velocity distribution through late diastole. Figure 4.17 shows velocity vectors in the vicinity of the valve and Figures 4.18 demonstrates pressure distribution through late diastole. It took 0.182 sec for the valve to reach its fully closed position. The maximum axial velocity was 1.13 m/sec at the instant of valve closure (t = 0.9 s) in the gap between the leaflet and the wall (Figure 4.19). The mean transvalvular pressure was 72.65 Pa. The maximum transvalvular pressure was 462 Pa, which occurred at the end of valve closing process (t = 0.9, Figure 4.20). No big change in the turbulent kinetic energy was observed (the average TKE = 8.58e-5 s^{-1}, maximum TKE = 1.95e-4 s^{-1} and minimum TKE = 1.59e-8 s^{-1}), indicating that the flow was prominently laminar.

Table 4.4 The bileaflet inlet valve closing behavior.

Parameter	Value
Maximum Axial Velocity	1.13 m/s
Maximum Pressure Drop Across the Valve	462 Pa
Average Pressure Drop Across the Valve	72.65 Pa
Valve Closing Time	0.182 s

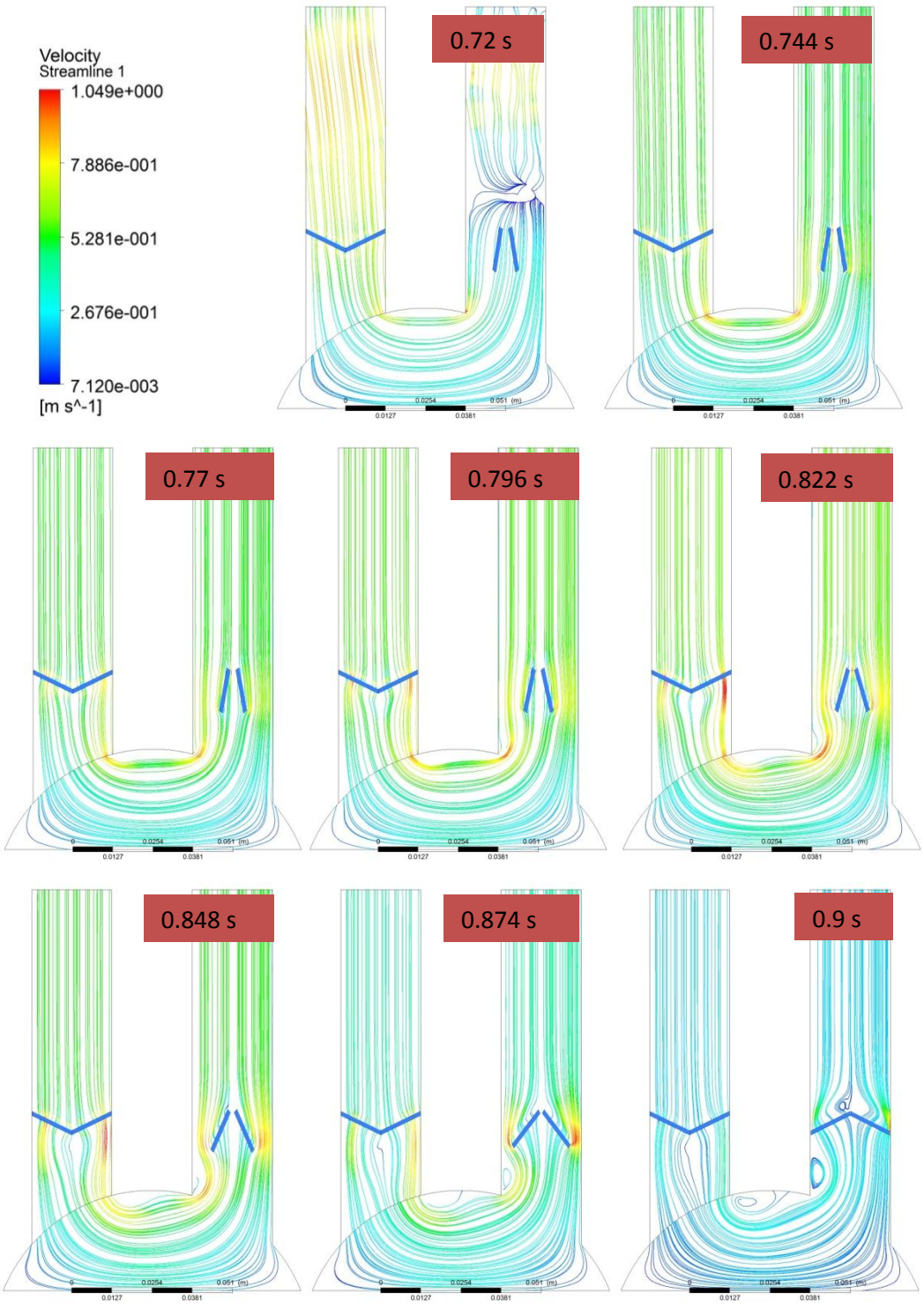

Figure 4.16 Velocity streamline during early systole when the bileaflet inlet valve closes.

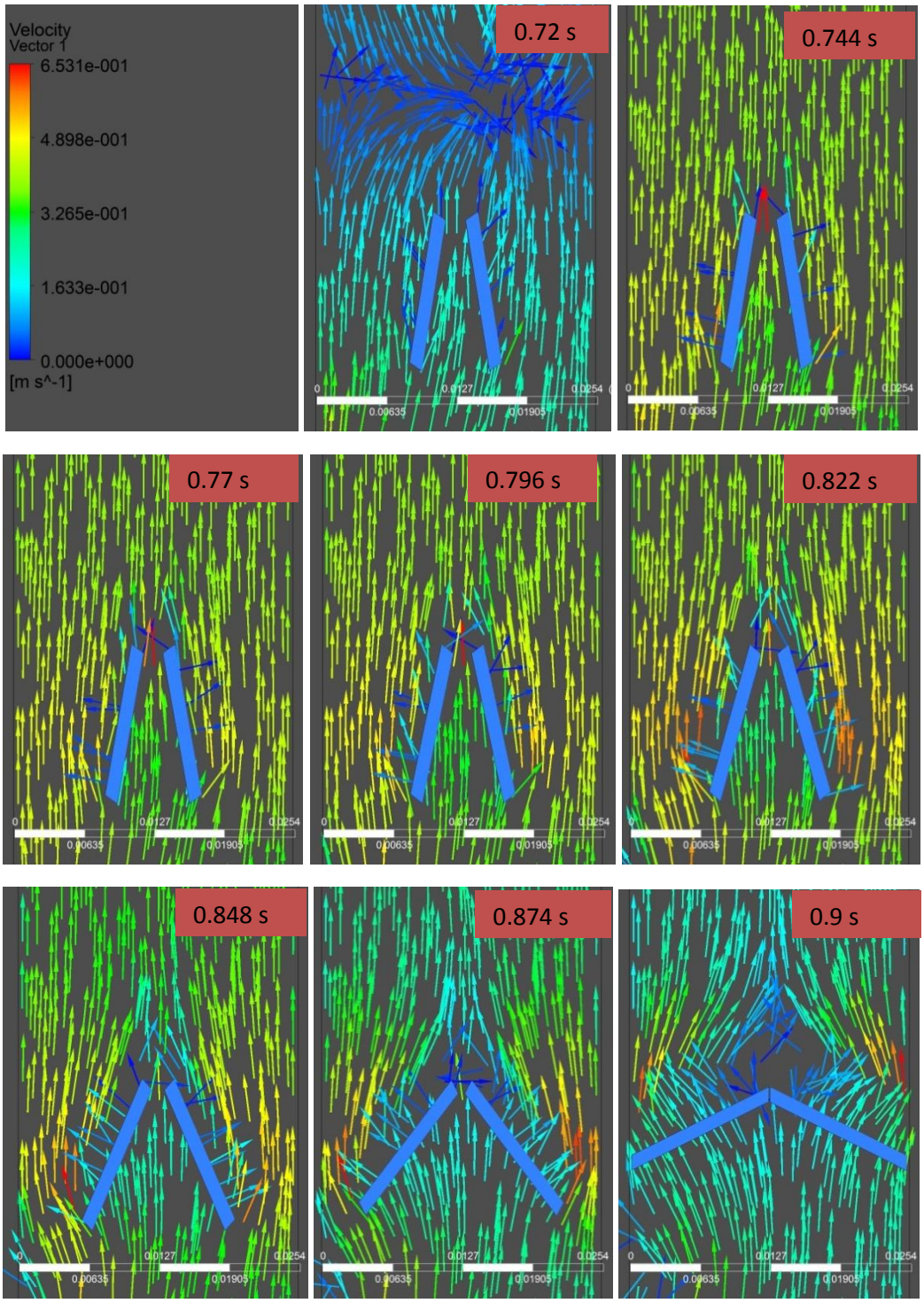

Figure 4.17 Velocity vectors in the bileaflet valve region during late diastole.

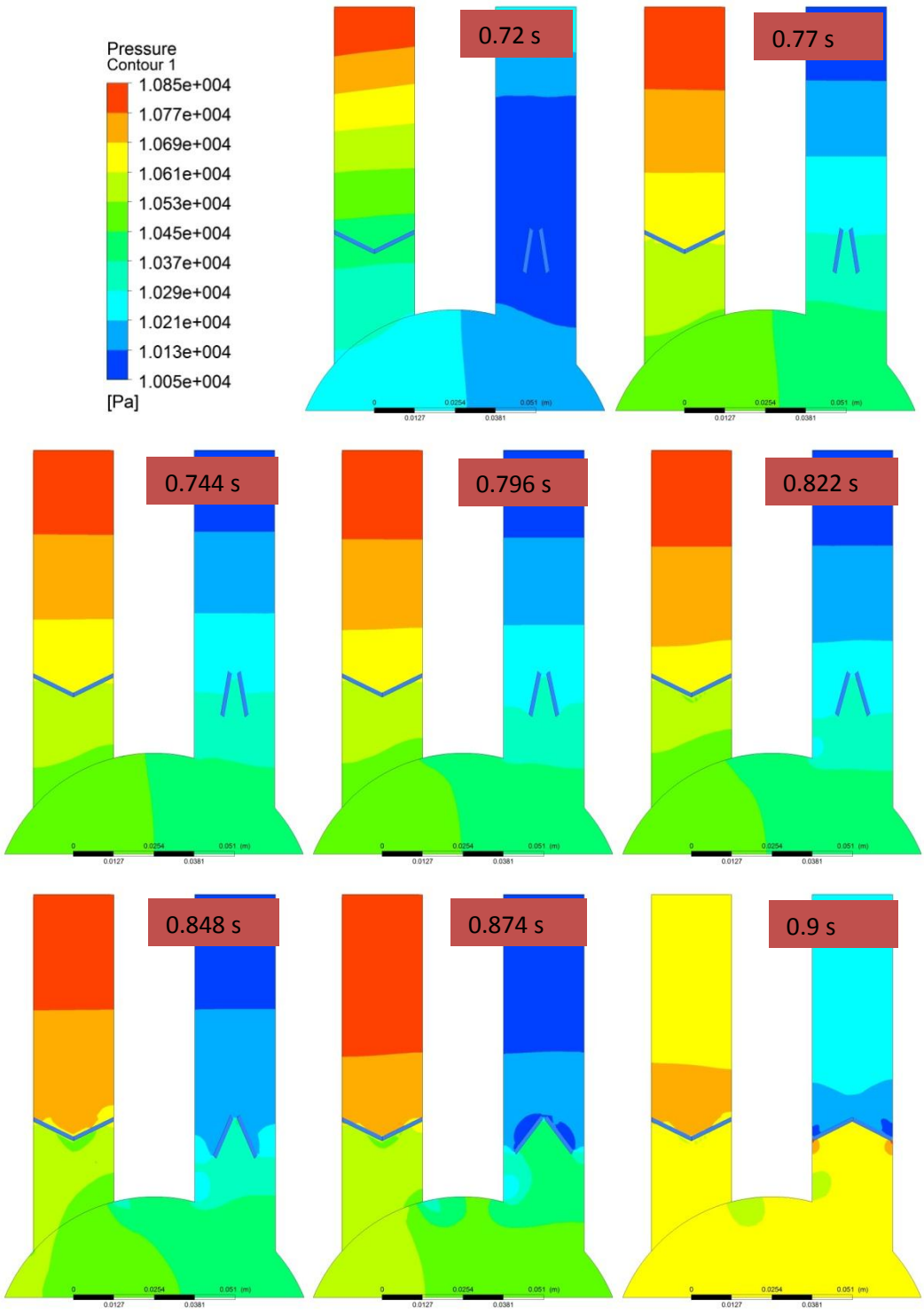

Figure 4.18 Pressure distribution during late diastole when the bileaflet inlet valve closes.

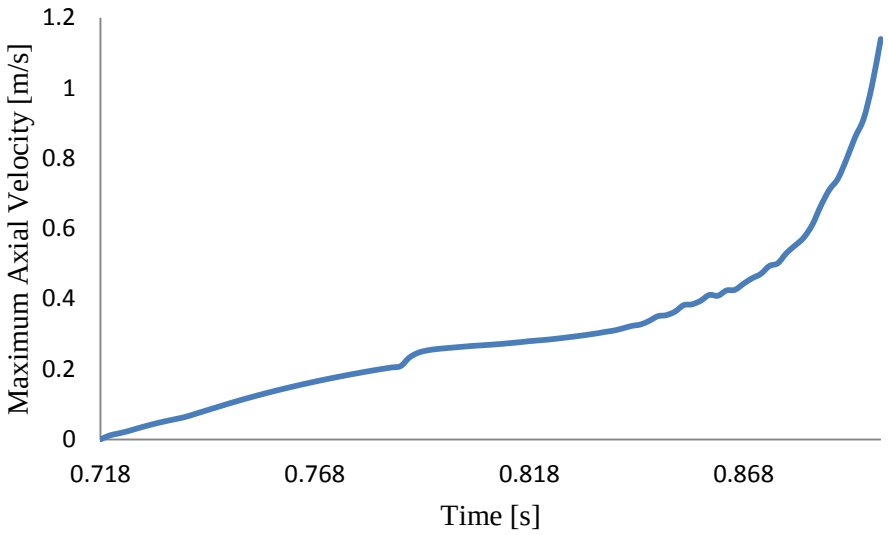

Figure 4.19 Maximum backflow velocity versus time for the bileaflet inlet valve closing measured on XY plane in the inlet tube.

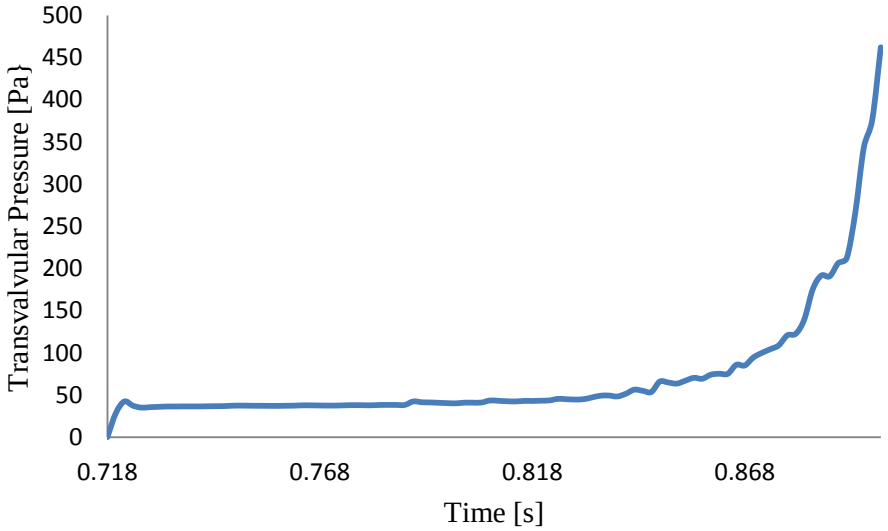

Figure 4.20 Transvalvular pressure versus time for the bileaflet inlet valve closing measured as the difference between average pressures on two planes 0.02 m apart before and after the valve.

4.1.2 THE MONOLEAFLET VALVE

4.1.2.1 THE OUTLET VALVE OPENNING BEHAVIOR

Using the 2D model, flow parameters around the outlet valve were calculated when the valve opening angle was 75°. Table 4.5 lists the maximum axial velocity and pressure conditions during the outlet valve opening. In this table, transvalvular pressure was defined as the difference between average pressure on two planes 0.02 m apart before and after the valve. Figure 4.21 depicts velocity distribution through systole. Figure 4.22 shows velocity vectors in the vicinity of the valve. Figure 4.23 shows pressure distribution through systole. It took 0.107 sec for the valve to reach the opening position (from 0° to 75°). The maximum velocity was 0.35 m/sec when the valve reached its maximum opening angle (t = 0.107 sec, Figure 4.24). At this moment, flow separated around the valve leaflets with high velocity. A recirculation zone developed approximately 20 mm in the outlet channel before the valve, due to the velocity gradient. Figure 4.25 shows the changes in pressure distribution in the model during systole. The mean transvalvular pressure was 64.68 Pa and the maximum transvalvular pressure was 266.64 Pa, which occurred right before the valve opening (t = 0.015 s). This value agrees with what reported by Zoghbe et al.[67], that the mean pressure gradient across the aortic valve during systole was less than 2666.44 Pa. In addition, no significant increase in turbulent kinetic energy was observed (the average TKE = 4.56e-6 s^{-1}, maximum TKE = 1.878e-3 s^{-1} and minimum TKE = 2.683e-9 s^{-1}) near the open valve which reveals that the flow was prominently laminar.

Table 4.5 Flow parameters related to the monoleaflet outlet valve opening when the opening angle was 75^{o}.

Parameter	Value
Maximum Axial Velocity	0.35 m/s
Maximum Pressure Drop Across the Valve	266.44 Pa
Average Pressure Drop Across the Valve	64.68 Pa
Valve Opening Time	0.107 s

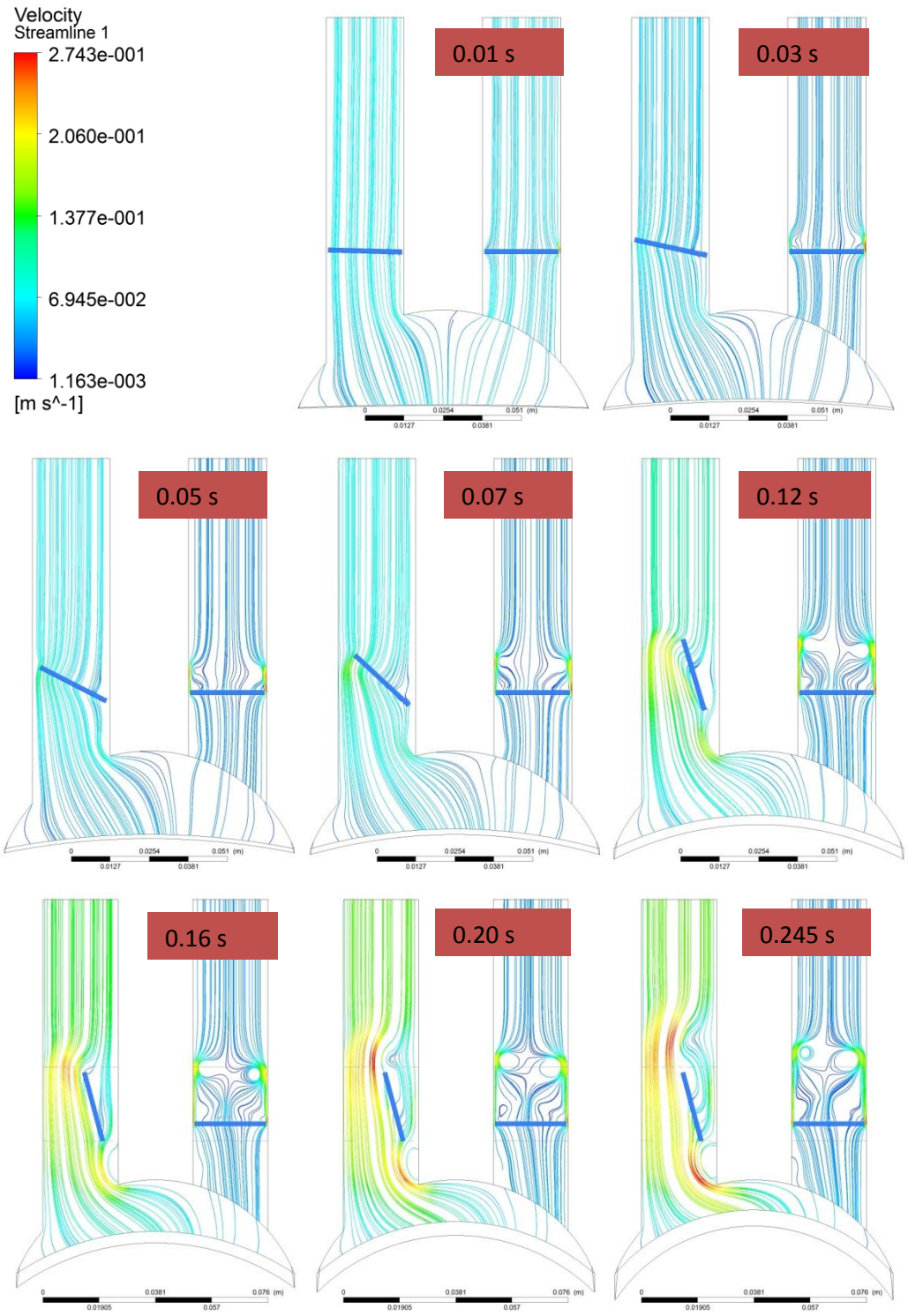

Figure 4.21 Velocity streamline during systole when the monoleaflet outlet valve opens.

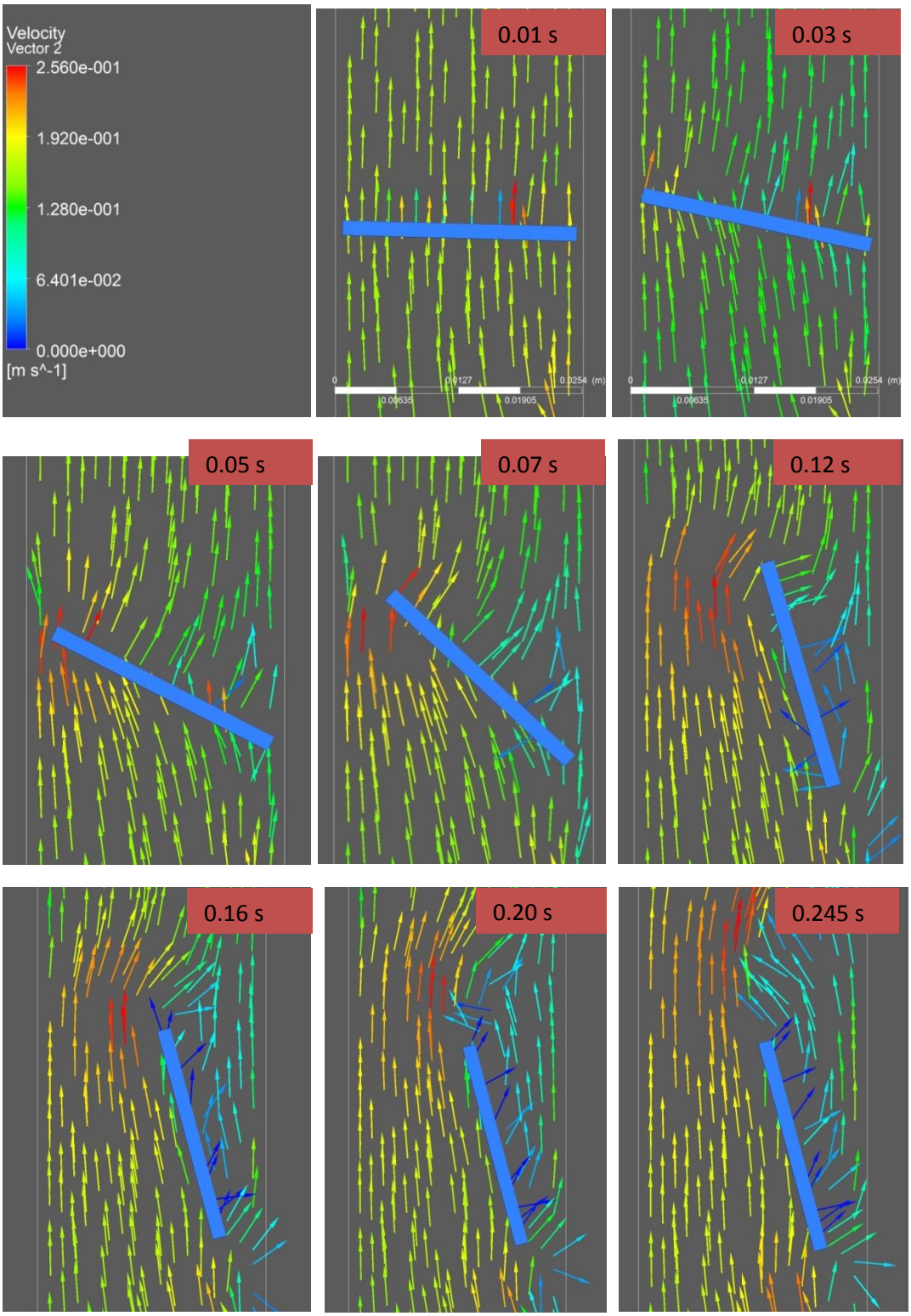

Figure 4.22 Velocity vectors in the outlet monoleaflet valve region during systole.

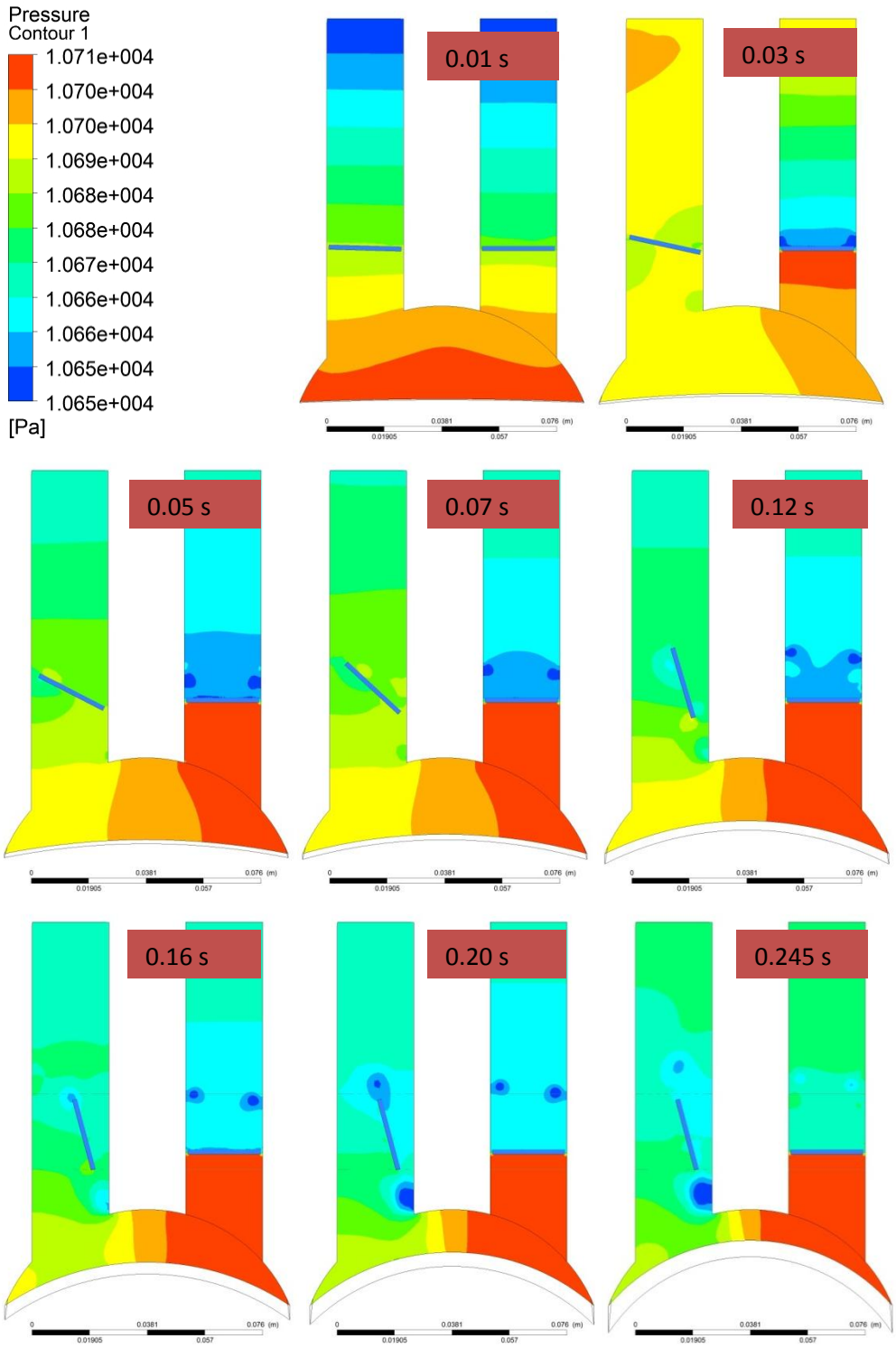

Figure 4.23 Pressure distribution for the monoleaflet outlet valve opening during the systole.

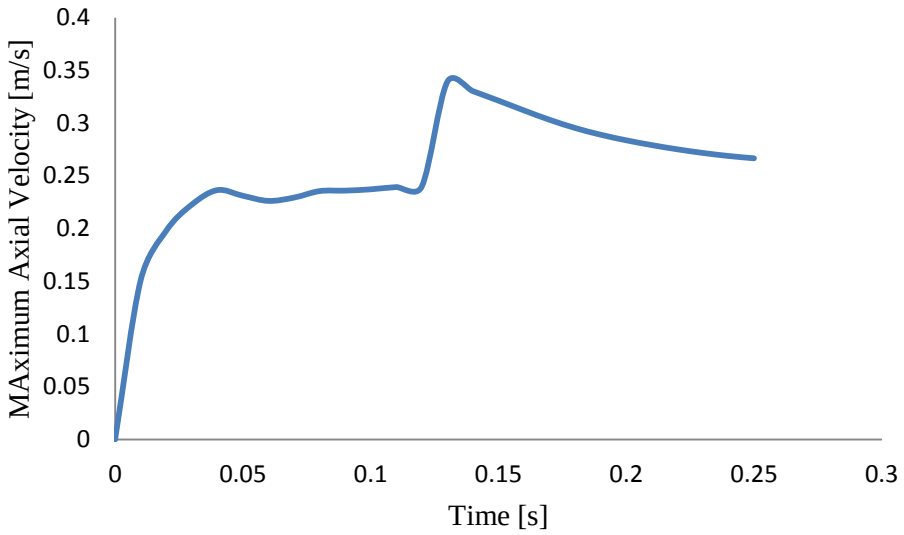

Figure 4.24 Maximum axial velocity versus time for the monoleaflet outlet valve opening measured on XY plane in the outlet tube.

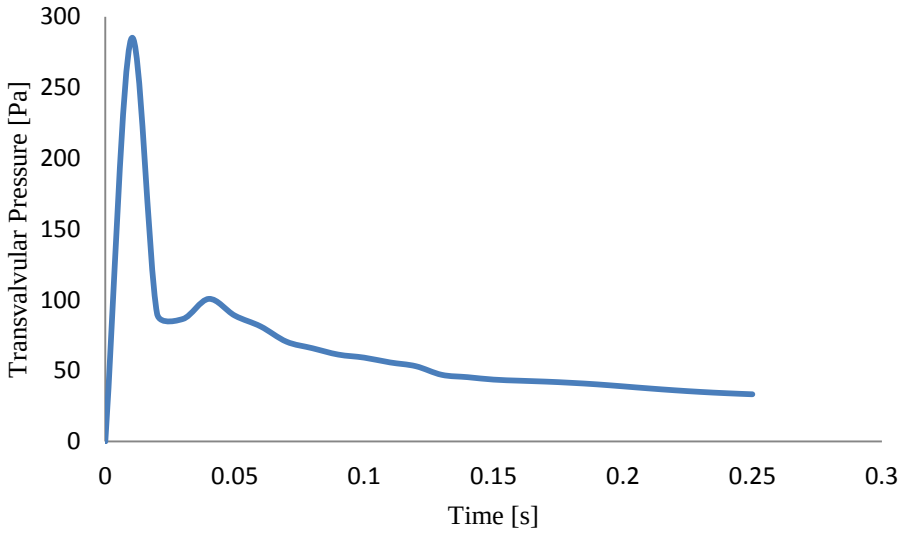

Figure 4.25 Transvalvular pressure versus time for the monoleaflet outlet valve opening measured as the difference between average pressure on two planes 0.02 m apart before and after the valve.

4.1.2.2 THE OUTLET VALVE CLOSING BEHAVIOR

Table 4.6 lists the maximum axial velocity and pressure conditions during the outlet valve closing. Figure 4.26 depicts velocity distribution and Figure 4.27 shows velocity vectors in the vicinity of the valve. Figure 4.28 demonstrates pressure distribution during the valve closing phase. It took 0.1046 sec for the valve to reach the fully closed position (0^o). The maximum backflow velocity was 0.78 m/sec and it occurred at the beginning of valve closure process (t = 0.26 s, Figure 4.29). The mean transvalvular pressure was 148.79 Pa and the maximum transvalvular pressure was 1500 Pa, shown in Figure 4.30. No significant increase in turbulent kinetic energy was observed (the average TKE = 4.56e-6 s^{-1}, maximum TKE = 1.878e-3 s^{-1} and minimum TKE = 2.683e-9 s^{-1}) near the open valve which reveals that the flow was prominently laminar.

Table 4.6 Flow parameters related to the monoleaflet outlet valve closing, when the opening angle was 75^o.

Parameter	Value
Maximum Backflow Velocity	0.78 m/s
Maximum Pressure Drop Across the Valve	1500 Pa
Average Pressure Drop Across the Valve	148.79 Pa
Valve Closing Time	0.1046 s

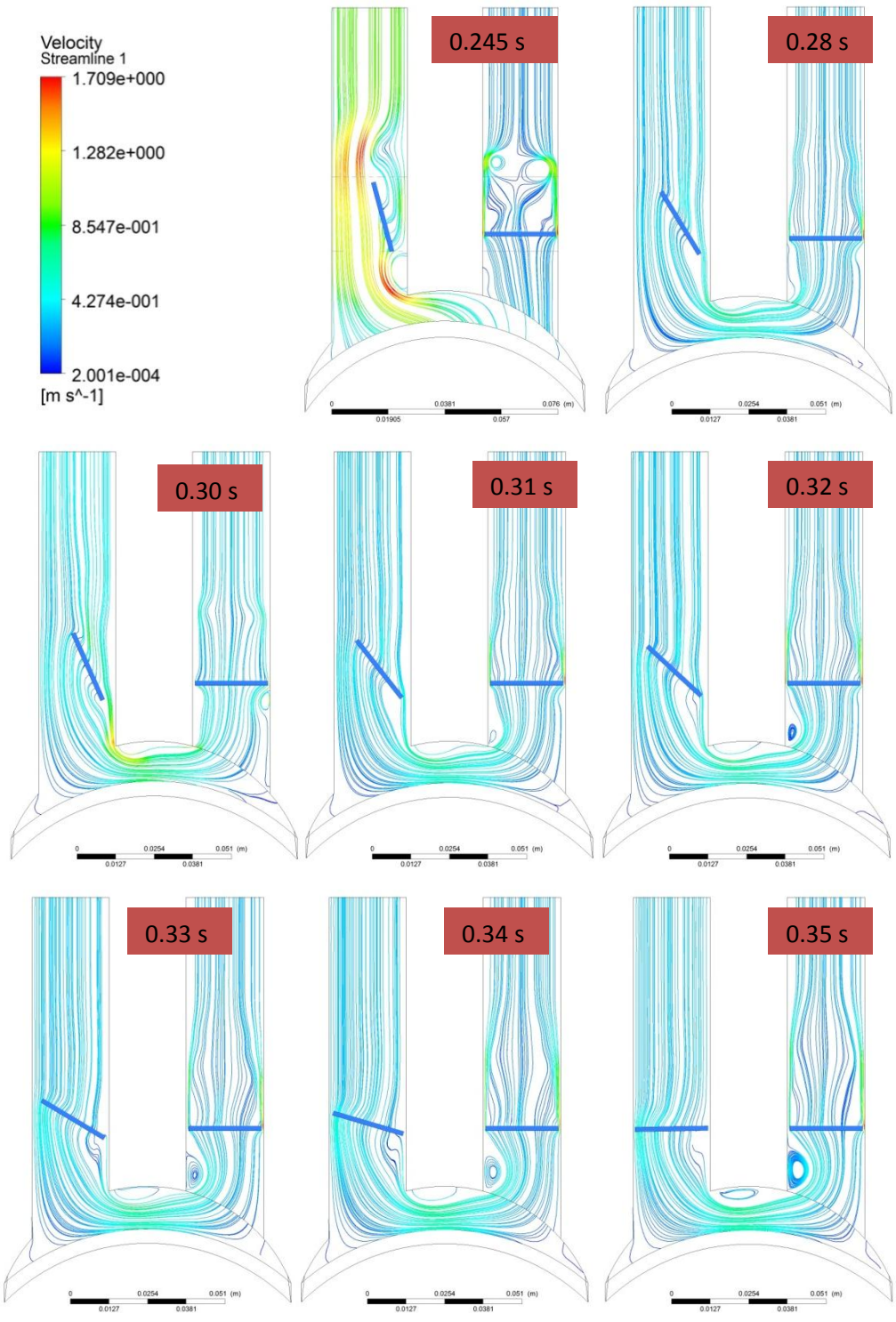

Figure 4.26 Velocity streamline during diastole when the monoleaflet valve closes.

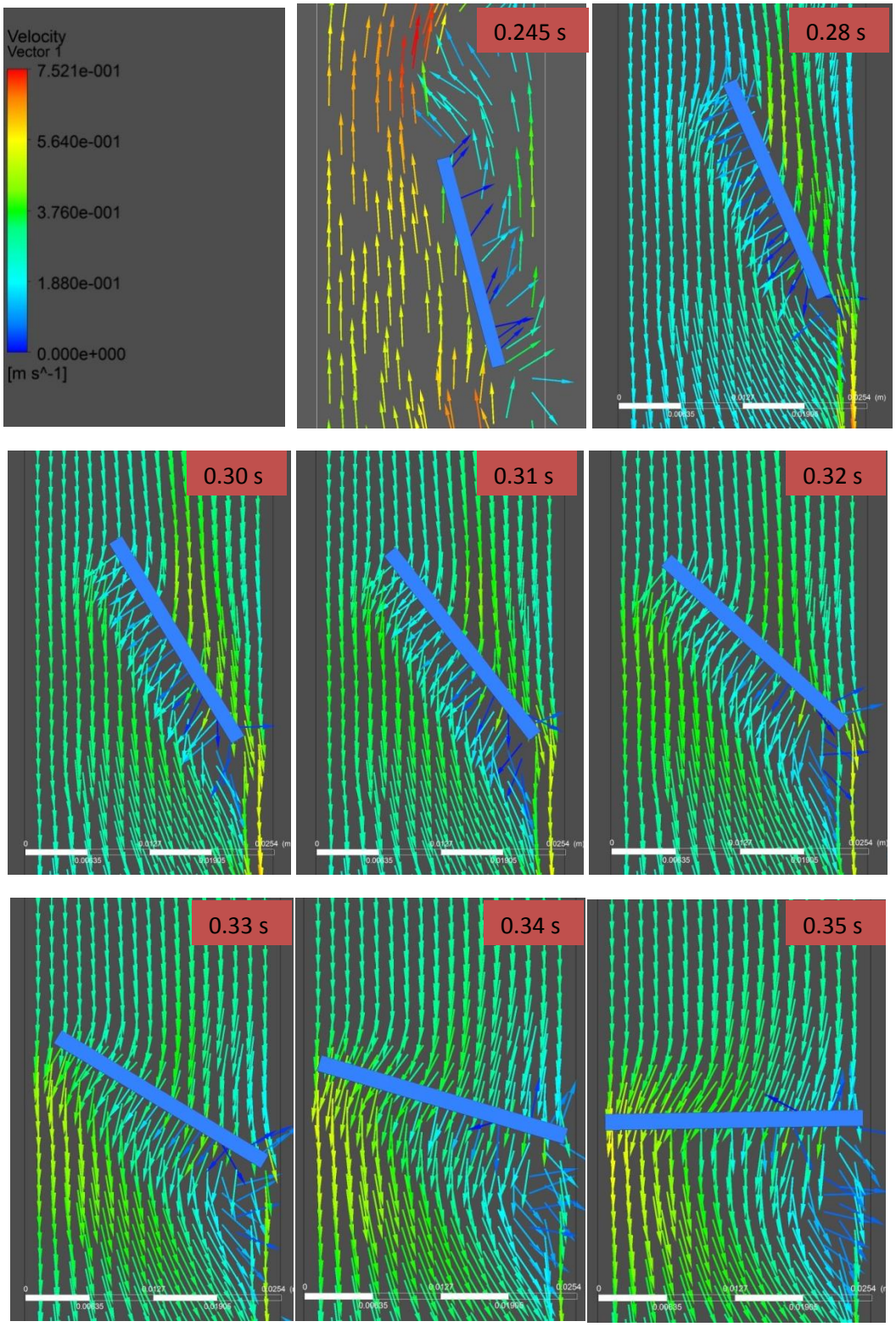

Figure 4.27 Velocity vectors in the valve region during diastole when the monoleaflet valve closes.

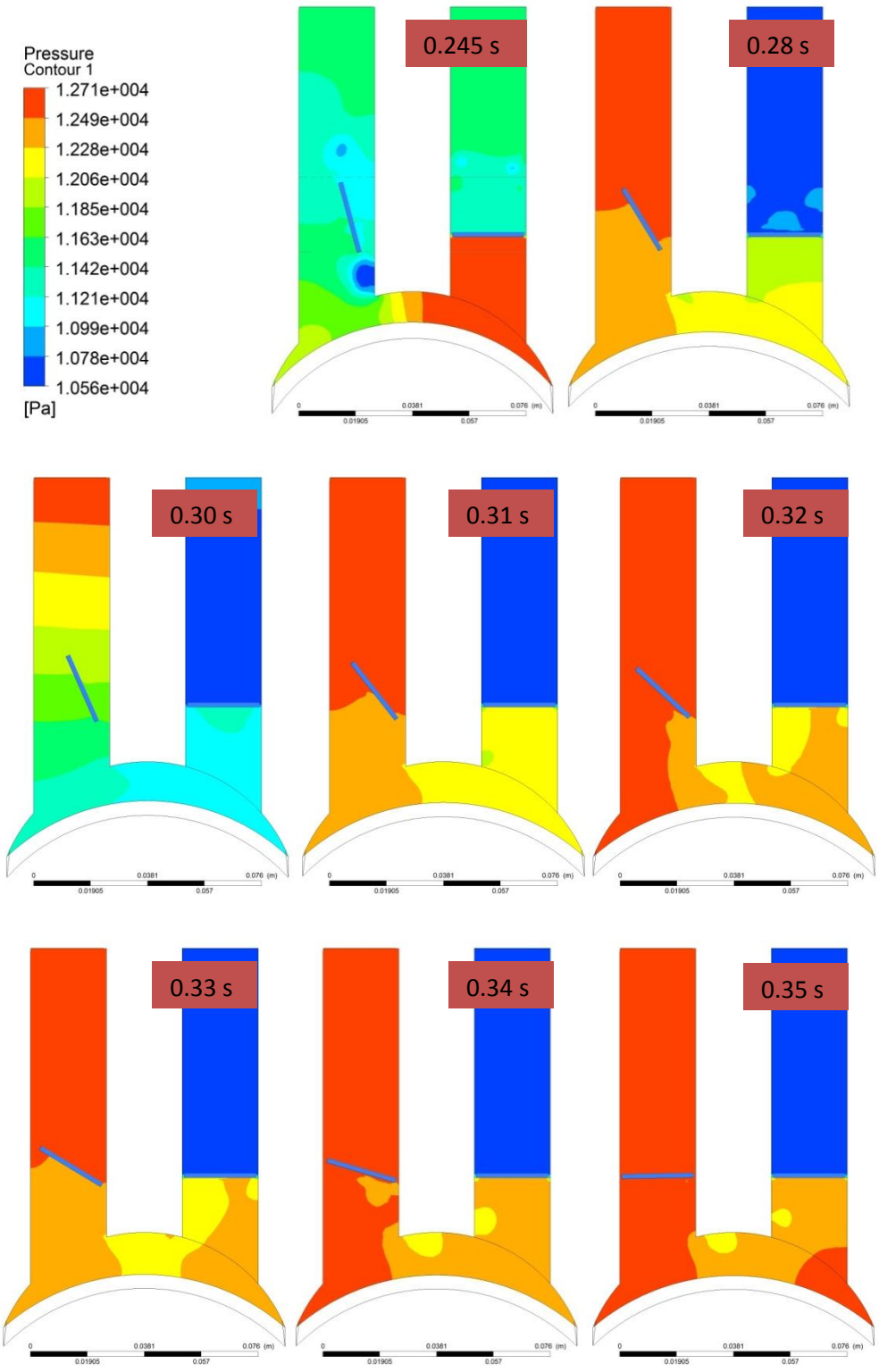

Figure 4.28 Pressure distribution for the monoleaflet outlet valve closing.

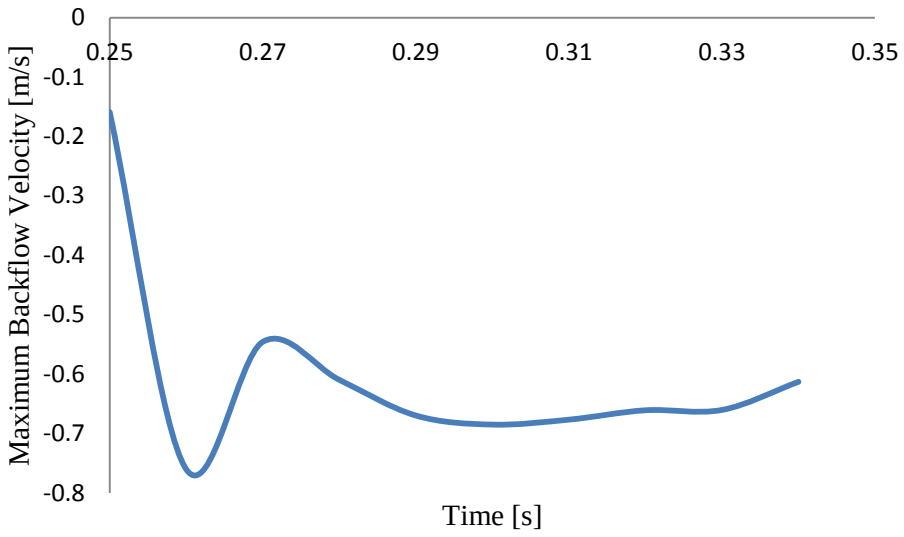

Figure 4.29 Maximum backflow velocity versus time for the monoleaflet outlet valve closing measured on XY plane in the outlet tube.

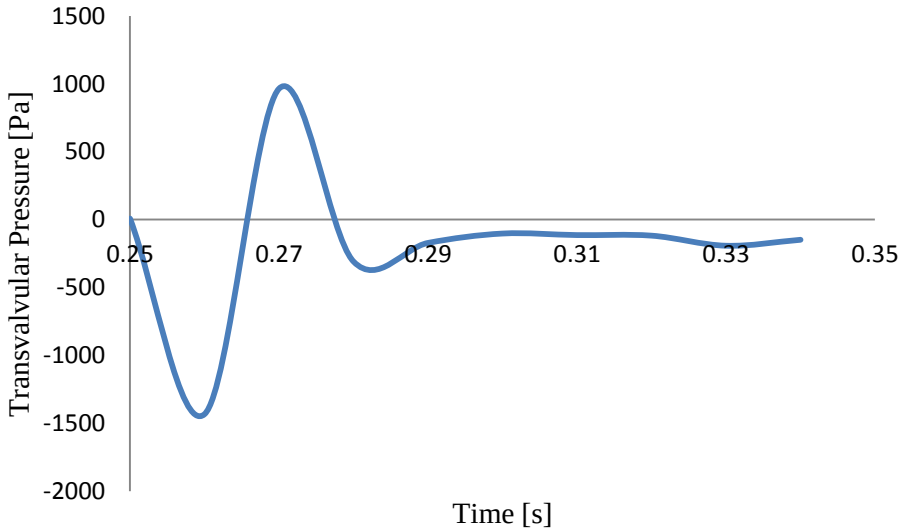

Figure 4.30 Transvalvular pressure versus time for the monoleaflet outlet valve closing

4.1.2.3 THE MONOLEAFLET INLET VALVE OPENING BEHAVIOR

In here, flow parameters around the inlet valve were calculated when the valve opening angle was kept at 75^{o}. Table 4.7 lists the maximum axial velocity and pressure conditions during the inlet valve opening. Figures 4.31, 4.32 and 4.33 depict velocity streamline, velocity vectors around the valve area and pressure distribution through diastole. It took 0.04 sec for the valve to reach the fully opened position and the maximum velocity was 2.5 m/sec (Figure 4.34). The mean transvalvular pressure was 291.82 Pa and the maximum transvalvular pressure was 5311 Pa, occurring at the moment of valve opening (t = 0.35s, Figure 4.35). The value for the mean transvalvular pressure agrees with what reported by Zoghbe et al.[67], that the mean pressure gradient across the mitral valve during diastole was less than 666.66 Pa. Moreover, no significant increase in the turbulent kinetic energy was observed (the average TKE = 6.84e-6 s^{-1}, maximum TKE = 6.845e-3 s^{-1} and minimum TKE = 2.607e-11 s^{-1}) in the model which reveals that the flow was prominently laminar.

Table 4.7 The monoleaflet inlet valve opening behavior.

Parameter	Value
Maximum Axial Velocity	-2.5 m/s
Maximum Pressure Drop Across the Valve	5311 Pa
Average Pressure Drop Across the Valve	291.82 Pa
Valve Opening Time	0.04 s

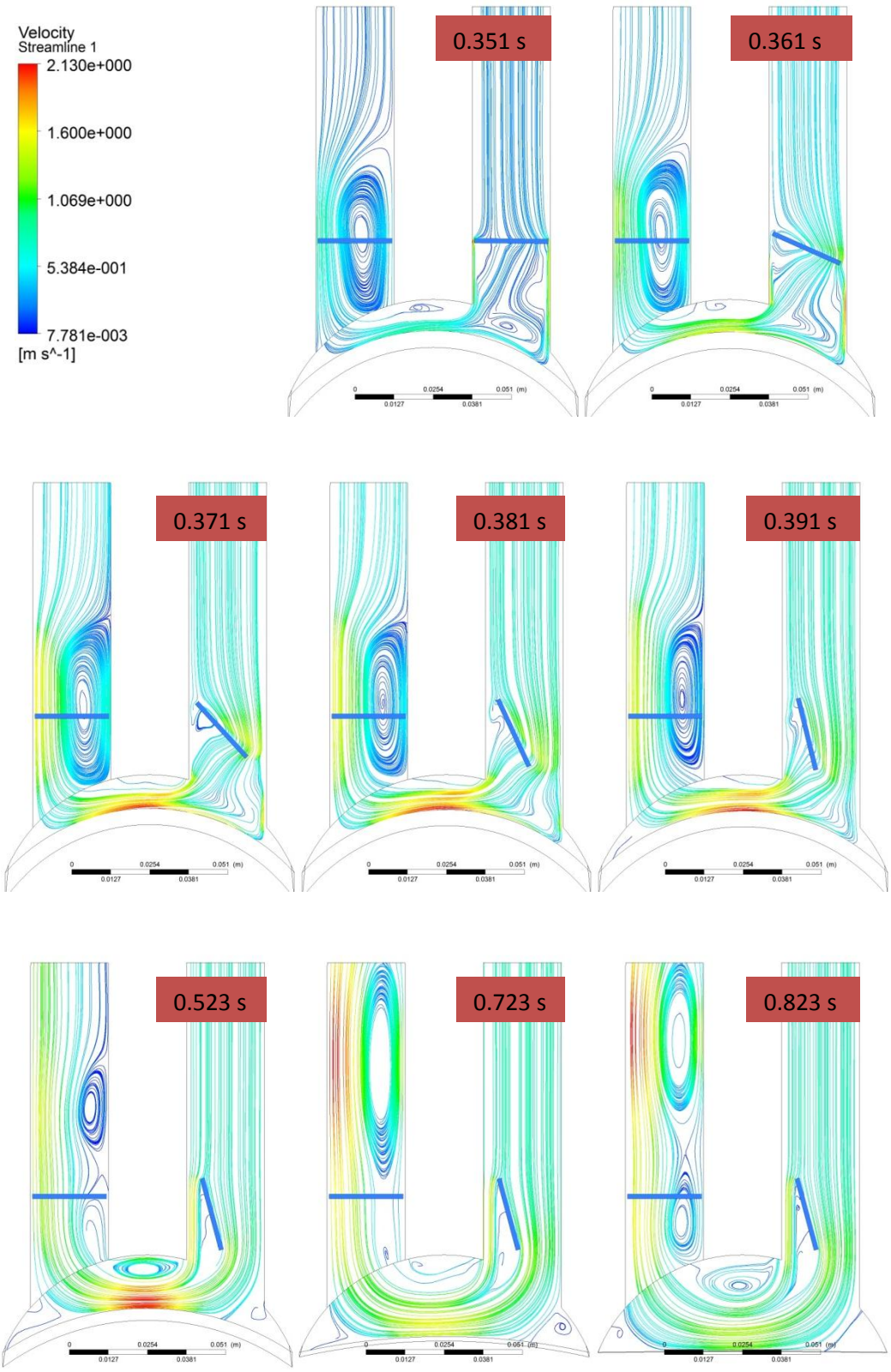

Figure 4.31 Velocity streamline during the inlet valve opening.

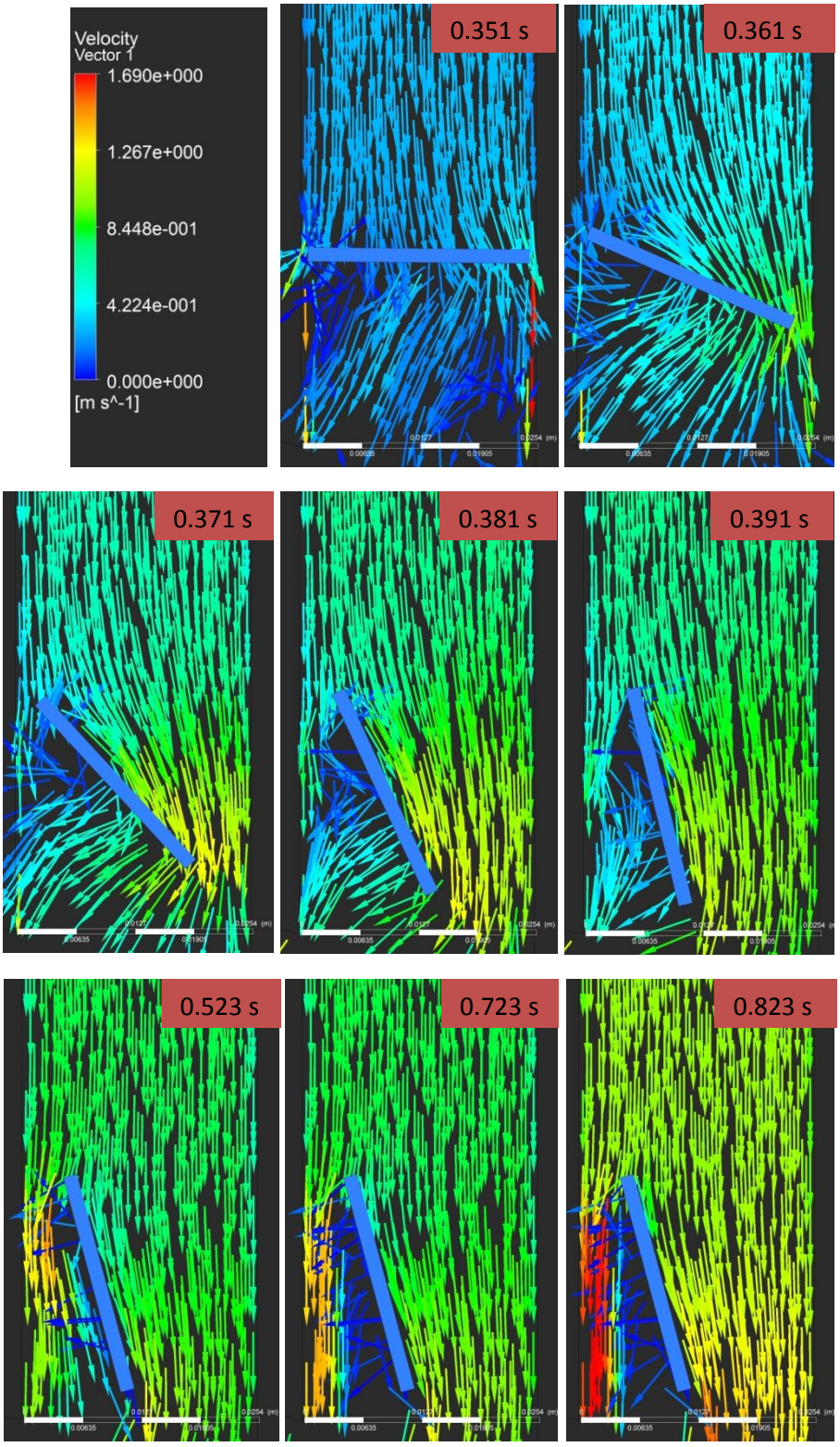

Figure 4.32 Velocity vectors in the valve region during the inlet valve opening.

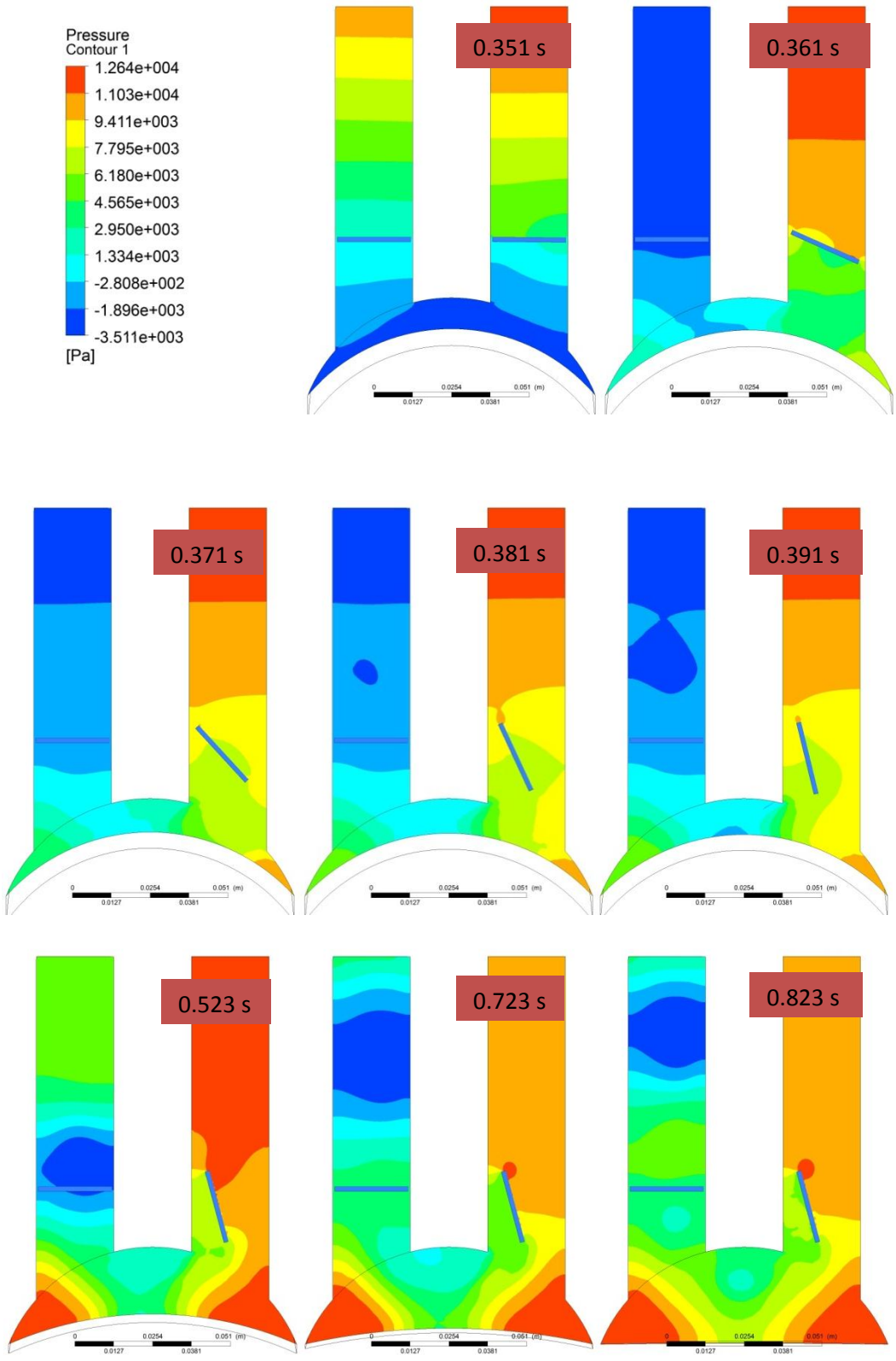

Figure 4.33 Pressure distribution for the monoleaflet inlet valve opening during diastole.

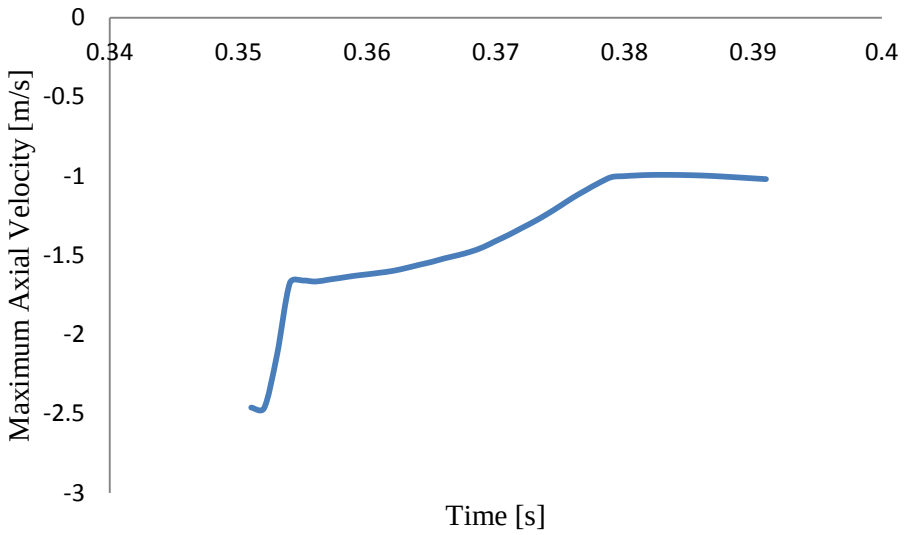

Figure 4.34 Maximum axial velocity versus time for the monoleaflet inlet valve opening measured on XY plane in the inlet tube.

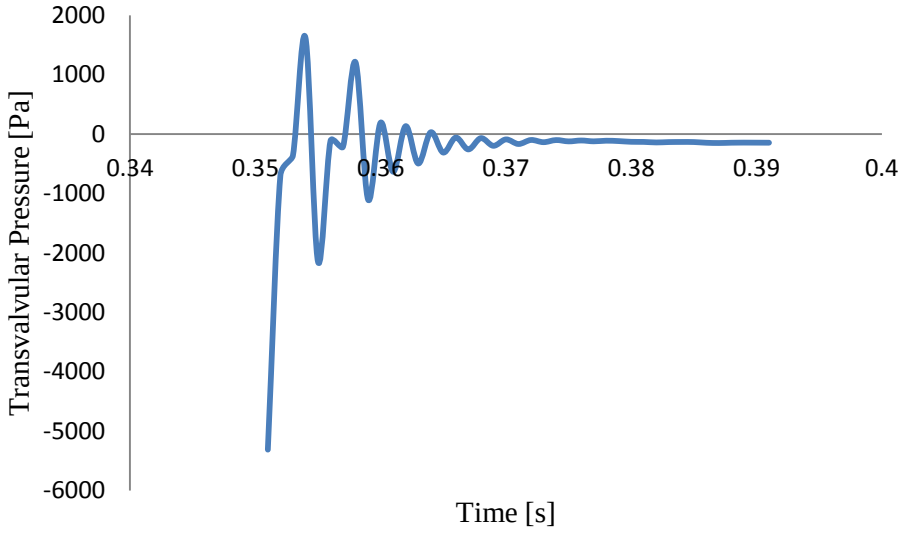

Figure 4.35 Transvalvular pressure versus time for the monoleaflet inlet valve opening measured as the difference between average pressures on two planes 0.02 m apart before and after the valve.

4.1.2.4 THE MONOLEAFLET INLET VALVE CLOSING BEHAVIOR

Table 4.8 lists the maximum axial velocity and pressure conditions during the inlet valve closing. In this table, transvalvular pressure was defined as the difference between average pressure on two planes 0.02 m apart, before and after the valve. Figures 4.36 and 4.39 depict velocity distribution through late diastole. Figure 4.37 shows velocity vectors in the vicinity of the valve. Figure 4.38 depicts pressure distribution through late diastole. It took 0.063 sec for the valve to reach the closed position (to reach from 75^0 to 0^o). During the valve closure the valve area was divided into a major and a minor area on each side of the leaflet. The maximum velocity in the gap between the leaflet and the wall in the minor area reached 0.98 m/s (t = 0.054 s) while the maximum velocity was 1.114 m/sec in the major area which occurred at the end of valve closure (t= 0.063s). Figure 4.38 shows the pressure distribution in the model during the valve closure. Due to Figure 4.40, the mean transvalvular pressure was 245.56 Pa. The maximum transvalvular pressure was 446.115 Pa which occurred as the valve was approaching the fully closed position (t = 0.893 s). In addition, no significant increase in turbulent kinetic energy was observed (the average TKE = 3.6 e-4 s^{-1}, maximum TKE = 7.288e-4 s^{-1} and minimum TKE = 7.56e-8 s^{-1}) near the open valve which reveals that the flow was prominently laminar.

Table 4.8 Flow parameters related to the monoleaflet inlet valve closing, when the opening angle was 75^{o}.

Parameter	Value
Maximum Axial Velocity	1.114 m/s
Maximum Pressure Drop Across the Valve	446.115 Pa
Average Pressure Drop Across the Valve	245.56 Pa
Valve Opening Time	0.063 s

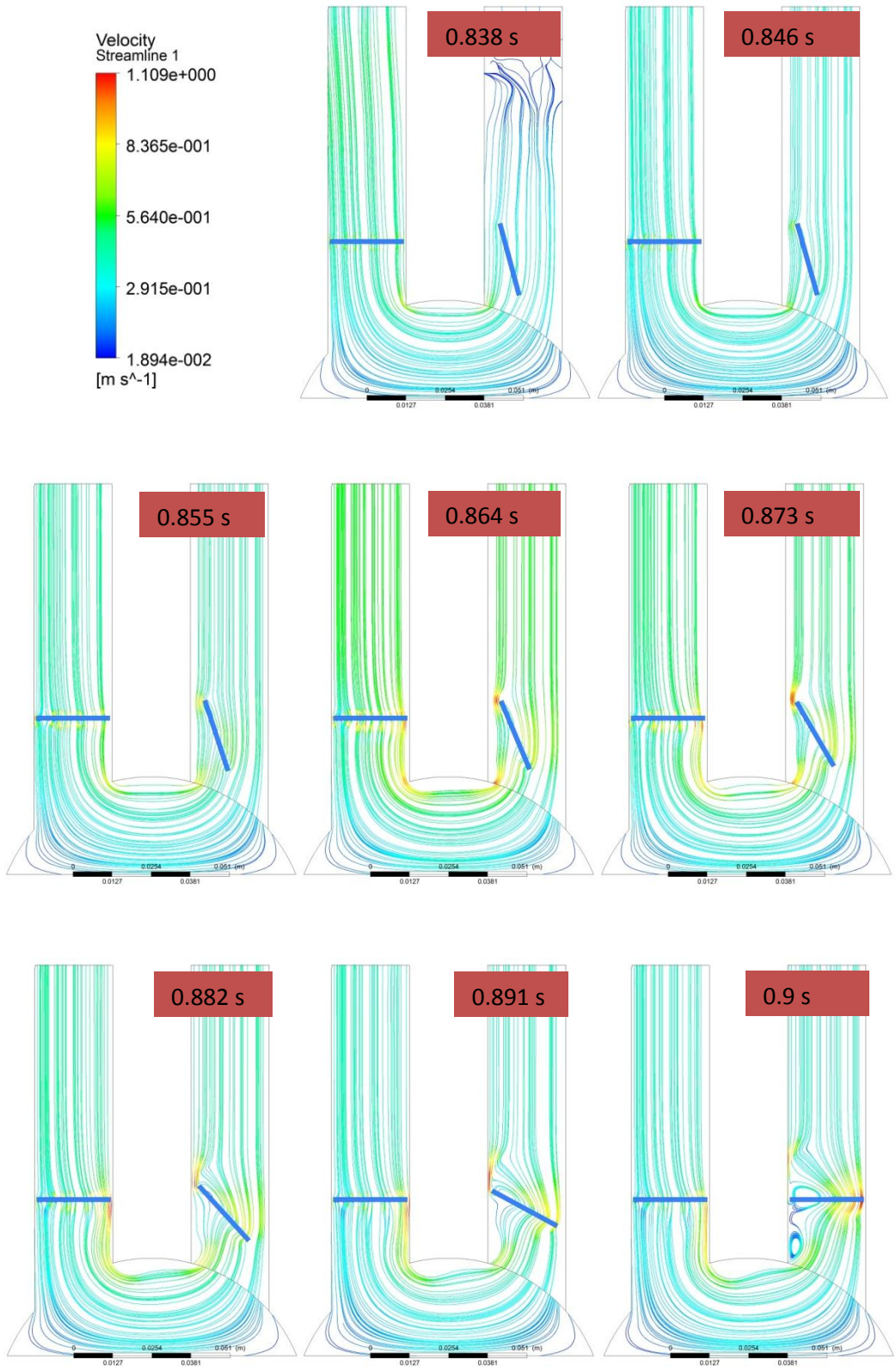

Figure 4.36 Velocity streamline during late diastole when the monoleaflet inlet valve closes.

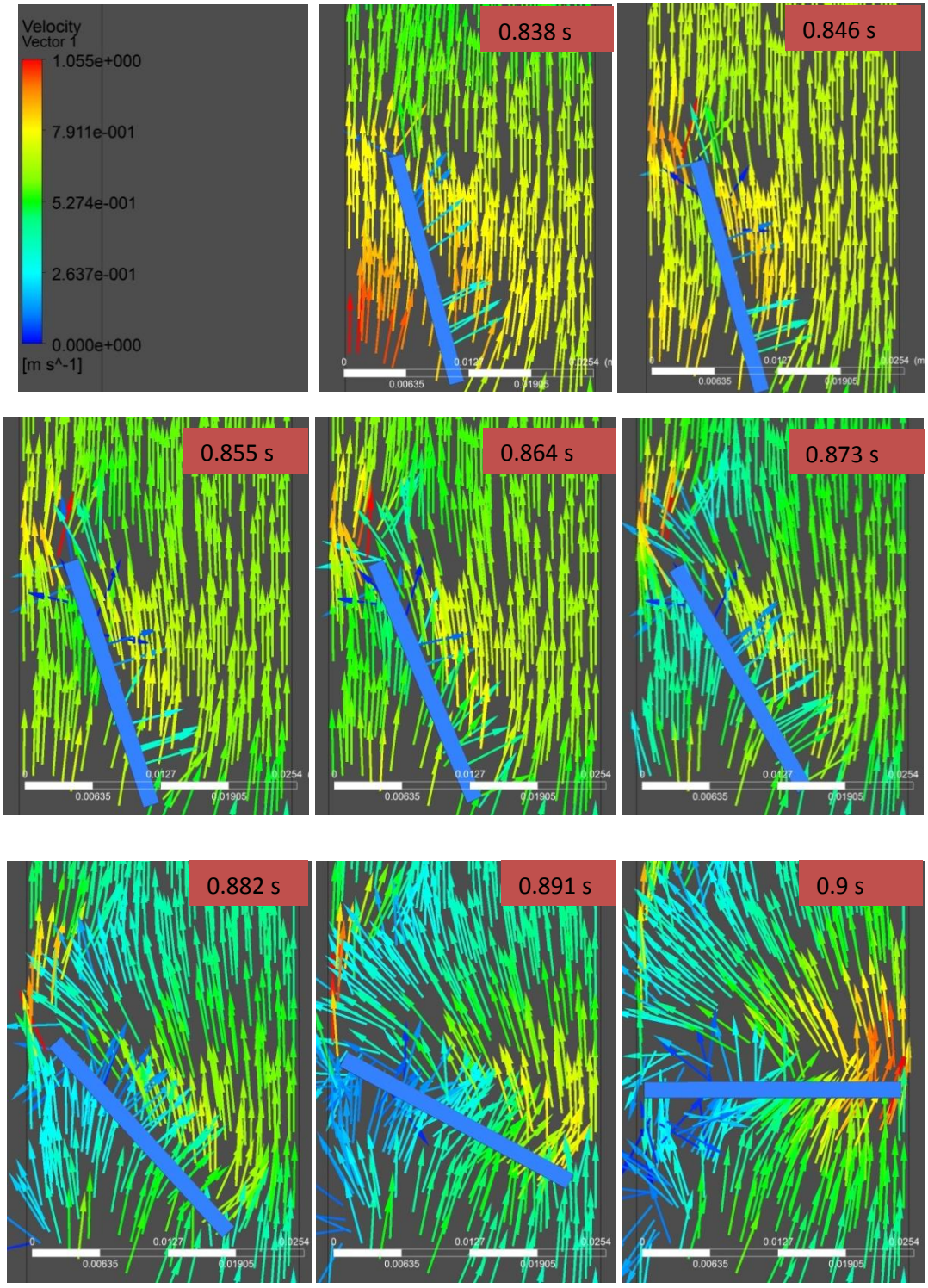

Figure 4.37 Velocity vectors in the valve region during late diastole when the monoleaflet inlet valve closes.

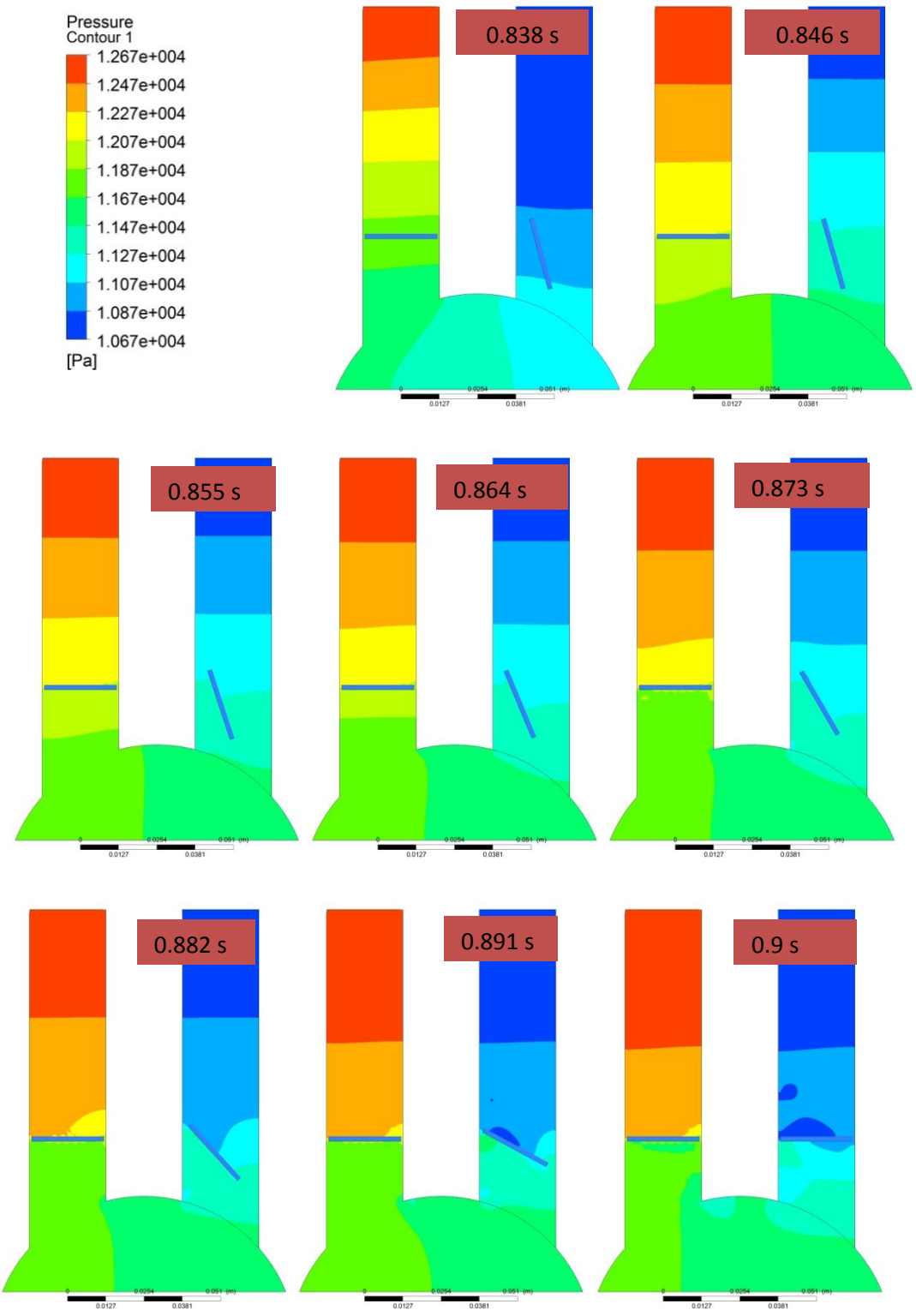

Figure 4.38 Pressure distribution for the monoleaflet inlet valve closing.

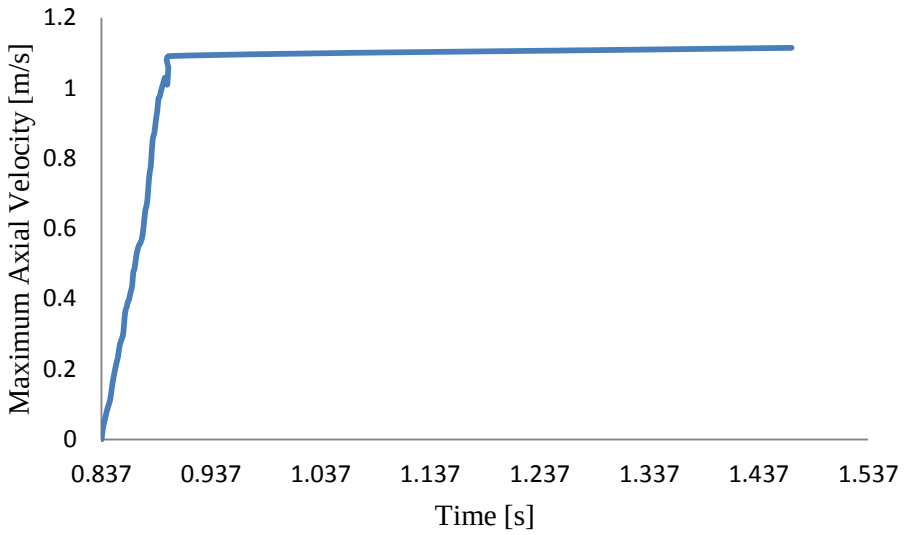

Figure 4.39 Maximum backflow velocity versus time for the monoleaflet inlet valve closing measured on XY plane in the inlet tube.

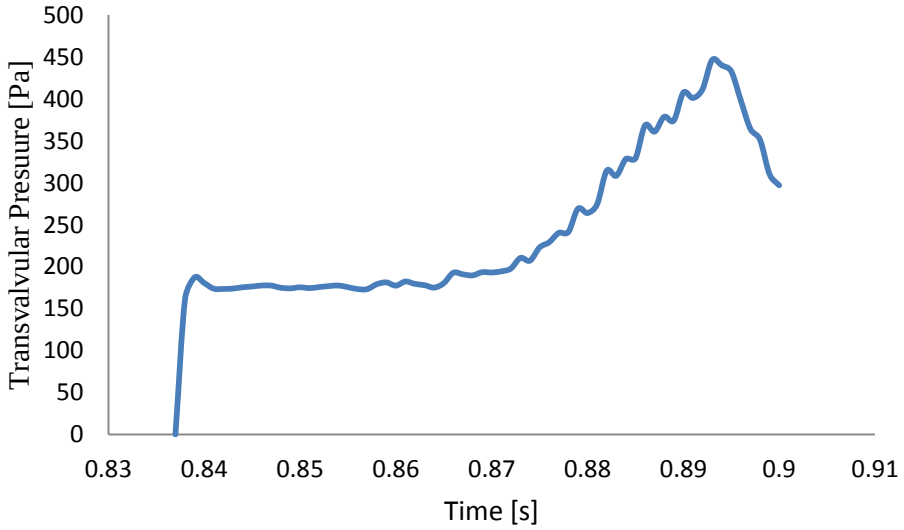

Figure 4.40 Transvalvular pressure versus time for the monoleaflet inlet valve closing measured as the difference between average pressures on two planes 0.02 m apart before and after the valve.

4.2 3D MODEL

4.2.1 THE BILEAFLET VALVE

4.2.1.1 THE BILEAFLET OUTLET VALVE OPENING

Flow conditions in the flow chamber with the bileaflet heart valve during systole were calculated with the valve opening and closing angles being at 85° and 25° respectively. Table 4.9 lists the maximum velocity, and mean and the maximum transvalvular pressures across the outlet valve during systole. Transvalvular pressure was defined as the difference between average pressure on two planes 0.02 m apart, before and after the valve. Figure 4.41 depicts velocity distribution through systole. Figure 4.42 shows velocity vectors in the vicinity of the valve. Figures 4.43 and 4.44 depict pressure distribution through systole. Figure 4.45 shows the computed leaflet position as a function of time for the 3D simulation. Euler Angle (Z), as it was explained in chapter III, was a representative for the opening angel (Θ) in radians. It took 0.022 sec for the valve to reach its fully opened position. When the valve was open, flow separated around the valve leaflets, rushing into three orifice areas. A recirculation zone developed approximately 10 mm in the outlet channel before the valve, due to the velocity gradient. Most of the flow passed through the left lateral orifice due to the skewed flow profile (Figure 4.41). The maximum velocity was 1.391 m/sec, occurring at the instant of valve opening (t = 0.004 s, Figure 4.42). Figure 4.43 shows the changes in pressure distribution in the model during systole. The mean transvalvular pressure was 117.716 Pa (Figure 4.43) which is less than the in vivo mean pressure gradient across the St. Jude Medical valves in aortic position (Δp mean = 586.61 Pa) measured by Laske et al.[66]. The maximum transvalvular pressure was 12000 Pa (Figure 4.21) which occurred right before valve opening (t = 0.001 s). In the study by Laske et al, the maximal pressure gradient at the moment of valve opening was 2199.81 Pa. In here, the calculated EOA was equal to 1.96 cm^2.

Table 4.9 the bileaflet outlet valve opening behavior for 85 degrees of opening angle

Parameter	Value
Maximum Velocity	1.391 m/s
Maximum Pressure Drop Across the Valve	12000 Pa
Average Pressure Drop Across the Valve	117.716 Pa
Valve Opening Time	0.022 s
EOA	1.96 cm^2

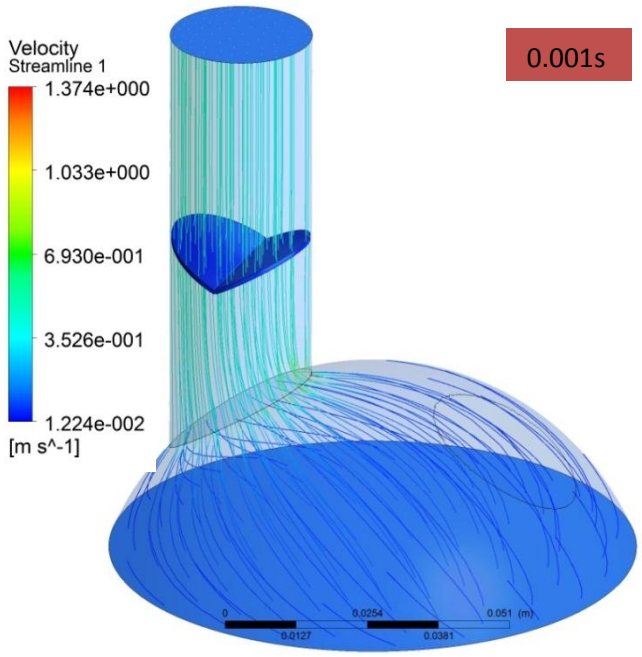
Velocity
Streamline 1
1.374e+000
1.033e+000
6.930e-001
3.526e-001
1.224e-002
[m s^-1]
0.001s
0
0.0254
0.051 (m)
0.0127
0.0381

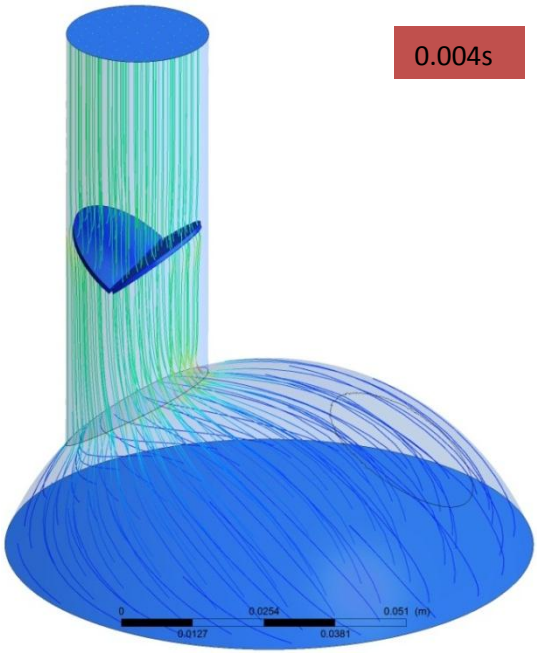
0.004s
0
0.0254
0.051 (m)
0.0127
0.0381

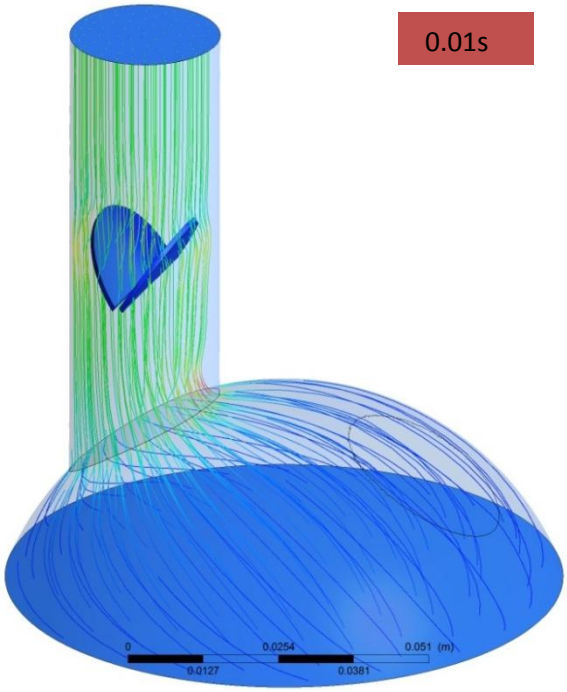
0.01s
0
0.0254
0.051 (m)
0.0127
0.0381

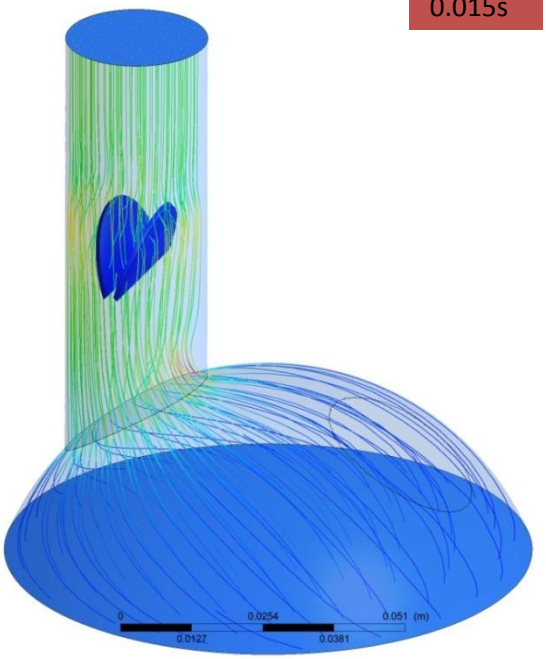
0.015s
0
0.0254
0.051 (m)
0.0127
0.0381

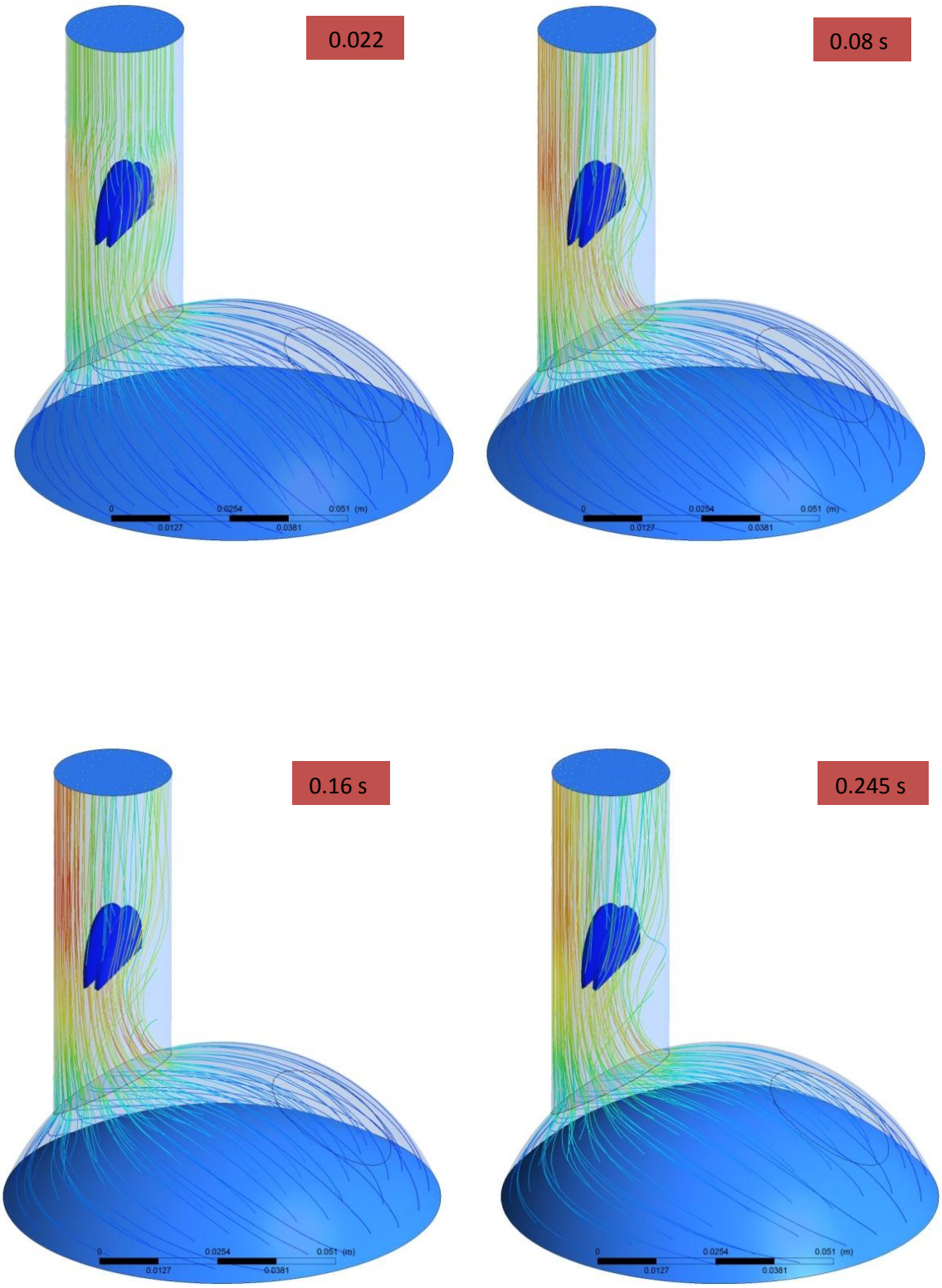

Figure 4.41 Velocity streamline during systole when the bileaflet valve opens.

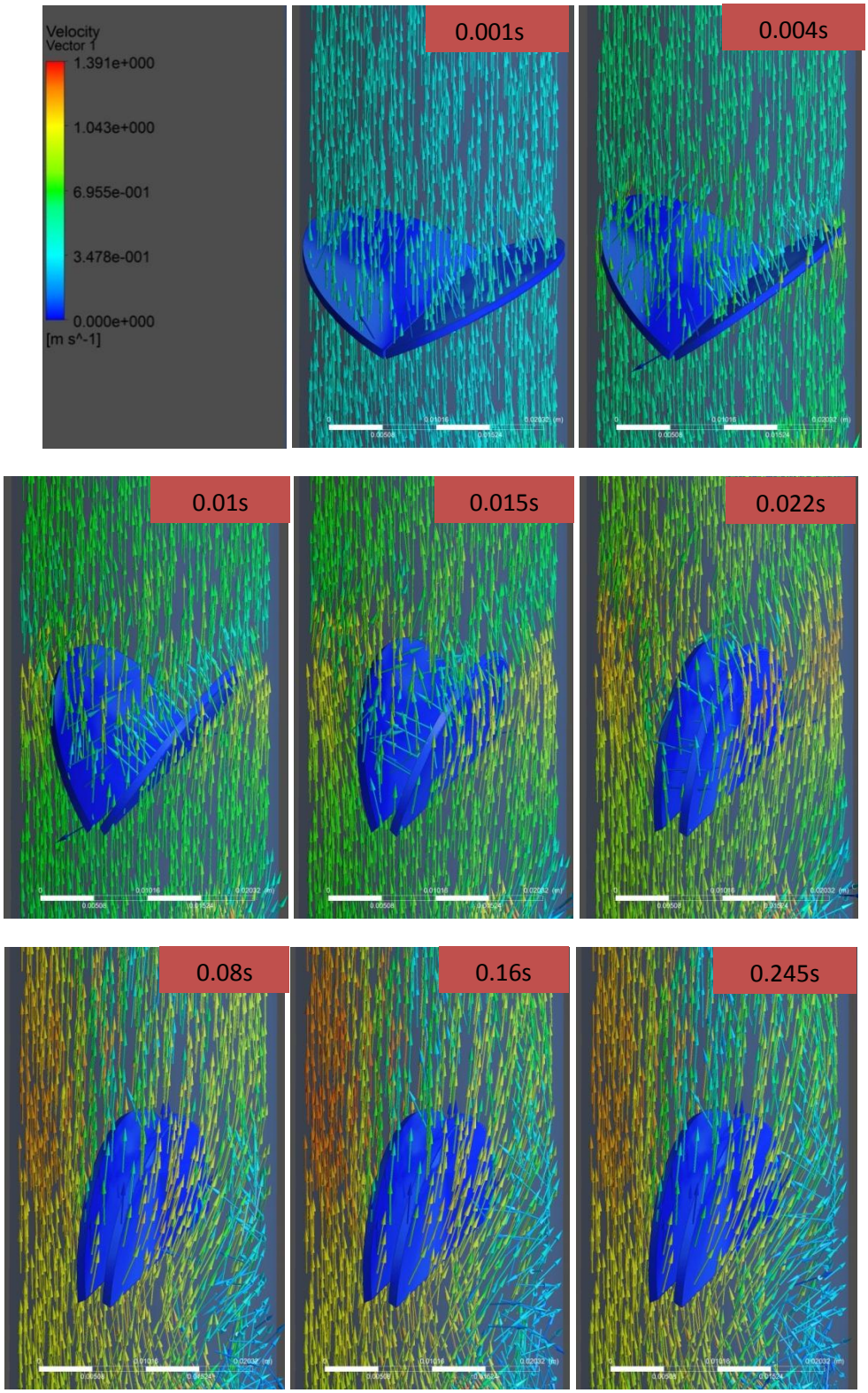

Figure 4.42 Velocity vectors during systole when the bileaflet valve opens.

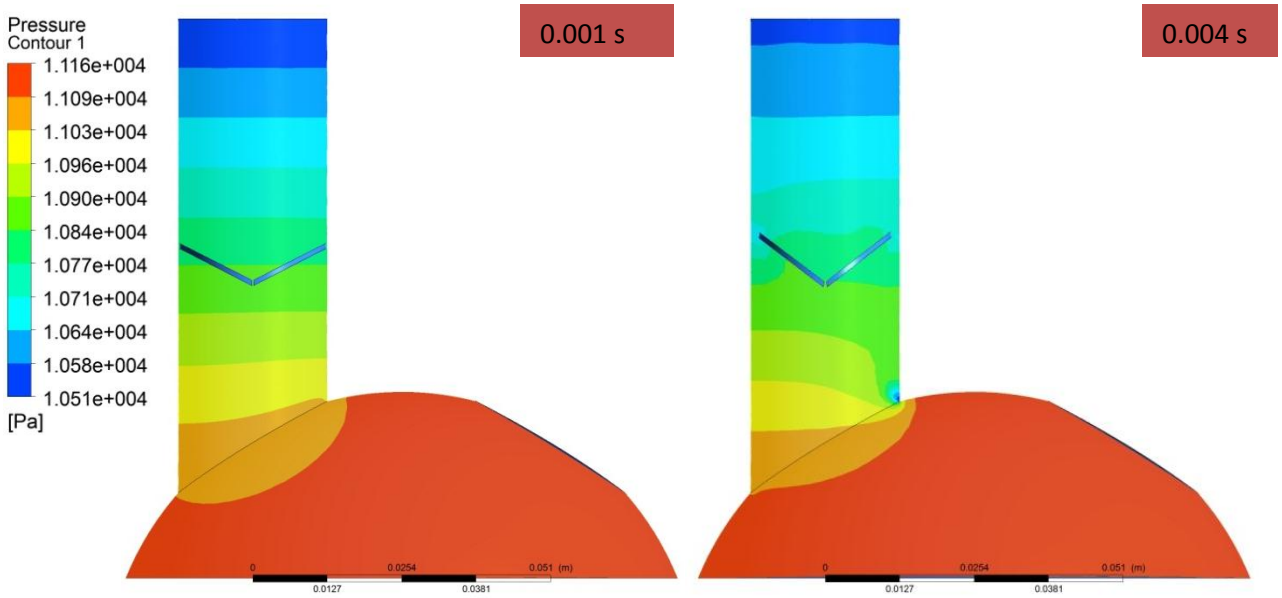
Pressure
Contour 1
1.116e+004
1.109e+004
1.103e+004
1.096e+004
1.090e+004
1.084e+004
1.077e+004
1.071e+004
1.064e+004
1.058e+004
1.051e+004
[Pa]
0.001 s
0.004 s
0
0.0254
0.051 (m)
0.0127
0.0381

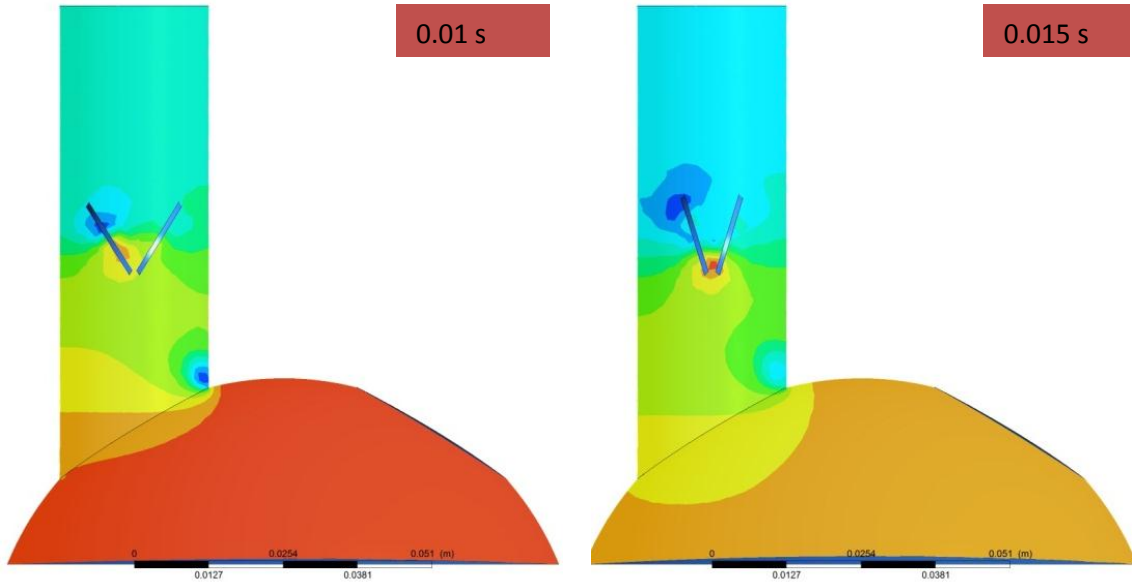
0.01 s
0.015 s
0
0.0254
0.051 (m)
0.0127
0.0381

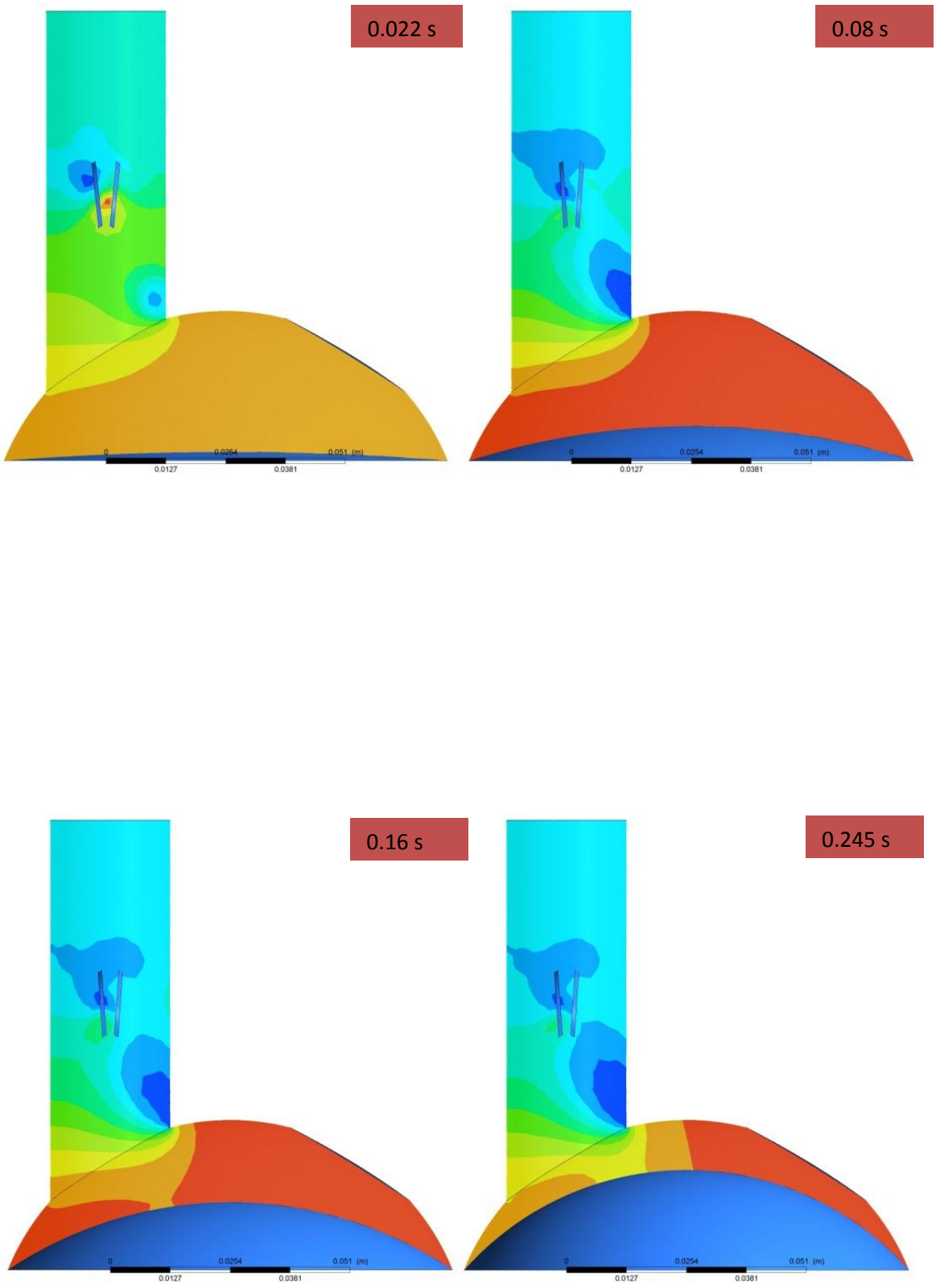

Figure 4.43 Pressure distribution during systole when the bileaflet valve opens (opening angle = 85^{o})

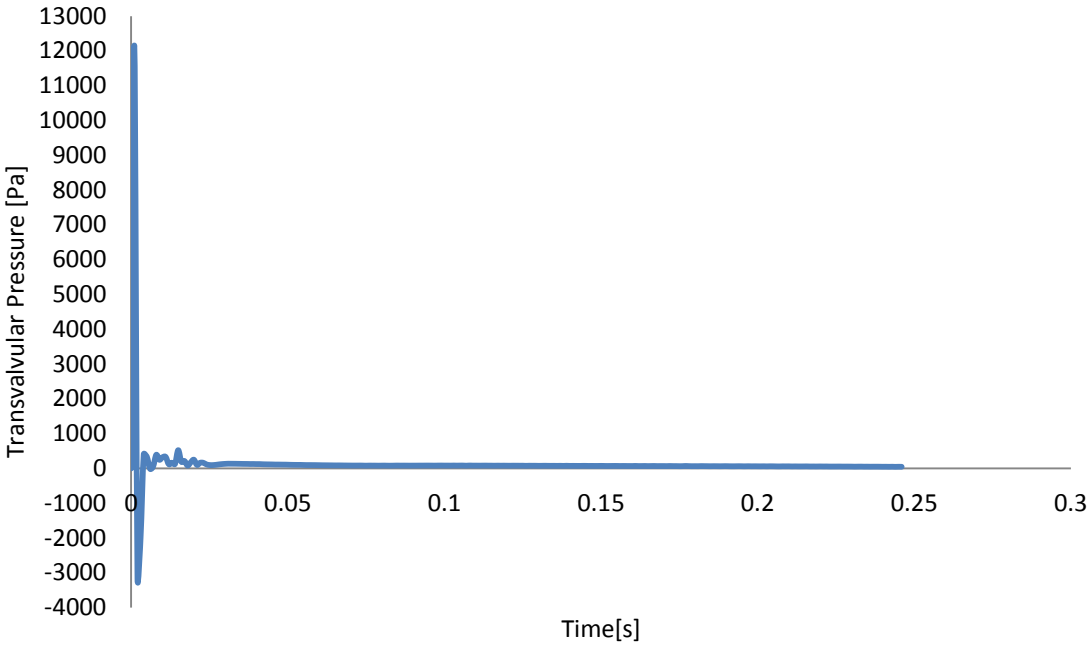

Figure 4.44 Transvalvular pressure versus time for the bileaflet outlet valve opening measured as the difference between average pressure on two planes 0.02 m apart, before and after the valve.

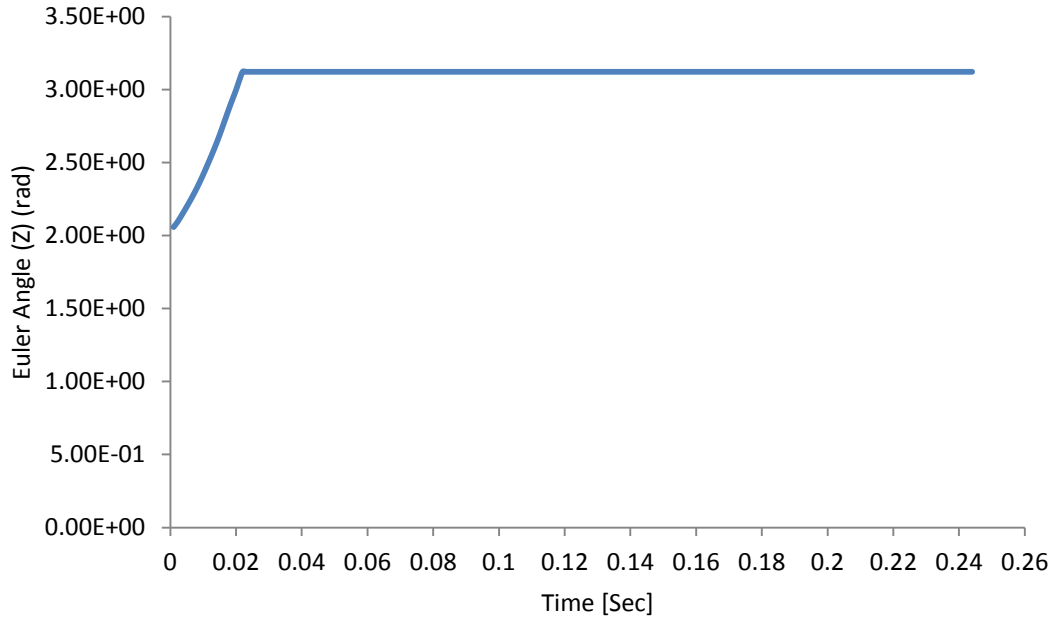

Figure 4.45 The bileaflet outlet valve opening angle (in terms of Euler angle (z)) versus time.

4.2.1.2 THE BILEAFLET OUTLET VALVE CLOSING

Table 4.10 lists the maximum velocity and pressure conditions during the outlet valve closure, when the opening and closing angles were 85° and 25° respectively. In this table, transvalvular pressure was defined as the difference between average pressure on two planes 0.02 m apart, before and after the valve. Figure 4.46 depicts velocity distribution through diastole. Figure 4.47 shows velocity vectors in the vicinity of the valve. Figures 4.48 and 4.49 depict pressure distribution through systole. It took 0.038 sec for the valve to reach the closing position (to reach from 85° to 25°). The maximum backflow velocity was 2.315 m/sec at the beginning of valve closure (t = 0.25 s). A region of high velocity flow (squeeze flow) developed in the gap between the right leaflet and the wall. The mean transvalvular pressure was 1251.29 Pa. All figures reveal the nonsymmetric closing behavior of the leaflets (i.e. the left leaflet stayed at the maximal opening angle at the beginning of the diastole while the right leaflet closed early).

Table 4.10 the bileaflet outlet valve closing behavior for 85 degrees of opening angle

Parameter	Value
Maximum backflow Velocity	-2.315 m/s
Maximum Pressure Drop Across the Valve	63790 Pa
Average Pressure Drop Across the Valve	1251.29 Pa
Valve Closing Time	0.038 s

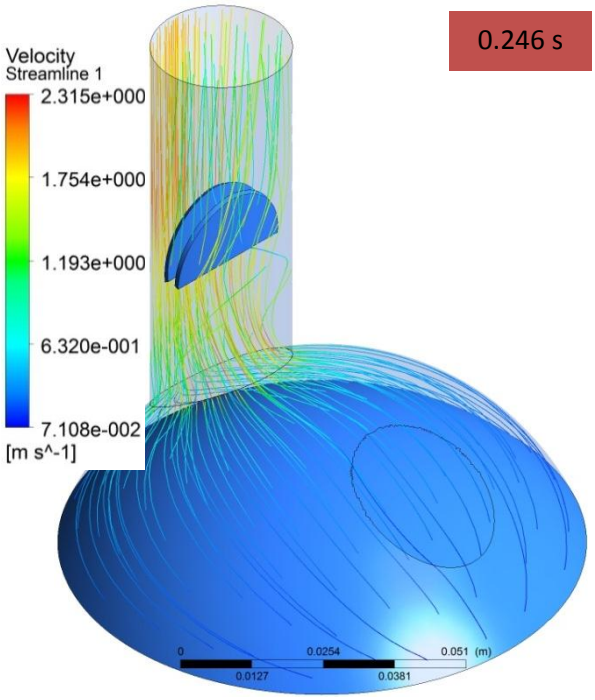

0.246 s

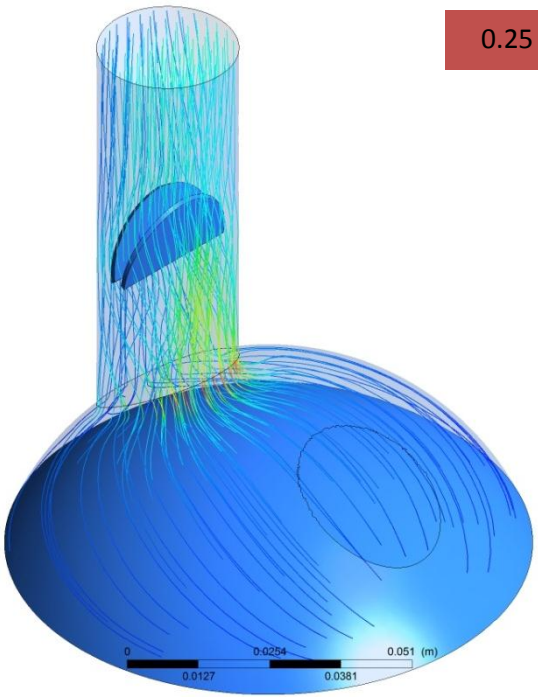

0.25 s

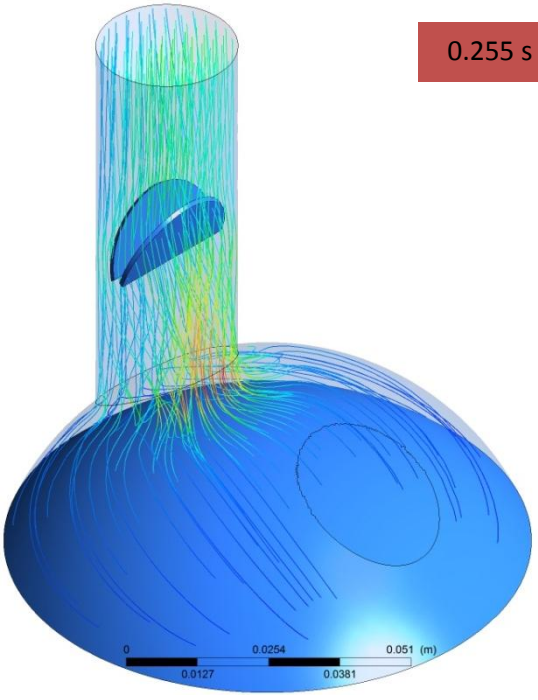

0.255 s

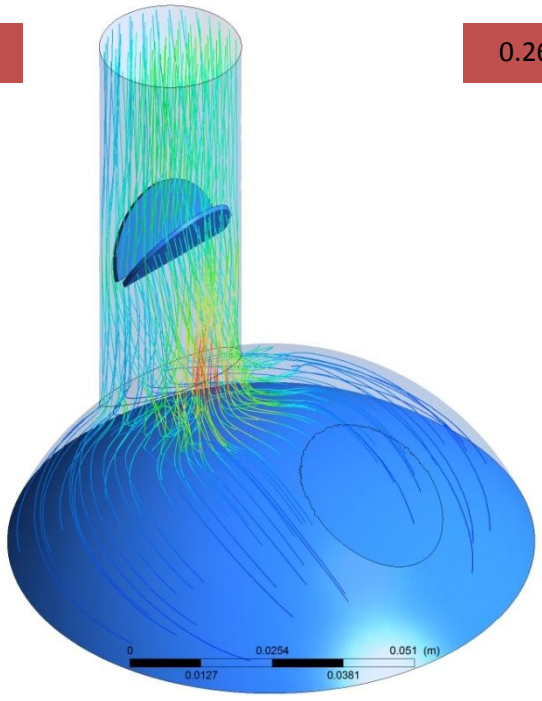

0.26 s

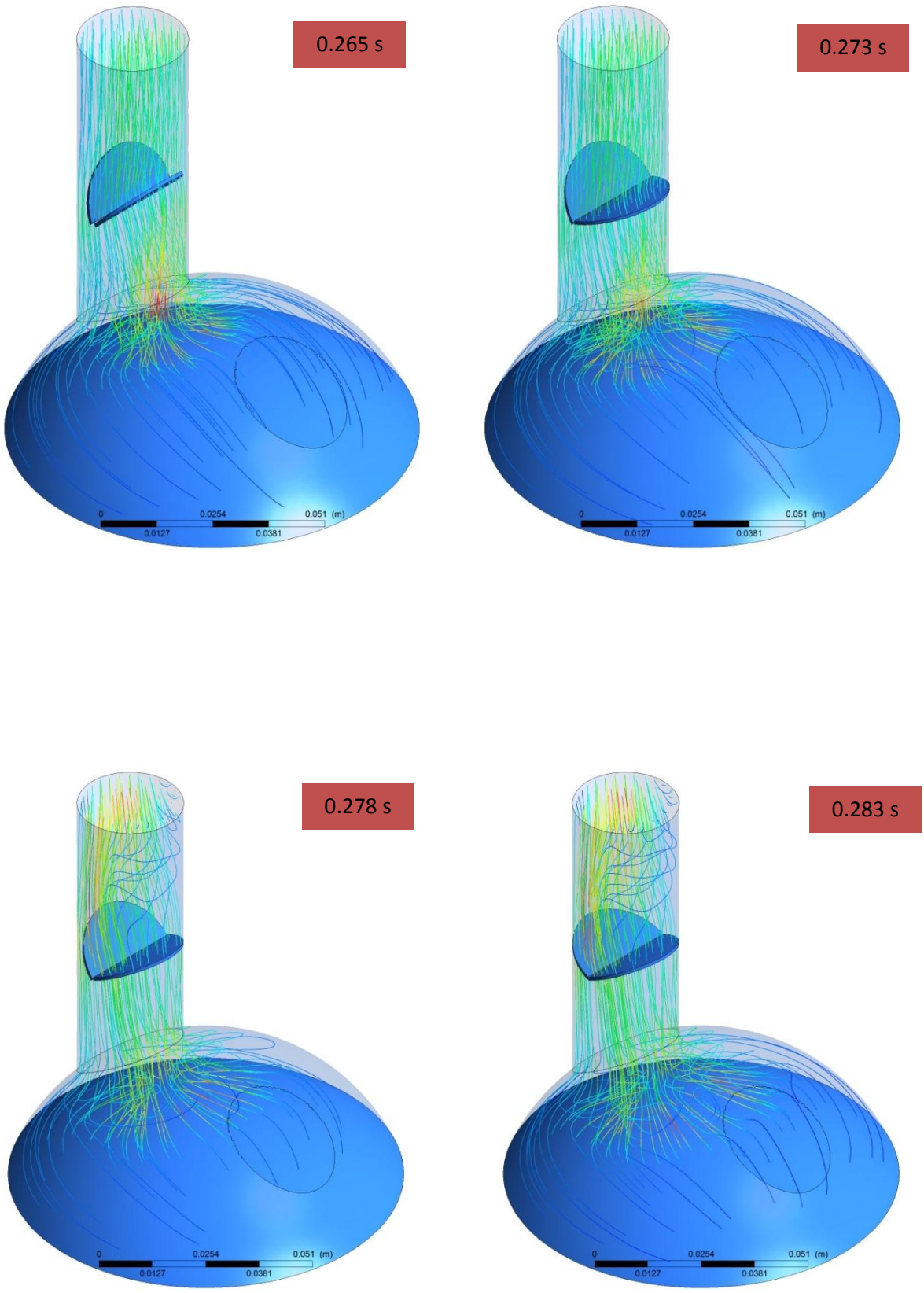

Figure 4.46 Velocity streamline for the bileaflet outlet valve closing (opening angle = 85^{O})

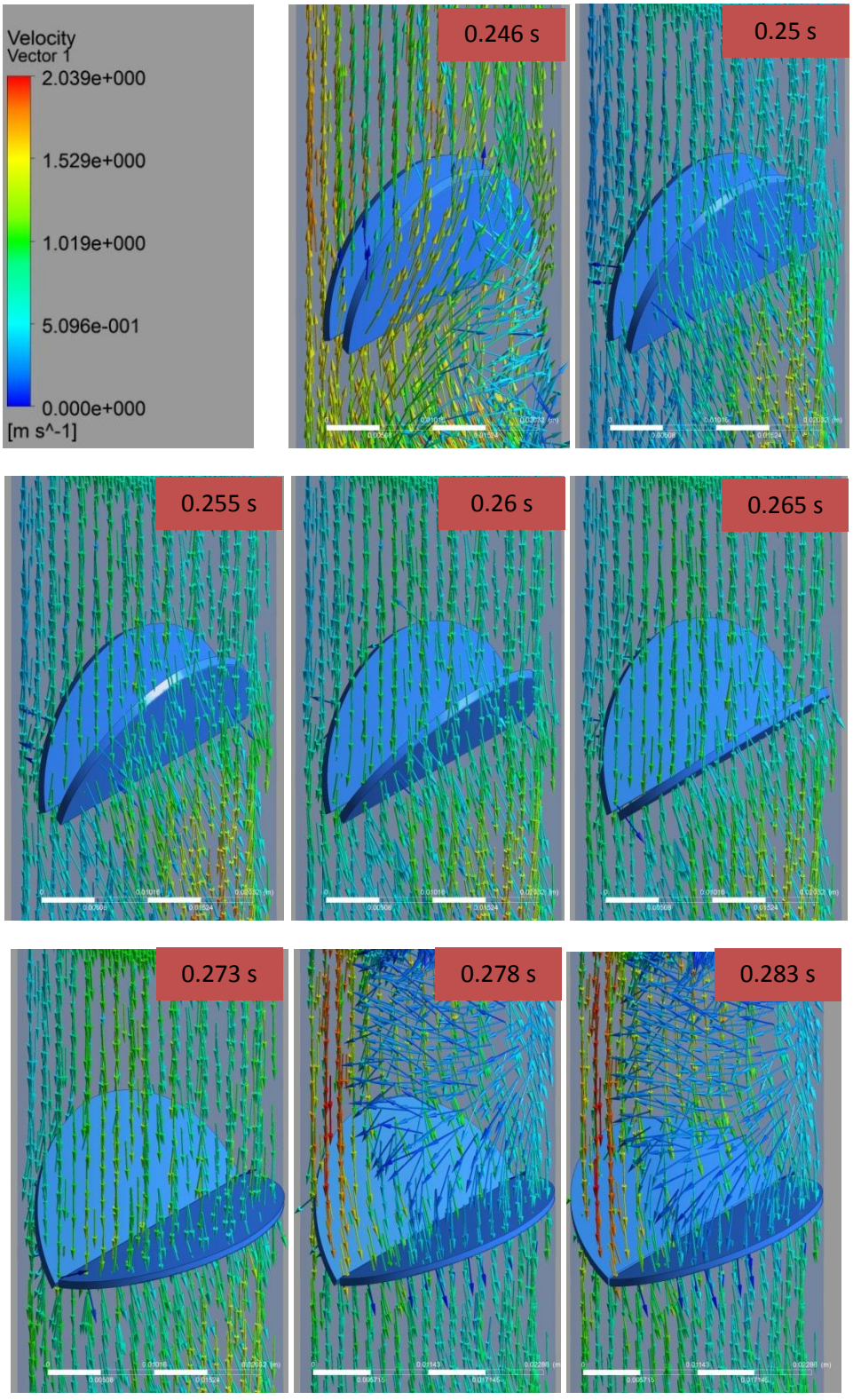

Figure 4.47 Velocity vectors in the bileaflet valve region during valve closure.

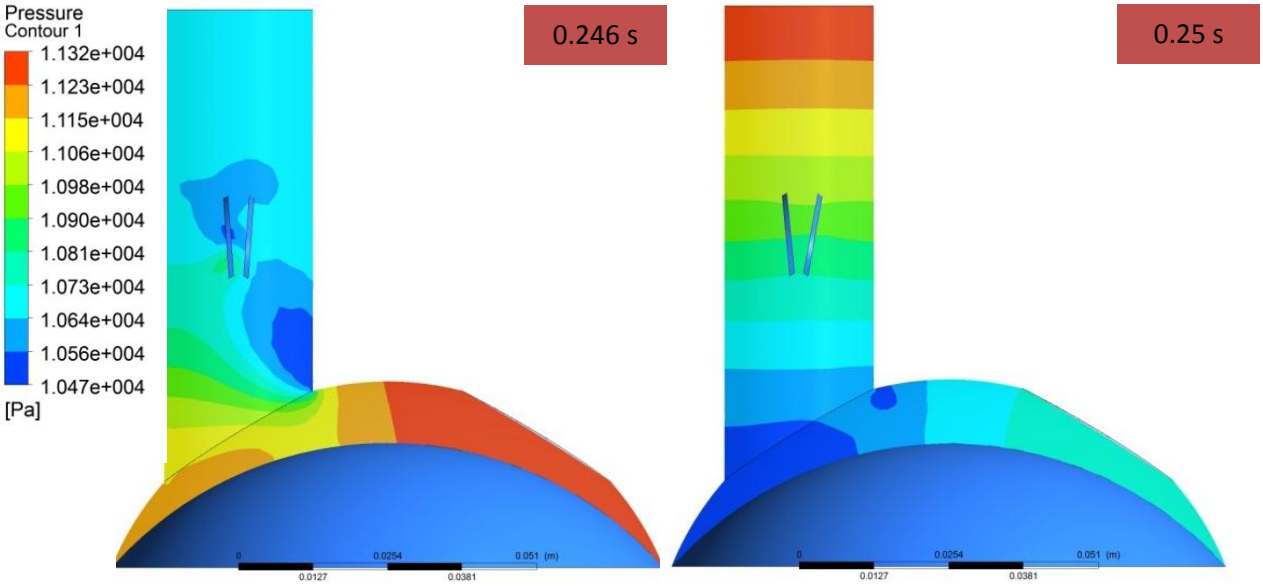
Pressure
Contour 1
1.132e+004
1.123e+004
1.115e+004
1.106e+004
1.098e+004
1.090e+004
1.081e+004
1.073e+004
1.064e+004
1.056e+004
1.047e+004
[Pa]
0.246 s
0.25 s
0
0.0254
0.051 (m)
0.0127
0.0381

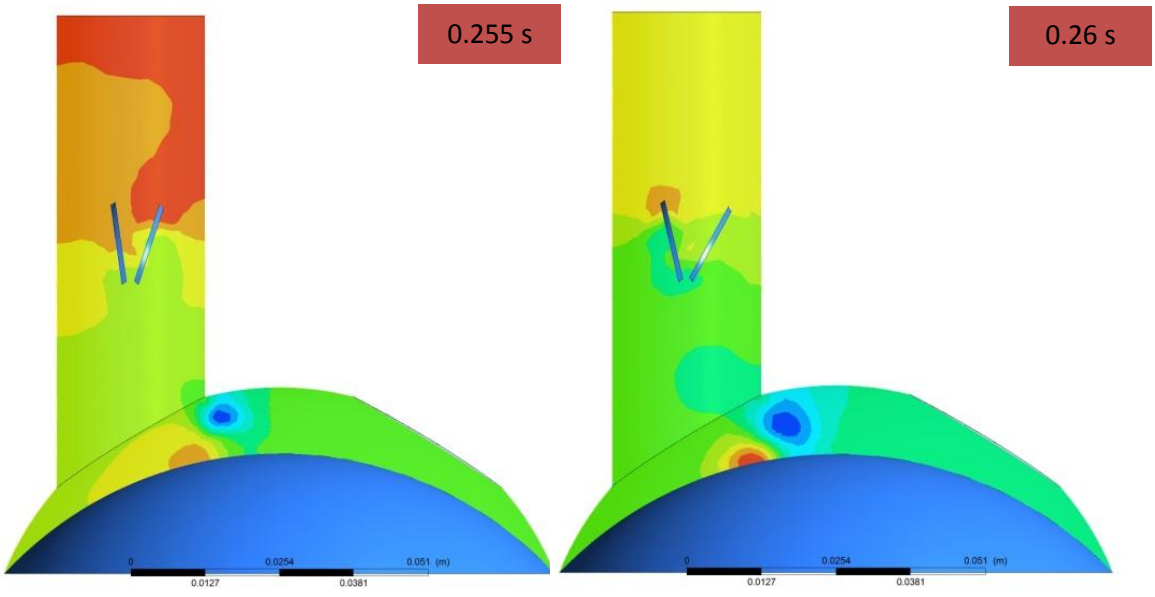
0.255 s
0.26 s
0
0.0254
0.051 (m)
0.0127
0.0381

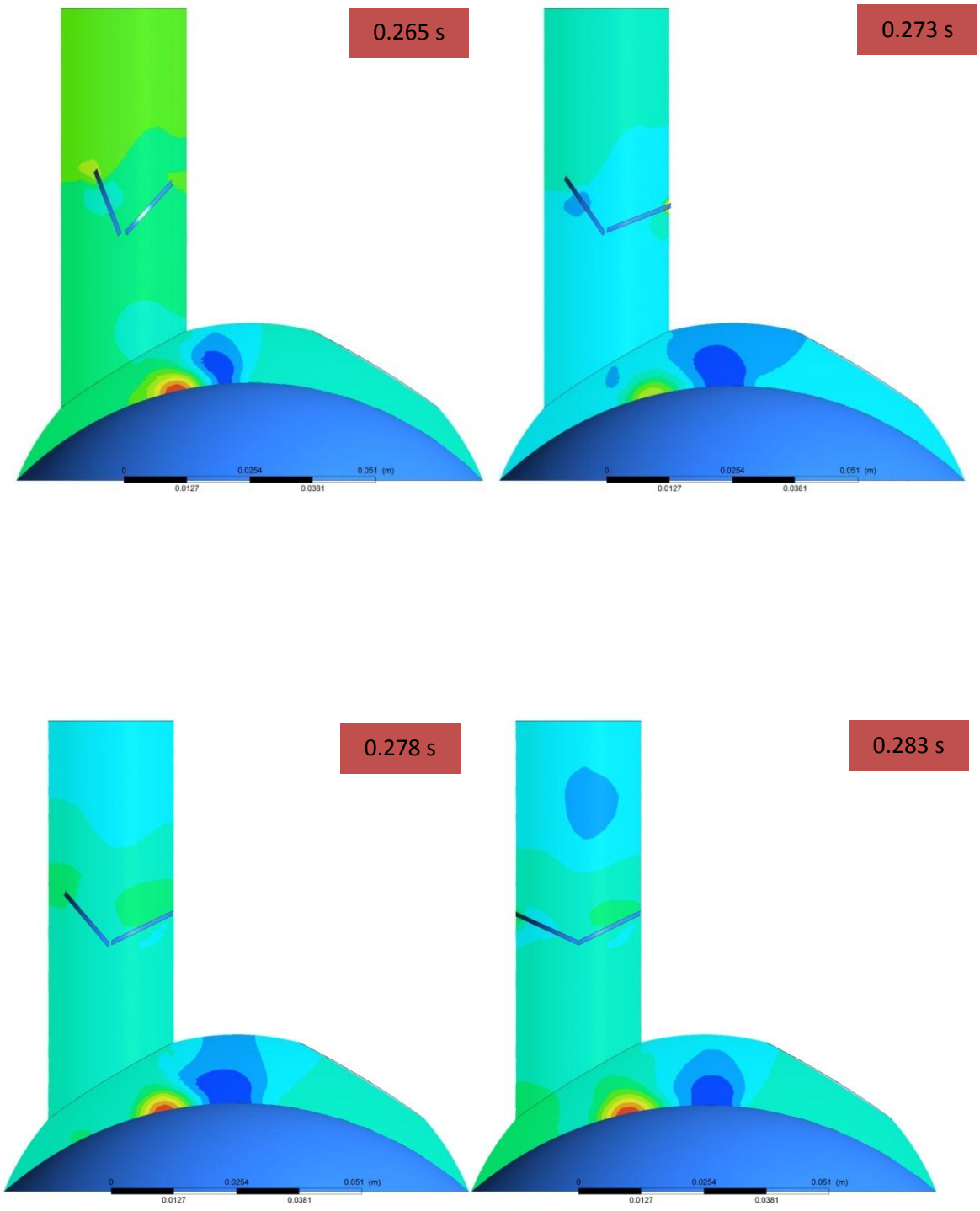

Figure 4.48 pressure distribution for the bileaflet outlet valve closing (opening angle = 85^{O})

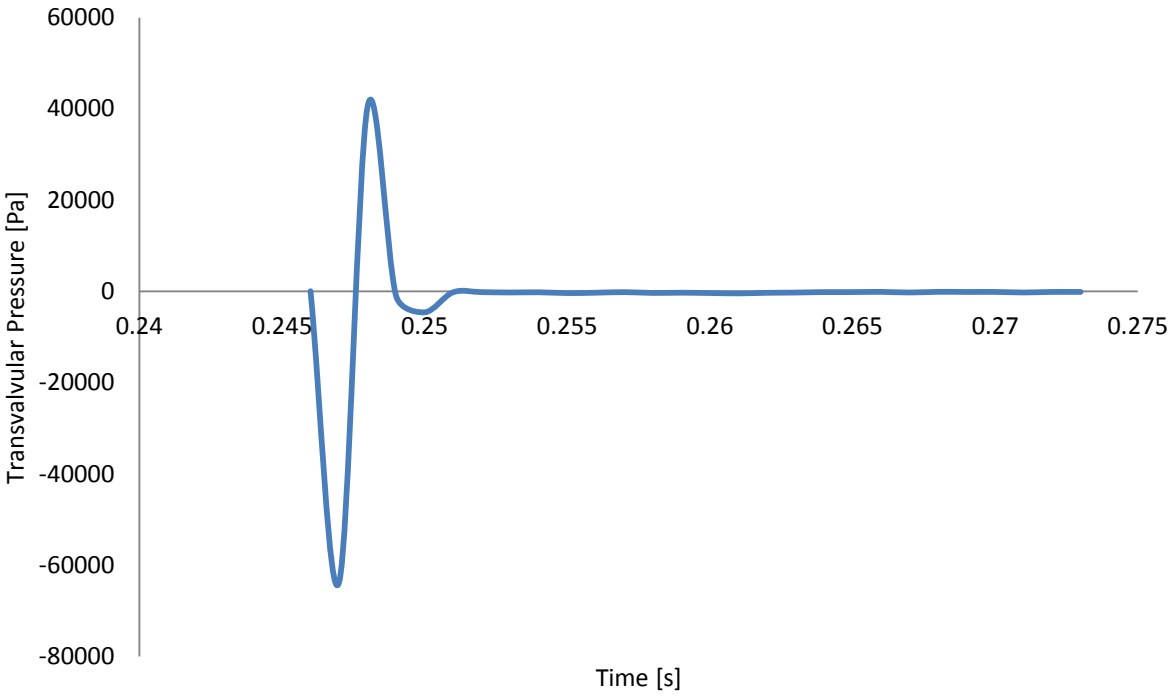

Figure 4.49 Transvalvular pressure versus time for the bileaflet outlet valve closing measured as the difference between average pressure on two planes 0.02 m apart, before and after the valve.

4.2.1.3 BILEAFLET INLET VALVE OPENING BEHAVIOR

Table 4.11 lists the maximum velocity and pressure conditions during the inlet valve opening. Transvalvular pressure was defined as the difference between average pressure on two planes 0.02 m apart, before and after the valve. Figure 4.50 depicts velocity distribution through diastole. Figure 4.51 shows velocity vectors in the vicinity of the valve. Figures 4.52 and 4.53 depict pressure distribution through diastole. It took 0.03 sec for the valve to reach the opening position (to reach from 0° to 85^{o}). Maximum velocity was 2.158 m/s in downward direction, at the end of diastole (t=0.85). The mean transvalvular pressure was 506.273 Pa. The value for mean pressure gradient was in agreement with what reported by Zoghbe et al.[67], that the mean pressure gradient across the mitral valve during diastole was less than 666.61 Pa. Figure 4.53 shows that the maximum transvalvular pressure was 2200 Pa, occurring at the instant of valve opening.

Table 4.11 the bileaflet inlet valve opening behavior with 85° opening angle

Parameter	Value
Maximum Velocity	-2.158
Maximum Pressure Drop Across the Valve	-2200
Average Pressure Drop Across the Valve	-506.273
Valve Opening Time	0.03

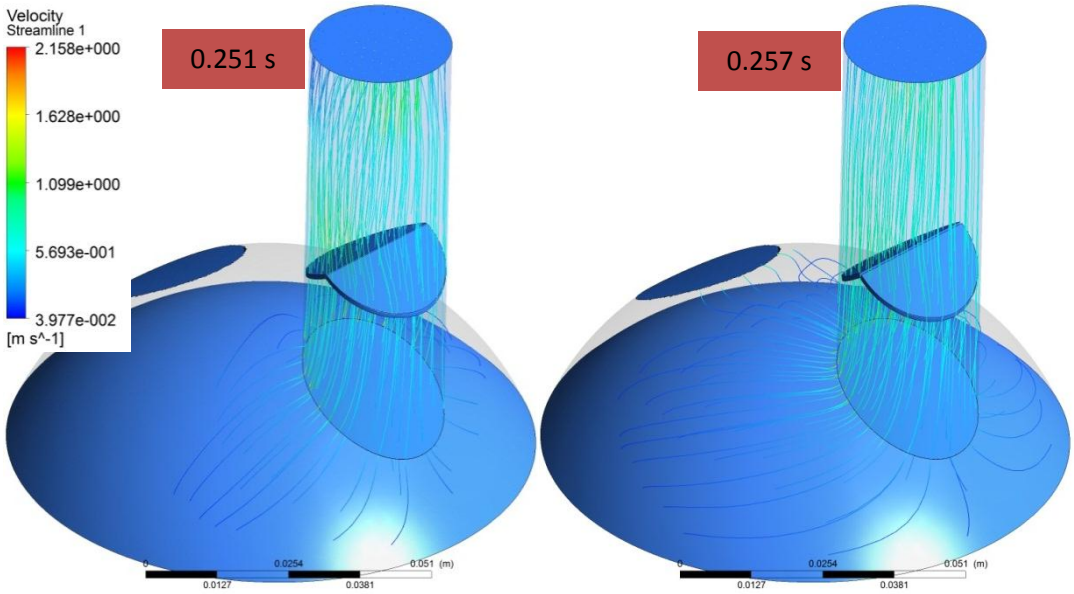
Velocity
Streamline 1
2.158e+000
1.628e+000
1.099e+000
5.693e-001
3.977e-002
[m s^-1]
0.251 s
0.257 s
0.0254
0.051 (m)
0.0127
0.0381

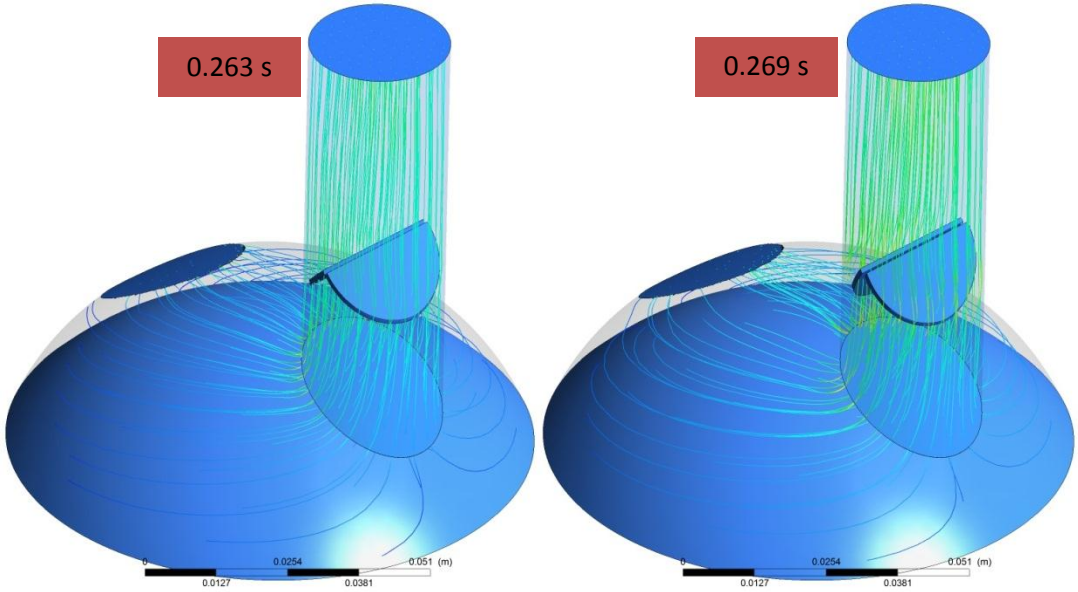
0.263 s
0.269 s
0.0254
0.051 (m)
0.0127
0.0381

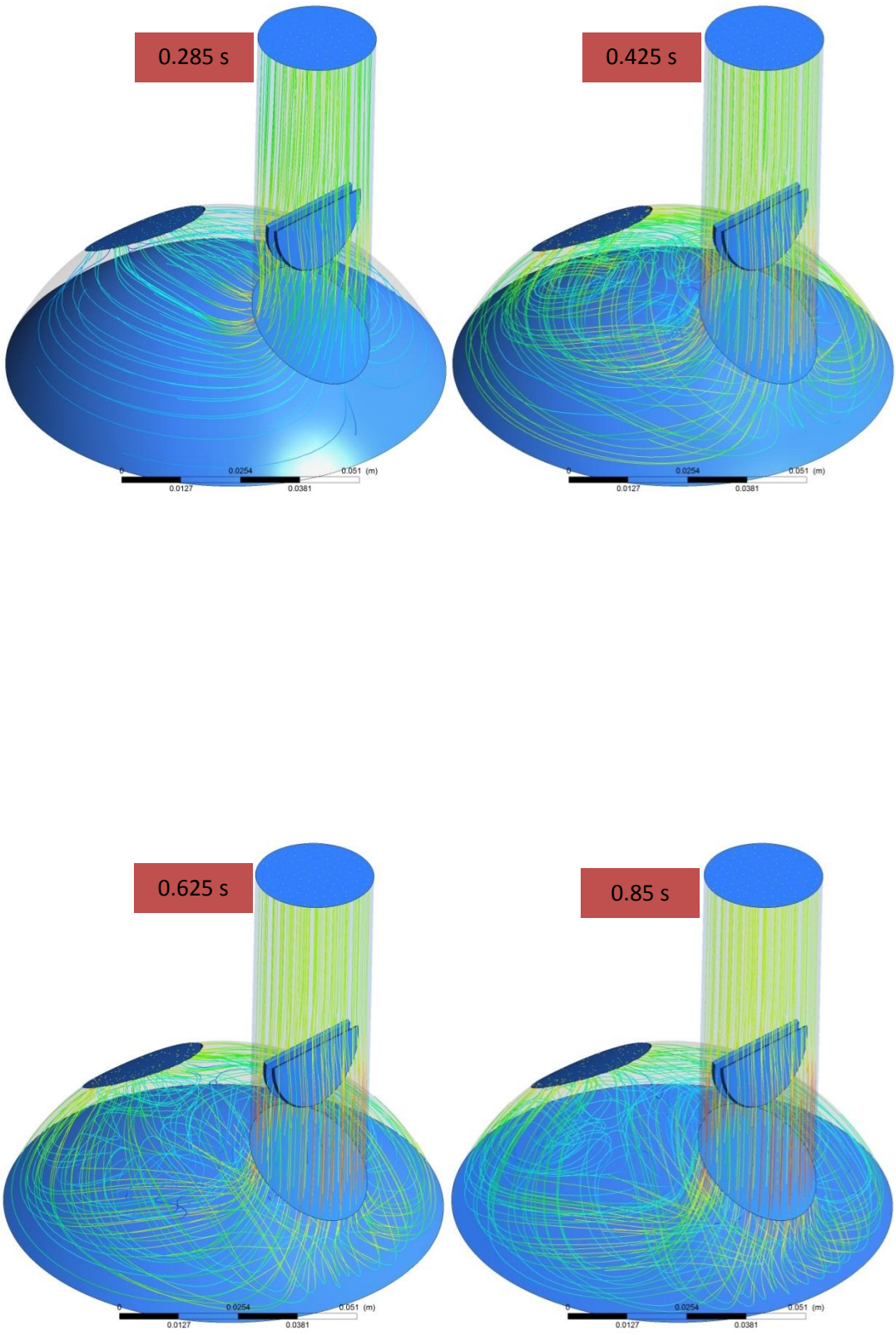

Figure 4.50 Velocity streamline for the bileaflet outlet valve closing (opening angle = 85^{O})

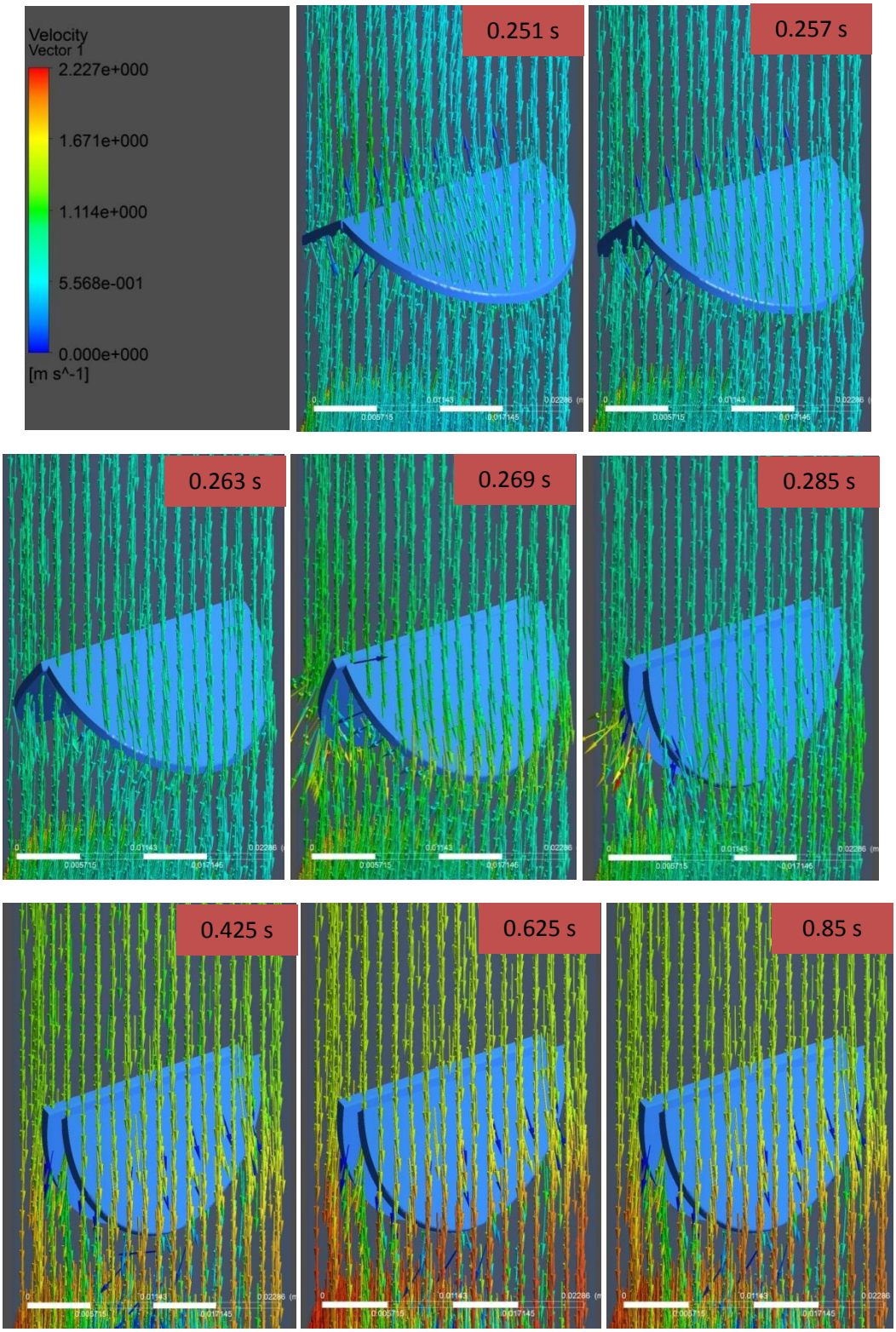

Figure 4.51 Velocity vectors in the bileaflet valve region during valve closure.

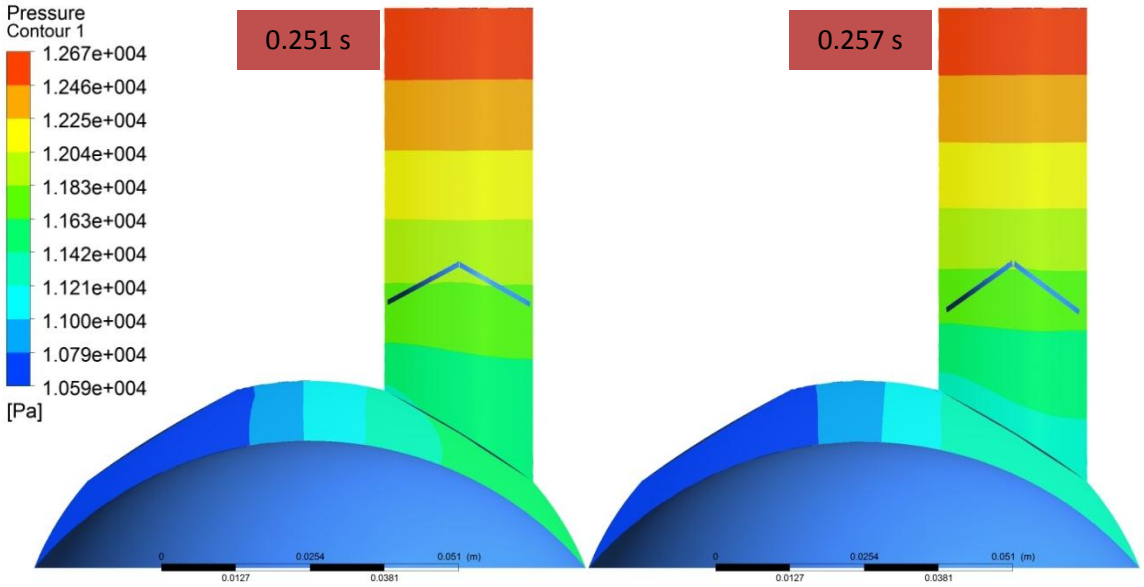
Pressure
Contour 1
1.267e+004
1.246e+004
1.225e+004
1.204e+004
1.183e+004
1.163e+004
1.142e+004
1.121e+004
1.100e+004
1.079e+004
1.059e+004
[Pa]
0.251 s
0.257 s
0
0.0254
0.051 (m)
0.0127
0.0381

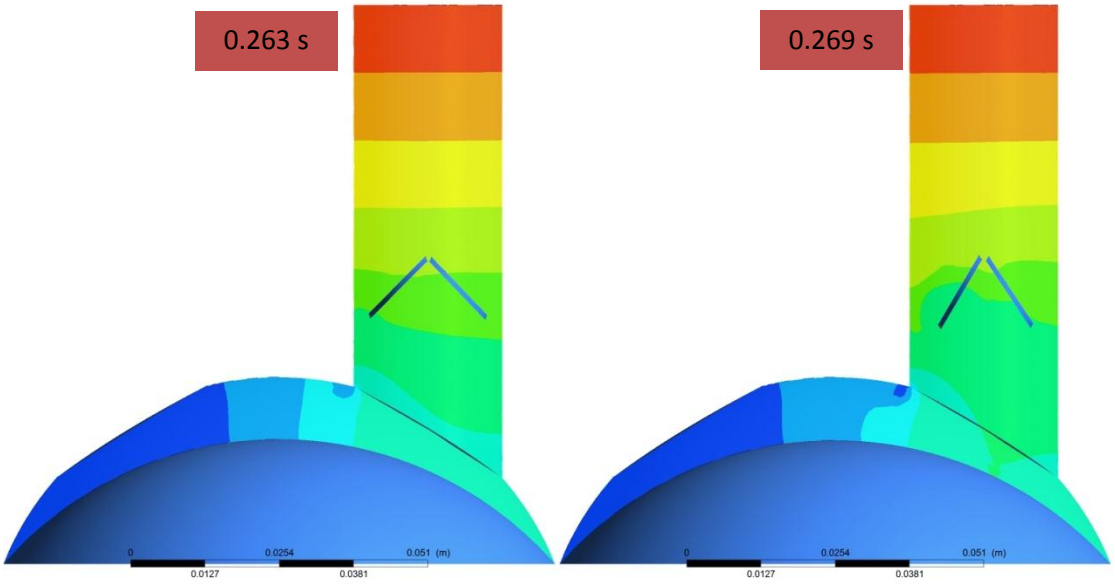
0.263 s
0.269 s
0
0.0254
0.051 (m)
0.0127
0.0381

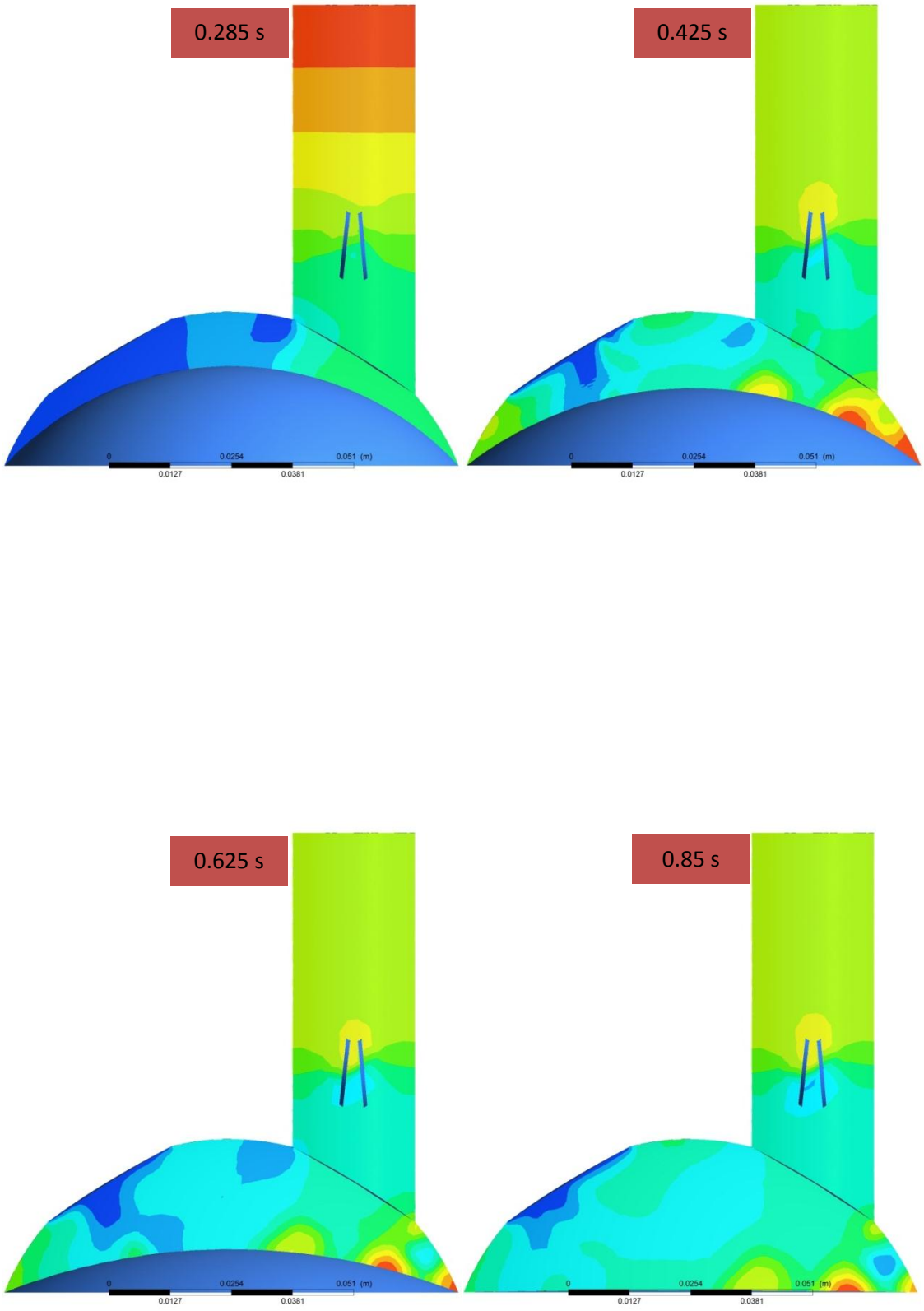

Figure 4.52 pressure distribution for the bileaflet outlet valve closing (opening angle = 85^{O})

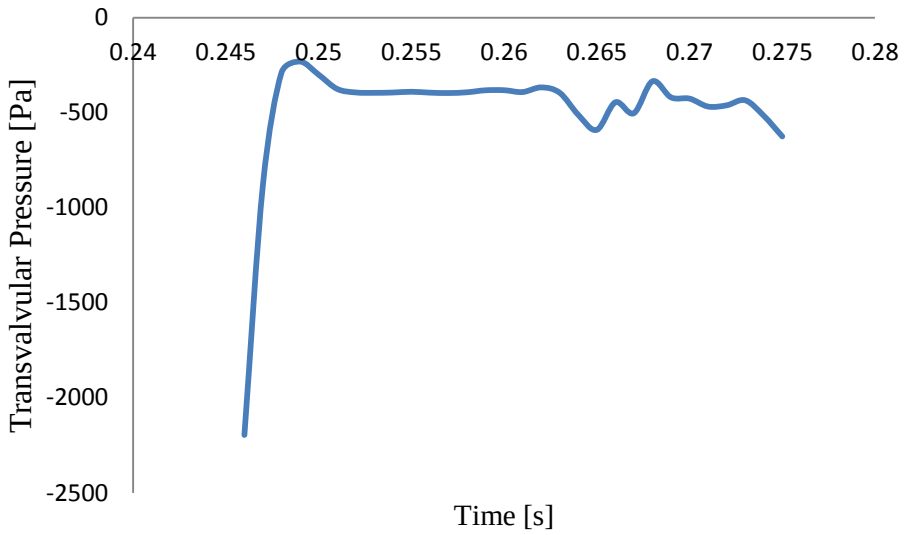

Figure 4.53 Transvalvular pressure versus time for the bileaflet outlet valve closing measured as the difference between average pressure on two planes 0.02 m apart, before and after the valve.

4.2.1.4 BILEAFLET INLET VALVE CLOSING BEHAVIOR

Table 4.12 lists the maximum velocity and pressure conditions during the inlet valve closing. In this table, transvalvular pressure was defined as the difference between average pressure on two planes of 0.02 m apart, before and after the valve. Figure 4.54 depicts velocity distribution through late diastole. Figure 4.55 shows velocity vectors in the vicinity of the valve. Figures 4.56 and 4.57 depict pressure distribution through late diastole. It took 0.04 sec for the valve to reach the fully closed position (to reach from 85° to 0°). The maximum velocity in the valve region reached 1.28 m/s at the instant of valve closure (t = 0.9 s). Figure 4.57 shows the pressure distribution in the model during the valve closure. The mean transvalvular pressure was 473.548 Pa. The maximum transvalvular pressure was 700 Pa which occurred at the end of valve closure process (t = 0.9 s).

Table 4.12 Flow parameters related to the bileaflet inlet valve closing, when the opening angle was 85°.

Parameter	Value
Maximum Velocity m/s	1.28
Maximum Pressure Drop Across the Valve Pa	700
Average Pressure Drop Across the Valve Pa	473.548
Valve closing Time m/s	0.04

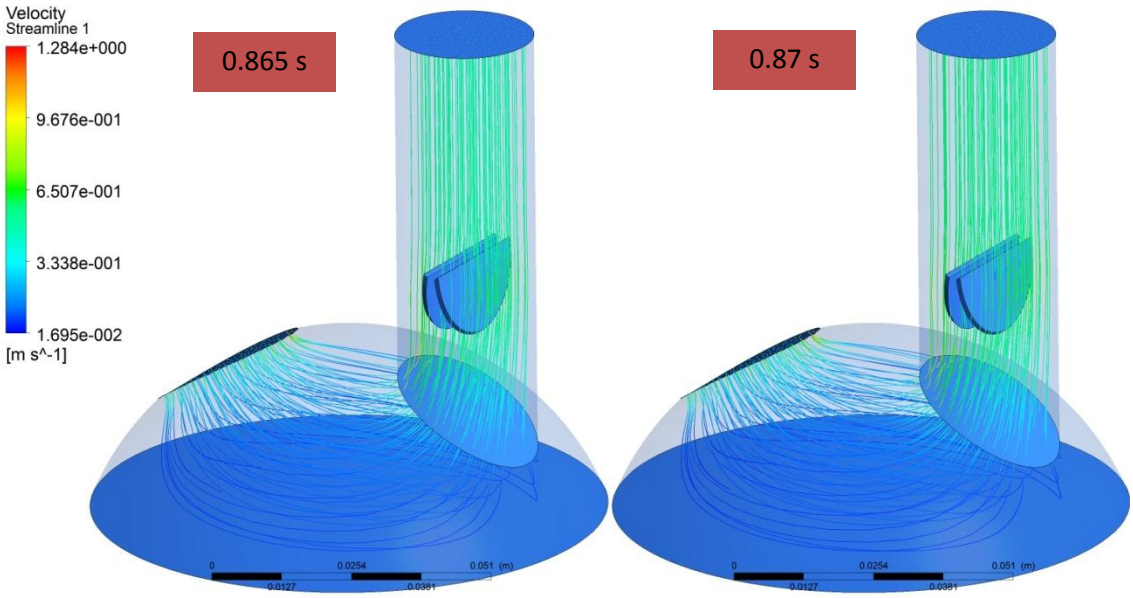
Velocity
Streamline 1
1.284e+000
9.676e-001
6.507e-001
3.338e-001
1.695e-002
[m s^-1]
0.865 s
0.87 s
0
0.0254
0.051 (m)
0.0127
0.0381

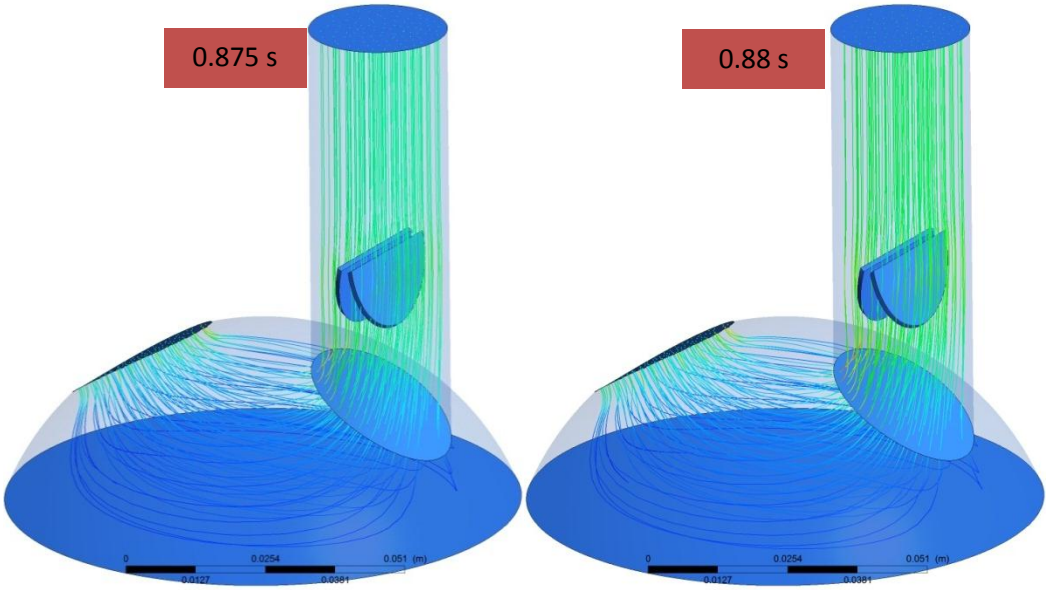
0.875 s
0.88 s
0
0.0254
0.051 (m)
0.0127
0.0381

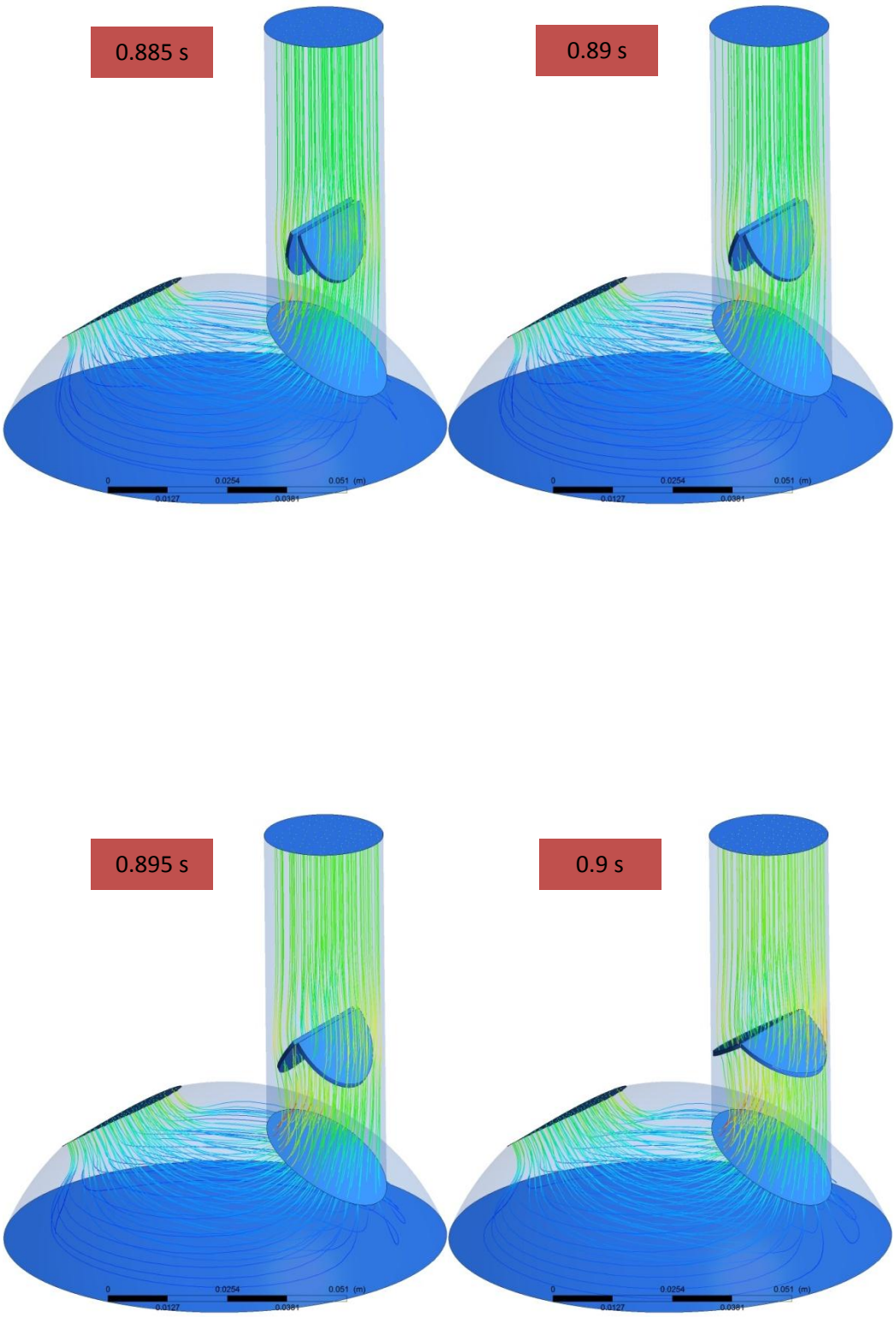

Figure 4.54 Velocity streamline for the bileaflet outlet valve closing (opening angle = 85^{O})

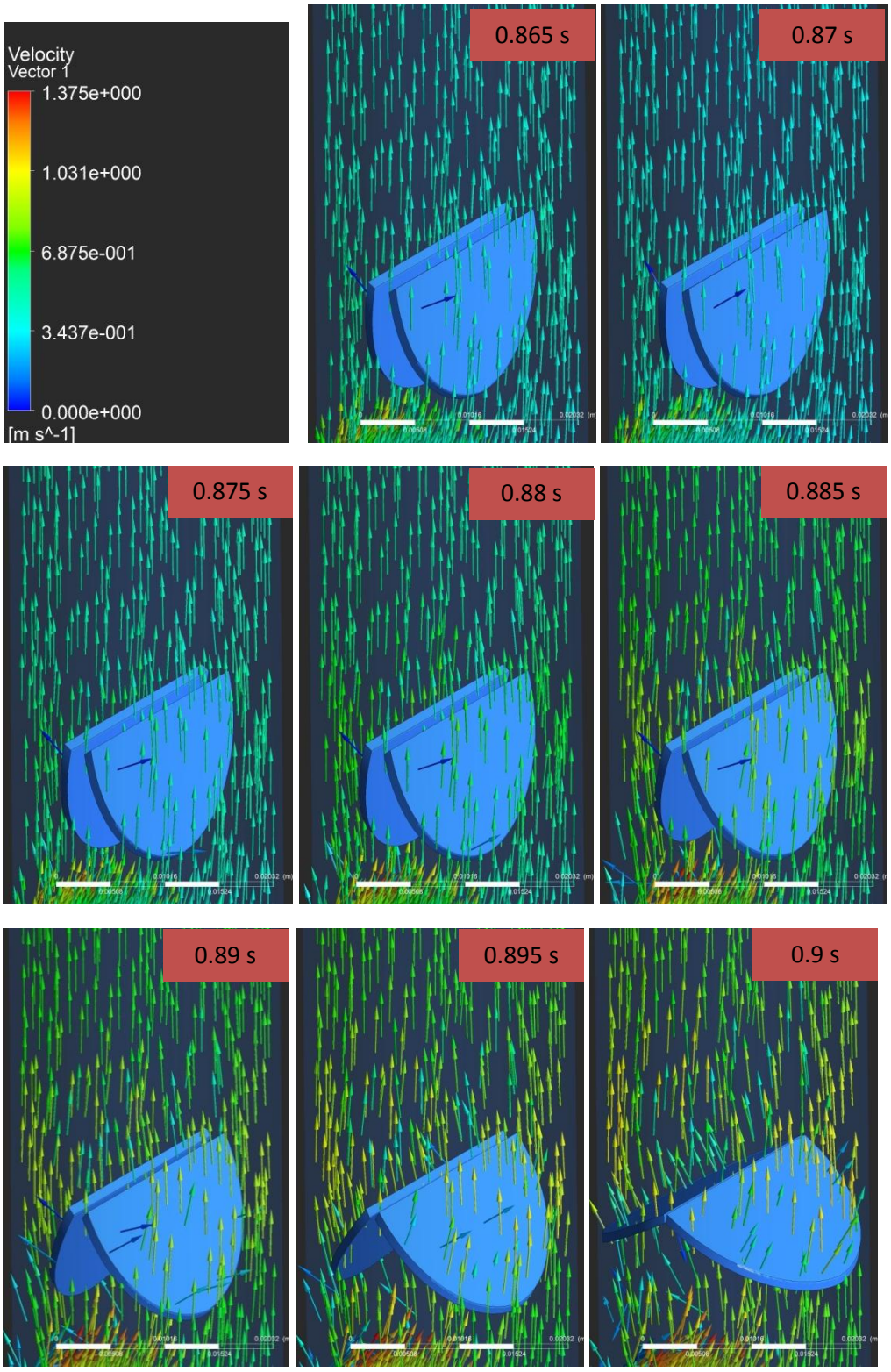

Figure 4.55 Velocity vectors in the bileaflet valve region during valve closure.

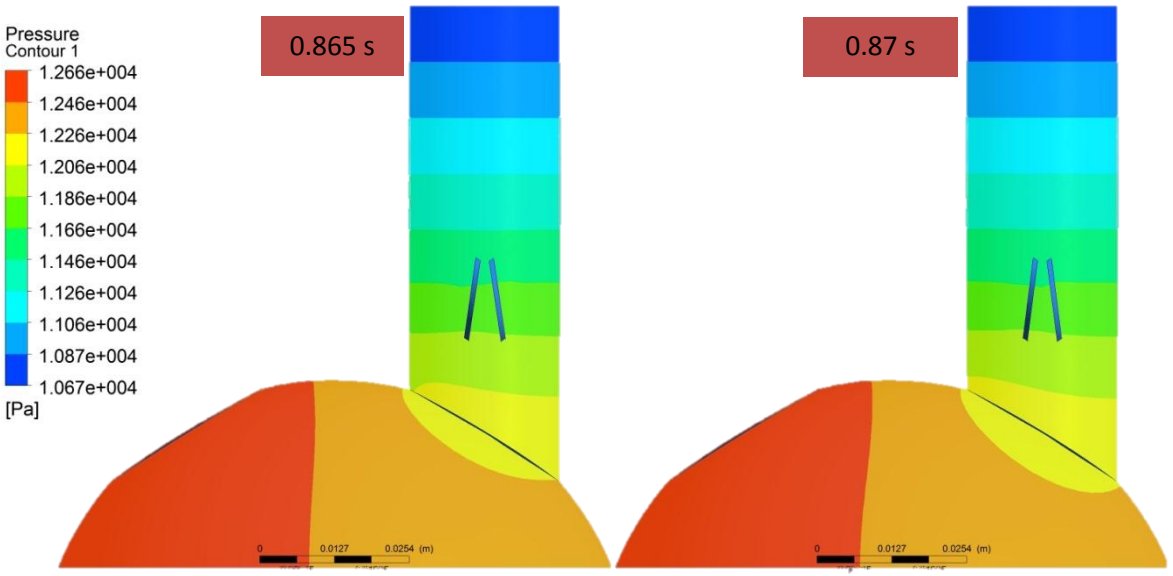
Pressure
Contour 1
1.266e+004
1.246e+004
1.226e+004
1.206e+004
1.186e+004
1.166e+004
1.146e+004
1.126e+004
1.106e+004
1.087e+004
1.067e+004
[Pa]
0.865 s
0.87 s
0
0.0127
0.0254 (m)

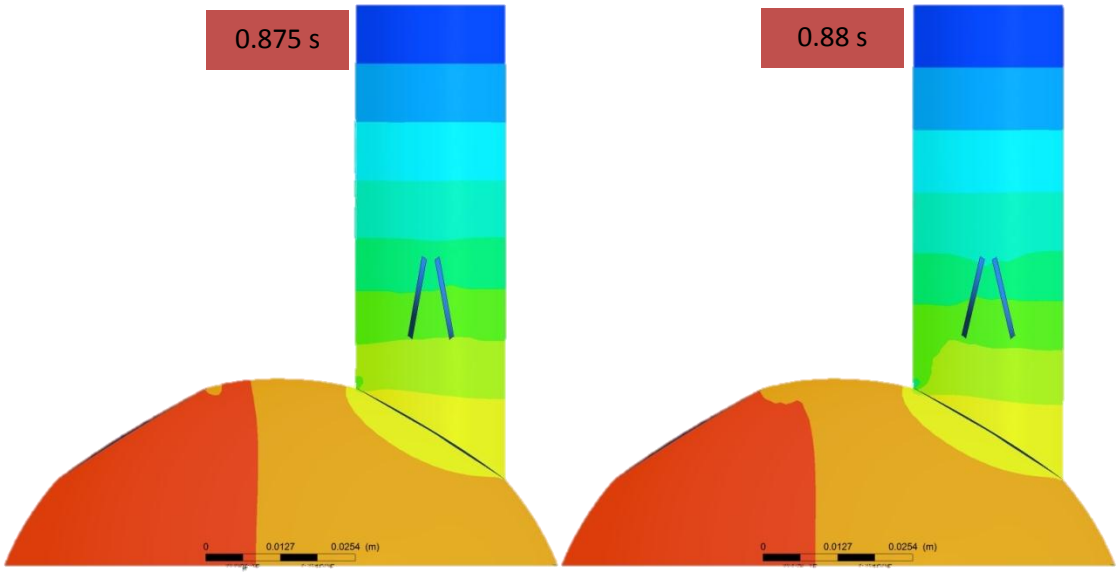
0.875 s
0.88 s
0
0.0127
0.0254 (m)

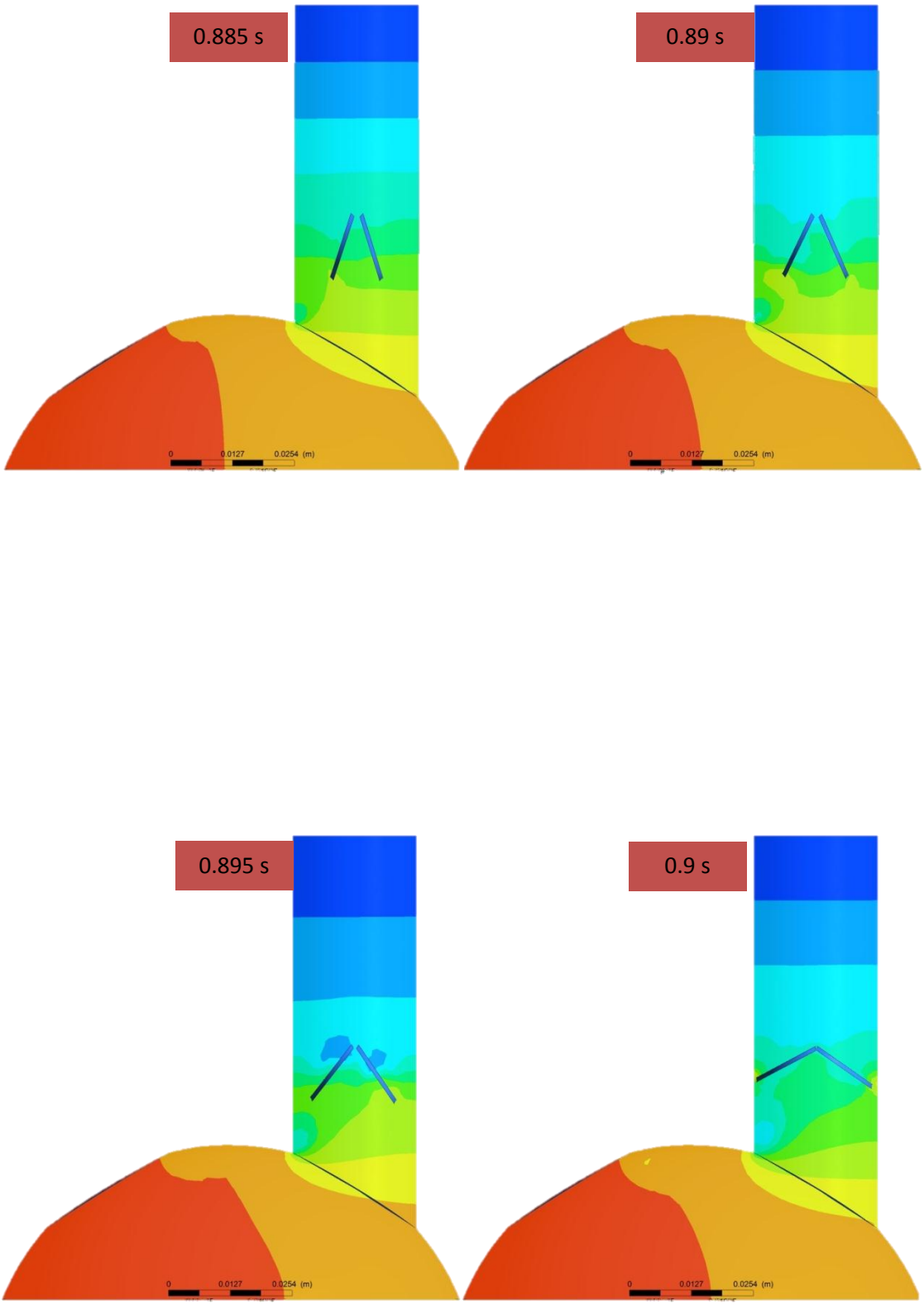

Figure 4.56 pressure distribution for the bileaflet outlet valve closing (opening angle = 85^{O})

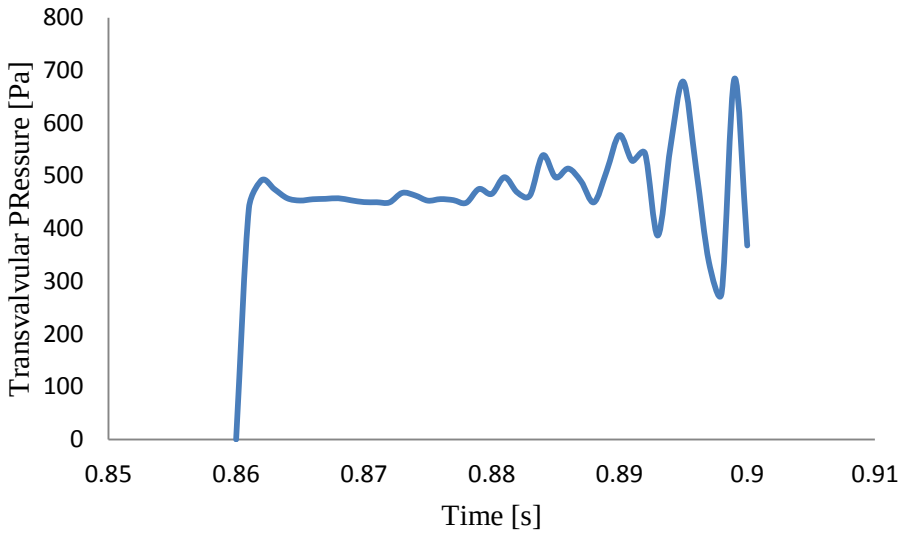

Figure 4.57 Transvalvular pressure versus time for the bileaflet outlet valve closing measured as the difference between average pressure on two planes 0.02 m apart, before and after the valve.

4.2.2 THE MONOLEAFLET VALVE

4.2.2.1 MONOLEAFLET OUTLET VALVE OPENING BEHAVIOR

In order to optimize the performance of monoleaflet heart valve, an optimum opening angle should be employed in the valve design. In this study, hemodynamic performance of monoleaflet valve with different opening angles including: 45, 60, 75, 80, and 85 degrees was investigated. The hemodynamic performance was evaluated based on effective orifice area (EOA), transvalvular pressure gradient, flow separation, and turbulence.

4.2.2.1.1 75 DEGREES OF OPENING ANGLE

Flow parameters around the outlet valve were calculated when the valve opening angle was kept at 75°. Table 4.13 lists the maximum velocity and pressure conditions during the outlet valve opening. Figure 4.58 depicts velocity distribution through systole. Figure 4.59 shows velocity vectors in the vicinity of the valve. Figures 4.60 and 4.61 depict pressure distribution through systole. Figure 4.62 shows the computed leaflet position as a function of time for the 3D simulation. Euler Angle (Z), as it was explained in chapter III, was a representative for the opening angel (Θ) in radians. It took 0.017 sec for the valve to reach the fully opened position (to reach from 0° to 75°). The maximum velocity was 1.058 m/sec at the end of systole (t = 0.2454 s). At t = 0.017 s, flow separated around the valve leaflet, forming a region of high velocity flow. A recirculation zone developed approximately 20 mm in the outlet channel before the valve, due to the velocity gradient (Figure 4.58). Due to Figure 4.61, the mean transvalvular pressure was 124.13 Pa. The value for mean pressure gradient agrees with what reported by Zoghbe et al.[67], that the mean pressure gradient across the aortic valve during systole was less than 2666.44 Pa. The maximum transvalvular pressure was 19700 Pa which occurred right before opening of the valve (t = 0.001 s). In here, the calculated EOA was equal to 1.91 cm^2.

Table 4.13 The monoleaflet outlet valve opening behavior for 75 degrees of opening angle

Parameter	Value
Maximum Velocity	1.058 m/s
Maximum Pressure Drop Across Valve	19700 Pa
Average Pressure Drop Across the Valve	124.13 Pa
Valve Opening Time	0.017 s
EOA	1.91cm^2

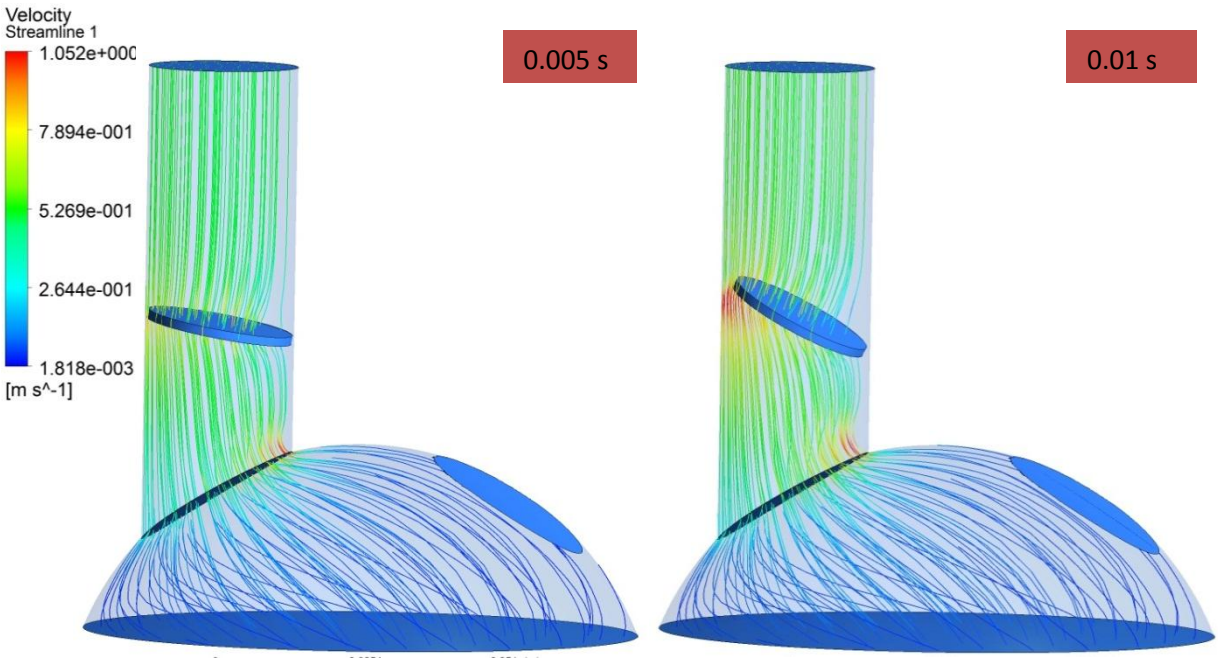
Velocity
Streamline 1
1.052e+000
7.894e-001
5.269e-001
2.644e-001
1.818e-003
[m s^-1]
0.005 s
0.01 s

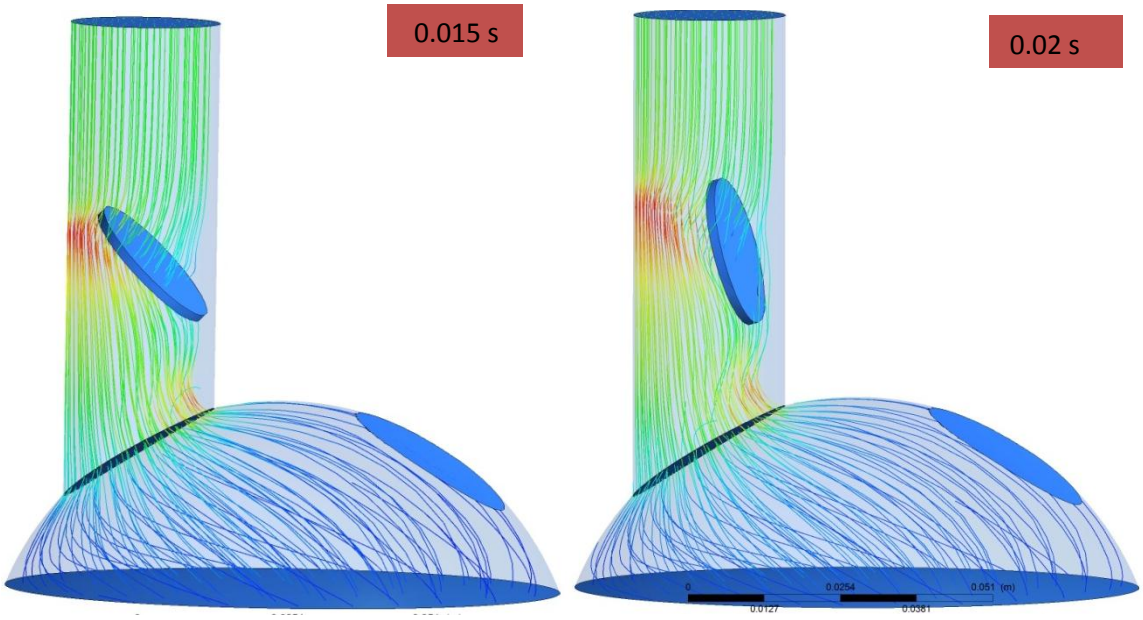
0.015 s
0.02 s
0
0.0254
0.051 (m)
0.0127
0.0381

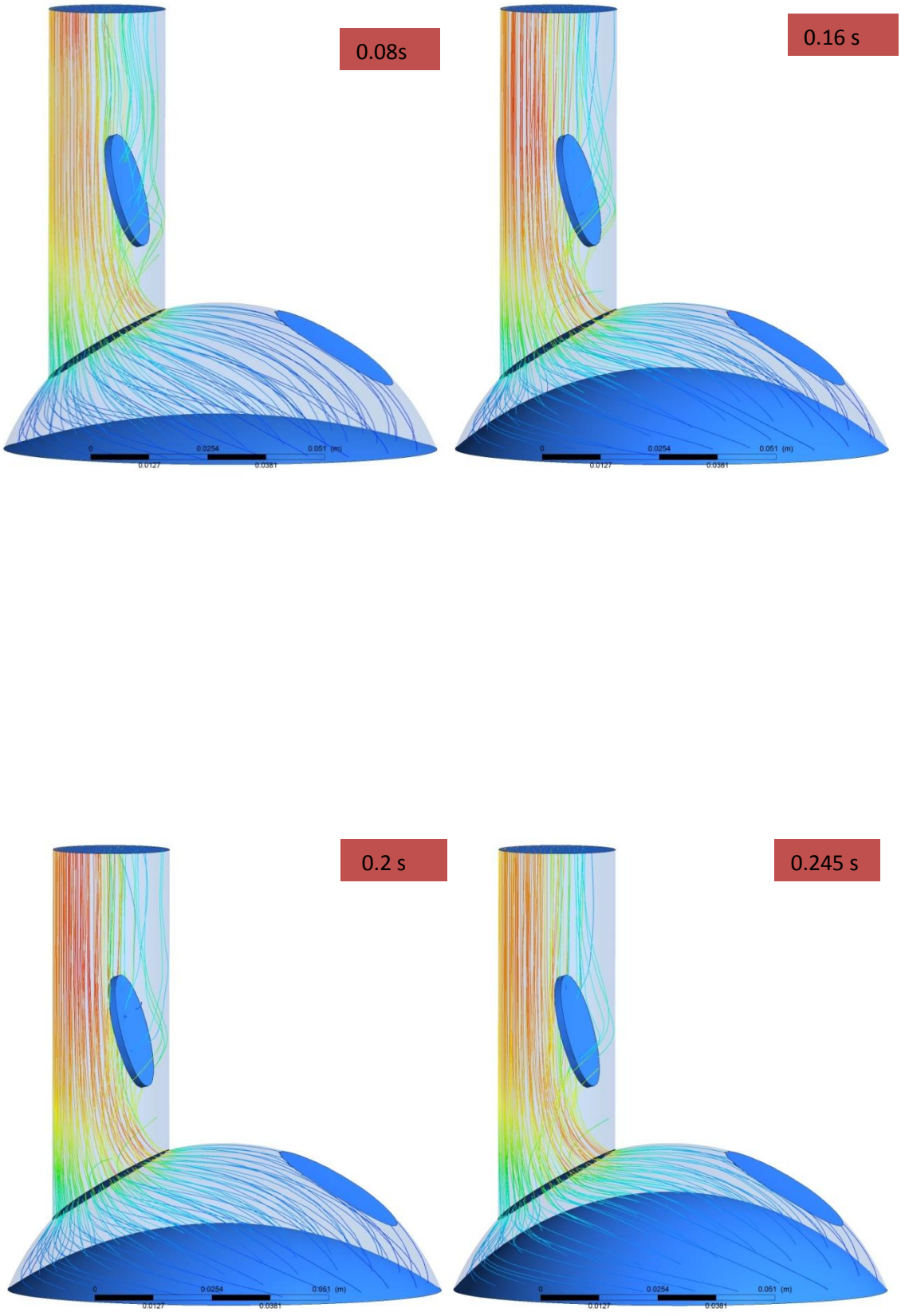

Figure 4.58 velocity stream line during systole when the monoleaflet valve opens (opening angle = 75°)

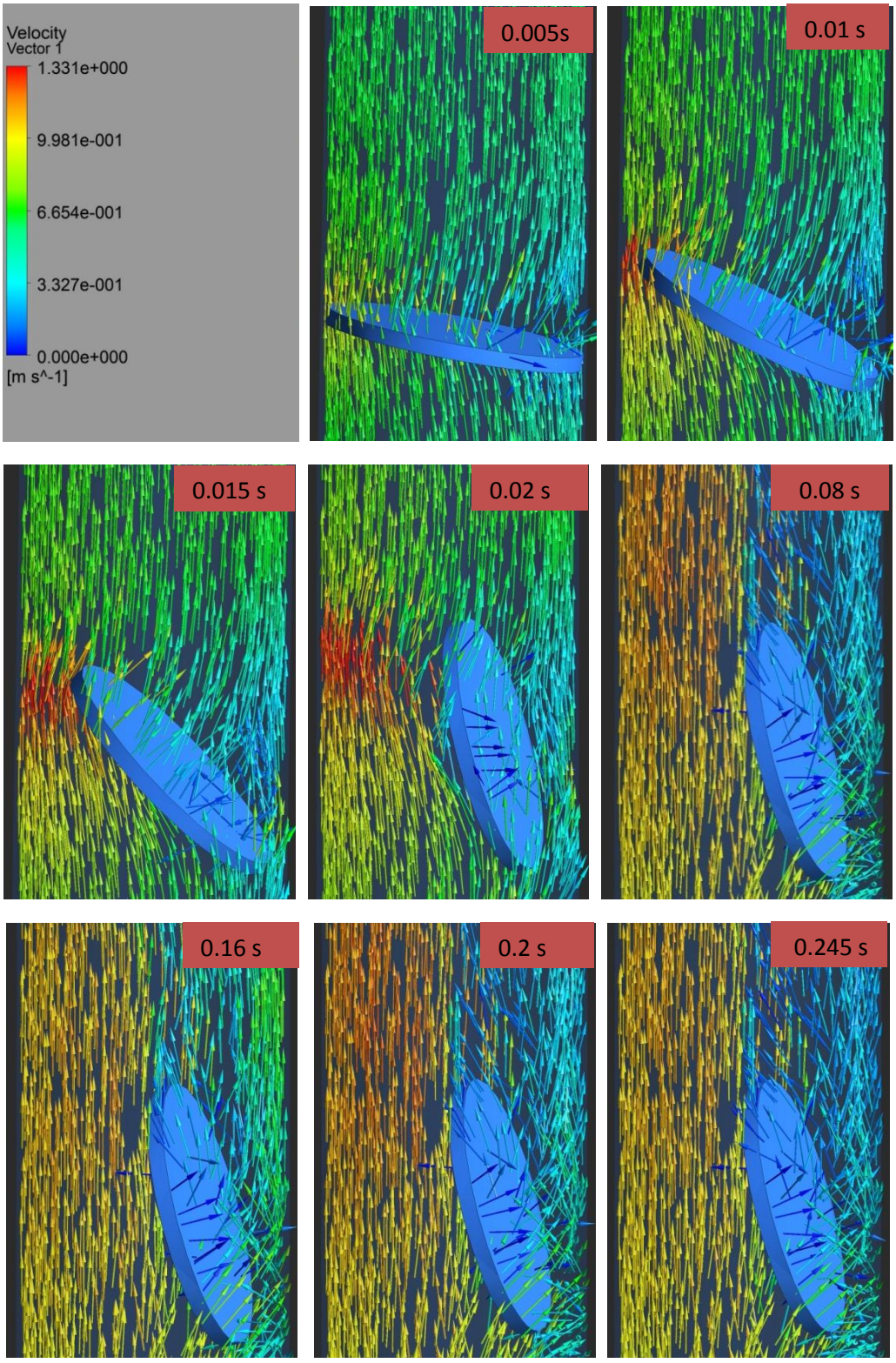

Figure 4.59 Velocity vectors in the outlet monoleaflet valve region during systole when the valve opens.

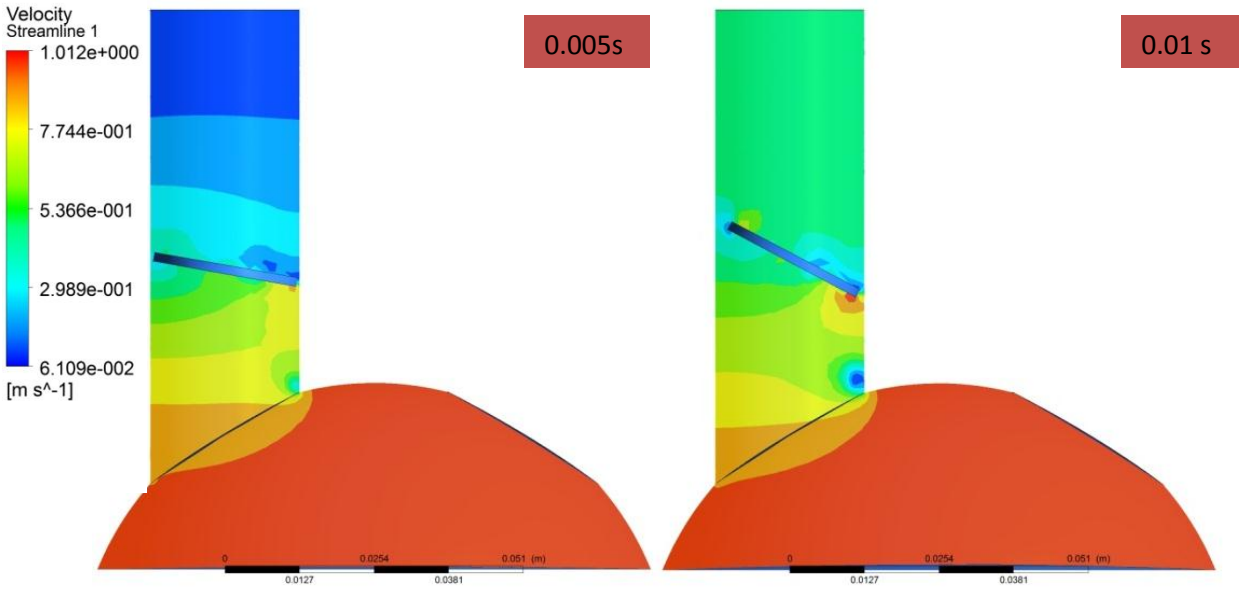
Velocity
Streamline 1
1.012e+000
7.744e-001
5.366e-001
2.989e-001
6.109e-002
[m s^-1]
0.005s
0.01 s
0
0.0254
0.051 (m)
0.0127
0.0381

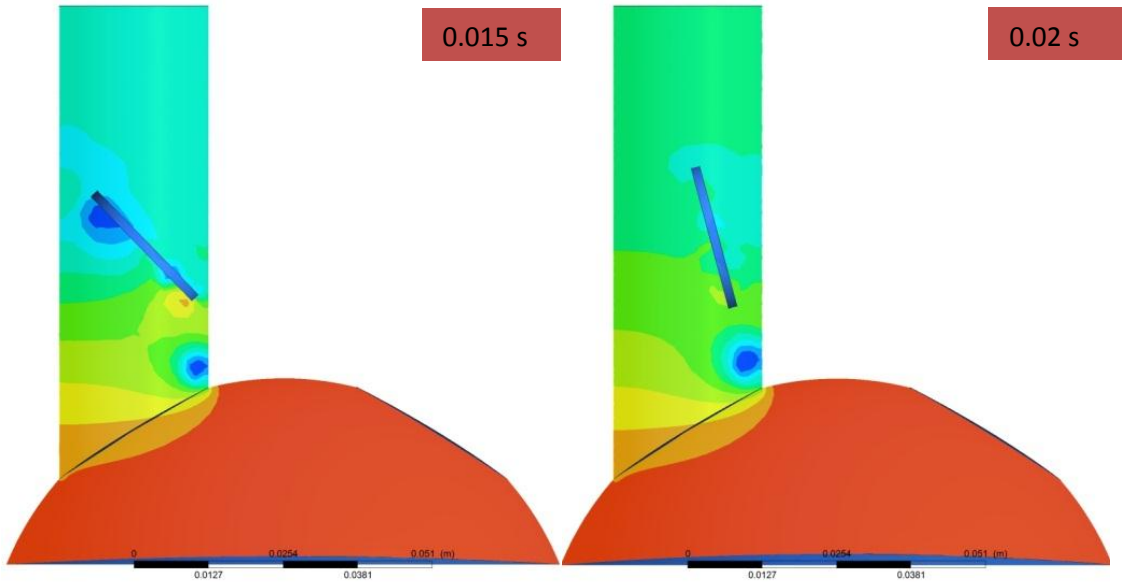
0.015 s
0.02 s
0
0.0254
0.051 (m)
0.0127
0.0381

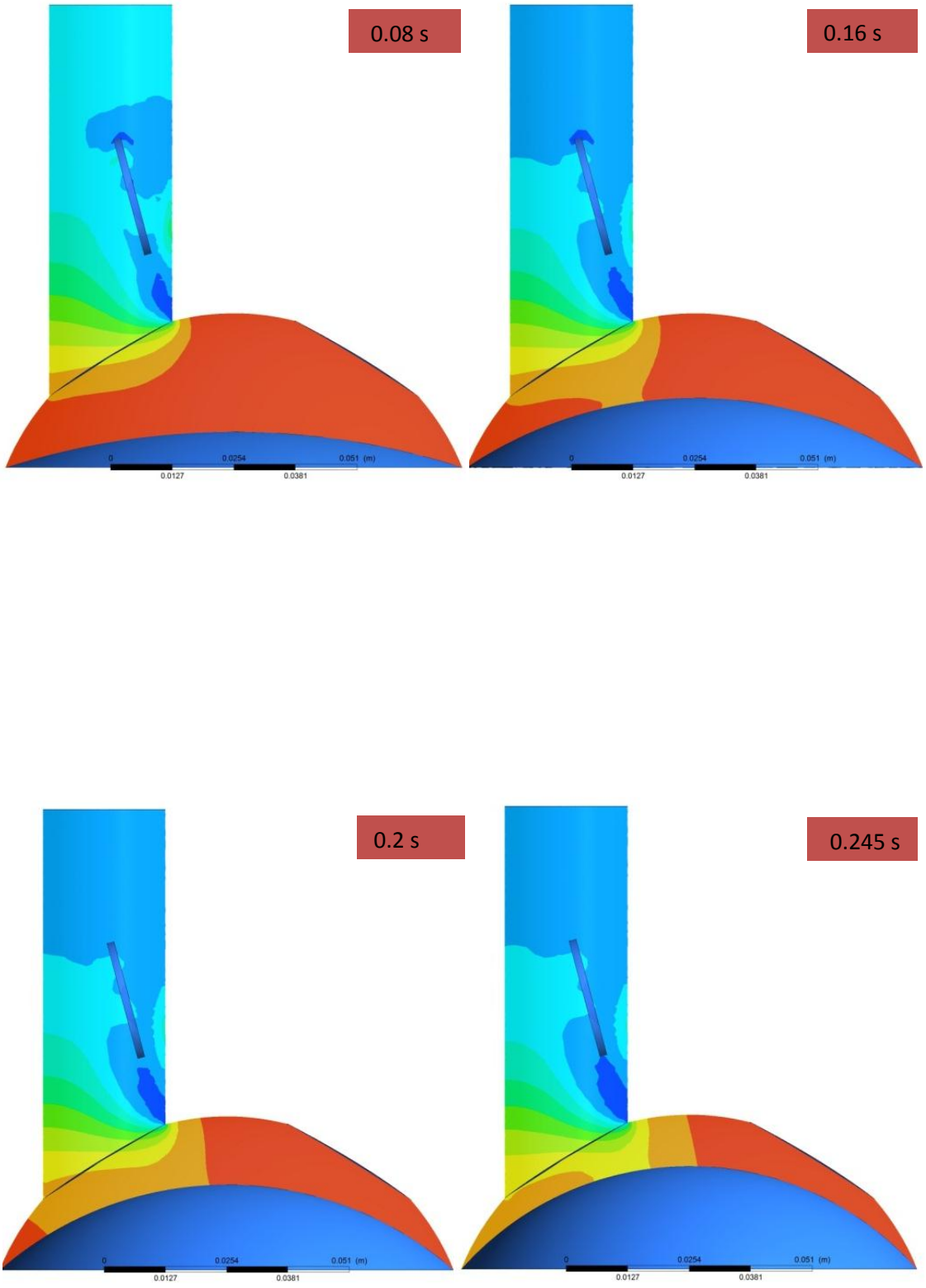

Figure 4.60 Pressure distribution for the monoleaflet outlet valve opening at t = 0.2454 s (opening angle = 75°)

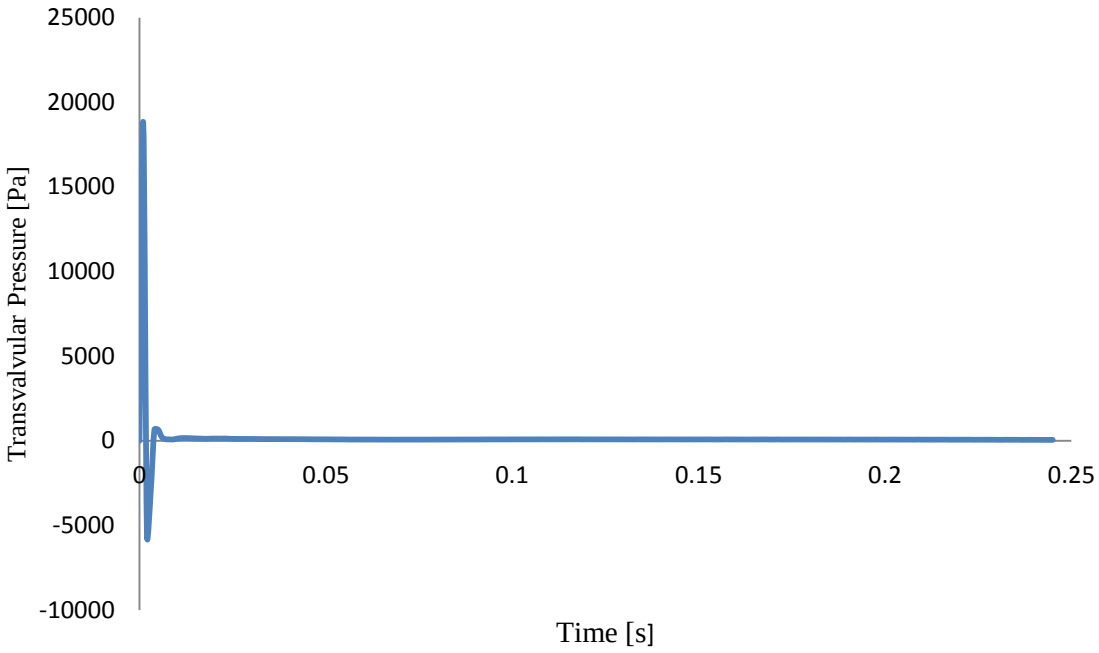

Figure 4.61 Transvalvular pressure versus time for the monoleaflet outlet valve opening measured as the difference between average pressure on two planes 0.02 m apart, before and after the valve. (opening angle = 75^{O})

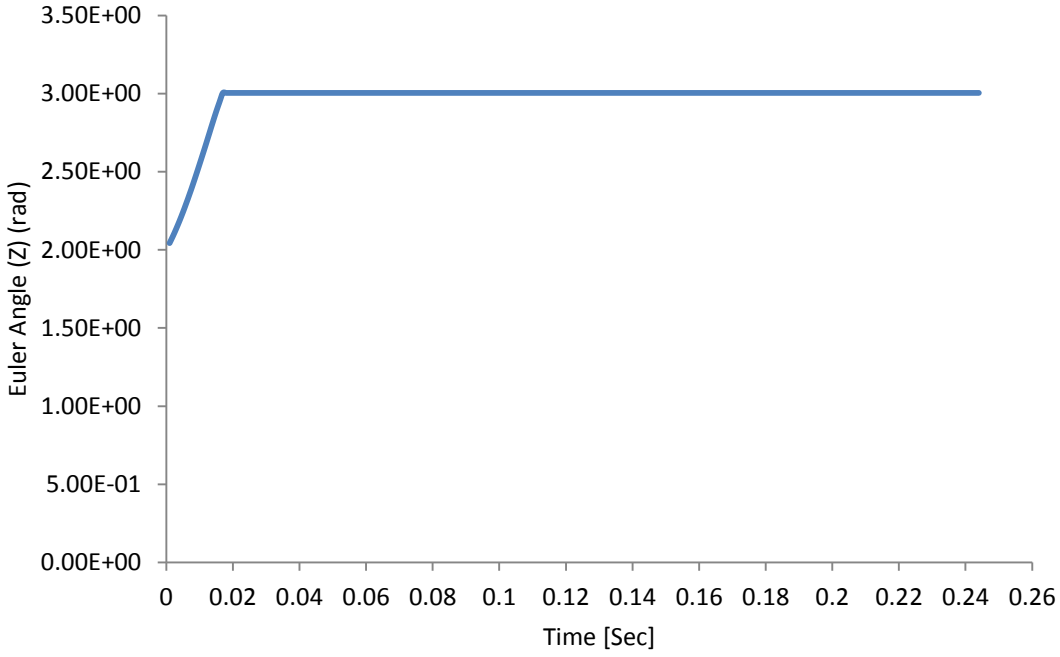

Figure 4.62 The monoleaflet outlet valve opening angle (in terms of Euler angle (z)) versus time (maximum opening angle = 75^{O})

4.2.2.1.2 45, 60, 80, AND 85 DEGREES OF OPENING ANGLE

In order to find the optimal opening angle for the monoleaflet outlet valve, the hemodynamic performance of monoleaflet valves with 45°, 60°, 75°, 80°, and 85° opening angle were studied. In Table 4.14 compared flow parameters when the opening angle of the monoleaflet outlet valve was 45, 60, 75, 80, and 85 degrees. In Figures 4.63 to 4.65, maximum flow velocity, transvalvular pressure and effective orifice area (EOA) are depicted as a function of valve opening angle. Figure 4.66 depicts the velocity streamline in the valve region for different opening angles at t=0.2454 s.

As it can be seen from Table 4.14 that as the opening angle approached 75°, the maximum velocity and transvalvular pressure decreased and the EOA increased. With the 80° opening angle, the maximum velocity and transvalvular pressure were almost the same as that at 75°. Increasing the opening angle further to 85^{o} caused a slight increase in the maximum velocity; however the transvalvular pressure decreased resulting in higher EOA. Figure 4.66 shows that increasing the maximum opening angle causes lower disturbance to the main flow.

Table 4.14 Comparison between flow conditions of the monoleaflet outlet valve opening with different opening angles

PARAMETER	45^{o}	60^{o}	75^{o}	80^{o}	85^{o}
Maximum Velocity m/s	1.342	1.155	1.058	1.057	1.065
Average Pressure Difference Across the Valve Pa	320	254.95	124.13	101.26	46.28
Valve Opening Time s	0.015	0.016	0.017	0.018	0.02
EOA cm^2	1.19	1.33	1.91	2.13	3.16

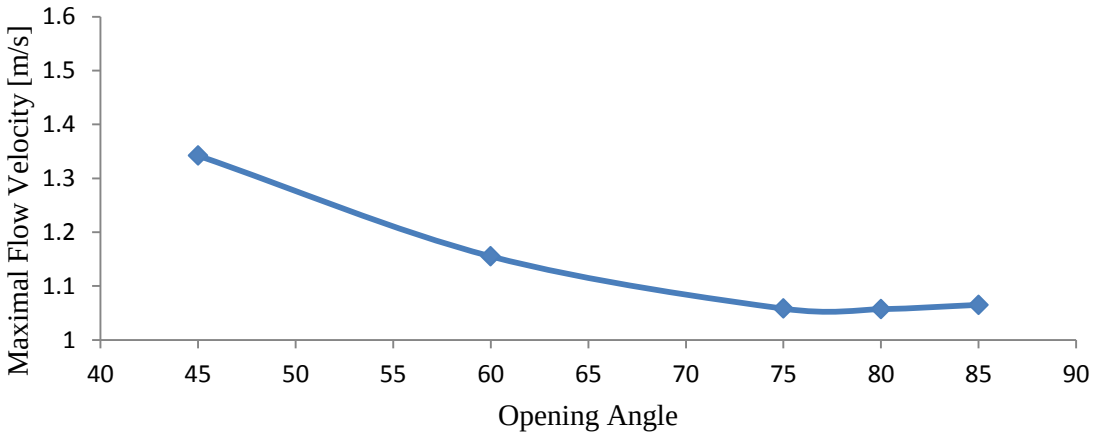

Figure 4.63 Relationship between the maximum flow velocity and the valve opening angle

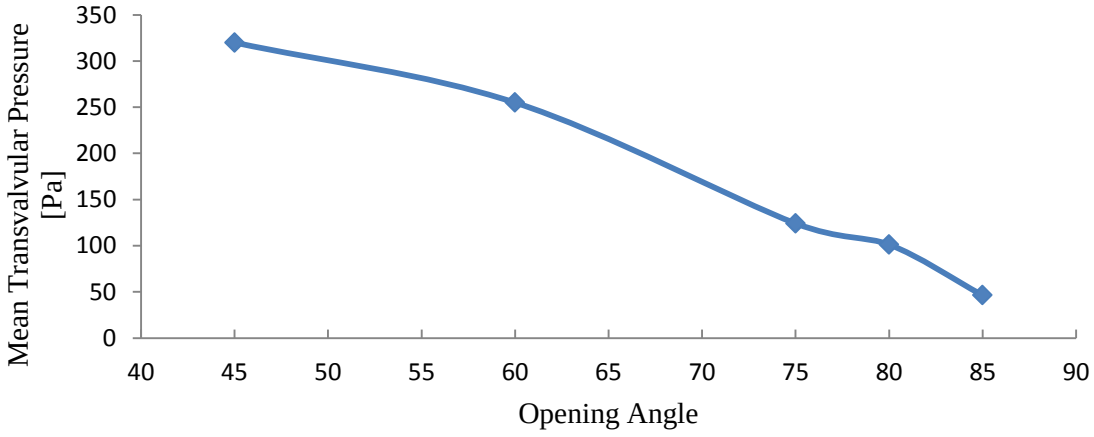

Figure 4.64 Relationship between the mean transvalvular pressure and the valve opening angle

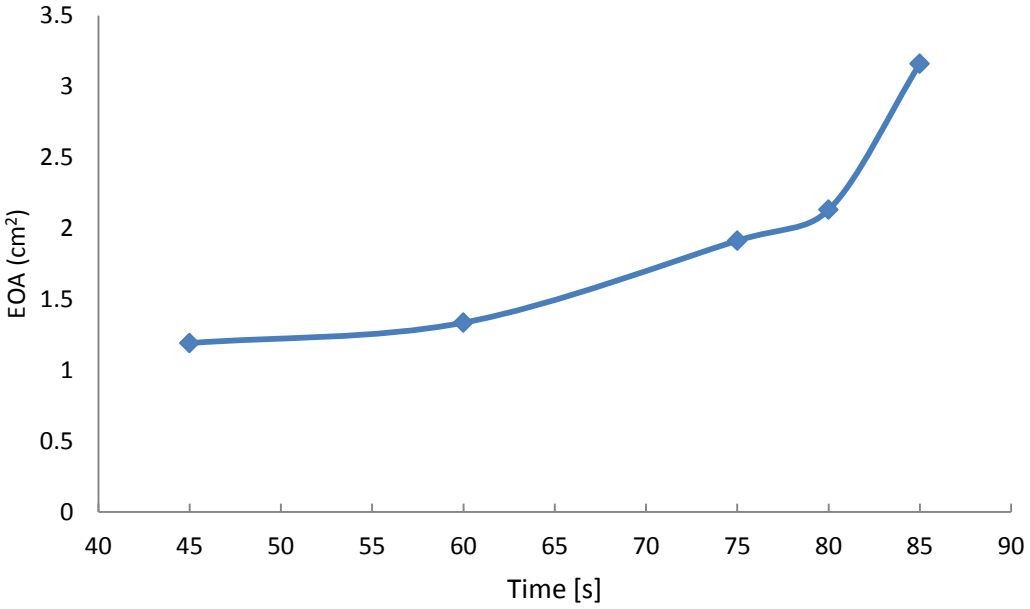

Figure 4.65 Relationship between EOA and the valve opening angle

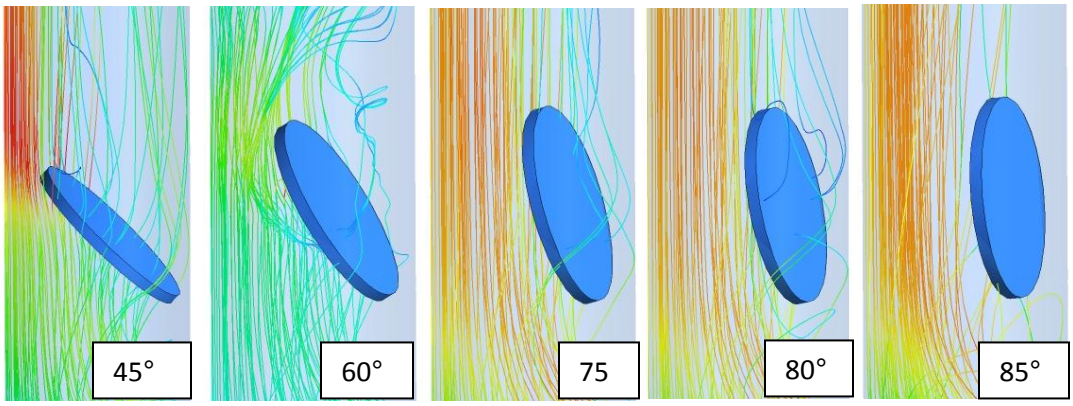

Figure 4.66 Stream line plot for 45°, 60°, 75°, 80°, and 85° degrees of opening angle at the end of valve opening.

4.2.2.2 THE MONOLEAFLET OUTLET VALVE CLOSING BEHAVIOR

4.2.2.2.1 75 DEGREES OF OPENING ANGLE

Table 4.15 lists the maximum velocity and pressure conditions during the outlet valve closure, when the opening angle was 75°. Figure 4.67 depicts velocity distribution through late systole. Figure 4.68 shows velocity vectors in the vicinity of the valve. Figures 4.69 and 4.70 depict pressure distribution. It took 0.036 sec for the valve to reach the fully closed position (from 75° to 0°). The maximum backflow velocity was 1.846 m/sec at t = 0.27 s, in a region of high velocity flow (squeeze flow) developed in the gap between the right side of the leaflet and the wall. The maximum and mean transvalvular pressures were 1460 Pa and 440.35 Pa respectively.

Table 4.15 The monoleaflet outlet valve closing behavior for 75 degrees of opening angle

Parameter	Value
Maximum Backflow Velocity	1.846 m/s
Maximum Pressure Drop Across Valve	17600 Pa
Average Pressure Drop Across the Valve	440.35Pa
Valve Closing Time	0.036 s

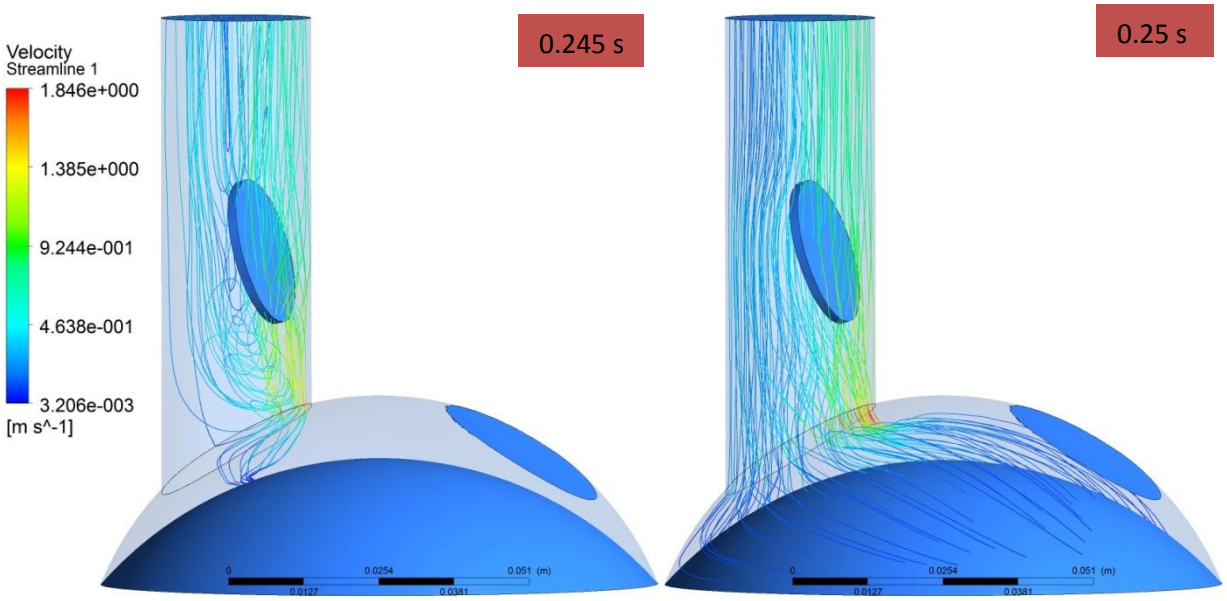
Velocity
Streamline 1
1.846e+000
1.385e+000
9.244e-001
4.638e-001
3.206e-003
[m s^-1]
0.245 s
0.25 s
0
0.0254
0.051 (m)
0.0127
0.0381

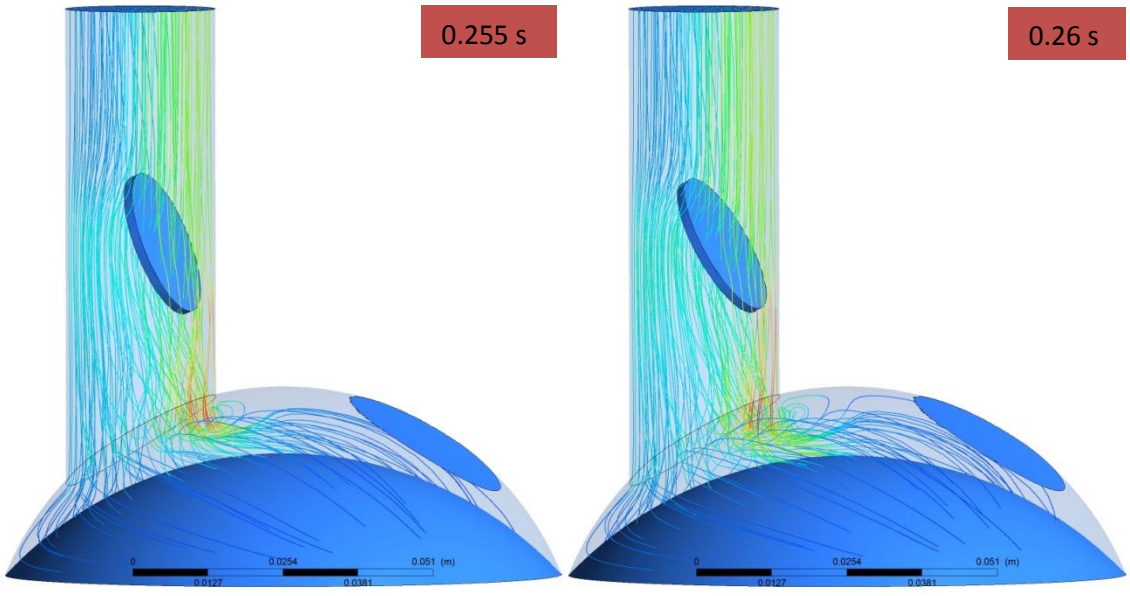
0.255 s
0.26 s
0
0.0254
0.051 (m)
0.0127
0.0381

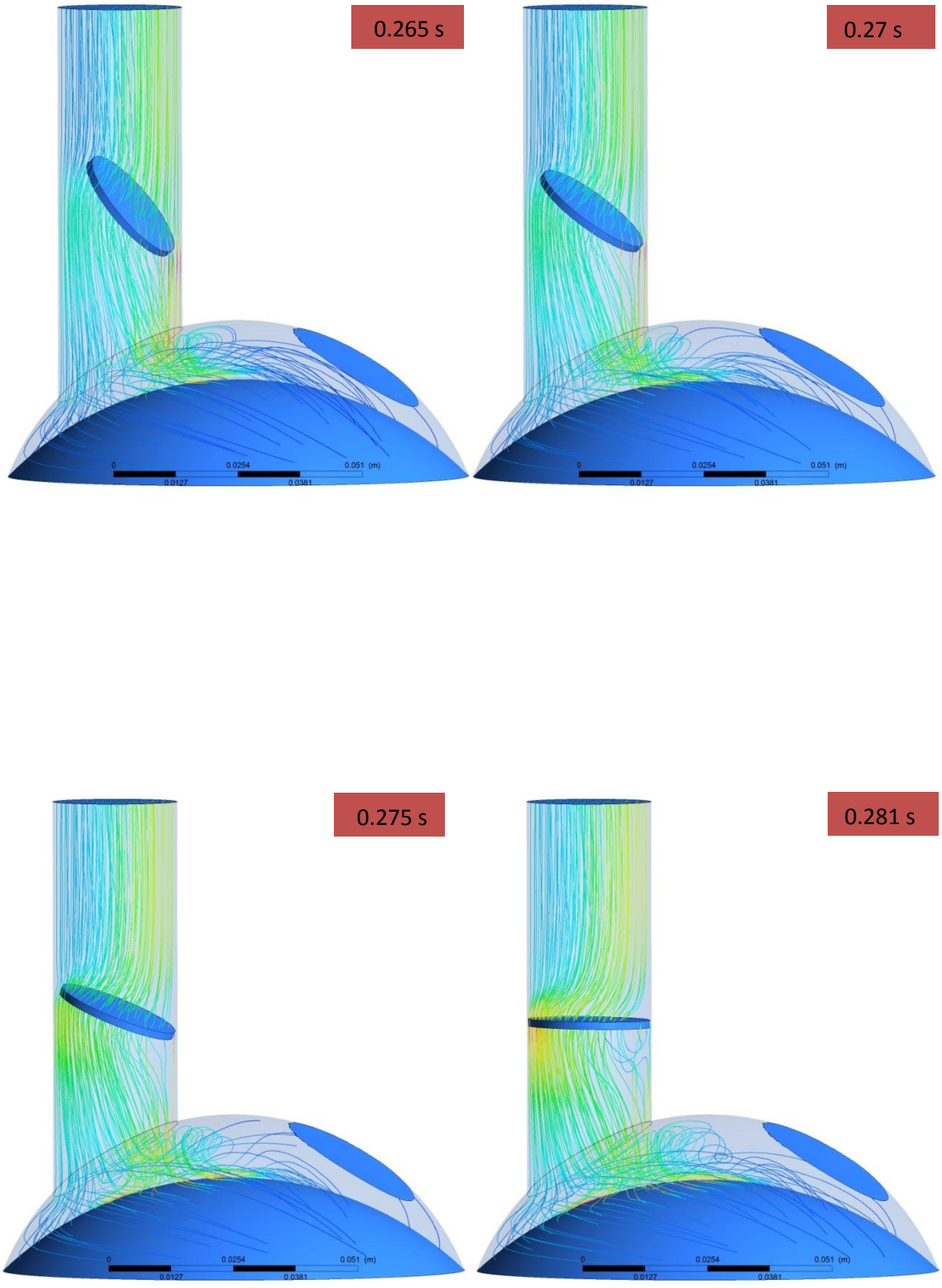

Figure 4.67 Velocity streamline for the monoleaflet outlet valve closure (opening angle = 75°)

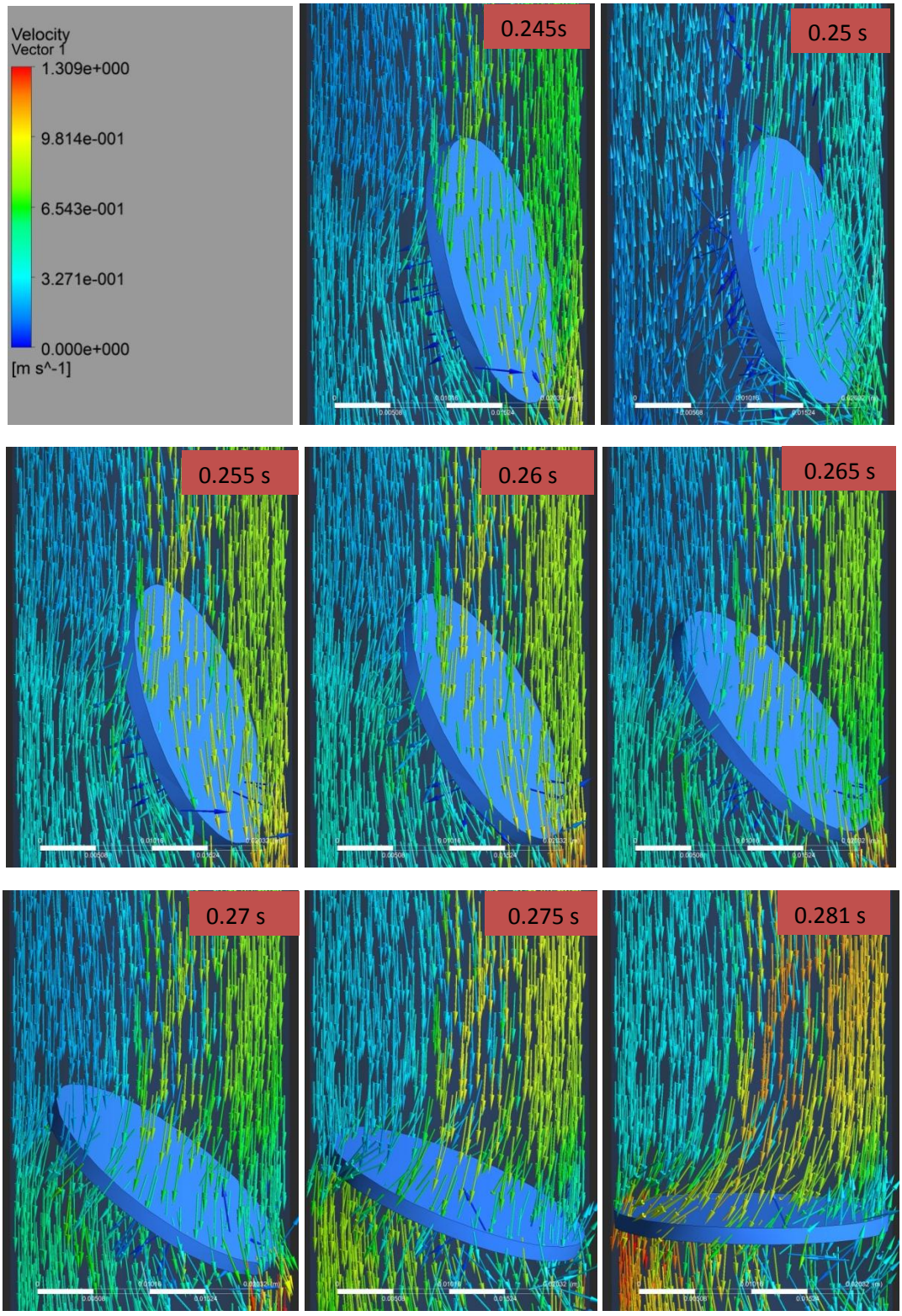

Figure 4.68 Velocity vectors in the valve region during diastole when the monoleaflet valve closes.

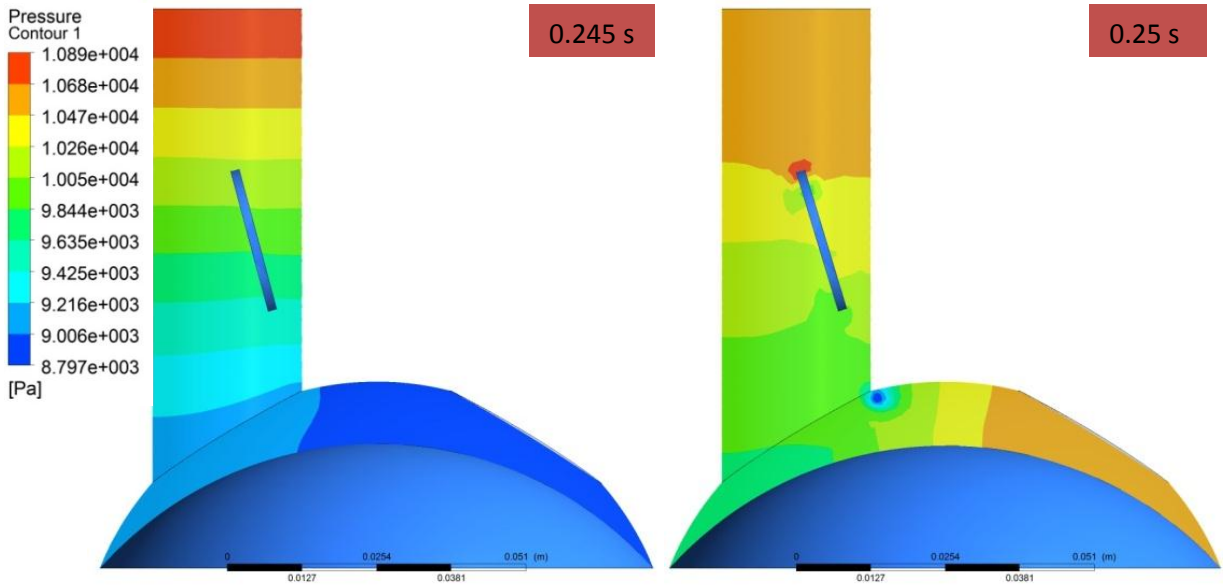
Pressure
Contour 1
1.089e+004
1.068e+004
1.047e+004
1.026e+004
1.005e+004
9.844e+003
9.635e+003
9.425e+003
9.216e+003
9.006e+003
8.797e+003
[Pa]
0.245 s
0.25 s
0
0.0254
0.051 (m)
0.0127
0.0381

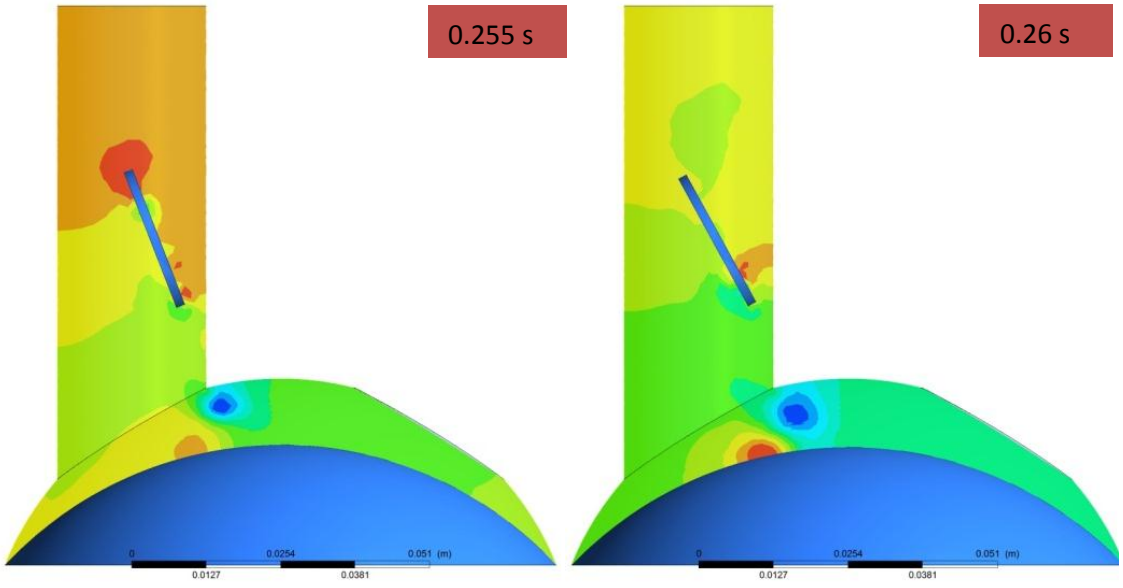
0.255 s
0.26 s
0
0.0254
0.051 (m)
0.0127
0.0381

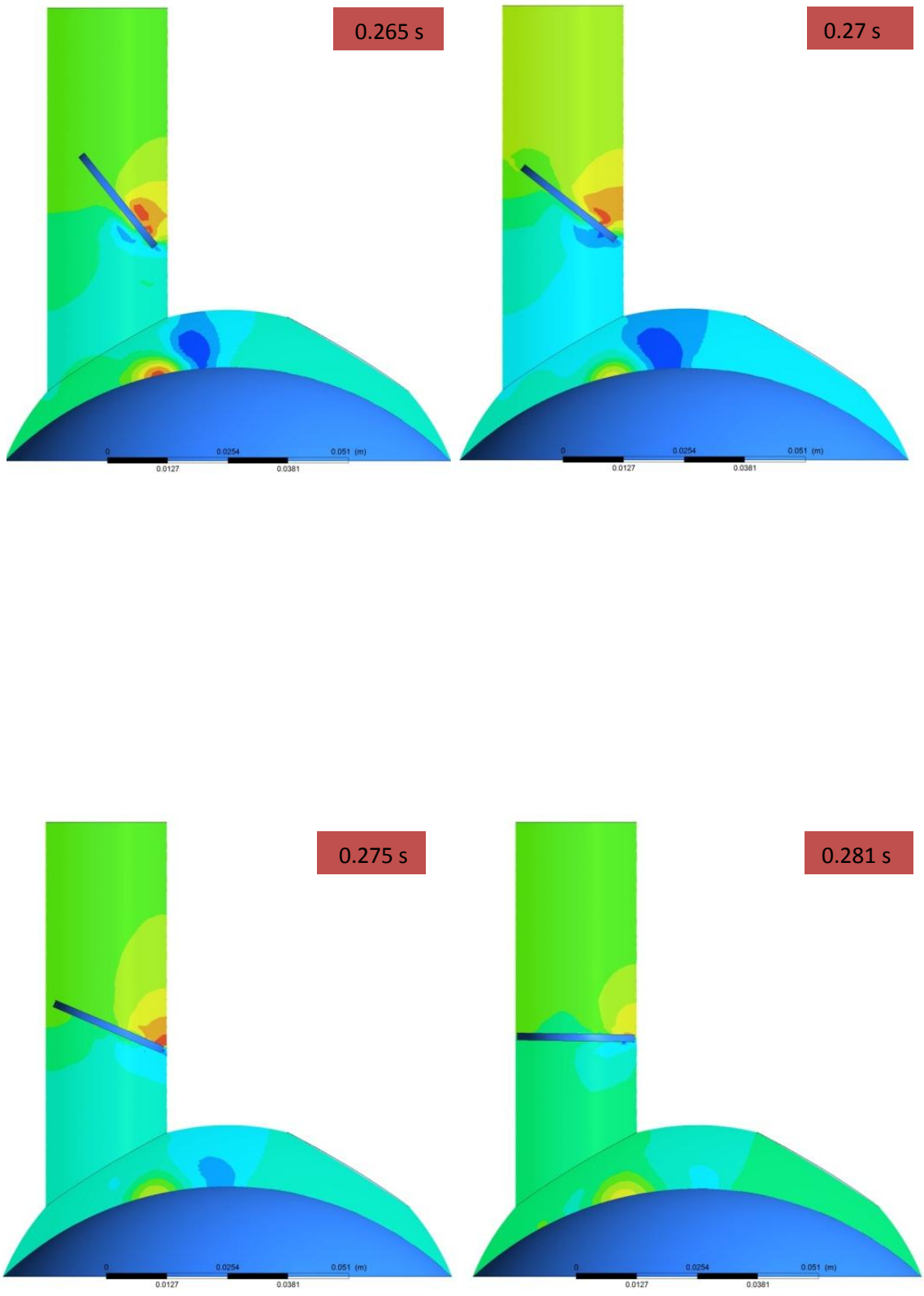

Figure 4.69 Pressure distribution for the monoleaflet outlet valve closing (opening angle = 75°)

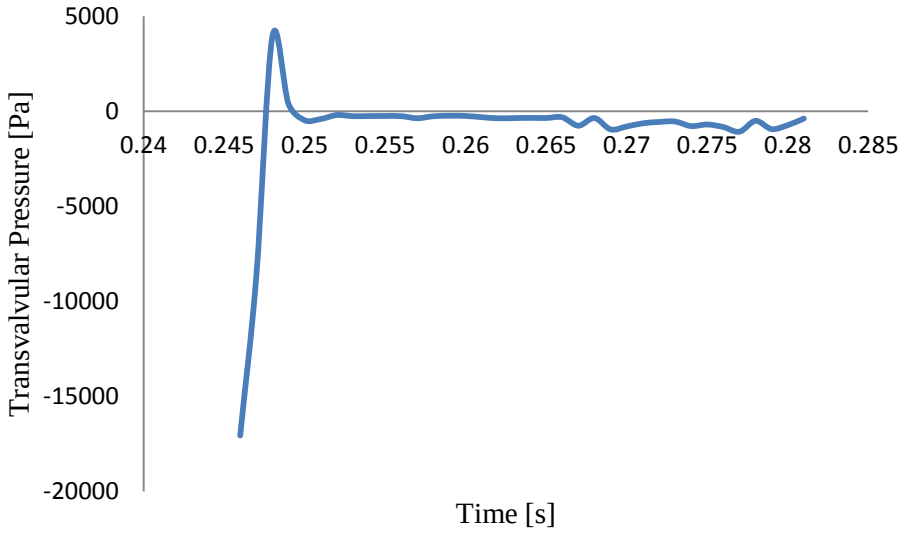

Figure 4.70 Transvalvular pressure versus time for the monoleaflet outlet valve closing measured as the difference between average pressure on two planes 0.02 m apart, before and after the valve. (opening angle = 75^{o})

4.2.2.1.2 45, 60, 80, AND 85 DEGREES OF OPENING ANGLE

In Table 4.16 compared flow parameters when the opening angle of the monoleaflet outlet valve was 45, 60, 75, 80, and 85 degrees. In Figure 4.71, maximum flow velocity is depicted as a function of valve opening angle. As it can be seen in Table 4.15 and Figure 4.71, 75^{o} opening angle has the lowest flow velocity. Results here demonstrated the closing complications of the valve with 85^{o} opening angle (i.e. the valve was not able to close due to the big opening angle).

Table 4.16 Comparison between flow conditions of the monoleaflet outlet valve closing with different opening angles

PARAMETER	45^{o}	60^{o}	75^{o}	80^{o}	85^{o}
Maximum Velocity m/s	14.13	5.35	1.846	4.197	5.076
Valve Closing Time s	0.005	0.01	0.036	0.022	N/A

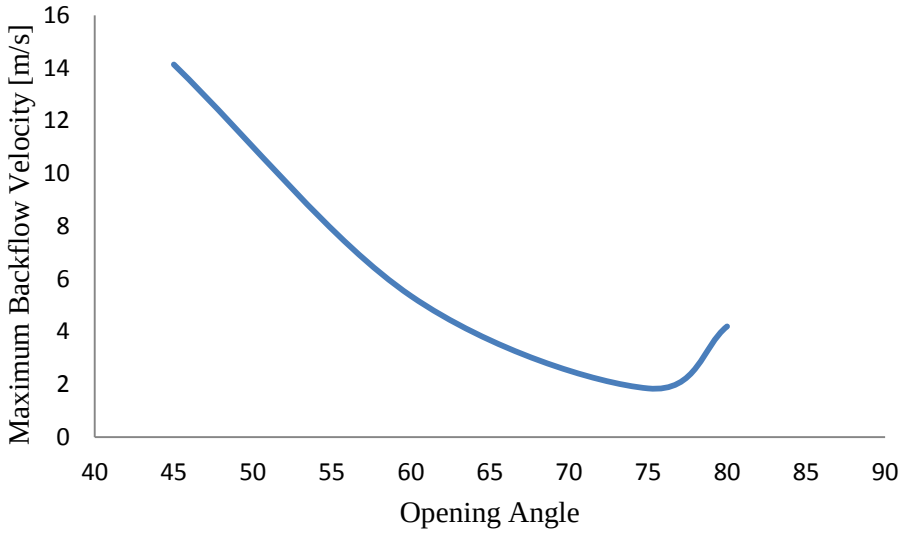

Figure 4.71 Relationship between the maximum flow velocity and the valve opening angle

4.2.2.3 THE MONOLEAFLET INLET VALVE OPENING BEHAVIOR

Based on the valve opening behavior described before, the monoleaflet valve with 75° or larger opening angles seemed to have better hemodynamic performance (i.e., lower maximum velocity, lower transvalvular pressure, larger EOA, etc.). Therefore, to investigate the flow conditions around the inlet monoleaflet valve, a 75° opening angle was chosen for the numerical simulation. Table 4.17 lists the maximum velocity and pressure conditions during the inlet valve opening. Transvalvular pressure was defined as the difference between average pressure on two planes 0.02 m apart, before and after the valve. Figure 4.72 depicts velocity distribution through diastole. Figure 4.73 shows velocity vectors in the vicinity of the valve. Figures 4.74 and 4.75 depict pressure distribution through diastole. It took 0.016 sec for the valve to reach the opening position (to reach from 0° to 75°). A region of high velocity flow (squeeze flow) was developed in the gap between the leaflet and inlet wall with a maximum velocity of 6.446 m/s in downward direction, at the beginning of valve opening process (t=0.283s). The mean transvalvular pressure was 304.075 Pa. Figure 4.75 shows that the maximum transvalvular pressure was 60901 Pa, occurring at the instant of valve opening. The value for mean pressure gradient was in agreement with what reported by Zoghbe et al.[67], that the mean pressure gradient across the mitral valve during diastole was less than 666.61 Pa.

Table 4.17 the monoleaflet inlet valve opening behavior for 75° opening angle

Parameter	Value
Maximum Velocity	-6.446 m/s
Maximum Pressure Drop Across the Valve	60901 Pa
Average Pressure Drop Across the Valve	304.07 Pa
Valve Opening Time	0.016 s

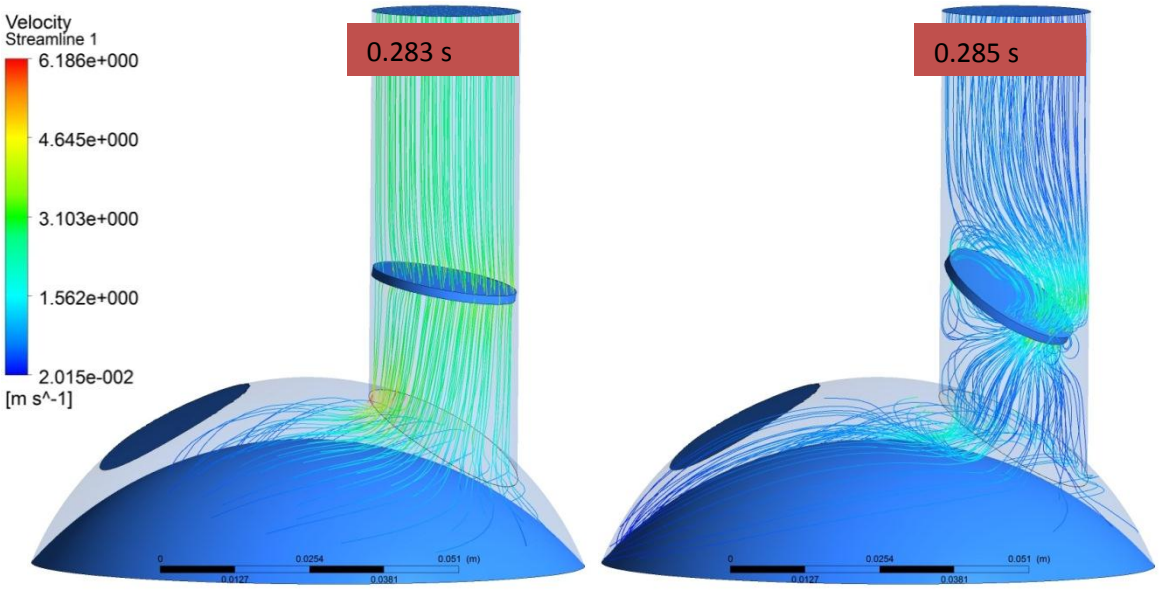
Velocity
Streamline 1
6.186e+000
4.645e+000
3.103e+000
1.562e+000
2.015e-002
[m s^-1]
0.283 s
0.285 s
0
0.0254
0.051 (m)
0.0127
0.0381

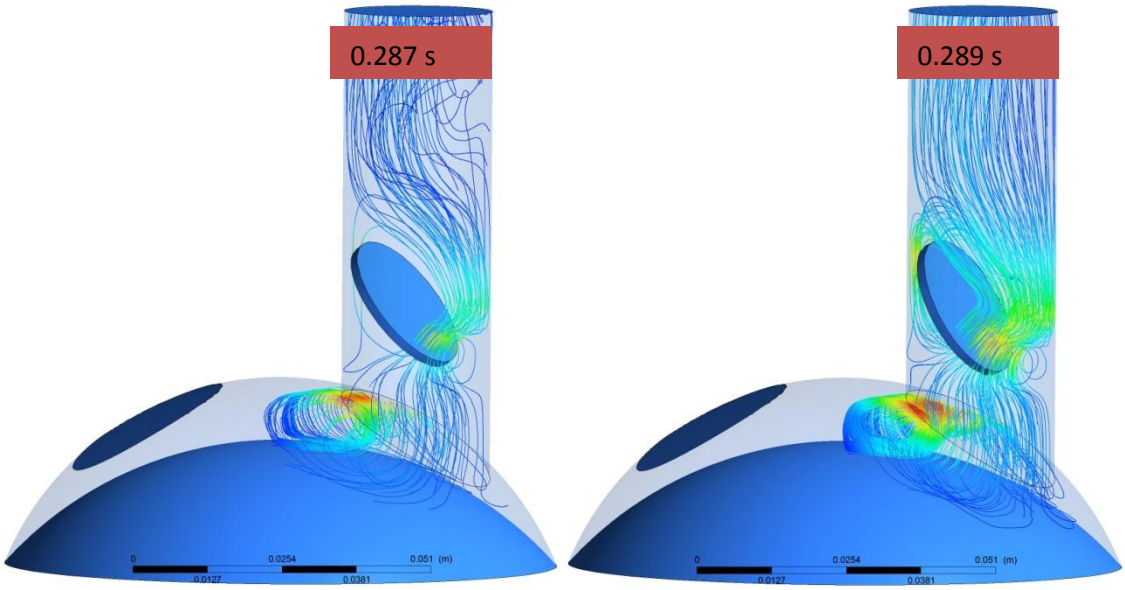
0.287 s
0.289 s
0
0.0254
0.051 (m)
0.0127
0.0381

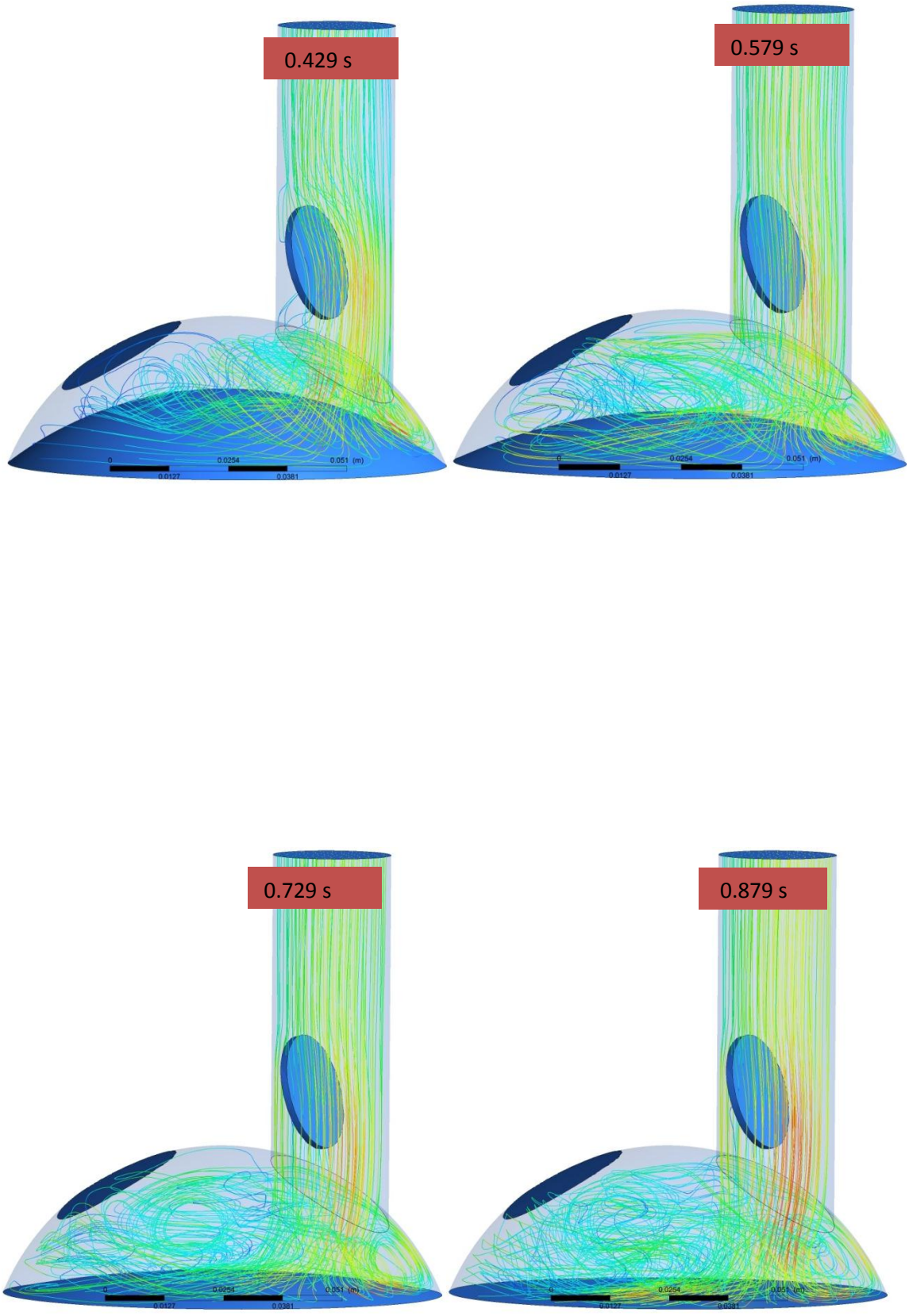

Figure 4.72 Velocity streamline for the monoleaflet inlet valve opening (opening angle = 75^{O})

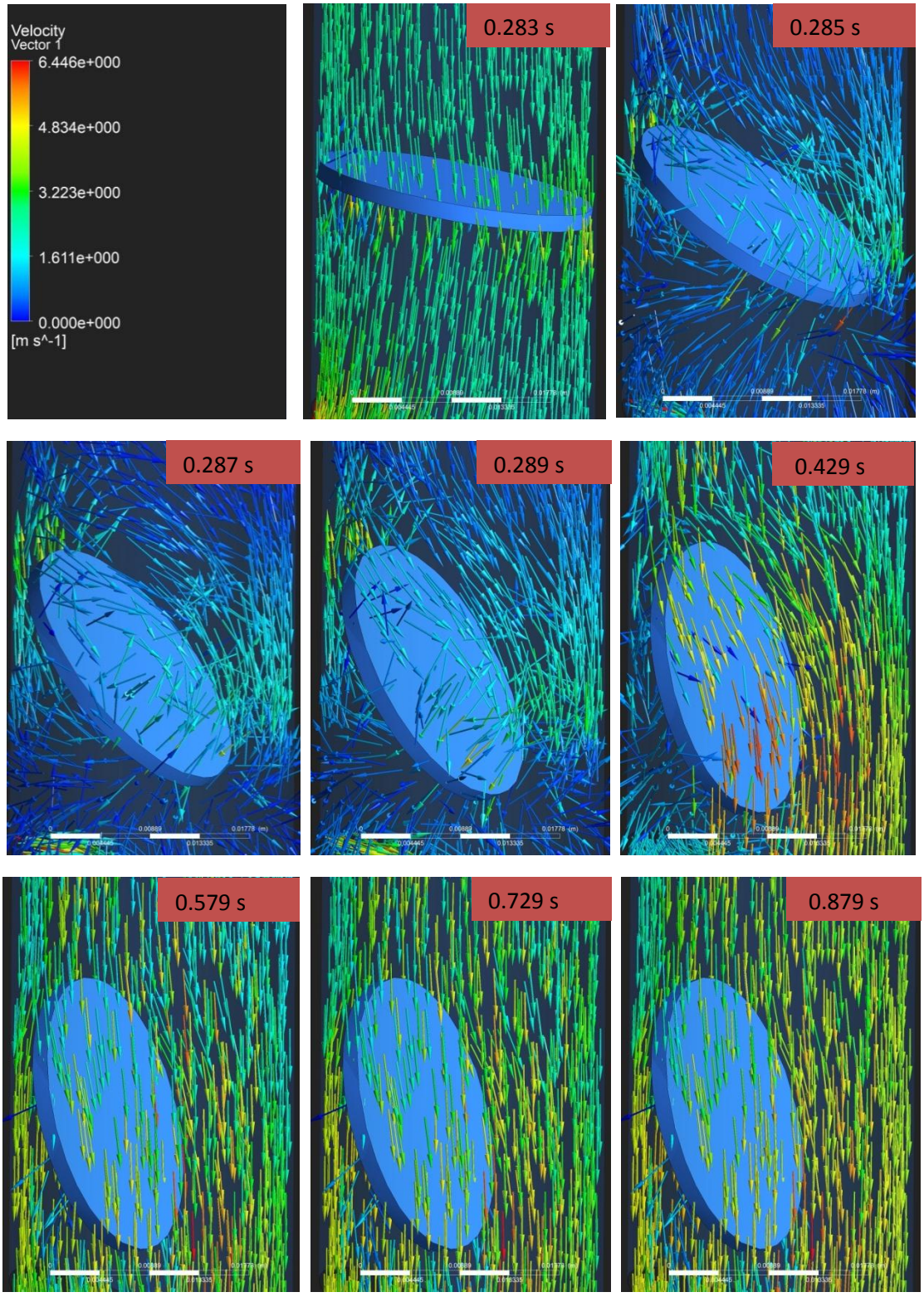

Figure 4.73 Velocity vectors in the valve region during the inlet valve opening.

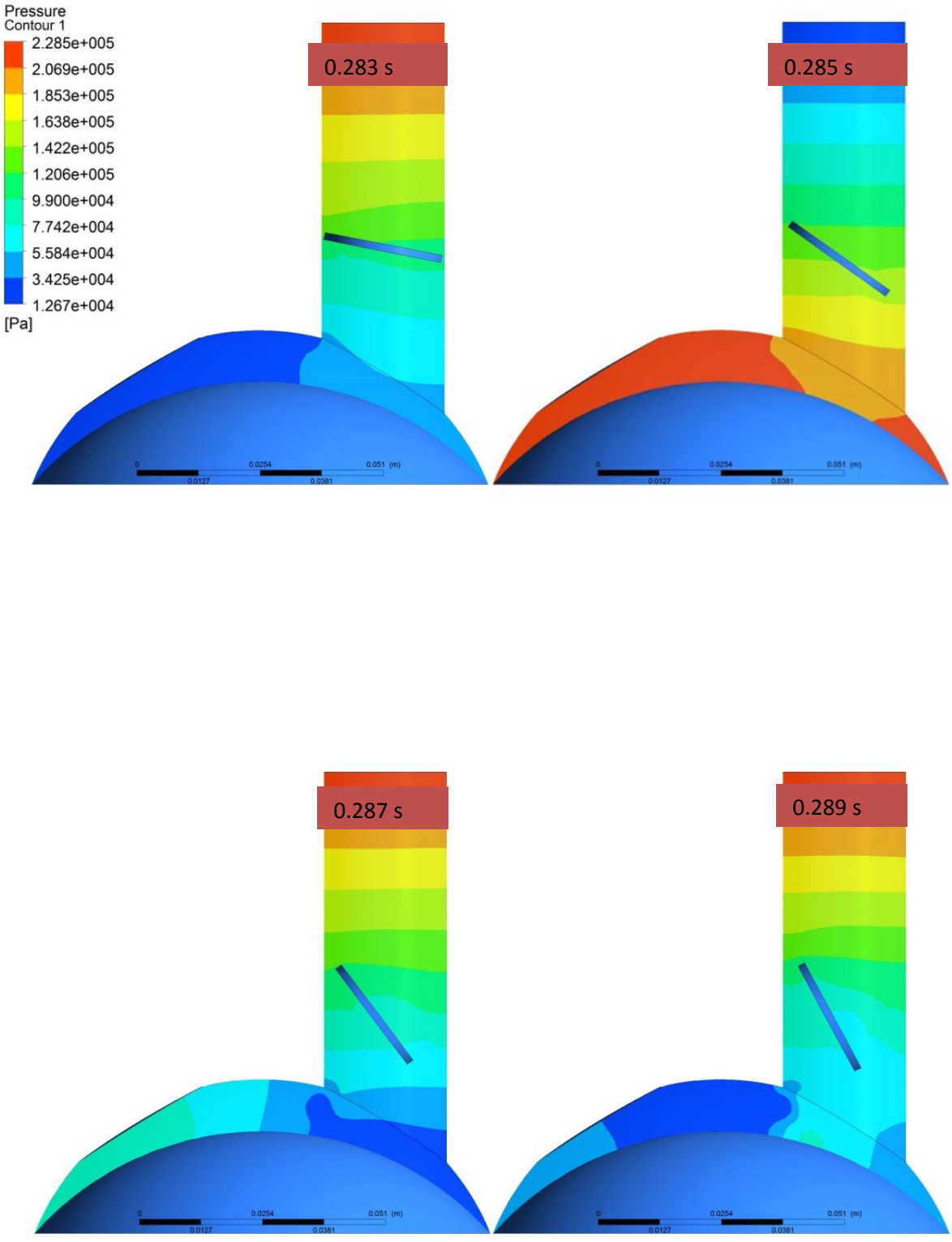
Pressure
Contour 1
2.285e+005
2.069e+005
1.853e+005
1.638e+005
1.422e+005
1.206e+005
9.900e+004
7.742e+004
5.584e+004
3.425e+004
1.267e+004
[Pa]
0.283 s
0.285 s
0.287 s
0.289 s

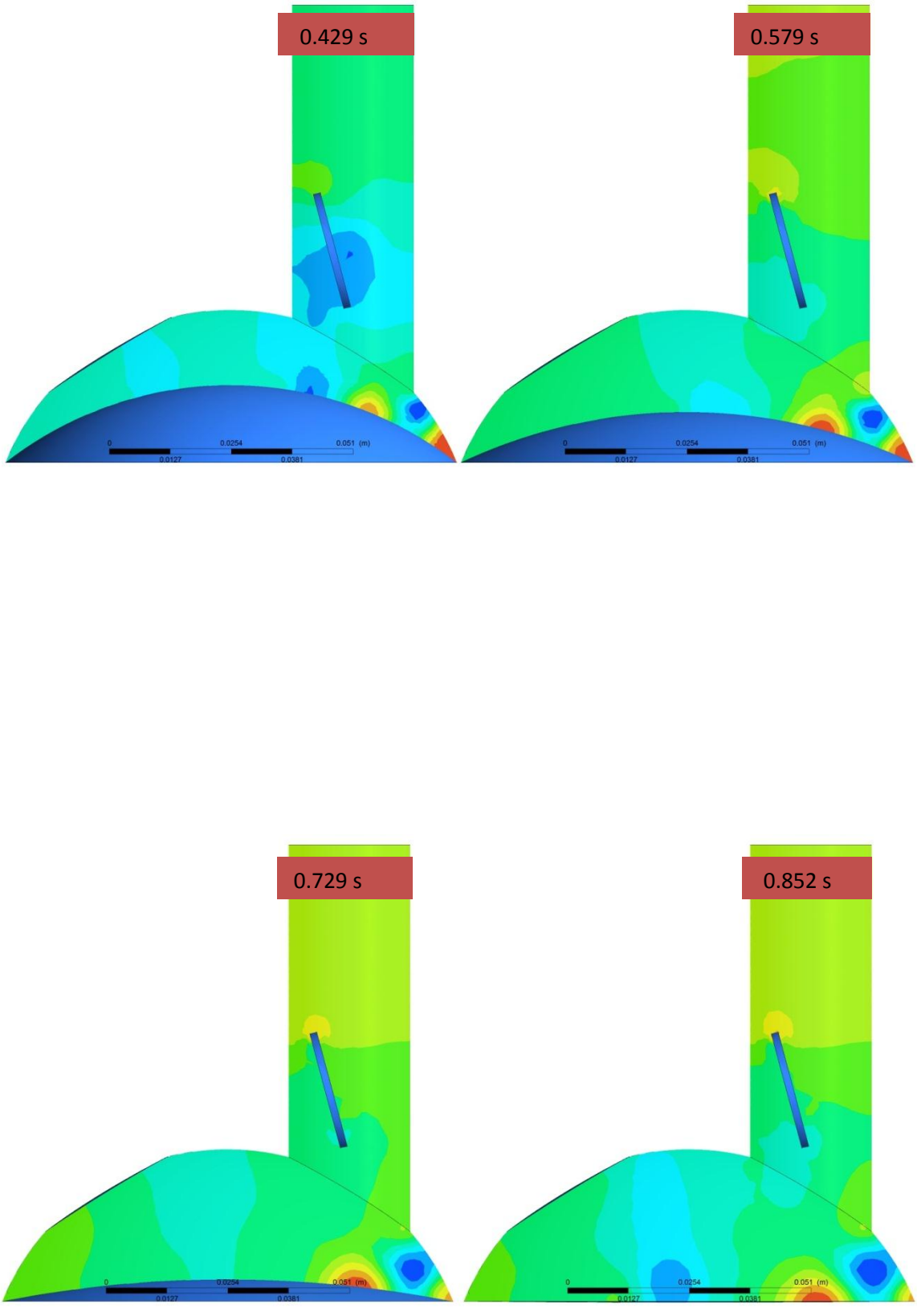

Figure 4.74 Pressure distribution for the monoleaflet inlet valve opening (opening angle = 75°)

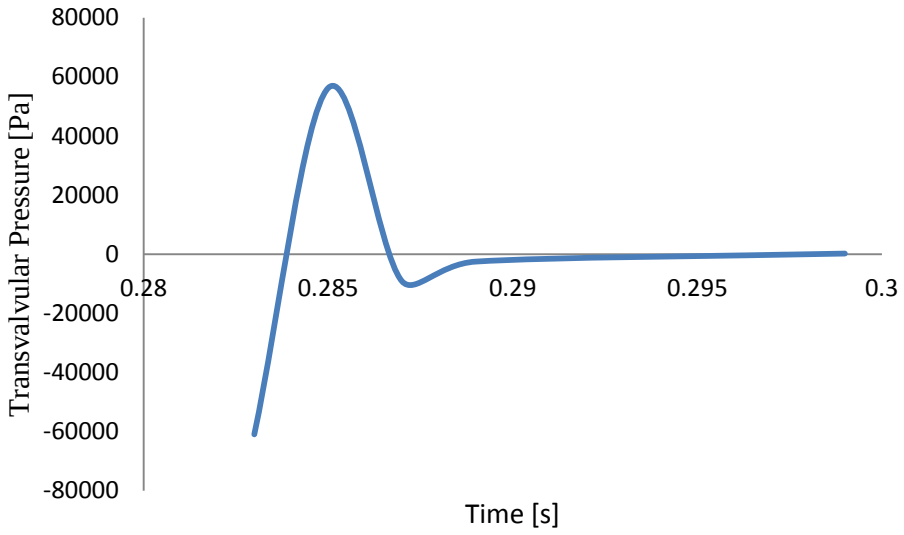

Figure 4.75 Transvalvular pressure versus time for the monoleaflet inlet valve opening measured as the difference between average pressure on two planes 0.02 m apart, before and after the valve. (opening angle = 75^{O})

4.2.2.4 THE MONOLEAFLET INLET VALVE CLOSING BEHAVIOR

Table 4.18 lists the maximum velocity and pressure conditions during the outlet valve closing. In this table, transvalvular pressure was defined as the difference between average pressure on two planes of 0.02 m apart, before and after the valve. Figure 4.76 depicts velocity distribution through late diastole. Figure 4.77 shows velocity vectors in the vicinity of the valve. Figures 4.78 and 4.79 depict pressure distribution through late diastole. It took 0.042 sec for the valve to reach the fully closed position (to reach from 75° to 0°). During the valve closure the valve area was divided into a major and a minor area on each side of the leaflet. The maximum velocity in the gap between the leaflet and the wall in the major area reached 1.57 m/s at the instant of valve closure (t = 0.9 s) while the maximum velocity was 1.256 m/sec in the minor area (t= 0.893s). Figure 4.80 shows the pressure distribution in the model during the valve closure. The mean transvalvular pressure was 565.93 Pa. The maximum transvalvular pressure was 918.23 Pa which occurred at the end of valve closure process (t = 0.9 s).

Table 4.18 Flow parameters related to the monoleaflet inlet valve closing, when the opening angle was 75^{o}.

Parameter	Value
Maximum Velocity	1.570 m/s
Maximum Pressure Drop Across the Valve	918.23 Pa
Average Pressure Drop Across the Valve	565.93 Pa
Valve closing Time	0.042 s

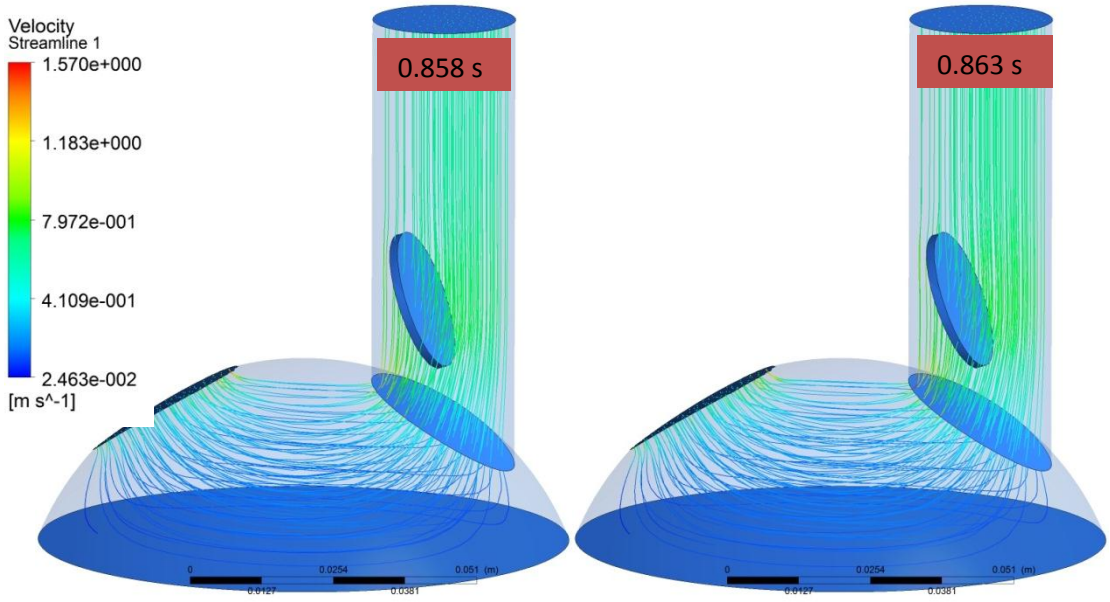
Velocity
Streamline 1
1.570e+000
1.183e+000
7.972e-001
4.109e-001
2.463e-002
[m s^-1]
0.858 s
0.863 s
0
0.0254
0.051 (m)
0.0127
0.0381

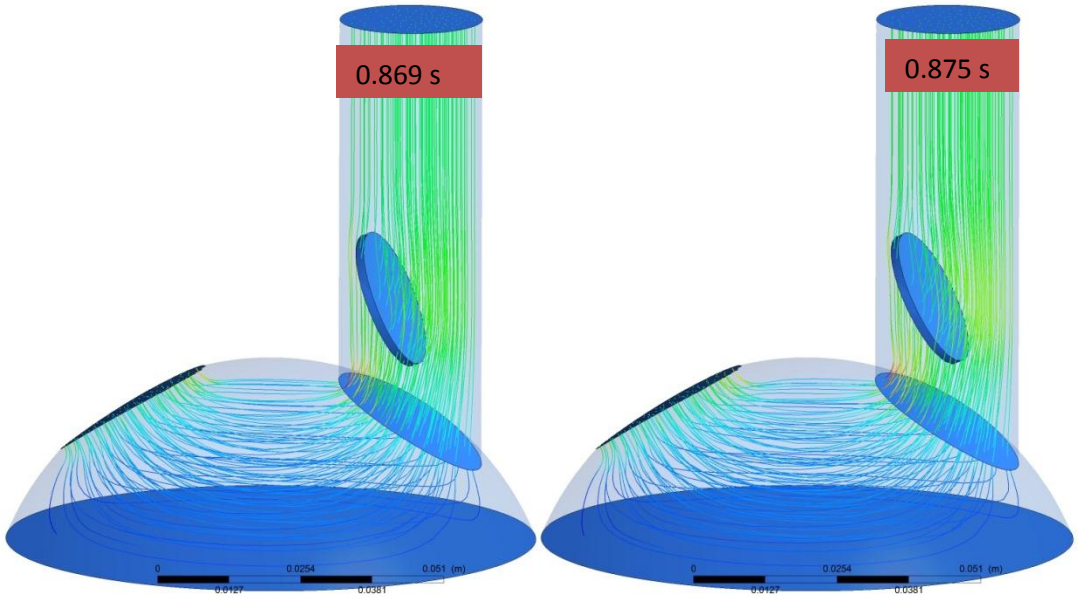
0.869 s
0.875 s
0
0.0254
0.051 (m)
0.0127
0.0381

Figure 4.76 Velocity streamline during early systole when the monoleaflet inlet valve closes.

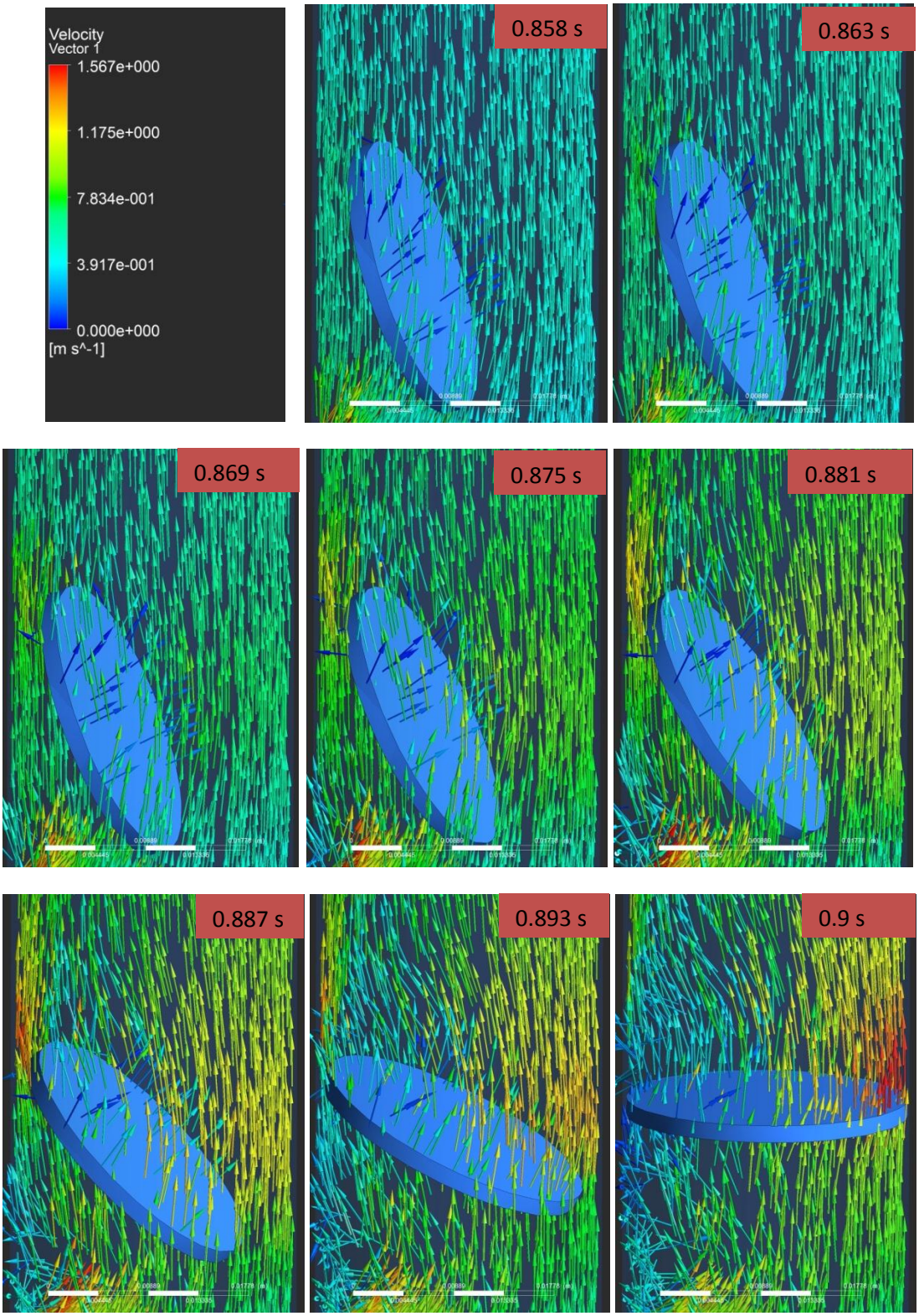

Figure 4.77 Velocity vectors in the valve region during early systole when the monoleaflet inlet valve closes.

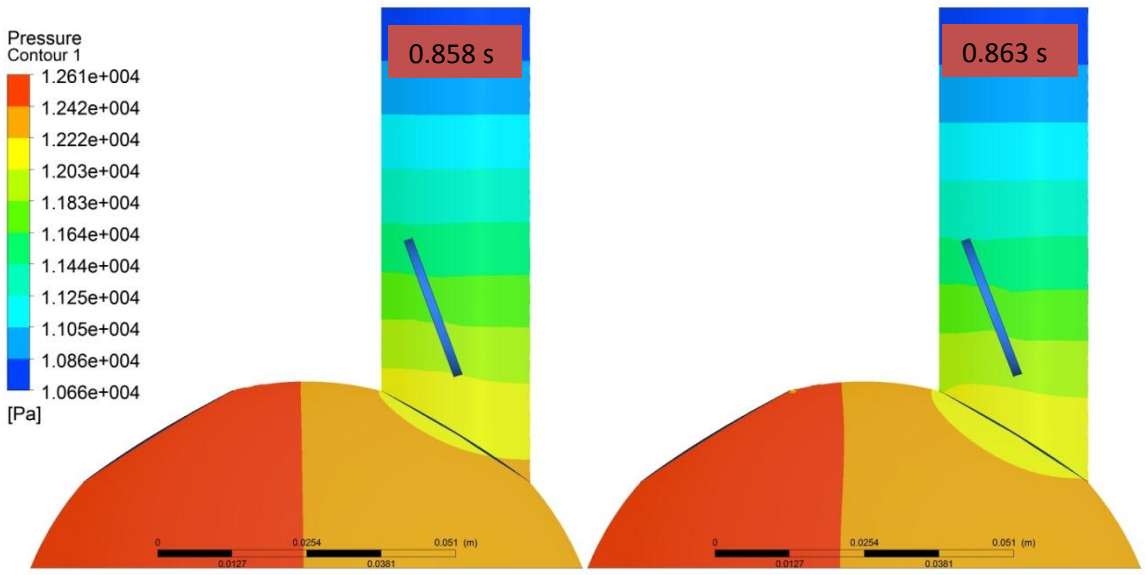
Pressure
Contour 1
1.261e+004
1.242e+004
1.222e+004
1.203e+004
1.183e+004
1.164e+004
1.144e+004
1.125e+004
1.105e+004
1.086e+004
1.066e+004
[Pa]
0.858 s
0.863 s
0
0.0254
0.051 (m)
0.0127
0.0381

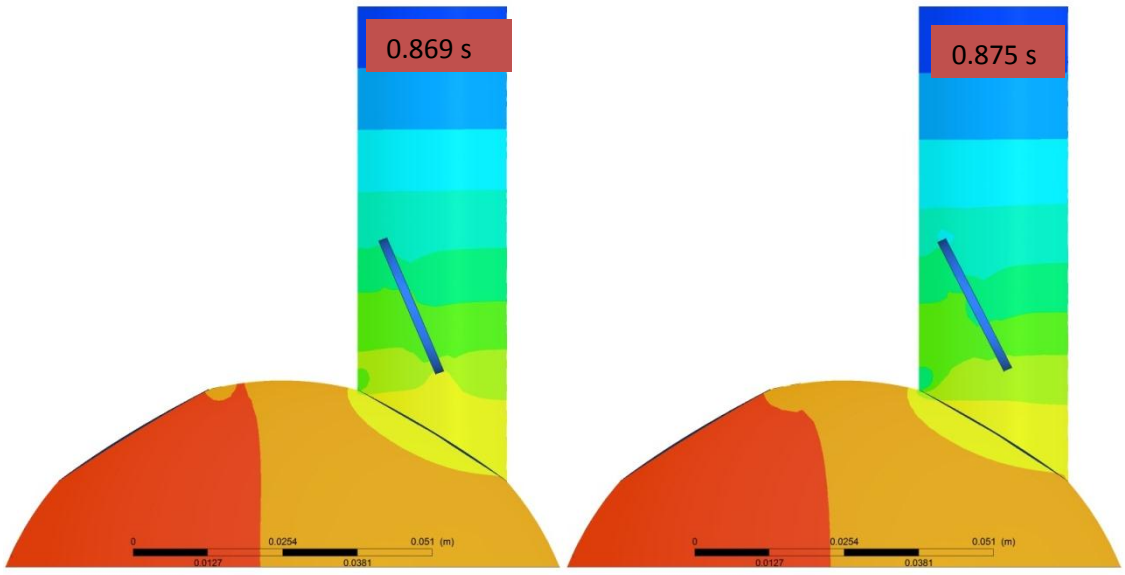
0.869 s
0.875 s
0
0.0254
0.051 (m)
0.0127
0.0381

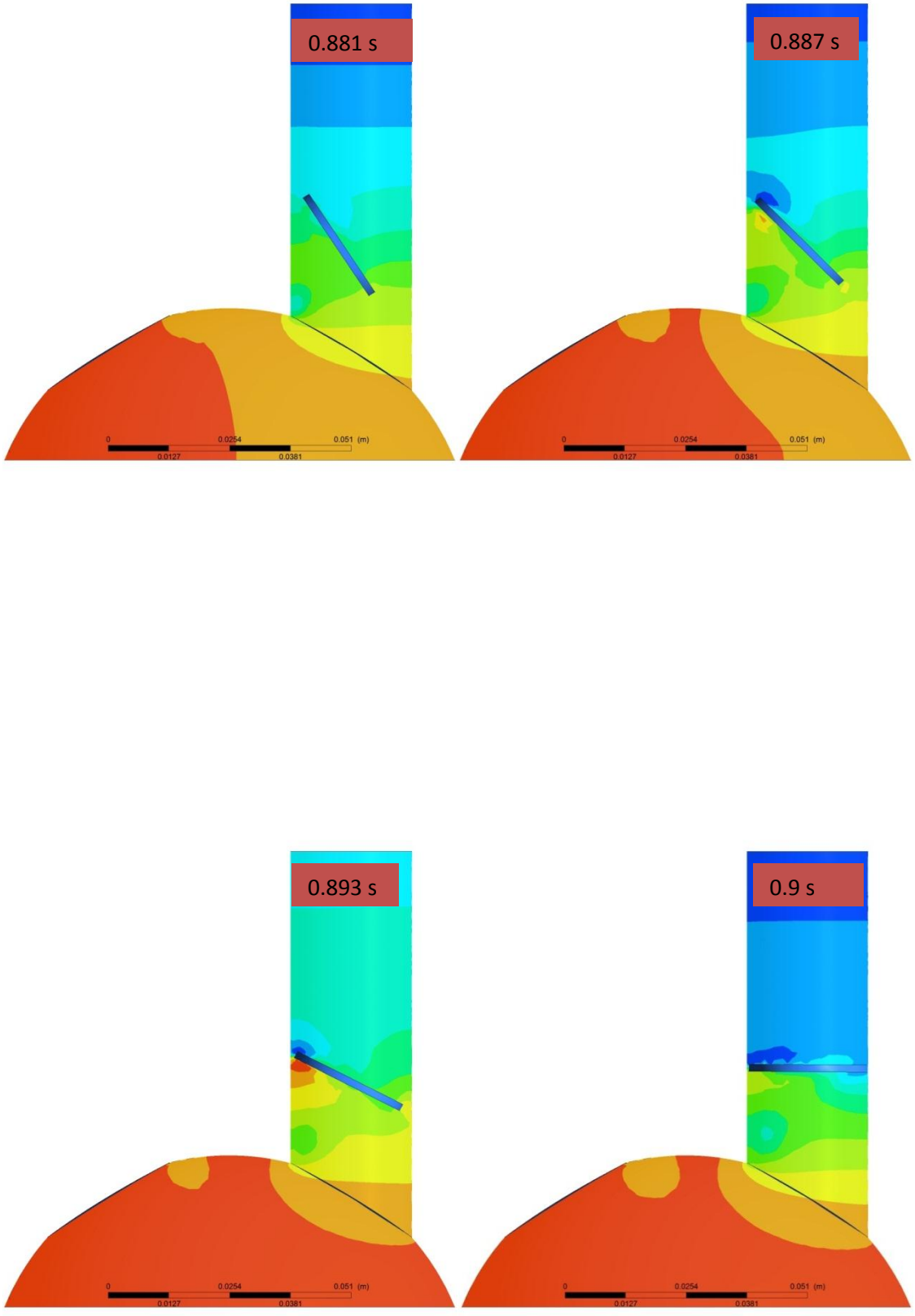

Figure 4.78 Pressure distribution for the monoleaflet inlet valve closing.

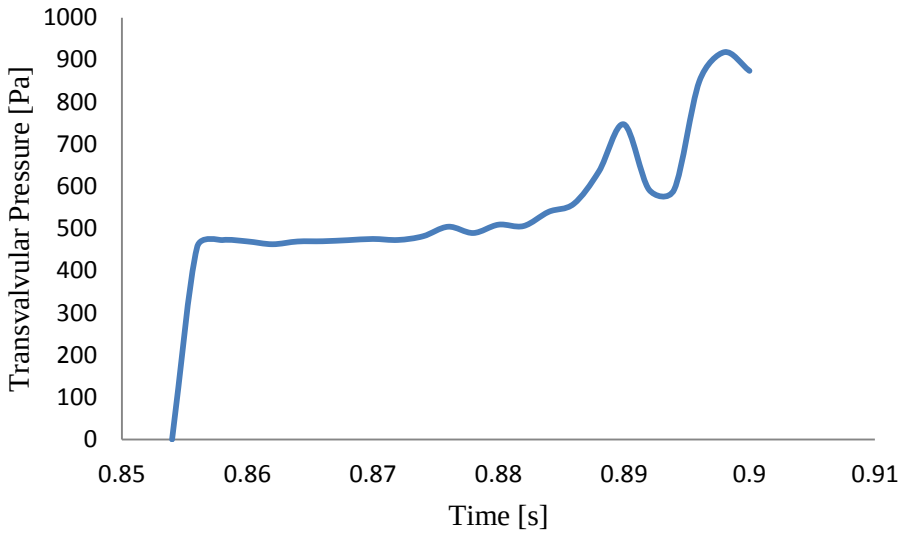

Figure 4.79 Transvalvular pressure versus time for the monoleaflet inlet valve closing measured as the difference between average pressures on two planes 0.02 m apart, before and after the valve.

CHAPTER V

DISCUSSION

In this study 2D and 3D Fluid Structure Interaction (FSI) models were developed to simulate the opening and closing behavior of monoleaflet and bileaflet mechanical heart valves, and to help to optimize the monoleaflet valve design. The FSI models were developed using the arbitrary Lagrangian-Eulerian (ALE) method for moving boundaries, coupled with user-defined functions to describe leaflet and diaphragm motion. Valve motion was determined by fluid dynamics inside the flow chamber; and the diaphragm motion was controlled by a pulsatile pump, following the experimental setup in Yin et al. *in vitro* studies[60].

5.1 COMPARISON BETWEEN 2D AND 3D MODELING RESULTS

The comparison between velocity profiles of 2D and 3D models for the bileaflet valves demonstrated that the two models had similar flow patterns (Table 5.1). The maximum flow velocities estimated using the 3D model of the bileaflet valves were closer to those reported in experimental studies[68, 69] (Table 5.1). The simplified geometry used in 2D models might have resulted in less accurate velocity estimations. Similarly, the 3D models of the monoleaflet valve produced more accurate estimation of flow velocities, compared to the 2D models (Figure 5.1). However, in case of the monoleaflet inlet valve opening, the estimated maximum flow velocity was higher than the measured value for prosthetic valves with echocardiography and Doppler ultrasound methods. One reason could be a minor error in the simulation convergence and also the different design of the flow chamber needs to be taken into consideration.

Table 5.1 Comparison between 2D and 3D maximum flow velocities and corresponding *in vivo* measurements

Maximum Velocity (m/s) in:	2D Model	3D Model	Experimental Measurements
Outlet Bileaflet Valve Opening	0.3099	1.391	3[67]
Outlet Bileaflet Valve Closing	0.745	2.315	1.5 - 2.5[68]
Inlet Bileaflet Valve Opening	2.5	2.158	1.9[67]
Inlet Bileaflet Valve Closing	1.13	1.28	1.9[67]
Outlet Monoleaflet Valve Opening	0.35	1.058	3[67]
Outlet Monoleaflet Valve Closing	0.78	1.846	1.5 - 2.5[68]
Inlet Monoleaflet Valve Opening	0.64	6.446	1.9[67]
Inlet Monoleaflet Valve Closing	1.114	1.570	1.9[67]

The average transvalvular pressures across the valve during the leaflet closing and opening process for the 2D and 3D simulations are listed in Table 5.2. 2D and 3D models generated quite different results on transvalvular pressures. In general, the 3D models generated higher transvalvular pressures compared to 2D models, except the case for the bileaflet outlet valve closing. When compared to experimental results obtained from ultrasound measurements, data obtained from the bileaflet outlet valve closing seemed to be the least accurate. The geometry difference between the flow chamber and the real heart may have contributed greatly to the difference we observed in the transvalvular pressure. Also, as it was mentioned in the *Results* section, during systole flow separated in the outlet tube and flow was skewed to the outside. Such a flow pattern resulted in an unsymmetrical closure of the outlet bileaflet valve. In a numerical study by Borazjani and Sotiropoulos[74], the asymmetric closing behavior of the aortic bileaflet valve was investigated as a function of valve orientation. They have reported that a valve which is oriented in the direction of the left ventricular outflow tract provided the minimum asymmetric closure of the leaflets. The asymmetric closure of the bileaflet valve can cause regurgitation (backward flow of blood to the left ventricle) and complex flow patterns in the valve area. Enchinger et al.[75], in an *in vitro* study, showed the asymmetric closure of a prosthetic bileaflet valve and corresponding regurgitation problem. Subsequently, *in vivo* studies have confirmed the asymmetric leaflet closure in bileaflet mechanical heart valves[76; 77].

Table 5.2 Comparison between 2D and 3D mean transvalvular pressure and corresponding experimental measurements

Mean Transvalvular Pressure (Pa) in:	2D Model	3D Model	Experimental Measurements
Outlet Bileaflet Valve Opening	91.60	117.716	586.61[69]
Outlet Bileaflet Valve Closing	3034.97	1251.29	586.61[69]
Inlet Bileaflet Valve Opening	227.436	506.273	666.61[67]
Inlet Bileaflet Valve Closing	72.65	473.548	666.61[67]
Outlet Monoleaflet Valve Opening	64.68	124.13	1466[67]
Outlet Monoleaflet Valve Closing	148.79	440.35	1466[67]
Inlet Monoleaflet Valve Opening	177.14	1970.21	666.61[67]
Inlet Monoleaflet Valve Closing	245.56	440.80	59,995[70]

The valve opening and closing times for different cases are compared in Table 5.3 between 2D and 3D simulations. In all cases, estimation from 2D simulations were much higher than that from 3D simulations, which are very close to results reported from experimental studies. The simplified geometry of the leaflets in 2D model had a lower momentum source compared to the 3D geometry. Due to the low momentum of the leaflet, the leaflet could be mildly permeable to flow. Therefore, when the movement of the fluid elements within the leaflet did not match the leaflet motion exactly, the movement of the leaflet would be retarded, resulting in longer opening and closing time.

Table 5.3 Comparison between the 2D and 3D models for valve opening and closing times and corresponding experimental measurements

Valve Opening/Closing Time (s) in:	2D Model	3D Model	Experimental Measurements
Outlet Bileaflet Valve Opening	0.16	0.022	0.025 - 0.035[71]
Outlet Bileaflet Valve Closing	0.042	0.038	0.035[72]
Inlet Bileaflet Valve Opening	0.106	0.03	-
Inlet Bileaflet Valve Closing	0.182	0.04	-
Outlet Monoleaflet Valve Opening	0.107	0.017	0.025 - 0.035[71]
Outlet Monoleaflet Valve Closing	0.104	0.036	0.05[73]
Inlet Monoleaflet Valve Opening	0.09	0.03	-
Inlet Monoleaflet Valve Closing	0.063	0.043	0.062[73]

Prosthetic heart valve opening and closing time has a significant effect on hemodynamic performance of the valve. During systole, longer opening time can cause higher resistance to the main flow. On the other hand, during diastole, higher closing velocities, or short closing time can intensify the cavitation possibility in the valve region[70].

Using the same computational source for 2D and 3D models (Intel 3.2 GHz dual processor, 12 Gb RAM), the CPU time was significantly lower for 2D simulations of the bileaflet valve compared to 3D ones. The results from 2D models were also easier to interpret. 3D models of the bileaflet valve used more CPU time and results from these models enabled us to estimate the three dimensional structure of flow across the valve and provided more detailed flow

information compared to 2D models. Similarly, the 3D models of the monoleaflet valve required more CPU time utilizing the same computational source as the 2D models and they were able to produce a more accurate estimation of the 3D flow patterns. Our results demonstrated that, in general, 2D flow analysis was able to capture the valve opening and closing dynamics but 3D models were required for high quality quantitative analysis.

5.2 THE OPTIMAL OPENING ANGLE FOR THE MONOLEAFLET OUTLET VALVE

In order to find the optimal opening angle for the monoleaflet outlet valve, the hemodynamic performance of monoleaflet valves at the opening angle of 45°, 60°, 75°, 80°, and 85° was compared. The hemodynamic performance was evaluated based on the effective orifice area (EOA), transvalvular pressure gradient, flow separation, and turbulence.

As it can be seen in Table 5.4, as the opening angle increased from 45° to 75° the maximum velocity and transvalvular pressure decreased and the EOA increased, indicating the improved hemodynamic performance. For an opening angle of 80°, the maximum velocity stayed about the same and the transvalvular pressure dropped slightly; but the EOA increased, indicating the further improvement of the valve performance. As the opening angle was further increased to 85° , there was a slight increase in the maximum velocity, while the decrease in transvalvular pressure and the increase in EOA were significant.

Table 5.4 Comparison between monoleaflet outlet valve opening behavior with different opening angles

PARAMETER	45^o	60^o	75^o	80^o	85^o
Maximum Velocity m/s	1.342	1.155	1.058	1.057	1.065
Average Pressure Difference Across the Valve Pa	320	254.95	124.13	101.26	46.28
Valve Opening Time s	0.015	0.016	0.017	0.018	0.02
EOA cm^2	1.19	1.33	1.91	2.13	3.16

For all the opening angles, as the leaflet reached its fully opened position, flow separated around the valve leaflet and a region of high velocity flow was formed on one side of the leaflet. On the other side, flow separated from the outlet wall and recirculation zones developed. As the opening angle increased, velocity fluctuation in the high velocity flow region decreased, producing a lower turbulent energy, which lowered the chance of flow transitioning into turbulence. In addition, as the opening angle increased, the area of the wake region behind the leaflet decreased.

Moreover, when the opening angles were less than 75° the jet flow in the high velocity region followed the inclination of the leaflet and then impinged on the outlet wall, which could increase the wall shear stress at the impingement region. When the opening angle was 75°, 80° or 85°, the fluid flow was more centralized and did not impinge on the outlet wall.

During the outlet valve closure, the monoleaflet valve with 75° of opening angle had the lowest maximum backflow velocity while the valve with the 85° opening angle was not able to close properly due to the big opening angle. At 80°, the valve was able to close but the maximum backflow velocity increased compared to the case with 75° of opening angle. These results demonstrated that the optimal opening angle should fall between 75° and 80°. As the opening angle further increased, even though the calculated flow parameters (i.e., transvalvular pressure and EOA) continued to improve, the large angle would prevent the valve to close properly, which would lead to the failure of the heart valve.

5.3 COMPARISON BETWEEN BILEAFLET AND MONOLEAFLET MECHANICAL HEART VALVES

The advantages of mechanical heart valves include good hemodynamic performance and high durability. Hemodynamic performance can be evaluated by measuring the following parameters: transvalvular pressure, flow recirculation regions, turbulent flow, stagnation and flow separation zones. In this study, using computational fluid dynamics (CFD) models, these parameters were estimated for bileaflet and monoleaflet MHVs during opening and closing processes. The St. Jude bileaflet valve had an opening angle of 85^{o}, while the optimal opening angle for the monoleaflet valve should be between 75^{o} and 80°. In the following discussion, the monoleaflet performance at its optimal opening angle was compared to that of the St. Jude bileaflet heart valve. Our simulation results demonstrated that the flow in the monoleaflet valve design had a lower maximum velocity compared to the bileaflet design during both opening and closing phases. Lower flow velocity lowered the chance for flow to transition to turbulence.

The mean and peak transvalvular pressures across the monoleaflet valve design were slightly higher than that of the bileaflet valve during the opening process. Higher pressure drop at the instant of valve opening for the monoleaflet design could be attributed to the higher moment of inertia of the leaflet in this design (1.21E-7 kg m^2) compared to the moment of inertia for the bileaflet valve design (8.1 E-9 kg m2). The similar pressure gradients across the monoleaflet and bileaflet valves resulted in an analogous EOA of 1.91 cm^2 and 1.96 cm^2 for these valves respectively, very similar.

Results for the bileaflet valve during closure showed nonsymmetrical closing behavior of the leaflets in this design (i.e. the left leaflet stayed at the maximal opening angle at the beginning of the diastole while the right leaflet closed early). The delayed closure of the bileaflet valve and its nonsymmetrical closing behavior could cause higher valve regurgitation compared to monoleaflet valve.

Our computational results also showed that there was no impingement region in both valve designs at their fully opened position. This would reduce the chance of high shear stress and shear stress gradient regions on the outlet wall. During valve closure, cavitation could be a big issue when the hemodynamic performance of a valve is considered. Cavitation is the formation of vaporous cavities due to large pressure drops resulting in fluid regions with lower pressure than vapor pressure of the blood. The major cause of cavitation is the regions of high velocity (squeeze flow) in the gap between the leaflet and the wall. Previous studies have revealed a direct link between the valve closing velocity and cavitation intensity in the valve region[70]. According to the results of this study during the valve closure phase, the maximum pressure drop for the bileaflet valve (-60000 Pa) was much bigger than the pressure drop for the monoleaflet valve (-17500 Pa), the bileaflet valve had higher chance of developing cavitation bubbles, especially when the leaflet tip velocity was also higher in the bileaflet design.

Due to the turbulent kinetic energy values from the two dimensional models, presented in the results section, the flow was maintained laminar in the whole model. This was in agreement with results from Ngwe numerical model[18]. Laminar flow condition was utilized in all three dimensional models without causing any convergence issues. The major limitation of this study was ignoring the diaphragm elasticity in all models. Considering the elasticity for the diaphragm could result in a better prediction of pressure and velocity distribution in the flow chamber. Another limitation of this study was lack of experimental results on flow conditions in the flow chamber and valve regions. Due to lack of an experimental study, results from this study were validated using physiological flow conditions for normal prosthetic heart valves extracted from different *in vivo* and *in vitro* studies. Further discussion on the verification and validation of results is provided in the next section.

5.4 VERFICATION AND VALIDATION OF THE RESULTS

The iterative convergence of all simulations in this study and consistency of the results were monitored. In all simulations, the solutions were converged at each time step (0.0005 s for the 3D models and 0.002 s for the 2D models) until the final time (t = 0.9 s) was reached. The results were independent from mesh density and mass conservation was maintained throughout the whole simulation.

Yin et al.[60] presented the maximum pressure drop and velocity for outlet and inlet valves during systole and diastole. Results from her study were comparable to 2D results of this research. However, results extracted from 3D models were showing higher values for pressure drop and velocities compared to Yin et al.[60]. Since there were no experimental studies on this kind of flow chamber, numerical results from this study were compared to experimental studies of similar prosthetic valves in different experimental setups (Table 5.1 – Table 5.3). These comparisons show that results from this study were within the range of other studies. Along with other numerical studies on prosthetic heart valves[28-32], this study contributed to our knowledge in mechanical heart valve performance under physiologically relevant dynamic environment, and brought new insight to optimal valve design.

CHAPTER V

CONCLUSION

The major goal of this study was to develop a high resolution numerical model to simulate the diaphragm motion and corresponding valve leaflet motions, to provide a more accurate estimation of the flow conditions in the Ngwe's flow chamber design[18]. The specific aims of this study were to develop two dimensional and three dimensional FSI models to simulate the diaphragm motion and corresponding bileaflet and monoleaflet valve motions, and evaluate flow dynamics around the valve area during systole and diastole. Also, it was an objective of this study to investigate the optimum opening angle for the monoleaflet mechanical heart valve and compare its hemodynamic performance to that of bileaflet heart valves.

Due to the results of this study, 2D flow analysis was able to capture the valve opening and closing dynamics but 3D models were required for high quality quantitative analysis. Results from this study demonstrated that the optimal opening angle should fall between 75° and 80°. As the opening angle further increased, even though the calculated flow parameters continued to improve, the large angle could prevent the valve to close properly, which might lead to the failure of the heart valve.

Furthermore, the hemodynamic performance of bileaflet and monoleaflet heart valves following the design of St. Jude bileaflet valve with 85° of opening angle and Bjork-Shiley

monoleaflet valve with 75° of opening angle was compared. Results demonstrated that monoleaflet mechanical heart valve has comparable hemodynamic performance to that of a bileaflet mechanical heart valve.

REFERENCES

1. Martorana C, W.Smith M, Nazario B, Chang L, Bhargava H, and J.Martin L. Heart Valve Disease. http://www.webmd.com/heart-disease/guide/heart-valve-disease. Accessed July 28, 2012.

2. Yoganathan AP, He ZM, Jones SC. Fluid mechanics of heart valves. *Annual Review of Biomedical Engineering* 2004;6:331-362.

3. Anderson GM, Grumbach K, Luft HS,et al. Use of coronary artery bypass surgery in the United States and Canada. Influence of age and income. *JAMA* 1993; 269: 1661–1666.

4. Vongpatanasin W, Hillis D, Lange R. Prosthetic heart valves. *N. Engl. J. Med*. 1996; 335: 407–416.

5. Emery RW, Petersen RJ, Kersten TE, et al. The initial United States experience with the ATS mechanical cardiac valve prosthesis. *Heart Surgery Forum*. 2001; 4(4):346-353.

6. Lee H, Tatsumi E, Taenaka Y. Flow Visualization of A Monoleaflet and Bileaflet Mechanical Heart Valve in A Pneumatic Ventricular Assist Device Using A PIV System. *Asaio Journal* 2010;56:186-193.

7. Kleine P, Perthel M, Nygaard H et al. Medtronic Hall versus St. Jude medical mechanical aortic valve: Downstream turbulences with respect to rotation in pigs. *Journal of Heart Valve Disease* 1998;7:548-555.

8. Kleine P, Perthel M, Hasenkam JM et al. High-intensity transient signals (HITS) as a parameter for optimum orientation of mechanical aortic valves. *Thoracic and Cardiovascular Surgeon* 2000;48:360-363.

9. Kleine P, Perthel M, Hasenkam JM et al. Downstream turbulence and high intensity transient signals (HITS) following aortic valve replacement with Medtronic Hall or St. Jude Medical valve substitutes. *European Journal of Cardio-Thoracic Surgery* 2000;17:20-24.

10. Kleine P, Scherer M, Abdel-Rahman U et al. Effect of mechanical aortic valve orientaion on coronary artery flow: Comparison of tilting disc versus bileaflet

prostheses in pigs. *Journal of Thoracic and Cardiovascular Surgery* 2002;124:925-932.

11. Laas J, Kleine P, Hasenkam MJ, Nygaard H. Orientation of tilting disc and bileaflet aortic valve substitutes for optimal hemodynamics. *Annals of Thoracic Surgery* 1999;68:1096-1099.

12. Laas J, Kseibi S, Perthel M et al. Impact of high intensity transient signals on the choice of mechanical aortic valve substitutes. *European Journal of Cardio-Thoracic Surgery* 2003;23:93-96.

13. Butany J, Ahluwalia MS, Munroe C et al. Mechanical heart valve prostheses: identification and evaluation (vol 12, pg 322, 2003). *Cardiovascular Pathology* 2003;12:322-344.

14. Pibarot P, Dumesnil JG. Prosthetic Heart Valves Selection of the Optimal Prosthesis and Long-Term Management. *Circulation* 2009;119:1034-1048.

15. Vansteenhoven AA, Verlaan CWJ, Veenstra PC, Reneman RS. Invivo Cinematographic Analysis of Behavior of the Aortic-Valve. *American Journal of Physiology* 1981;240:286-292.

16. Nerem RM, Seed WA. In-Vivo Study of Aortic Flow Disturbances. *Cardiovascular Research* 1972;6:1-14.

17. Weston MW, LaBorde DV, Yoganathan AP. Estimation of the shear stress on the surface of an aortic valve leaflet. *Annals of Biomedical Engineering* 1999;27:572-579.

18. Ngwe EC. A biocompatible flow chamber to study the hemodynamic performance of prosthetic heart valves. 2010. Oklahoma State University. Ref Type: Thesis/Dissertation.

19. Sotiropoulos F, Borazjani I. A review of state-of-the-art numerical methods for simulating flow through mechanical heart valves. Medical & Biological Engineering & Computing 2009;47:245-256.

20. Dasi LP, Simon HA, Sucosky P, Yoganathan AP. Fluid Mechanics of Artificial Heart Valves. *Clinical and Experimental Pharmacology and Physiology*. 2009;36(2):225-237.

21. Iqbal A. Human anatomy. http://www.mananatomy.com/. Accessed July 16, 2012.

22. Martini F, Nath JL. Fundamentals of anatomy & physiology (ed 8th). San Francisco: Pearson/Benjamin Cummings; 2009.

23. Fatemeh F. Pirapezeshki. http://pirapezeshki90.blogfa.com. Accessed July 13, 2012.

24. Nkomo VT, Gardin JM, Skelton TN, et al. Burden of valvular diseases: a population-based study. The Lancet Online. 2006;368:1005-1011.

25. Yoganathan AP, He Z, Casey Jones S. Fluid mechanics of heart valves. *Annu Rev Biomed Eng*. 2004;6:331-362.

26. Butany J, Ahluwalia MS, Munroe C, et al. Mechanical heart valve prostheses: identification and evaluation (erratum). *Cardiovasc Pathol*. 2003;12(6):322-344.

27. Gott VL, Alejo DE, Cameron DE. Mechanical heart valves: 50 years of evolution. *Annals of Thoracic Surgery*. 2003;76(6):S2230-S2239.

28. Morse D, Steiner RM, Fernandez J. Cardiac valve identification atlas and guide. In: Dryden Morse RM, Sa JF editor. Guide to prosthetic cardiac valves. New York: Springer-Verlag; 1985; 257–346

29. Bloomfield P. Choice of heart valve prosthesis. *Heart*. 2002;87(6):583-589.

30. Emery RW, Arom KV, Kshettry VR, et al. Decision-making in the choice of heart valve for replacement in patients aged 60-70 years: twenty-year follow up of the St. Jude Medical aortic valve prosthesis. *J Heart Valve Dis*. 2002;11 Suppl 1:S37-44.

31. Marchand MA, Aupart MR, Norton R, et al. Fifteen-year experience with the mitral Carpentier-Edwards perimount pericardial bioprosthesis. *Annals of Thoracic Surgery*. 2001;71(5):S236-S239.

32. Westaby S, Huysmans HA, David TE. Stentless aortic bioprostheses: Compelling data from the second international symposium. *Annals of Thoracic Surgery*. 1998;65(1):235-240.

33. Mancini MC. Bioprosthetic heart valves. http://emedicine.medscape.com/article/1971075-overview. Accessed July 13, 2012.

34. Nair K, Muraleedharan CV, Bhuvaneshwar GS. Developments in mechanical heart valve prosthesis. *Sadhana-Academy Proceedings in Engineering Sciences*. 2003;28:575-587.

35. Mouneimne K., et al. Testing Transcatheter Heart Valve Devices. Vol. 1. Los Angeles, CA, ETATS-UNIS: Canon Communication; 2010.

36. Jimenez JH, Soerensen DD, He ZM, Ritchie J, Yoganathan AP. Mitral valve function and chordal force distribution using a flexible annulus model: An In vitro study. *Annals of Biomedical Engineering*. 2005;33(5):557-566.

37. Ritchie J, Jimenez J, He ZM, Sacks MS, Yoganathan AP. The material properties of the native porcine mitral valve chordae tendineae: An in vitro investigation. *Journal of Biomechanics*. 2006;39(6):1129-1135.

38. Yoffe B, Vaysbeyn I, Urin Y, et al. Experimental study of a novel suture-less aortic anastomotic device. *European Journal of Vascular and Endovascular Surgery*. 2007;34(1):79-86.

39. Day SW, McDaniel JC. PIV measurements of flow in a centrifugal blood pump: Steady flow. *Journal of Biomechanical Engineering-Transactions of the Asme*. 2005;127(2):244-253.

40. Timms D, Hayne M, Tan A, Pearcy M. Evaluation of left ventricular assist device performance and hydraulic force in a complete mock circulation loop. *Artificial Organs* 2005;29:573-580.

41. Aluri S, Chandran KB. Numerical simulation of mechanical mitral heart valve closure. *Annals of Biomedical Engineering*. 2001;29(8):665-676.

42. Gill-Jeong C, Chandran KB. Dynamics of a mechanical monoleaflet heart valve prosthesis in the closing phase: effect of squeeze film. *Annals of Biomedical Engineering*. 1995;23(2):189-197.

43. King MJ, Corden J, David T, Fisher J. A three-dimensional, time-dependent analysis of flow through a bileaflet mechanical heart valve: Comparison of experimental and numerical results. *Journal of Biomechanics*. 1996;29(5):609-618.

44. King MJ, David T, Fisher J. Three-dimensional study of the effect of two leaflet opening angles on the time-dependent flow through a bileaflet mechanical heart valve. *Medical Engineering & Physics*. 1997;19(3):235-241.

45. Krafczyk M, Cerrolaza M, Schulz M, Rank E. Analysis of 3D transient blood flow passing through an artificial aortic valve by Lattice-Boltzmann methods. *Journal of Biomechanics*. 1998;31(5):453-462.

46. Chandran KB, Lee CS, Chen LD. Pressure field in the vicinity of mechanical valve occluders at the instant of valve closure: correlation with cavitation initiation. *The Journal of heart valve disease*. 1994;3 Suppl 1:S65-75; discussion S75-66.

47. Lee CS, Chandran KB. Numerical simulation of instantaneous backflow through central clearance of bileaflet mechanical heart valves at closure: shear stress and pressure fields within clearance. *Medical & biological engineering & computing*. 1995;33(3):257-263.

48. Lai YG, Chandran KB, Lemmon J. A numerical simulation of mechanical heart valve closure fluid dynamics. *Journal of Biomechanics*. 2002;35(7):881-892.

49. Rosenfeld M, Avrahami I, Einav S. Unsteady effects on the flow across tilting disk valves. *Journal of Biomechanical Engineering-Transactions of the Asme*. 2002;124(1):21-29.

50. Krishnan S, Udaykumar HS, Marshall JS, Chandran KB. Two-dimensional dynamic simulation of platelet activation during mechanical heart valve closure. *Ann Biomed Eng*. 2006;34(10):1519-1534.

51. Yin W, Alemu Y, Affeld K, Jesty J, Bluestein D. Flow-induced platelet activation in bileaflet and monoleaflet mechanical heart valves. *Ann Biomed Eng*. 2004;32(8):1058-1066.

52. Simon HA, Ge L, Sotiropoulos F, Yoganathan AP. Simulation of the Three-Dimensional Hinge Flow Fields of a Bileaflet Mechanical Heart Valve Under Aortic Conditions. *Annals of Biomedical Engineering*. 2010;38(3):841-853.

53. De Hart J. Fluid-Structure intraction in the aortic heart valve. Vol. PhD. Eindhoven: eindhoven University of Thecnology; 2002.

54. Govindarajan V, Udaykumar HS, Herbertson LH, Deutsch S, Manning KB, Chandran KB. Two-dimensional FSI simulation of closing dynamics of a tilting disc mechanical heart valve. *Journal of medical devices*. 2010;4(1):11001.

55. Cheng R, Lai YG, Chandran KB. Three-dimensional fluid-structure interaction simulation of bileaflet mechanical heart valve flow dynamics. *Annals of Biomedical Engineering*. 2004;32(11):1471-1483.

56. Nobili M, Morbiducci U, Ponzini R, et al. Numerical simulation of the dynamics of a bileaflet prosthetic heart valve using a fluid-structure interaction approach. *Journal of Biomechanics*. 2008;41(11):2539-2550.

57. Sotiropoulos F, Borazjani I. A review of state-of-the-art numerical methods for simulating flow through mechanical heart valves. *Medical & Biological Engineering & Computing*. 2009;47(3):245-256.

58. Weston MW, et al. Estimation of the shear stress on the surface of an aortic valve leaflet, *Annals of. Biomedical Engineering*. 27(4), 1999;572-579.

59. Frazier OH. Current status of cardiac transplantation and left ventricular assist devices. *Tex.Heart Inst.J* 2010;37:319-321.

60. Yin W, Ngwe Ch, Rubenstein DA. A Biocompatible Flow Chamber to Study the Hemodynamic Performance of Prosthetic Heart Valves. *Biomedical Engineering* 2012;58:470-480.

61. Cheng R, Lai YG, Chandran KB. Three-dimensional fluid-structure interaction simulation of bileaflet mechanical heart valve flow dynamics. *Ann.Biomed.Eng* 2004;32:1471-1483.

62. Gill-Jeong C, Chandran KB. Dynamics of a mechanical monoleaflet heart valve prosthesis in the closing phase: effect of squeeze film. *Ann.Biomed.Eng* 1995;23:189-197.

63. ANSYS® user's guide: Academic Research. (Release 13.0). ANSYS, Inc. 2012

64. Hirt CW, Amsden AA, Cook JL. An arbitrary Lagrangian-Eulerian computing method for all flow speeds. *Journal of Computational Physics* 1974;14:227-253.

65. Chandran KB, Udaykumar HS, Reinhardt JM. Image-Based Computational Modeling of the Human Circulatory and Pulmonary Systems. 2011.

66. Andreas Laske, MD, Rolf Jenni, MD, Michel Maloigne, MD, Giuseppe Vassalli, MD, Osmund Bertel, MD, Marko I. Turina, MD (1996), Pressure Gradients Across Bileaflet Aortic Valves by Direct Measurement and Echocardiography. *Ann Thorac Surg* 1996;61:48-57.

67. Zoghbi WA, Chambers JB, Dumesnil JG, et al. Recommendations for evaluation of prosthetic valves with echocardiography and doppler ultrasound: a report From the American Society of Echocardiography's Guidelines and Standards Committee and the Task Force on Prosthetic Valves, developed in conjunction with the American College of Cardiology Cardiovascular Imaging Committee, Cardiac Imaging Committee of the American Heart Association, the European Association of Echocardiography, a registered branch of the European Society of Cardiology, the Japanese Society of Echocardiography and the Canadian Society of Echocardiography, endorsed by the American College of Cardiology Foundation, American Heart Association, European Association of Echocardiography, a registered branch of the European Society of Cardiology, the Japanese Society of Echocardiography, and Canadian Society of Echocardiography. *Journal of the American Society of Echocardiography*. 2009;22(9):975-1014.

68. Chandran KB, Lee CS, Chen LD. Pressure field in the vicinity of mechanical valve occluders at the instant of valve closure: correlation with cavitation initiation. *The Journal of heart valve disease*. 1994;3 Suppl 1:S65-75; discussion S75-66.

69. Laske A, Jenni R, Maloigne M, Vassalli G, Bertel O, Turina MI. Pressure gradients across bileaflet aortic valves by direct measurement and echocardiography. *The Annals of thoracic surgery*. 1996;61(1):48-57.

70. Lee H, Tsukiya T, Homma A, et al. A study on the mechanism for cavitation in the mechanical heart valves with an electrohydraulic total artificial heart. *Jsme International Journal Series C-Mechanical Systems Machine Elements and Manufacturing*. 2004;47(4):1043-1048.

71. Van Steenhoven AA, Verlaan CW, Veenstra PC, Reneman RS. In vivo cinematographic analysis of behavior of the aortic valve. *The American journal of physiology*. 1981;240(2):H286-292.

72. Lu PC, Liu JS, Huang RH, Lo CW, Lai HC, Hwang NH. The closing behavior of mechanical aortic heart valve prostheses. *ASAIO journal (American Society for Artificial Internal Organs*. 2004;50(4):294-300.

73. Lee H, Tsukiya T, Homma A, Taenaka Y, Tatsumi E, Takano H. Measurement of the closing behavior of the bjork-shiley monoleaflet mechanical heart valve with an electrohydraulic total artificial heart. *Artif Organs*. 2003;27(8):744-748.

74. Borazjani I, Sotiropoulos F. The Effect of Implantation Orientation of a Bileaflet Mechanical Heart Valve on Kinematics and Hemodynamics in an Anatomic Aorta. *J Biomech Eng.* 2011;132(11:)111005.

75. Eichinger W, Hettich I, Bleiziffer S, Günzinger R, Hutter A, Bauern-schmitt R, Lange R. Intermittent Regurgitation Caused by Incomplete Leaflet Closure of the Medtronic ADVANTAGE Bileaflet Heart Valve: Analysis of the Underlying Mechanism. J. *Thorac. Cardiovas. Surg*. 2010;140(3):611–616.

76. Ikeda K, Okazaki Y, Furukawa K, Ohtsubo S, Yunoki J, Natsuaki M, Itoh T. Direct imaging of bileaflet mechanical valve behavior in the tricuspid position. *Eur J Cardiothorac Surg*. 2006;29(6):1014-9.

77. Lorenz H, Matthias D, Bettina H, Friedrich-C. R. Structural valve failure with every beat regurgitation observed using the Medtronic Advantage aortic valve. *J Thorac Cardiovasc Surg.* 2007;134:1344-1345.

VITA

Morteza Kimiaghalam

Candidate for the Degree of

Master of Science

Thesis: FLUID-STRUCTURE SIMULATION OF BILEAFLET AND MONOLEAFLET MECHANICAL HEART VALVE FLOW DYNAMICS

Major Field: MECHANICAL ENGINEERING

Biographical:

Education:

Completed the requirements for the Master of Science in Mechanical Engineering at Oklahoma State University, Stillwater, Oklahoma in December, 2012.

Completed the requirements for the Bachelor of Science in Mechanical Engineering at Ferdowsi University of Mashhad, Mashhad, Iran in 2010.

Relevant Experience:

Research and Development Engineer September 2012 – Present
Rupture Pin Technology, Oklahoma City, United States.

Graduate Research Assistant January 2011 – July 2012
School of Mechanical and Aerospace Engineering, Oklahoma State University

HVAC Designer September 2009 - January 2010
Paya Idea Karamad Toos Co. Mashhad, Iran.

Summer Intern July 2009- August 2009
Iran Khodro Khorasan Co. Mashhad, Iran.

Undergraduate Research Assistant January 2009 – May 2009
School of Mechanical and Aerospace Engineering, Ferdowsi University of Mashhad

Name: Morteza Kimiaghalam Date of Degree: May, 2013

Institution: Oklahoma State University Location: Stillwater, Oklahoma

Title of Study: FLUID-STRUCTURE SIMULATION OF BILEAFLET AND MONOLEAFLET MECHANICAL HEART VALVE FLOW DYNAMICS

Pages in Study: 190 Candidate for the Degree of Master of Science

Major Field: Mechanical Engineering

In this study, opening and closing behavior of monoleaflet and bileaflet prosthetic heart valves was simulated using 2D and 3D Fluid Structure Interaction (FSI) models. The FSI models were based on the arbitrary Lagrangian-Eulerian (ALE) method for moving boundaries. Leaflet and diaphragm motions were described by means of user-defined functions following the experimental setup in a previous study. The hemodynamic performance of monoleaflet valves at the opening angle of 45°, 60°, 75°, 80°, and 85° was compared and results from this study demonstrated that the optimal opening angle should fall between 75° and 80°. As the opening angle further increased, even though the calculated flow parameters continued to improve, the large angle could prevent the valve to close properly, which might lead to the failure of the heart valve. Furthermore, the hemodynamic performance of bileaflet and monoleaflet heart valves following the design of St. Jude bileaflet valve with 85° of opening angle and Bjork-Shiley monoleaflet valve with 75° of opening angle was compared. Results demonstrated that the flow in the monoleaflet valve design had a lower maximum velocity compared to the bileaflet design during both opening and closing phases which resulted in lower chance for flow to transition to turbulence. The mean pressure gradients across the monoleaflet and bileaflet valves were similar and resulted in an analogous EOA for these valves. According to the results of this study, the bileaflet valve had higher chance of developing cavitation bubbles during the valve closure because of higher pressure drops across the valve.